Essentials of dynamic walking

Analysis and design of two-legged robots

Martijn Wisse

Essentials of dynamic walking
Analysis and design of two-legged robots

Proefschrift

ter verkrijging van de graad van doctor
aan de Technische Universiteit Delft,
op gezag van de Rector Magnificus prof. dr ir J.T. Fokkema,
voorzitter van het College voor Promoties,
in het openbaar te verdedigen op maandag 20 september 2004 om 10:30 uur
door Martijn WISSE
werktuigkundig ingenieur
geboren te Delft.

Dit proefschrift is goedgekeurd door de promotoren:
Prof. dr ir H.G. Stassen
Prof. dr F.C.T. van der Helm

Samenstelling promotiecommissie:
Rector Magnificus, voorzitter
Prof. dr ir H.G. Stassen, Technische Universiteit Delft, promotor
Prof. dr F.C.T. van der Helm, Technische Universiteit Delft, promotor
Dr ir A.L. Schwab, Technische Universiteit Delft
Prof. dr A. Ruina, Cornell University
Prof. dr ir M. Steinbuch, Technische Universiteit Eindhoven
Prof. dr P.J. Beek, Vrije Universiteit Amsterdam
Dr ir S. Stramigioli, Universiteit Twente
Prof. dr ir D.J. Rixen, Technische Universiteit Delft, reservelid

Dr ir R.Q. van der Linde en ing. J. van Frankenhuyzen hebben een belangrijke bijdrage geleverd aan het onderzoek beschreven in dit proefschrift.

Het onderzoek werd financieel mogelijk gemaakt door de Technologiestichting STW, projectnummer DWT4551.

ISBN 90-77595-82-1

Summary

Human beings can walk stably and efficiently on all sorts of terrain, apparently without much effort. From an engineering point of view, this apparent ease is remarkable given the fact that the walking motion is a complex dynamic phenomenon. Walking on two legs involves highly non-linear and multi-variable dynamics, a limited foot-ground interaction (only compressive forces), naturally unstable dynamics (the system is an inverted pendulum pivoting at the foot), it involves discrete events (such as heel strike) and a varying configuration (alternating stance and swing phases). To be able to replicate this complex walking motion, for example for the development of rehabilitation aids or for walking robots, it is necessary to find the essentials of the locomotive system design that make human walking so natural and effortless.

To find the essentials of human walking, this thesis applies the approach of gait synthesis (building artificial walking systems) rather than gait analysis (studying the existent human system). In a problem-solving manner, an artificial walking system is built up feature by feature. This approach ensures a focus on the essentials of walking; for each additional feature it is known exactly why it is necessary and how it adds to human-like walking.

The approach in this thesis differs from the approach used in most walking robot projects. Usually, the design and control of two-legged robots is based on standard robot manipulator technology; strong actuators and stiff structural components are combined with sophisticated control algorithms so that the entire system can accurately follow prescribed trajectories. We argue that this leads to unnecessarily complex, heavy, and energy inefficient walking machines, because accurate trajectory following is not a necessary condition for successful locomotion. The key insight is that stability does not necessarily need to be obtained within a single step (the trajectory control approach), as long as the walking motion is stable *over the course of multiple steps*. In other words, the walking motion must be regarded as a cyclic motion which only needs to be stabilized in its entirety. Thus, the fundamental trajectory instability within a step (the system is an inverted pendulum) can simply be allowed to exist!

Our research is based on the well known concept of 'passive dynamic walking', in which the potential of the cyclic approach is convincingly demonstrated. Purely passive mechanisms consisting of two legs with knees can perform a stable, cyclic walk down a shallow slope. With their unactuated hip and knee joints, these walkers obtain cyclic stability without any control input. Not only are such

walkers extremely simple mechanical constructions, also their walking motion is highly natural and efficient; the swing leg moves forward in its natural frequency requiring no energy input and giving a natural, fluent impression. Only at the end of the step, a bit of energy is lost at the heel strike impact, which is usually replenished by walking down a shallow slope. The stability of such walkers is a result of the regulating effect of the impact at heel strike and it depends on the parameter values of the model. To analyze the stability of a passive dynamic walker by means of computer simulations, the method of Poincaré Mapping is usually applied. The system state is monitored once per cycle (at heel strike), and it is analyzed how this state progresses from step to step. If a certain state repeats itself step after step ('it maps onto itself'), then the system is said to be in a *limit cycle*. The stability of the limit cycle is analyzed by regarding the linearized effects of small deviations from the limit cycle. This is the method that has been applied in previous research on passive dynamic walking and it forms the basis for the stability research in this thesis.

The goal of this thesis is to find the essentials of dynamic, human-like walking, taking the concept of passive dynamic walking as the point of departure. So, what are the limitations of the current state of the art in passive dynamic walking? The answer consists of a long list of capabilities and features that have not yet been incorporated in passive dynamic walking; stability against large disturbances, an upper body, 3D stability, starting and stopping, standing up after a fall, climbing stairs, turning, etcetera. This thesis focuses on three of the problems in this list. First, although the passive walkers are stable for small disturbances, larger disturbances quickly lead to a fall. Therefore, the first requirement is a method to analyze the large disturbance behavior, with the help of which we should find simple and efficient design or control solutions to improve the large disturbance behavior. Second, a major limitation of passive dynamic walking is the fact that currently all designs consist of legs only, as there exists no passive solution to add an upper body. Third, in passive dynamic walking the 3D stability results are still meagre. Almost all of the prototypes are two-dimensional; they move in the plane by means of a double symmetric construction with two pairs of legs, one outer pair and one inner pair (cf. walking with crutches). The few existent prototypes with genuine 3D dynamics (which can fall also sideways because they have only two legs) are only barely stable. In summary, the goal of this thesis is to solve the following three problems:

1. understanding and improving the large disturbance behavior,
2. adding the upper body,
3. obtaining 3D stability.

First, to study the large disturbance behavior, we introduced the analysis of the *basin of attraction* of the limit cycle. The basin of attraction is the collection of all the states that still lead to the steady limit cycle. All states outside the basin of attraction eventually lead to a failure. We analyzed the basin of attraction for the most elementary walking model, a two-dimensional model with straight legs and point masses at the hip and feet. We found that the main failures are falling backward (not sufficient energy to pass mid stance) and falling forward (the swing leg is not timely in a forward position to catch the walker for the next step). The simulation study provided the following conclusions:

- Compared to the original, linearized stability analysis, the basin of attraction provides a better insight in the large disturbance behavior, and thus it enables a better prediction of successful locomotion under realistic circumstances.
- The basin of attraction for purely passive walkers is extremely small, indicating a very weak tolerance for larger disturbances.
- The most frequent failure is a fall forward. The fully passive swing leg moves forward in its natural frequency and thus it requires a fixed amount of time to complete the step. If the walker moves too fast due to a disturbance, the swing leg is not timely in a forward position to catch the robot for the next step.

To improve the large disturbance behavior, we proposed to take a step away from the fully passive approach and to add actuation in the hip joint. With an actuator at the hip it is possible to accelerate the swing leg to ensure a timely arrival at a forward position. A simulation study showed that this solution can completely remove the risk of falling forward, albeit at a small energetic cost. Moreover, we found that there is no complex control required for this solution; the swing leg can simply be moved to a preset forward position. No measurements of the actual state of the robot are required, the actuation can be identical at every step. A simple spring-damper combination at the hip joint is sufficient; all that is required is to switch the equilibrium position of the spring once per step. An additional benefit of the proposed actuation is that it injects a sufficient amount of energy in the system so that the walkers are no longer dependent on a downhill slope for their energy input.

The proposed solution was validated with an autonomous, two-dimensional prototype with knees. The prototype weighs 7 kg and stands 0.7 m tall, and it can walk at 0.4 m/s (0.6 s per step). The hip joint is actuated with McKibben muscles which provide a joint stiffness proportional to their internal CO_2 pressure. By alternatingly using only one muscle out of a pair of antagonistic muscles, the hip joint is given a stiffness and a forward set point at each step. In this manner, the swing leg is accelerated forward according to our proposed control rule. The prototype was made to take a step-down during a steady walk, and the maximal step-down height was recorded as a function of the hip muscle pressure (hip joint stiffness). It was shown that a higher pressure indeed allows a larger step-down (maximally 14 mm). Thus, the proposed hip actuation indeed improves the large disturbance behavior.

Second, to add an upper body, we introduced the bisecting hip mechanism. It constrains the upper body to the bisection angle of the two legs. In this manner, the addition of the upper body does not introduce an extra degree of freedom.

The upper body is not an unstable inverted pendulum (with the hip as pivot point), but rather its mass and inertia are mapped onto the two legs. Therefore, there is no additional stability control required and we can maintain the simple system design of the original passive walkers. A simulation study revealed that the presence of such an upper body results in an improved energy efficiency without deteriorating the large disturbance behavior. From these results we concluded that the bisecting hip mechanism forms a practical and simple solution to construct efficient bipedal walking robots with an upper body, in agreement with the concept of passive dynamic walking.

The proposed solution was validated with an second prototype. The walker is an autonomous, two-dimensional prototype with knees and an upper body. The prototype weighs 10 kg and stands 1.1 m tall (0.7 m leg length), and it walks at 0.4 m/s (0.8 s per step). The actuation system and most of the design is an improved copy of the first prototype. The prototype walks stably and efficiently, while the motions and the disturbance behavior match perfectly with a detailed simulation model. We found both in the model study and in the prototype that the fore-aft position of the center of mass of the upper body is a powerful parameter for the stability of the walking motion. Conversely, the hight of the center of mass, the total mass and the mass distribution have no noticeable influence on the stability. The prototype experiments validate the use of a bisecting hip mechanism to add a passive upper body in a simple manner to dynamically walking robots.

Third, to obtain stability for three-dimensional walking motions, we studied a special ankle joint. The ankle joint points forward and downward, quite unlike the human ankle. The effect of the ankle joint is a dynamic stability; it only provides stability when the robot is walking with sufficient forward velocity. The effect is similar to the stabilizing dynamic effects found in bicycles and skateboards. In all of these systems, a sideways leaning angle (the main cause for instability in 3D walking systems) is coupled to a steering angle so that the systems steers in the direction that it is falling. With sufficient forward velocity, the coupling results in a stabilization of the sideways leaning angle. A simulation study revealed that the orientation of the ankle joint axis has an important effect on the stability. The general rule is that the more horizontal the axis is oriented, the higher is the required minimal velocity for stability. The simulation also showed that the hip actuation as described earlier is a prerequisite for stable 3D walking with this ankle joint. A final result is that the ankle joint provides a simple means to make (weak) turns while walking; an asymmetry in the mass distribution automatically leads to a turn, as the asymmetry can be seen as a continuous sideways disturbance which is stabilized by (automatically) steering in that direction. In summary, the simulation results convincingly showed that the special ankle joint can result in stable 3D walking motions.

The idea of a special ankle joint for 3D stability was validated with a final prototype. The prototype weighs 8 kg and stands 1.5 m tall (0.7 m leg length), and it walks at 0.4 m/s (0.8 s per step). The prototype leaves a much more human impression than any of the previous machines. It has two legs (not four legs in symmetric pairs) with knees and the special ankle joints, and an upper body (with a lightweight head and counter-swinging arms, features more for appearance than for function yet). The human impression is especially strong when the prototype walks; the natural swing of the legs including a passive knee motion, the slight sideways oscillation from step to step, and the overall effortless forward progression all give the prototype a highly natural appearance. With its successful walking performance, the third prototype validates the implementation of a special ankle joint that couples lean to steering as a solution for dynamic stability in 3D walking machines.

The most significant achievement is that the three prototypes can walk naturally, stably, and efficiently while using a minimal control system; the entire control system for all three prototypes consists of only two foot switches which trigger only three on/off actuators (one hip actuator and two knee latches). With these results, we have demonstrated that knowledge of the essentials of dynamic, human-like walking can lead to extremely simple yet highly natural walking machines.

Martijn Wisse, 2004

Contents in brief

1 Introduction 3

Part I Elementary model studies 15

2 Basin of Attraction of the Simplest Walking Model 17

3 How to keep from falling forward; Elementary swing leg action for passive dynamic walkers 33

4 Passive Dynamic Walking Model with Upper Body 51

5 Skateboards, bicycles, and 3D biped walkers; Velocity dependent stability by means of kinematic and dynamic lean-to-yaw coupling 67

Part II Prototype experiments 89

6 Design and Construction of 'Mike'; A 2D autonomous biped based on passive dynamic walking 91

7 Adding the upper body to passive dynamic walking robots by means of a bisecting hip mechanism 105

8 Three additions to passive dynamic walking; Actuation, an upper body, and 3D stability 123

9 Discussion, conclusions, and future directions 143

Contents

Summary **i**

Contents in brief **vii**

Contents **ix**

1 Introduction **3**
  1.1 Essentials of dynamic walking 3
  1.2 Motivation 4
  1.3 Gait synthesis instead of biomechanical analysis 5
  1.4 The difficulty with gait synthesis 6
  1.5 Two possible points of departure 8
  1.6 State of the art and problem statement 10
  1.7 Goal 11
  1.8 Approach 11
  1.9 Thesis outline 12

Part I Elementary model studies **15**

2 Basin of Attraction of the Simplest Walking Model **17**
  2.1 Introduction 18
  2.2 The Simplest Walking Model 18
  2.3 Analysis of the Model 19
    2.3.1 Equations of Motion 20
    2.3.2 Heelstrike 21
    2.3.3 Stride function 23
  2.4 Step-to-step behavior 24
    2.4.1 Failure modes 24
    2.4.2 Cyclic motion 25
    2.4.3 Cell mapping method 27
  2.5 Results 28
    2.5.1 Basin of Attraction 28
    2.5.2 Basin of attraction versus slope angle 29
  2.6 Conclusion 32

3 How to keep from falling forward; Elementary swing leg action for passive dynamic walkers 33
- 3.1 Introduction 34
- 3.2 Modeling and analysis 34
  - 3.2.1 The simplest walking model 34
  - 3.2.2 Limit cycle analysis 35
  - 3.2.3 Linearized stability, local stability 37
  - 3.2.4 Basin of attraction, global stability 38
- 3.3 Swing leg action for a larger basin of attraction 40
  - 3.3.1 Largest possible basin of attraction 40
  - 3.3.2 The rimless wheel 42
  - 3.3.3 A realistic actuation model 43
- 3.4 Prototype experiments 44
  - 3.4.1 Mike 44
  - 3.4.2 Actuation system 45
  - 3.4.3 Stability results 45
- 3.5 Discussion 47
  - 3.5.1 Level floor 47
  - 3.5.2 Distributed leg mass 47
  - 3.5.3 Feet 48
  - 3.5.4 Knees and muscles 48
  - 3.5.5 Human walking 48
- 3.6 Conclusion 49

4 Passive Dynamic Walking Model with Upper Body 51
- 4.1 Introduction 52
- 4.2 Passive walking model with upper body 52
- 4.3 Results 55
  - 4.3.1 Walking motion 55
  - 4.3.2 Inherent stability 56
- 4.4 Parameter study 58
  - 4.4.1 Slope and spring stiffness; speed and step length 58
  - 4.4.2 Upper body height and weight 59
  - 4.4.3 Limits to stability 60
- 4.5 Conclusion 61

5 Skateboards, bicycles, and 3D biped walkers; Velocity dependent stability by means of kinematic and dynamic lean-to-yaw coupling 67
- 5.1 Introduction 68
- 5.2 Two examples of advantageous lean-to-yaw coupling 68
  - 5.2.1 Skateboard 68
  - 5.2.2 Bicycle 70
- 5.3 Simplest passive walking model with lean-to-yaw coupling 74
  - 5.3.1 Model 74
  - 5.3.2 Equations of motion 75

5.3.3 Simulation procedure 76
5.4 Simulation results 77
5.4.1 Fully passive model 78
5.4.2 Model with hip actuation 81
5.4.3 Stability versus velocity 83
5.4.4 Walking and steering 85
5.5 Discussion 87
5.5.1 Applicability in walking robots 87
5.6 Conclusion 88

Part II Prototype experiments 89

6 Design and Construction of 'Mike'; A 2D autonomous biped based on passive dynamic walking 91
6.1 Introduction 92
6.2 Foot Shape 93
6.2.1 Foot shape in literature 93
6.2.2 Test machine for foot roll-over shape 93
6.2.3 Construction 94
6.3 McKibben Muscles as Adjustable Springs 95
6.3.1 Background and requirements 95
6.3.2 Operating principle, technical realization and results 95
6.4 Pneumatic System 97
6.4.1 Background and presumptions 97
6.4.2 Requirements 97
6.4.3 System overview 98
6.5 Pressure Control Unit 99
6.5.1 Background and requirements 99
6.5.2 Operating principle 99
6.5.3 Technical realization and results 100
6.6 Walking Experiments 101
6.6.1 Downhill walking 101
6.6.2 Walking on level floor 102
6.7 Conclusion 103

7 Adding the upper body to passive dynamic walking robots by means of a bisecting hip mechanism 105
7.1 Introduction 106
7.2 Main concepts 106
7.2.1 Passive dynamic walking 106
7.2.2 Hip actuation for stability 107
7.2.3 Bisecting hip mechanism 108
7.3 Methods 109
7.3.1 Simulation model 109

    7.3.2 Simulation procedure 110
    7.3.3 Default parameter values 111
    7.3.4 Construction of the prototype 111
  7.4 Results 115
    7.4.1 Resultant motion and gait characteristics 115
    7.4.2 Stability 116
    7.4.3 Parameter sensitivity 118
    7.4.4 Energy efficiency 120
  7.5 Conclusion 121

8 Three additions to passive dynamic walking; Actuation, an upper body, and 3D stability 123
  8.1 Introduction 124
  8.2 Passive Dynamic Walking 125
    8.2.1 Historical background 125
    8.2.2 State of the art 126
    8.2.3 Stability analysis 126
  8.3 Hip actuation for power input and stability 127
    8.3.1 Elementary model study 127
    8.3.2 Prototype experiments 129
    8.3.3 Conclusion 132
  8.4 Bisecting hip mechanism for passive yet stable upper body 133
    8.4.1 Elementary model study 133
    8.4.2 Prototype experiments 133
    8.4.3 Conclusion 135
  8.5 Skateboard-like ankle joint for 3D stability 136
    8.5.1 Elementary model study 136
    8.5.2 Prototype experiments 137
    8.5.3 Conclusion 139
  8.6 General conclusions 140

9 Discussion, conclusions, and future directions 143
  9.1 Essentials of dynamic walking 143
  9.2 On general design guidelines for stability 143
  9.3 On stability measures and disturbances 147
  9.4 On actuation 149
  9.5 On foot contact in simulations 151
  9.6 On human walking 152
  9.7 General conclusions 153
  9.8 Future directions 154

Appendix A First steps in Passive Dynamic Walking 157
  A.1 Introduction 158
  A.2 Forward dynamic simulation 159
  A.3 Step-to-step stability analysis 165
  A.4 Conclusion 168

Appendix B Video material 169

References 173

Samenvatting 181

Dankwoord 187

Curriculum Vitae 191

Chapter 1

Introduction

1.1 Essentials of dynamic walking

The topic of this thesis is the search for the essentials of dynamic, human-like walking. This search is motivated by needs from rehabilitation and from robot design (Section 1.2). The search is conducted by means of gait synthesis (the construction of walking simulations and robot prototypes) rather than gait analysis (the biomechanical study of human locomotion), because this will lead to the more fundamental dynamic insights (Section 1.3). The main difficulties in gait synthesis arise from the involved nonlinear and variable dynamics and from the unilateral foot contact (Section 1.4). To overcome these difficulties, two general approaches are known (Section 1.5); industry builds on classical robotic control techniques whereas some academic research institutes build on dynamical systems theory. This thesis applies the second approach. The state of the art is represented by 'passive dynamic walking' robots; mechanical contraptions that demonstrate extremely natural walking motions without the need for any control action (Section 1.6). Of all the work that needs to be done in this field, this thesis focuses on three issues (Section 1.7): 1) robustness, 2) upper body, and 3) 3D stability. These three issues are resolved via a comparison (Section 1.8) between simulations and three successfully walking prototypes (one for each problem) as outlined in Section 1.9.[1]

---

[1] Note that chapters 2-8 are exact reproductions (except for page lay-out) of journal articles or conference articles as they have appeared or have been submitted.

1.2 Motivation

The oldest motivation to search for knowledge on dynamic walking is the field of rehabilitation. Archeological findings[2] have shown that already in the prehistory, humans were fitted with prostheses (limb replacement) and orthoses (limb function support). Then and now, these artificial limbs have two purposes: to restore the function of the limb (prostheses and orthoses) and to hide the weakness or disfiguredness of a missing limb (mostly prostheses). In ancient history, most of the amputations were a result of human conflicts, and this is not different in the more recent history, as World Wars I and II brought tens of thousands of amputees each, while other parts of the world continue to suffer from large scale conflicts. In addition, the late 1950's saw the 'Thalidomide tragedy'; approximately ten thousand babies were born with deformed or missing limbs due to disastrous side effects of this insomniac drug taken during pregnancy[3]. In the Netherlands, currently most amputations are a result of an accident or are necessary because of a vascular disease (mostly elderly patients), and add up to over 2000 amputations per year in the Netherlands alone [42].

For most part of history, leg protheses have been constructed the same way, with a wooden peg leg, leather straps and a soft leather or linen lining. In the sixteenth century Paré heralded an era of mechanical refinement comprising better materials and more degrees of freedom, especially for the upper extremities. For the legs, however, even the most advanced prostheses still have only one degree of freedom, the knee. Foot designs have evolved to incorporate damping and compliance, but most of these developments were experience-based. This is also the case for the modern prostheses with computer controlled damping in the knee. Almost none of the design features of today's prostheses are based on knowledge of the dynamics of walking. This lack of knowledge results in unnatural dynamic behavior of the prosthetic leg, which the amputee will try to hide by means of extra effort [72]. This demonstrates the relevance of knowledge on the essentials of dynamic walking and the current lack thereof.

Another motivation for the search for knowledge on dynamic walking comes from the field of entertainment, an industry with less urgency but much more economic thrust than the field of rehabilitation. The billion dollar markets of computer games and motion pictures make more and more use of computer generated actors [35]. The generated motions must be of high quality because the human eye is very perceptive for deviations from natural walking motions. Although virtual gravity is a little more forgiving than the real thing, knowledge of the underlying dynamics is imperative for the development of realistic animations.

More recently, the entertainment industry has been opening up the market for entertainment robots. After SONY's four-legged AIBO-dog, several companies [68, 46, 41, 45] are now developing two-legged *humanoid* robots, see Fig. 1.1. Although the current products are still based on classic robotic technology (see Section 1.5), the attractiveness of the human appearance of these robots has already resulted in huge media coverage and public interest, providing the developing companies with an effective means to show their technological disposition. It is expected that the human-like form of locomotion will eventually also prove useful for tasks other than entertainment; a two-legged design provides functionality in environments that are especially designed for humans such as dangerous factory environments, construction workplaces, and the homes of private robot owners. Various reports [74, 66] predict a steady development from the current research and entertainment products towards highly versatile machines, parallel to the stages of development seen in the short history of the PC. For the development of two-legged walking robots, the need for knowledge of the essentials of human-like walking is self-evident.

---

[2] The remarks with respect to the history of gait analysis and prosthetics in this chapter are based on the *Clinical Gait Analysis* webpages, `http://www.univie.ac.at/cga/`

[3] The 'Thalidomide tragedy' ('Softenon drama' in Dutch) was one of the incentives to start research into prosthetics at Delft University of Technology, the technology of which has been the base for our research into biped robots.

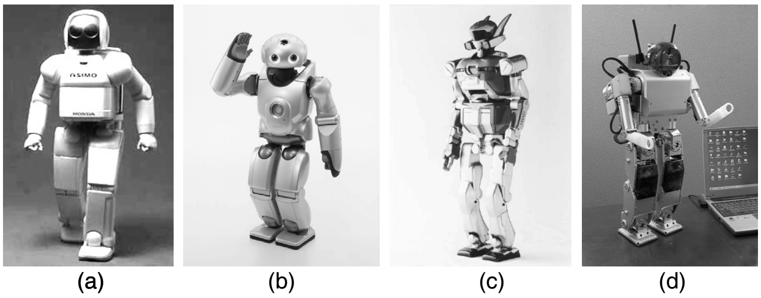
(a) (b) (c) (d)

Figure 1.1: *Several companies are now developing two-legged humanoid robots: (a) Honda's ASIMO [68], (b) Sony's SDR-4X [46], (c) Kawada's HRP2 [41], and (d) Fujitsu's HOAP-1 [45].*

1.3 Gait synthesis instead of biomechanical analysis

To obtain knowledge on human walking, there are two distinct approaches; descriptive gait analysis and predictive gait synthesis. The most obvious approach, gait analysis, has been a central research topic in biomechanics since early history, such as Hippocrates' treatment of people with a hip joint dislocation [32] around 400 BC. The early modern times have produced beautiful treatments on human motion (e.g., Borelli [9] in 1680). As soon as photography became available in the late nineteenth century, Marey [47] and Muybridge [55] applied it to perform two-dimensional (2D) kinematic analyses. The first 3D kinematic analysis was performed in 1891 by Braüne and Fischer [10]. Elftman [22] developed the force plate in 1938 which he used to perform the first inverse-dynamics gait analysis. Although the tools have improved enormously since then (e.g.

with the introduction of the 3D computerized data acquisition and even real-time inverse-dynamics analysis), the basic analytical approach has remained the same ever since; the motions and ground reaction forces are measured and the joint torques or muscle forces are then calculated using a model of the human body.

In the search for the essentials of human-like walking, the biomechanical approach of gait analysis is not suitable. First, it is hard to discriminate between essential and non-essential features, because the system has to be studied in its entirety. For example, it is rather impossible to switch off certain sensors (e.g. Golgi tendon organs which measure muscle force) and study the result. Second, some essential features might be overlooked because of their sustained presence in all experiments. For example, many studies based on inverse-dynamics calculations ignore the problem of stability and thus fail to recognize the importance of related features such as local feedback control loops.

The goal of this thesis, finding the essentials of dynamic walking, is better served with the approach of gait synthesis. In a problem-solving manner, an artificial walking system is built up feature by feature. This approach ensures a focus on the essentials of walking. Moreover, for each additional feature it is known exactly why it is necessary and how it adds to human-like walking. This is the approach taken throughout the research presented in this thesis.

1.4 The difficulty with gait synthesis

The synthesis of bipedal gait is difficult because it requires a complete understanding of the system characteristics; it is impossible to focus on a detail (e.g. knee motion) and temporarily ignore a fundamental problem such as stability. Following Pratt [63], we distinguish the following characteristics that make two-legged systems a complicated topic:

- **Non-linear dynamics.** The leg excursions are distinctly outside the linearizable region so that the full non-linear dynamics must be accounted for. The non-linear nature of the system is especially dominant when three-dimensional dynamics are considered.

- **Multi-variable dynamics.** Walking systems are modeled as multibody systems with rigid links and low-impedance joints. The interaction between the various degrees of freedom is important and should not be overlooked, especially in three dimensions (e.g. a simplification into two planar models, one for the lateral plane and one for the frontal plane, is guaranteed to provide erroneous answers).

- **Naturally unstable dynamics.** Grosso modo, the entire system can be seen as a (naturally unstable) inverted pendulum balancing on the stance leg. This necessitates to study the dynamic balance of the system over the entire walking cycle, which requires a much more involved analysis than the more common study of static balance.

- **Limited foot-ground interaction.** The unilateral nature of the foot-ground contact (only compressive contact forces) makes biped systems fundamentally underactuated. The system must use the control over its internal joints to cope also with the uncontrollable foot-ground contact. In addition, the system has no permanent contact to an inertial reference frame and so it cannot directly determine its absolute orientation in space.

- **Discretely changing dynamics.** The alternation of foot contact represents a discrete change in boundary conditions of the dynamical system. In addition, in many idealized models of biped machines there is the occurrence of impacts (e.g. heel strike) which result in discrete velocity changes.

Due to these characteristics, biped systems belong to a general class of systems that form an interesting topic for dynamical systems theory and a definite challenge to control theory [86].

However, it should be realized that the requirements for successful bipedal walking are not identical to those for successful robotic manipulation for manufacture, the classical interpretation of robotics. Where speed and positioning accuracy are the main requirements for successful manufacturing, these characteristics are not important for bipedal walking, warranting a different approach to dealing with the above mentioned intricacies. Instead of speed and positioning accuracy, successful biped systems meet the following requirements:

- **Stability.** The biped should not fall when challenged with (a predefined range of) disturbances.

- **Efficiency.** In most cases the biped system is useful only if it is autonomous, i.e. it has to carry its own energy supply. Depending on the required sustained operational time, it has to use its resources efficiently.

- **Naturalness.** Depending on its purpose, the biped has to demonstrate more or less human-like natural motions. Note that playing back prerecorded human walking motions on an artificial system with slightly differing dimensions can quickly result in a highly unnatural appearance to the human observer.

- **Versatility.** Depending on the application, the biped system should be capable to manoeuvre, vary velocities, climb stairs, avoid obstacles, etc.

- **Safety.** When applied in a human environment, the biped system should be unable to harm human beings, i.e. it should be lightweight and low-powered.

These requirements make the synthesis of walking systems a challenge that is clearly different from classical robot design, and in some ways the solutions might prove simpler, depending on the design approach as detailed in the following section.

1.5 Two possible points of departure

To synthesize gait and build biped walking systems, two possible points of departure exist:

- the industry-oriented *static* bipeds
- the academic oriented *passive* bipeds

Each starting point has its benefits and drawbacks, but both require substantial research to arrive at human-like walking; the *static* bipeds have sufficient versatility but must be developed towards *dynamic* (more natural and efficient) walking, whereas the *passive* bipeds already possess an efficient, natural dynamic gait but must be provided with actuation and must be developed towards more robustness and versatility. The points of departure are detailed below.

Static bipeds

The standard approach to robot control as applied in industrial manufacturing robots is to ensure direct control over all degrees of freedom. By application of strong actuators and stiff structural components, the robot manipulators can be controlled to accurately follow prescribed trajectories. This approach can be used as a starting point for the construction and control of biped robots. To deal with the fundamental characteristics of limited foot contact and discretely changing dynamics, the bipeds are programmed to walk slowly and to keep the center of mass above the foot contact area (hence 'static' bipeds). Thanks to these constraints, the stance foot remains in full, flat contact with the floor and thus 'simulates' direct control over all degrees of freedom. An extension towards a more dynamic approach is the so-called 'Zero Moment Point' [82] (center of pressure [28]) control; by keeping the center of pressure inside the foot contact, full and flat foot contact can also be ensured. Note that this is not sufficient to prevent the biped from falling, it would just fall while keeping full foot contact. Usually, the 'Zero Moment Point' calculation serves as a constraint to trajectory generators so that faster (than fully static) walking motions can be generated while ensuring that the foot maintains full, flat contact with the floor. The actual stability of the gait results from the ability to robustly follow the generated trajectory. One of the first research robots based on this approach was built at Waseda University in 1970 [1]. Many followed, especially in Japan, and work towards a more dynamic gait is in progress.

The benefit of the static approach is that a complete system can be built from the start; it has all the degrees of freedom needed to make it look human and thus it is immediately ready for commercialization, e.g. for entertainment purposes. Making it more dynamic, natural, efficient and cheaper are topics for gradual improvement, as illustrated with the succession of prototypes by Honda [33, 68] and Sony [46]. This benefit makes the static approach a good starting point for industrial developers. The drawback is that it is unlikely that this approach will yield clearly presented fundamental insights in the problem of walking, making it an unattractive starting point for academic research.

Passive bipeds

Biomechanical research has provided several hints towards the possible role of passive dynamic motions in human walking. A remarkably relevant hypothesis posed by Weber and Weber [84] as early as 1836 reads: 'Die Beine können am Rumpfe wie Pendel hin und her schwingen. (...) Unsere aufmerksamkeit wird für diese schwingende Bewegung nicht erfordert.' ('The leg can swing back and forth like a pendulum suspended from the body. ... Our attention is not required to produce this swinging motion.') Mochon and McMahon [53] arrived at the same conclusion after comparing the swing leg motion with a passive double pendulum. Another hint in that direction is given by Ralston [65] who discovered that there exists an optimal walking velocity for humans; at approximately 5 km/h the specific resistance (also termed specific cost of transport, i.e. energy cost per weight per distance traveled) is minimal, a phenomenon that indicates the use of the natural frequencies of the mechanical system.

Early toy makers [23] (Fig. 1.2a) proved the applicability of the ideas by showing that the human walking motion can at least partially be generated with passive mechanisms that move and oscillate at their natural frequencies. In 1989, McGeer [49] proposed that those passive mechanisms could serve as an alternative point of departure for the synthesis of bipedal gait. He parallelled this to the approach of the Wright Brothers, who first mastered passive gliding before they added an engine to their aeroplane. McGeer showed that a completely unactuated and therefore *uncontrolled* robot can perform a stable walk [48] when walking down a gentle slope (Fig. 1.2b). Since then, his work has been extended gradually by Ruina's group at Cornell University [18, 15, 27, 24, 19] (Fig. 1.2c) up to the point where the passive approach can be regarded beyond doubt as a valid starting point for bipedal gait synthesis and robot construction.

The benefits of the passive approach are the inherent efficiency of the walking motion, the natural-looking motions, and the simplicity of the required construction. The development towards a more human-like versatility should be taken step-by-step (figuratively), which can be seen as both a benefit and a drawback of this approach. The drawback is that, although the motions of the early machines are uncannily natural, the general public is quickly disappointed with the incompleteness of the system (e.g. no upper body, lateral constraints to ensure only two-dimensional dynamics, no velocity control). This makes the passive approach unattractive for industrial developers. The required incremental addition of versatility does, however, provide ample opportunities to discover fundamental dynamic properties. As such, the passive approach is the most appropriate point of departure for academic research into gait synthesis.

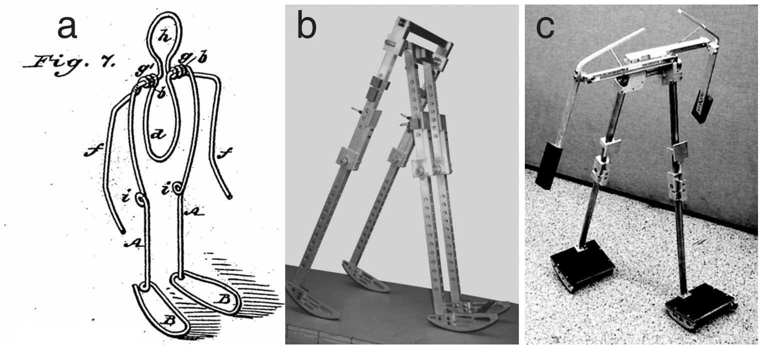

Figure 1.2: *Previous realizations of passive walkers demonstrate the feasibility of the concept of passive dynamic walking: (a) Figure from 1888 patent by Fallis [23], (b) Garcia's copy of McGeer's 2D kneed walker [48], (c) Collins' 3D passive walker with knees and counterswinging arms [19].*

1.6 State of the art and problem statement

Since McGeer, much research has been done on passive dynamic walking, but even more remains to be done. McGeer built and simulated bipeds with and without knees which were laterally constrained (2D dynamics) by a symmetric construction with two pairs of legs. Simulation studies on fully passive models were performed by Garcia [27] and Goswami [30], whereas Hurmuzlu [38], Spong [73], Van der Linde [78] and Asano [8] added some form of actuation and control. Wisse [90], Piiroinen [60], Adolfsson [6, 7], and Kuo [43] simulated near-3D models, whereas Coleman [17] simulated a fully passive, full 3D model, for which also a physical prototype was built [18]. Other prototypes were built by Collins [19], Van der Linde [77], Ono [57, 58] and Tedrake [75], whereas Pratt [62] included passive dynamics in an otherwise active robot.

Almost all walkers in this list consist of legs only, most of them are fully passive, and many exist only as computer models. Also, all of them require a disturbance-free environment. To advance from this state of the art towards human-like walking capabilities, at least the following topics need to be addressed:

- increasing the robustness in 2D,
- adding an upper body,
- obtaining robustness in 3D,
- enabling control of the walking velocity,
- enabling the walker to start and stop,
- enabling the walker to turn,

- enabling the walker to stand up after a fall.

These increases in complexity and actuation must be carried out step-by-step. For each addition, it should be ensured that the beneficial characteristics of passive walking (efficiency, naturalness, and simplicity) are preserved, and that the fundamental dynamic properties and effects in the entire system with the new addition are understood. This is clearly a long-term research goal, much broader than can be captured in one PhD study. Therefore, this thesis is confined to the first three topics; an increased robustness in 2D, the addition of an upper body, and the search for robustness in 3D.

1.7 Goal

The goal of this thesis is to answer the following three questions:

1. How can the robustness of 2D walking motions be increased?
2. How can an upper body be added?
3. How can robustness for 3D walking motions be obtained?

While answering to these issues, it is pursued to:

- preserve the efficiency, naturalness, and elegant simplicity of passive dynamic walking, and
- present an understanding of the fundamental dynamic principles.

1.8 Approach

The research approach taken in this thesis is based on two cornerstones. On the one hand, irreducibly simple simulation models are studied to generate an understanding of the underlying dynamic principles. On the other hand, the hypotheses and concepts that result from the simulation studies are verified and validated with real-world prototypes, one for each of the three questions mentioned above. The validation can take place on three levels of detail, where each level subsumes the previous one:

- **Single-bit.** The robot walks or it does not. If the irreducibly simple simulation predicts a stable walking motion for a certain morphology within certain boundaries, and the corresponding prototype indeed demonstrates a successful walking motion, then the concept is verified. In many cases a validation on this lowest level of detail is already sufficient, as most objections can easily be countered with 'It works!'.

- **Qualitative effects.** A certain effect (such as an increased stability with a parameter change in a certain direction) is found both in the simulation and in the prototype. If the predicted qualitative effect can be reproduced in the prototype, then the most important goal is achieved; the model has indeed provided an understanding of the fundamental dynamic effects. These are the main research results. The validation in the corresponding prototype guarantees applicability of the concepts for gait synthesis.
- **Quantitative gait characteristics.** The gait characteristics such as walking velocity, step length, energy consumption and disturbance rejection can be quantitatively predicted with the simulation model. This requires a simulation model with adjustable parameters to accurately model the mass distribution, friction, damping, etc. As such, the model is no longer 'irreducibly simple', which might jeopardize the goal of generating an understanding of the fundamental dynamic principles. Therefore, a validation on this level of detail requires a second, more detailed model in addition to the irreducibly simple model. Although a validation on this level merely demonstrates a skill of data matching, the results can help in making the validation on the qualitative level more convincing. Also, the development of such an accurate model is imperative for the optimization of the correlating prototype.

In this thesis, a validation at the level of qualitative effects is applied, enriched with a validation of quantitative gait characteristics where this provides added value. The first level of validation ('It works') is still the most convincing, especially when seen in motion; please refer to the website `http://dbl.tudelft.nl` or to Appendix B (consisting of text and a CD-ROM) for a collection of videos of the robots presented in this thesis.

1.9 Thesis outline

This thesis contains two parts, Part I with four chapters on irreducibly simple simulation models, and Part II with three chapters on real-world prototypes. Each chapter is a complete article, unmodified with respect to the form in which it was published or submitted. Therefore, there exists some overlap between the two parts, as an article on simulation results sometimes requires a brief prototype section and vice versa. The three questions that constitute the goal of this thesis are addressed in the following chapters:

1. How can the robustness of 2D walking motions be increased?
    - **Part I, Chapter 2** presents the analysis of the basin of attraction to study the large-disturbance behavior,
    - **Part I, Chapter 3** presents a simple control rule for the swing leg which increases the robustness against large disturbances,

  - **Part II, Chapter 6** presents a validation of this rule with the prototype 'Mike'.

2. How can an upper body be added?
   - **Part I, Chapter 4** presents the concept of a bisecting hip mechanism which allows the addition of a passive yet stable upper body,
   - **Part II, Chapter 7** presents a validation of this concept with the prototype 'Max'.

3. How can robustness for 3D walking motions be obtained?
   - **Part I, Chapter 5** presents the concept of tilted ankle axis which couples lean to yaw for 3D stability,
   - **Part II, Chapter 8** presents a validation of this concept with the prototype 'Denise'.

Finally, **Chapter 9** presents a discussion and a general conclusion. In addition, **Appendix A** provides a tutorial text to get started with 'passive dynamic walking' and **Appendix B** (consisting of text and a CD-ROM) provides a collection of videos of the walking robots and models presented in this thesis.

Part I

Elementary model studies

Chapter 2

Basin of Attraction of the Simplest Walking Model

A. L. Schwab and M. Wisse

ASME Design Engineering Technical Conferences, Sep. 2001; Pittsburgh,
Pennsylvania.

Passive dynamic walking is an important development for walking robots, supplying natural, energy-efficient motions. In practice, the cyclic gait of passive dynamic prototypes appears to be stable, only for small disturbances. Therefore, in this paper we research the basin of attraction of the cyclic walking motion for the simplest walking model. We present a general method for deriving the equations of motion and impact equations for the analysis of multibody systems, as in walking models. Application of the cell mapping method shows the basin of attraction to be a small, thin area. Our measures of the basin of attraction are not directly related to the stability of the cyclic motion.

2.1 Introduction

The past few decades robotics research has made huge developments in the area of biped locomotion, running from prosthesis development to entertainment industries. Several major institutes have succeeded in building successful walking bipeds. One of the under-addressed problems is energy consumption. Most existing bipeds need an 'umbilical cord' for power supply. Honda Motor Co. [33] developed a completely autonomous humanoid robot, but it has to carry 20 kilograms of batteries for a 15 minute walk.

A solution for energetic efficiency is the exploitation of the 'natural dynamics' of the locomotive system. In 1989 McGeer [49] introduced the idea of 'passive dynamic walking', inspired by research of Mochon and McMahon [53]. They showed that in human locomotion the motion of the swing leg is merely a result of gravity acting on an unactuated double pendulum. McGeer extended the idea and showed that a completely unactuated and therefore *uncontrolled* robot can perform a stable walk [48].

The walking motion of a passive dynamic walker is started by launching the robot with such initial values for the leg angles and velocities, that the end of that step (the beginning of a new step) is nearly identical to the starting conditions. A periodic or cyclic walking motion will then result. At each step, when the heel strikes the floor, the impact will result in loss of energy. This loss can be compensated for by having the robot walk down a shallow slope or by periodically supplying energy with an actuator.

A recent study by Garcia *et al.* [27] showed that the simplest passive dynamic walking model can have stable cyclic motion. Experience with real prototypes however reveals that even a very small disturbance may result in failure. This leads us to believe that the size of allowable disturbances is at least as important as the stability of the cyclic solution. Therefore, in this paper we will investigate the basin of attraction of the cyclic motion and the failure modes for the simplest walking model.

2.2 The Simplest Walking Model

The subject of this research is the simplest mechanical model still possessing the ability to perform a bipedal walking motion, as conceived by Garcia *et al.* [27]. The model, shown in Figure 2.1, consists of two rigid links with unit length, connected by a frictionless hinge at the hip. The mass is distributed over three point masses; one with unit mass at the hip, and two with mass β at the feet. The limit case where the foot mass is negligible in comparison with the hip mass, $\beta \to 0$, is investigated. This unactuated two-link system walks down a slope in a gravity force field with unit magnitude. The scaled model of the walker now only has one free parameter, the slope angle γ.

A walking step is started with both feet on the slope. The front foot has just made ground contact, the hind foot has a velocity away from the floor. During a step, the stance foot is modeled as a hinge, connected to the floor. The swing foot is moving freely as the other end of a double pendulum. At about midstance, the swing foot will briefly be below floor level ('foot-scuffing'), which is inevitable for a walker with straight legs. Knees ([50], [88], [7], [19]) or other leg shortening measures ([76]), as well as 3D motion ([43], [76] [78]) would solve the problem but increase complexity of the model. After this short through-pass, the second time that the swing foot reaches floor level is regarded as heel-strike, the end of the step. The former swing foot makes a fully inelastic collision and becomes the new stance leg. Instantaneously, the former stance leg loses ground contact, and a new step begins.

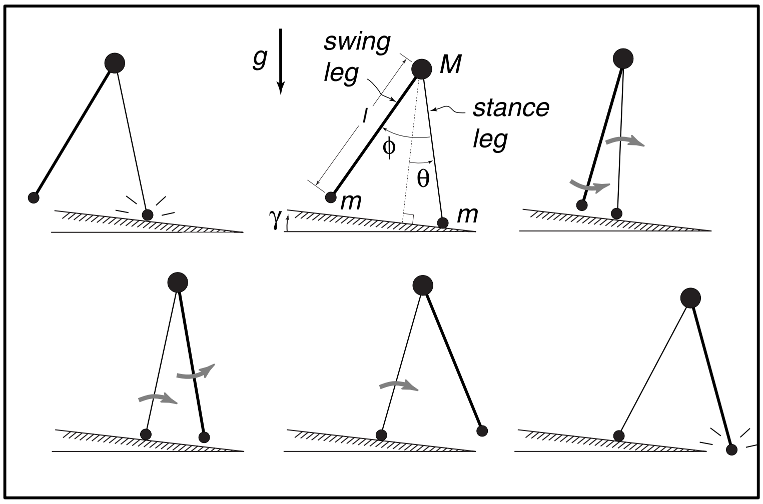

Figure 2.1: *A typical passive walking step. The new stance leg (lighter line) has just made contact with the ramp in the upper left picture. The swing leg (heavier line) swings until the next heelstrike (bottom right picture). The top-center picture gives a description of the variables and parameters that we use. θ is the angle of the stance leg with respect to the slope normal. ϕ is the angle between the stance leg and the swing leg, M is the hip mass, m is the foot mass, l is the leg length, γ is the ramp slope, and g is the acceleration due to gravity. Reprinted with permission from Garcia et al. [27]*

2.3 Analysis of the Model

In the analysis of the passive dynamic walking motion, three stages can be distinguished. First, the derivation of the equations of motion for the walker during the support phase. They will be derived in terms of independent coordinates by the principle of virtual power and will be solved by numeric integration. Second, we formulate and apply the impact equations governing the heelstrike. Third and last, we will formulate the support exchange and combine the results from the previous stages in a stride function. The 'stride function' [51] is a

Poincaré map relating the state during one part of a step with the state during the same part of the next step.

2.3.1 Equations of Motion

The configuration of the walker is defined by the coordinates of the three point masses; the stance foot, the hip and the swing foot, which can be arranged in a global vector $\mathbf{x} = (x_{stl}, y_{stl}, x_{hip}, y_{hip}, x_{swl}, y_{swl})^T$. These coordinates are not independent owing to the two distance constraints imposed by the stance and the swing leg. In order to eliminate the constraint forces from the start, we shall express the equations of motion in terms of independent generalized coordinates. Let Oxy be a fixed orthogonal system of coordinates with Ox along the walking slope and Oy directed upward. Then u and v are the coordinates of the contact point of the stance foot. During walking motion they will be fixed, but at heelstrike they will have no boundary condition in order to fulfill the 'lifting stance foot'-assumption. Furthermore, θ is the angle between the stance leg and Oy, and ϕ the clockwise angle between the stance leg and the swing leg. The configuration of the walker can be described by the vector of generalized coordinates $\mathbf{q} = (u, v, \theta, \phi)^T$. The coordinates $\mathbf{x}$ can locally be expressed as functions of the generalized coordinates $\mathbf{q}$, the kinematic degrees of freedom (configuration coordinates), by means of a transfer function $\mathbf{F}$ as

$$\mathbf{x} = \mathbf{F}(\mathbf{q}) \rightarrow \begin{bmatrix} x_{stl} \\ y_{stl} \\ x_{hip} \\ y_{hip} \\ x_{swl} \\ y_{swl} \end{bmatrix} = \begin{bmatrix} u \\ v \\ u - \sin(\theta) \\ v + \cos(\theta) \\ u - \sin(\theta) + \sin(\theta - \phi) \\ v + \cos(\theta) - \cos(\theta - \phi) \end{bmatrix}. \tag{2.1}$$

The unreduced equations of motion for the system are obtained by assembling the contribution to the virtual power equation of all point masses in a global mass matrix $\mathbf{M}$ and a global force vector $\mathbf{f}$, which results in a virtual power balance

$$\delta\dot{\mathbf{x}}^T[\mathbf{f} - \mathbf{M}\ddot{\mathbf{x}}] = 0. \tag{2.2}$$

Here, $\delta\dot{\mathbf{x}}$ are kinematically admissible virtual velocities, which satisfy all instantaneous kinematic constraints. By differentiating the transfer function (2.1) we obtain

$$\dot{\mathbf{x}} = \mathbf{F}_{,\mathbf{q}}\dot{\mathbf{q}}, \quad \delta\dot{\mathbf{x}} = \mathbf{F}_{,\mathbf{q}}\delta\dot{\mathbf{q}} \quad \text{and} \quad \ddot{\mathbf{x}} = \mathbf{F}_{,\mathbf{q}}\ddot{\mathbf{q}} + \mathbf{F}_{,\mathbf{qq}}\dot{\mathbf{q}}\dot{\mathbf{q}}. \tag{2.3}$$

Here a subscript comma followed by one or more variables denotes partial derivatives with respect to these variables. The way in which higher-order derivatives have to be multiplied by the juxtaposed vectors goes without saying. Substitution of these expressions in the virtual power equation (2.2) and adding on the left-hand side the contribution, $\delta\dot{\mathbf{q}}^T\mathbf{Q}$, from the generalized forces $\mathbf{Q}$ dual to the coordinates $\mathbf{q}$, yields the reduced equations of motion

$$[\mathbf{F}_{,\mathbf{q}}^T\mathbf{M}\mathbf{F}_{,\mathbf{q}}]\ddot{\mathbf{q}} = \mathbf{F}_{,\mathbf{q}}^T[\mathbf{f} - \mathbf{M}\mathbf{F}_{,\mathbf{q}\mathbf{q}}\dot{\mathbf{q}}\dot{\mathbf{q}}] + \mathbf{Q}. \tag{2.4}$$

For the walker the global mass matrix is

$$\mathbf{M} = \mathrm{Diag}(\beta, \beta, 1, 1, \beta, \beta), \tag{2.5}$$

and the applied forces, only gravity, are

$$\mathbf{f} = \mathbf{M}[\sin(\gamma), -\cos(\gamma), \sin(\gamma), -\cos(\gamma), \sin(\gamma), -\cos(\gamma)]^T, \tag{2.6}$$

and zero for the generalized forces Q_θ and Q_ϕ. The contact condition on the stance foot gives the boundary conditions $u = 0$ and $v = 0$. This contact is only valid for compressive vertical contact force, $Q_v > 0$, and will be checked during the simulation. After solving the unknown accelerations of the generalized coordinates $\ddot{\mathbf{q}}$ from the reduced equations of motion (2.4) and then taking the limit yields

$$\lim_{\beta\to 0}\ddot{\mathbf{q}} = \left[\begin{array}{c}\ddot{\theta}\\ \ddot{\phi}\end{array}\right] = \left[\begin{array}{l}\sin(\theta-\gamma)\\ \sin(\phi)(\dot{\theta}^2 - \cos(\theta-\gamma)) + \sin(\theta-\gamma)\end{array}\right], \tag{2.7}$$

and for the unknown contact forces

$$\lim_{\beta\to 0}\left[\begin{array}{c}Q_u\\ Q_v\end{array}\right] = \left[\begin{array}{r}\sin(\theta)(\dot{\theta}^2 - \cos(\theta-\gamma))\\ -\cos(\theta)(\dot{\theta}^2 - \cos(\theta-\gamma))\end{array}\right]. \tag{2.8}$$

In the case of a more complicated walker, as for example in the 3D passive dynamic biped with yaw and roll compensation [88], it will be impractical to solve symbolically for the accelerations of generalized coordinates. A numerical evaluation of every individual contribution to the reduced equations of motion (2.4) and its solution is more practical. A limit case can be handled by a small order perturbation.

2.3.2 Heelstrike

We assume that the heel strike behaves as a fully inelastic impact (no slip, no bounce), which is in accordance with observations on existing passive dynamic walking prototypes. Also, double stance is assumed to occur instantaneously. As soon as the swing foot hits the floor the stance foot lifts up, not interacting with the ground during impact. The resulting vertical velocity of the lifting foot should then be pointed upward. If this is confirmed after the impact equations are solved, the assumption is verified. Otherwise, the walker would come to a complete stop. Treating heel strike as an impact, we assume that velocities change instantaneously. These velocity jumps are enforced by very high values of the contact forces acting only during a small time interval of contact. In the limit case the forces go to infinity and the time interval goes to zero. The integral of the force with respect to time over the duration of the impact, the impulse, has a finite value which is the cause of the velocity jump. While the impact takes place all positions as well as all non-impulsive forces of the system remain constant. The impact is usually divided into a compression and an expansion phase. Newton's impact law links these two phases by stating that the relative speed after impact equals e times the relative speed before impact but in opposite direction. The factor e is the coefficient of restitution. A value of $e = 1$ corresponds with a fully elastic impact whereas the value of $e = 0$ represents a completely inelastic impact in which the two parts "stick" together after impact. The reduced equations of motion (2.4) written in terms of the generalized coordinates $\mathbf{q}$ are

$$\bar{\mathbf{M}}\ddot{\mathbf{q}} = \bar{\mathbf{f}}, \tag{2.9}$$

with the reduced mass matrix and force vector

$$\bar{\mathbf{M}} = [\mathbf{F}_{,\mathbf{q}}^T \mathbf{M} \mathbf{F}_{,\mathbf{q}}], \quad \bar{\mathbf{f}} = \mathbf{F}_{,\mathbf{q}}^T [\mathbf{f} - \mathbf{M}\mathbf{F}_{,\mathbf{qq}}\dot{\mathbf{q}}\dot{\mathbf{q}}] + \mathbf{Q}. \tag{2.10}$$

Note that the 'lifting stance foot'-assumption implies that the system has no boundary conditions on the former stance foot and consequently there are more degrees of freedom during impact than during smooth motion. The uni-lateral constraints at heel strike are expressed by the contact functions $\mathbf{g}$, the coordinates of the swing foot expressed in terms of the generalized coordinates as

$$\mathbf{g}(\mathbf{q}) = \begin{bmatrix} g_x \\ g_y \end{bmatrix} = \begin{bmatrix} x_{swl} \\ y_{swl} \end{bmatrix} = \begin{bmatrix} u - \sin(\theta) + \sin(\theta - \phi) \\ v + \cos(\theta) - \cos(\theta - \phi) \end{bmatrix}. \tag{2.11}$$

When contact occurs, detected by a change of sign in the swing foot vertical clearance function g_y, the former swing foot becomes constrained in both the x and y direction and the equations of motion become

$$\bar{\mathbf{M}}\ddot{\mathbf{q}} + \mathbf{g}_{,\mathbf{q}}^T \boldsymbol{\lambda} = \bar{\mathbf{f}}, \tag{2.12}$$

with the Lagrangian multipliers $\boldsymbol{\lambda}$ dual to the relative contact velocities $\dot{\mathbf{g}}$. These multipliers can be interpreted as the contact forces. Integration of these equations of motion over the time of impact and taking the limit case yields

$$\lim_{t^- \uparrow t^+} \int_{t^-}^{t^+} (\bar{\mathbf{M}}\ddot{\mathbf{q}} + \mathbf{g}_{,\mathbf{q}}^T \boldsymbol{\lambda}) dt = 0. \tag{2.13}$$

The reduced force vector $\bar{\mathbf{f}}$ only contains non-impulsive forces and therefore the right-hand side vanishes. Under the introduction of the contact impulses,

$$\boldsymbol{\rho} = \lim_{t^- \uparrow t^+} \int_{t^-}^{t^+} \boldsymbol{\lambda} dt, \tag{2.14}$$

and noting that the mass matrix, in general a function of the generalized coordinates, remains constant during impact, the momentum equations for the system become

$$\bar{\mathbf{M}}\dot{\mathbf{q}}^+ + \mathbf{g}_{,\mathbf{q}}^T \boldsymbol{\rho} = \bar{\mathbf{M}}\dot{\mathbf{q}}^- \tag{2.15}$$

with $\dot{\mathbf{q}}^-$ the velocities before and $\dot{\mathbf{q}}^+$ the velocities of the system after impact. Together with Newton's impact law,

$$\dot{\mathbf{g}}^+ = -e\dot{\mathbf{g}}^-, \quad \text{or} \quad \mathbf{g}_{,\mathbf{q}}\dot{\mathbf{q}}^+ = -e\mathbf{g}_{,\mathbf{q}}\dot{\mathbf{q}}^-, \tag{2.16}$$

we have a complete set of linear equations reading

$$\begin{bmatrix} \bar{\mathbf{M}} & \mathbf{g}_{,\mathbf{q}}^T \\ \mathbf{g}_{,\mathbf{q}} & \mathbf{0} \end{bmatrix} \begin{bmatrix} \dot{\mathbf{q}}^+ \\ \boldsymbol{\rho} \end{bmatrix} = \begin{bmatrix} \bar{\mathbf{M}}\dot{\mathbf{q}}^- \\ -e\mathbf{g}_{,\mathbf{q}}\dot{\mathbf{q}}^- \end{bmatrix} \tag{2.17}$$

From these equations the velocities after impact $\dot{\mathbf{q}}^+$ together with the contact impulses $\boldsymbol{\rho}$ can be found. Because Newton's impact law (2.16) is often contradicted experimentally in case of multiple impacts, a restriction to simple impacts is made. The contact configuration for the walker is denoted by $u = 0$, $v = \text{constant}$, and $\phi = 2\theta$. The velocities of the stance foot before impact are zero. Solving the impact equations at the contact configuration and subsequently taking the limit case yields for the velocities after impact

$$\lim_{\beta \to 0} \dot{\mathbf{q}}^+ = \begin{bmatrix} \dot{u}^+ \\ \dot{v}^+ \\ \dot{\theta}^+ \\ \dot{\phi}^+ \end{bmatrix} = \begin{bmatrix} -\sin(\theta)\cos(2\theta)\sin(2\theta) \\ \cos(\theta)\cos(2\theta)\sin(2\theta) \\ \cos^2(2\theta) \\ \cos(2\theta)(\cos(2\theta)-1) \end{bmatrix} \dot{\theta}^-, \tag{2.18}$$

and for the contact impulses

$$\lim_{\beta \to 0} \boldsymbol{\rho} = \begin{bmatrix} \rho_x \\ \rho_y \end{bmatrix} = \begin{bmatrix} -\sin(\theta)\sin(2\theta) \\ \cos(\theta)\sin(2\theta) \end{bmatrix} \dot{\theta}^-. \tag{2.19}$$

The limit case, with the only moving mass in the hip, gives us some easy to verify results. First, the velocities after impact are only a function of the stance leg angle θ and its angular velocity $\dot{\theta}^-$. This velocity is in fact the hip velocity. Second, the contact impulse at the heel strike is directed along the swing leg with magnitude $\sin(2\theta)\dot{\theta}^-$, which is the projection of the hip velocity just before impact on the swing leg. And last, the stance foot velocity after impact is $\cos(2\theta)\sin(2\theta)\dot{\theta}^-$ in the direction of the stance leg, this is the hip velocity after impact projected on this leg.

2.3.3 Stride function

The mapping from the initial conditions $\mathbf{v} = (\mathbf{q}, \dot{\mathbf{q}})$, from one step to the next is the so-called 'stride function' [51], reading

$$\mathbf{v}_{n+1} = \mathbf{S}(\mathbf{v}_n). \tag{2.20}$$

If we start the walker with the initial conditions on the state as $(\theta, \phi, \dot{\theta}, \dot{\phi})_0$, then after the first heelstrike (2.18) two initial conditions drop out and the next state is only dependent on θ and $\dot{\theta}^-$. In this paper we look for a motion of the walker were the two legs pivot and swing, no full turns, and return to the same state after one heelstrike, the so called period-one gait cycle. For the analysis of the gait we have to swap the stance and swing leg variables from step n to step $n+1$ as

$$\begin{aligned} \theta_{n+1} &= \theta_n - \phi_n \\ \phi_{n+1} &= -\phi_n. \end{aligned} \tag{2.21}$$

At heelstrike, the swing leg angle ϕ^- is equal to $2\theta^-$, and combining the time derivatives of (2.21) with the velocities after impact (2.18), gives us the initial conditions after heelstrike as

$$\begin{aligned} \theta_{n+1} &= -\theta_n^- \\ \phi_{n+1} &= -2\theta_n^- \\ \dot{\theta}_{n+1} &= \cos(2\theta^-)\dot{\theta}_n^- \\ \dot{\phi}_{n+1} &= \cos(2\theta^-)(1-\cos(2\theta^-))\dot{\theta}_n^- . \end{aligned} \tag{2.22}$$

The stride function for the simplest walker is now; starting with $(\theta_n, \dot{\theta}_n)$ as the initial conditions at the beginning of the n^{th} step, numerically integrating the equations of motion (2.4) until heelstrike occurs, then calculating the velocities after heelstrike and finally swapping the legs (2.22), resulting in the initial conditions $(\theta_{n+1}, \dot{\theta}_{n+1})$ of the next step.

2.4 Step-to-step behavior

For a large range of initial conditions at step n, the stride function has no result; the model does not make a complete walking step so that there cannot be a subsequent step. Usually, the stride function has one or two cyclic solutions: initial conditions that map onto themselves. If a cyclic solution is stable, there exists a region surrounding it, which asymptotically leads to this solution. This region is called the basin of attraction. We will determine this basin of attraction by the cell mapping method.

2.4.1 Failure modes

We limited the searching area for practical reasons by exclusion of uninteresting and unfeasible initial conditions. First, as mentioned in Section 3.3, after the first heelstrike there are only two independent initial conditions, θ and $\dot{\theta}$. This reduces the Poincaré section to a 2D area. Second, only forward walking is investigated, so $\theta > 0$ and $\dot{\theta} < 0$. And last, from (2.22) it is clear that after heelstrike, $\dot{\theta}_{n+1}$ can only be negative (forward motion) if $\theta < \frac{\pi}{4}$ $[\mathrm{rad}]$. Within this area, the general behavior is classified in Figure 2.2. Exemplary motion of the walker is at a slope $\gamma = 0.004$ $[\mathrm{rad}]$. The area of possible initial conditions is roughly bisected by the line $\dot{\theta}_0 = -\theta_0 + \gamma$. Above this line, the input energy (initial velocity) is not enough to overcome the 'dead point' (compare this with an inverted pendulum), and the walker falls Backward. Below this line, the walker falls Forward. This occurs when the swing foot does not rise above floor level, after the short through-pass at midstance. In between these areas, a small region exists in which a walking step can occur. Some of these steps lead to failure (F or B) after a sequence of steps, while others will lead to perpetual walking, the small basin of Attraction. At large angles and high speeds, walking is not possible. In the model, a tensile vertical foot contact force occurs, $Q_v < 0$. Real walking mechanisms would lose foot contact and with both feet in the air we classify this as Running. Note that this is more or less equal to the commonly used boundary of Froude number $v^2/(gl) > 1$.

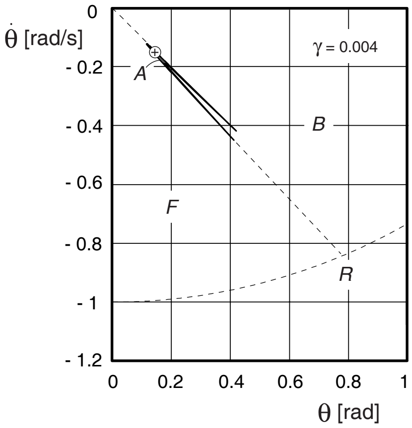

Figure 2.2: *Poincaré section for the simplest walker with initial stance leg angle* θ *and velocity* $\dot{\theta}$ *together with failure modes; falling Forward, falling Backward and Running, and the basin of Attraction of the cyclic walking motion* $(\theta, \dot{\theta}) = (0.1534, -0.1561)$ [rad] *at a slope of* $\gamma = 0.004$ [rad].

2.4.2 Cyclic motion

If the model is started inside the basin of attraction, it settles eventually into a repetitive motion, the attractor. The walker is in cyclic motion if the stride pattern repeats itself after a fixed number of strides. Looking at the Poincaré map of the state of the system at the beginning of each step we recognize this cyclic motion as a fixed point. The method for finding cyclic gait, as commonly used in passive dynamic walking research, is as follows. A walking cycle is specified by the requirement that the vector of initial conditions $\mathbf{v}_n$ results in identical initial conditions for the k^{th} subsequent step:

$$\mathbf{v}_{n+k} = \mathbf{v}_n \tag{2.23}$$

A vector with initial conditions satisfying this requirement is a cyclic solution $\mathbf{v}_c$, which maps onto itself:

$$\mathbf{S}^k(\mathbf{v}_c) = \mathbf{v}_c \tag{2.24}$$

The main interest is symmetric walking, or $k = 1$. Such cyclic solution can be found by a linearization of the stride function

$$\begin{array}{rcl} \mathbf{S}(\mathbf{v} + \Delta\mathbf{v}) & \approx & \mathbf{S}(\mathbf{v}) + \mathbf{J}\Delta\mathbf{v} \\ \text{with} \quad \mathbf{J} = & \frac{\partial \mathbf{S}}{\partial \mathbf{v}} & \end{array} \tag{2.25}$$

and applying a Newton-Raphson iteration procedure, starting with a set of initial conditions $\mathbf{v}$ close to the cyclic solution $\mathbf{v}_c$

```
repeat
    $\Delta\mathbf{v} = [\mathbf{I} - \mathbf{J}]^{-1}(\mathbf{S}(\mathbf{v}) - \mathbf{v})$
    $\mathbf{v} = \mathbf{v} + \Delta\mathbf{v}$
until $|\Delta\mathbf{v}| < \epsilon$
```
(2.26)

where $\mathbf{I}$ is the identity matrix. The Jacobian $\mathbf{J}$ is calculated by a perturbation method, which involves simulation of a full walking step for every initial condition. The eigenvalues of $\mathbf{J}$ quantify the stability of the cyclic motion. If both eigenvalues are inside the unit circle in the complex plane, a basin of attraction exists, with at least the size of the perturbation used to calculate the Jacobian. From Garcia, it is known that the simplest walking model has a stable cyclic walking motion for slopes up to 0.015 [rad], see Figure 2.3.

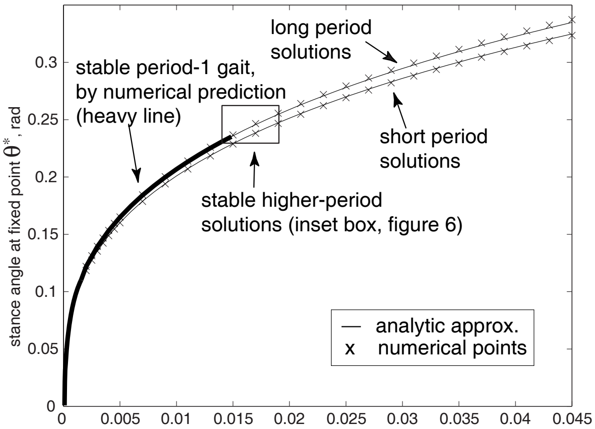

Figure 2.3: *Stance leg angle θ at fixed point versus slope angle γ. Reprinted with permission from Garcia et al. [25].*

2.4.3 Cell mapping method

The general behavior of the stride function can be studied with the aid of the cell mapping method [36]. The region of feasible initial conditions is subdivided into a large number (N) of small cells. All unfeasible initial conditions are regarded as a small number (z) of very large cells, so called *sink cells*. The cells are numbered 1 to N+z. By application of the stride function to the centre of each cell, all of the N+z cells point to initial conditions inside one of the other cells, except the sink cells which point to themselves by definition. Starting with cell 1, a sequence of cells appears by following the pointers. This sequence either ends in a sink cell or in a repetitive cycle. This cycle can consist of one self-repeating cell (a fixed point, which could be a sink cell), or a number of cells (comparable to multiple-period walking, Garcia [25]). The repetitive cycle is identified and all cells in the sequence are labeled as basin of attraction of that cycle. Then the procedure is repeated with all N cells. As soon as a known cell (from a previous sequence) is encountered, the procedure can be stopped, and all cells in that sequence are labeled as basin of attraction of that last cell.

Application of the cell mapping method results in a list with all attractors (cyclic solutions) and classification of all discretization points into this list. Not only period-one walking gaits can be found, also period-*k* walking gaits. Results of the cell mapping method are as accurate as the discretization, within these tolerances fixed points may come and go. For example, what appears to be a fixed cell might in fact be slowly changing initial conditions (smaller changes than the discretization) of subsequent steps.

2.5 Results

All initial conditions leading to perpetual walking are contained inside the basin of attraction, which for the simplest walker is roughly speaking a small, pointy boomerang. If started inside the basin of attraction, the initial conditions of a sequence of steps spiral toward the self-repeating cyclic solution. The size and shape of the basin of attraction diminish at increasing slope angle. Above a certain slope angle, the basin of attraction completely disappears and no stable cyclic solutions exist.

2.5.1 Basin of Attraction

From Figure 2.2 it is obvious that the basin of attraction is only a very small region. For better insight in the shape, Figure 2.2 is zoomed in and sheared, leading to Figure 2.4. The vertical axis now represents the sum of the stance leg angle and scaled angular velocity. The horizontal line at $\theta + \dot{\theta} = 0$ corresponds with the '-45 degree'-line in Figure 2.2. Figure 2.4 is obtained with application of the cell mapping method with a discretization of about 200×250 points ($\Delta\theta = 0.002$ [rad], $\Delta(\theta + \dot{\theta}) = 0.0002$ [rad]), the drawn lines are a manual continuous interpretation of the discrete boundary of the basin of attraction.

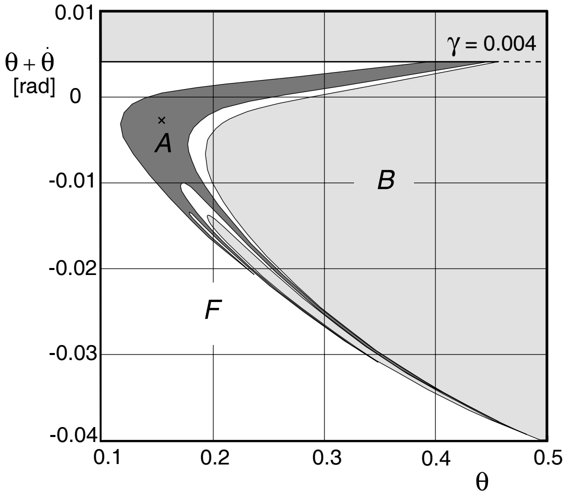

Figure 2.4: *Poincaré section for the simplest walker, enlarged and sheared section from Figure 2.2, together with failure modes; falling Forward, falling Backward, and the basin of Attraction of the cyclic walking motion.*

Figure 2.4 shows that the small basin of attraction is mostly bounded by falling backward on one side and falling forward on the other side. The basin of attraction seems to be a continuous and tailing area. The different areas show fractal-like entanglement. We will discuss the behavior of the walker in these areas by going over a vertical line, $\theta = 0.2$ [rad], in Figure 2.4 from area F to area B, crossing the basin of attraction at least four times. Point ($\theta = 0.2$ [rad], $\dot{\theta} = -0.23$ [rad]) lies in area F. If started with such initial conditions, the walking model will fall forward; the swing leg is allowed to pass through the floor to ignore the otherwise inevitable foot-scuffing, but does not rise above floor level anymore. Going up, the area changes from falling Forward to the basin of Attraction. Just before crossing this boundary, the behavior changes. Not the first step after these initial conditions is failing, but the model first walks some steps before eventually falling forward. The closer to the basin of attraction, the more steps it takes before failure. If started in the first tail of the basin of attraction, encountered when going up, the walker will eventually settle into steady cyclic walking with initial conditions of the fixed point. The path toward the fixed point is presented in Figure 2.5 and in Table 2.1. The motion of the legs is shown in Figure 2.6. After nine steps, the walker is close to the fixed point, and continuing the simulation will show asymptotic approach. Even more up on the line ($\theta = 0.2$), area F is encountered again. Starting there leads to falling forward after a number of steps. In this manner, A, B, and F are crossed several times, until we reach $\theta + \dot{\theta} = \gamma$. Above this boundary, the stance leg will not reach midstance and fall backward. In general, if started inside the basin of attraction, the initial conditions spiral toward the fixed point. If started just outside the basin of attraction, the walker will take a few steps but eventually fail. The further away, the smaller the amount of successful steps before failure.

step	θ [rad]	$\dot{\theta}$ [rad]	$\theta + \dot{\theta}$ [rad]
1	0.2000	-0.2165	-0.01645
2	0.1788	-0.1917	-0.01290
3	0.1756	-0.1841	-0.00850
4	0.1878	-0.1888	-0.00100
5	0.1586	-0.1599	-0.00134
6	0.1459	-0.1488	-0.00295
7	0.1492	-0.1526	-0.00337
8	0.1539	-0.1569	-0.00302
9	0.1558	-0.1583	-0.00256
⋮	⋮	⋮	⋮
f.p.	0.1534	-0.1561	-0.00269

Table 2.1: *Initial conditions of a number of subsequent steps, started just inside the basin of attraction and going to the fixed point.*

2.5.2 Basin of attraction versus slope angle

The size of the basin of attraction determines the amount of disturbance that the walker can handle without falling. The stability of the fixed point determines if,

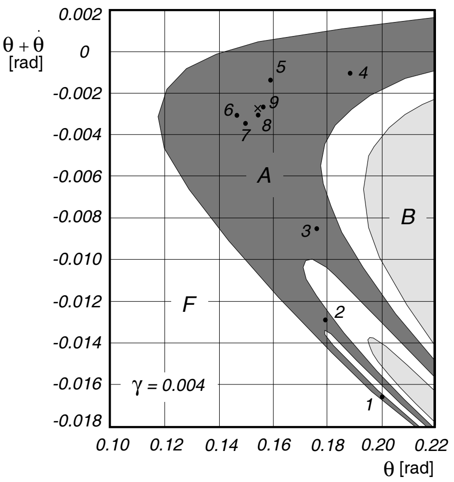

Figure 2.5: *A number of steps, started just inside the basin of attraction and going to the fixed point. Together with failure modes; falling Forward, falling Backward, and the basin of Attraction of the cyclic walking motion.*

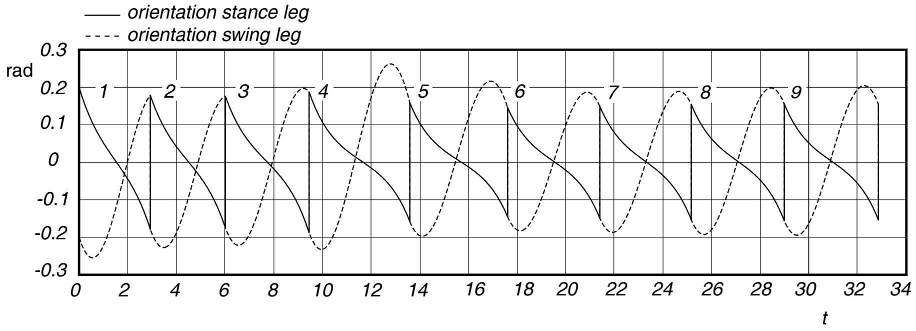

Figure 2.6: *Orientation of the stance leg, solid line, and swing leg, dotted line, with respect to the normal on the slope for a walker started just inside the basin of attraction and going to the fixed point.*

and how fast the walker recovers from a small disturbance. The latter analysis is less time-consuming and therefore very useful to determine the existence of a basin of attraction. The applicability of the walker however depends on the allowable size of disturbances. Therefore, we investigate the dependency of the basin of attraction on the only model parameter, the ramp slope γ. Figure 2.7 shows the development of the basin of attraction for an increasing ramp slope γ. As the slope increases, the basin of attraction decreases in size and gets more and more tails at the boundaries, which appear to be fractal-like. At and beyond a slope angle of 0.019 [rad] the basin of attraction has vanished, leaving fractal-like boundaries between the regions of falling forward and falling backward.

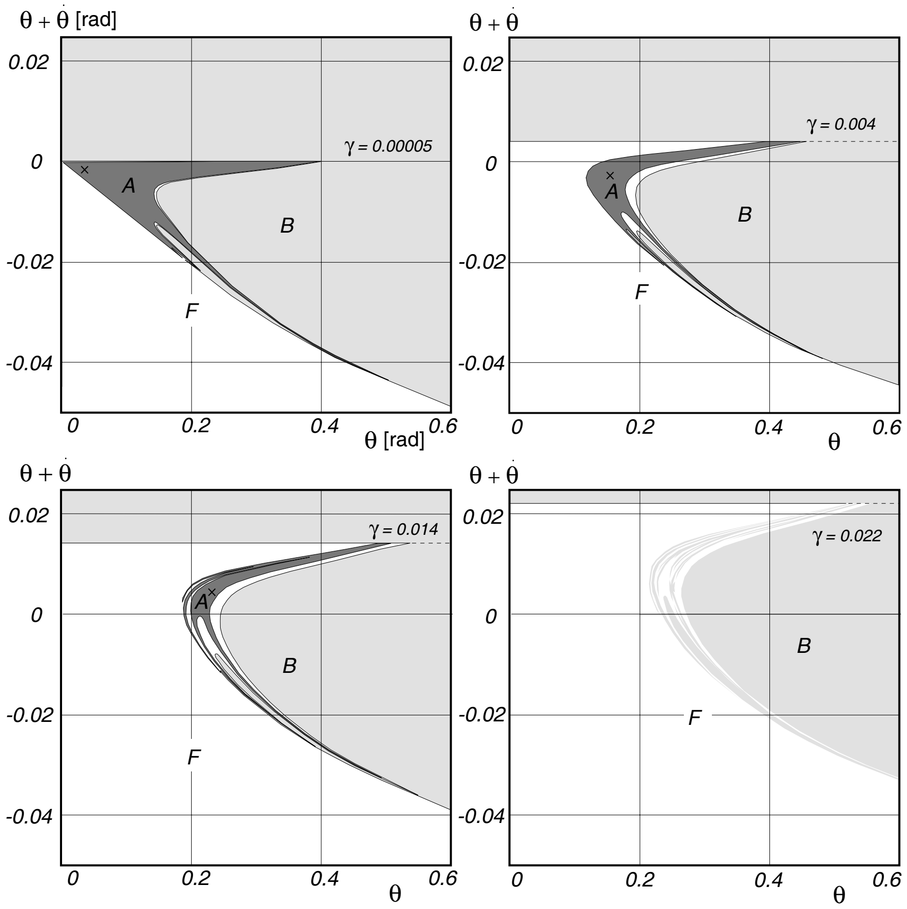

Figure 2.7: *Development of the basin of attraction with increasing floor slopes, together with failure modes; falling Forward, falling Backward, and the basin of Attraction of the cyclic walking motion.*

We compare the size of the basin of attraction with the stability of the cyclic motion, see Figure 2.8. The stability is measured as the largest of the two eigenvalues (modulus) of the linearized stride function (2.25). As stated by Garcia *et al.* [25], for $0 < \gamma < 0.0151$ [rad] the period-one gait is stable. For higher slopes, only higher-period gaits are stable, having a small basin of attraction. The eigenvalues would lead to believe that a slope $\gamma = 0.012$ [rad] would be preferable. However, the basin of attraction, measured as the number of cells inside the basin of attraction times the area of one cell, is not at its maximum. Clearly, there is no direct relation between the stability of the cyclic motion and its basin of attraction.

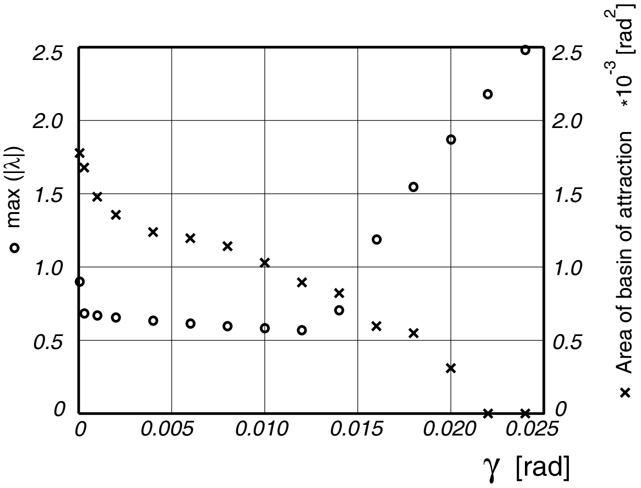

Figure 2.8: *The stability of the cyclic motion and the area of the basin of attraction versus slope angle* γ.

2.6 Conclusion

The basin of attraction of the simplest walking model is very small. This explains why physical models only walk successfully if started carefully on a very flat and rigid surface. The basin of attraction is surrounded by a region of initial conditions that lead to successful walking for a limited number of steps, eventually resulting in failure. The simplest walker has two failure modes; falling forward and falling backward. We expect to find qualitatively similar failure behavior in more complex walkers, although these would have more failure modes.

Our research shows that there is no obvious relation between the size of the basin of attraction and the stability of the fixed point. Therefore, the most robust design would probably not be the one with the best linearized stability, but the one with the largest basin of attraction. It is our intention to continue this research and find in which manner various passive and active measures on the walker can increase the basin of attraction.

Acknowledgements

This research is funded by the Dutch national technology foundation STW. We would like to thank Richard van der Linde for pointing out the necessity of this research, and Jaap Meijaard for his guidance toward the cell mapping method. Finally, a thanks to Andy Ruina for proofreading and Mariano Garcia for supplying Figures 2.1 and 2.3.

Chapter 3

How to keep from falling forward; Elementary swing leg action for passive dynamic walkers

M. Wisse, A. L. Schwab, R. Q. van der Linde and F. C. T. van der Helm
To appear in *IEEE Transactions on Robotics*, 2004.

Stability control for walking bipeds has been considered a complex task. Even in 2D, fore-aft stability in dynamic walking appears to be difficult to achieve. In this paper we prove the contrary, starting from the basic belief that in nature stability control must be the sum of a number of very simple rules. We study the global stability of the simplest walking model by determining the basin of attraction of the Poincaré map of this model. This shows that the walker, although stable, can only handle very small disturbances. It mostly falls, either forward or backward. We show that it is impossible for any form of swing leg control to solve backward falling. For the problem of forward falling, we devise a simple but very effective rule for swing leg action: "You will never fall forward if you put your swing leg fast enough in front of your stance leg. In order to prevent falling backward the next step, the swing leg shouldn't be too far in front." The effectiveness of this rule is demonstrated with our prototype 'Mike'.

3.1 Introduction

When designing a practical locomotion system, the engineer usually chooses wheels or tracks. On the one hand, legged locomotion seems complicated, even more so with only two legs, when static stability is out of the question. On the other hand, for some reason human beings have been equipped with two legs, and seem to have no difficulty with locomotion. Moreover, walking doesn't seem to require any attention, as one can concentrate on complicated thoughts while walking. Is bipedal walking then really as complicated as the engineer suspects?

No, it can quite simply be the natural mode of a purely mechanical system. Connect two rods by a hinge, and the system can walk down a shallow slope, the legs swinging in their natural frequency. Patents over 100 years old (e.g. [23]) already use this principle. In 1989, McGeer [49] performed rigorous numerical and practical experiments, showing that *passive dynamic walking*, as he termed it, even allows for knees. The key to passive dynamic walking is the repetitive nature of the walking motion, a limit cycle. If such a limit cycle is existent and stable, the walking motion is successful. McGeer, Garcia [27], Van der Linde [78], Goswami [29] among others researched the influence of different parameters on the stability of such walking cycles. It is now known that by applying round feet, a large hip mass compared to the leg mass, and not too steep a slope, a passive dynamic walker can be constructed that is stable enough for manual startup by an experienced person.

However, human beings can deal with much larger disturbances. On top of the passive locomotory system, humans are actively reacting to perturbations of the walking cycle. We presume that the human control scheme is of the same elegant simplicity as the passive dynamic walking motion. A basic assumption in our research is that the human walking motion is stabilized by a number of very simple, modular control rules. In this paper, we focus on one of those modules; swing leg control. We take the simplest walking model and ask the question: “Can we achieve global stability for the simplest walking model with a simple swing leg control rule?”. The answer is then validated with our prototype ‘Mike’, see Fig. 3.1.

3.2 Modeling and analysis

3.2.1 The simplest walking model

This research starts with the simplest mechanical model still possessing the ability to perform a bipedal walking motion, as conceived by Garcia *et al.* [27]. The model, shown in Fig. 3.2, consists of two rigid links with unit length, connected by a frictionless hinge at the hip. The mass is distributed over three point masses; one with unit mass M at the hip, and two with infinitesimally small mass m at the feet. This unactuated two-link system walks down a slope in a

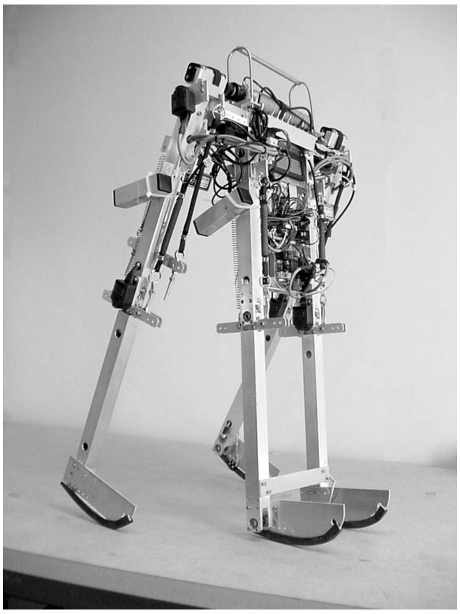

Figure 3.1: *Prototype 'Mike'; a 2D passive dynamic walking robot with pneumatic McKibben muscles at the hip.*

gravity force field with unit magnitude. The scaled model of the walker now only has one free parameter, the slope angle γ.

A walking step is started with both feet on the slope. The front foot has just made ground contact, the hind foot has a velocity away from the floor. During a step, the stance foot is modeled as a hinge, connected to the floor. The swing foot is moving freely as the other end of a double pendulum. At about midstance, the swing foot is briefly allowed to be below floor level ('foot-scuffing'), which is inevitable for a walker with straight legs. Knees ([50], [90], [7], [19]) or other leg shortening measures ([76]), as well as 3D motion ([43], [18] [79]) would solve the problem but increase complexity of the model. After this short through-pass, the second time that the swing foot reaches floor level is regarded as heel-strike, the end of the step. The swing foot makes a fully inelastic collision and becomes the new stance leg. Instantaneously, the former stance leg looses ground contact, and a new step begins.

3.2.2 Limit cycle analysis

According to common practice, the dynamic behavior of the simplest walking model is investigated with the following computer simulation procedure. The simulation of one step comprises smooth leg swing motion, an abrupt collision at heel strike, and the switching of leg function. A simple and efficient method for deriving the necessary equations of motion is given in [71]. Here we will only

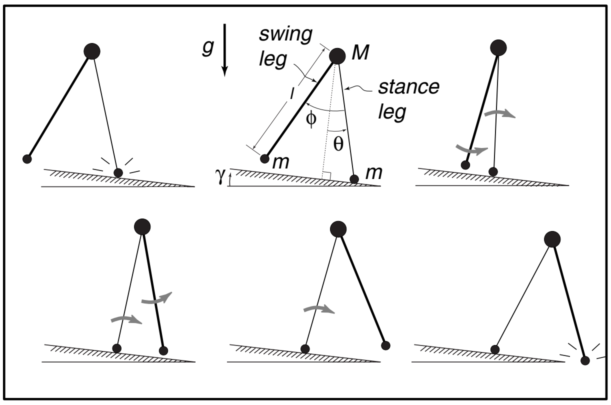

Figure 3.2: *A typical passive walking step. The new stance leg (lighter line) has just made contact with the ramp in the upper left picture. The swing leg (heavier line) swings until the next heelstrike (bottom right picture). The top-center picture gives a description of the variables and parameters that we use. θ is the angle of the stance leg with respect to the slope normal. ϕ is the angle between the stance leg and the swing leg, M is the hip mass, m is the foot mass, l is the leg length, γ is the ramp slope, and g is the acceleration due to gravity. Reprinted with permission from Garcia et al. [27].*

supply a brief overview of the simulation procedure for one walking step. Then, this procedure is applied to investigate how initial conditions change from one step to the next.

The model has two independent degrees of freedom, the absolute stance leg angle θ, and the relative swing leg angle ϕ. The equations of motion, as presented in [27] and [71], read:

$$\begin{bmatrix} \ddot{\theta} \\ \ddot{\phi} \end{bmatrix} = \begin{bmatrix} \sin(\theta-\gamma) \\ \sin(\phi)(\dot{\theta}^2 - \cos(\theta-\gamma)) + \sin(\theta-\gamma) \end{bmatrix} \tag{3.1}$$

The state of the system at the start of step n ($\phi_n = 2\theta_n$) is completely determined by $\theta_n, \dot{\theta}_n$, and $\dot{\phi}_n$. Shortly it will be clear that also $\dot{\phi}_n$ is a dependent initial condition, leaving only two independent initial conditions describing the start of a step. With these initial conditions, the equations of motion are numerically integrated until the end of step n (thus the start of step $n+1$) is detected (when again $\phi = 2\theta$).

At heel strike just before the start of step $n+1$, the collision of the former swing foot with the floor, simultaneous with the loss of ground contact of the former stance leg, leads to an instantaneous velocity change from the pre-collision state ($-$) to the post-collision state ($+$) calculated with:

$$\begin{bmatrix} \dot{\theta}^+_{n+1} \\ \dot{\phi}^+_{n+1} \end{bmatrix} = \begin{bmatrix} \cos(2\theta_{n+1}) \\ \cos(2\theta_{n+1})(1-\cos(2\theta_{n+1})) \end{bmatrix} \dot{\theta}^-_{n+1} \tag{3.2}$$

From the collision equation Eq. (3.2), it is obvious that the initial conditions of the next step are only a function of θ and $\dot{\theta}$. Therefore, in continuous walking there are only two independent initial conditions. This is a result of the peculiar mass distribution into three point masses. The final part of the simulation is switching the stance and swing leg, resulting in initial conditions for the next step. The simulation has now completed one walking step, and can be repeated with the new initial conditions.

The above simulation procedure is regarded as a step-to-step function **S**:

$$\begin{bmatrix} \theta_{n+1} \\ \dot{\theta}_{n+1} \end{bmatrix} = \mathbf{S}\left(\begin{bmatrix} \theta_n \\ \dot{\theta}_n \end{bmatrix}\right) \tag{3.3}$$

Monitoring the state of the system only once per cycle like this is known as Poincaré mapping, with the event of heel strike taken as the Poincaré Section. The walker is in a limit cycle if, logically, $[\theta_{n+1}, \dot{\theta}_{n+1}] = [\theta_n, \dot{\theta}_n]$. These initial conditions are then a fixed point on the Poincaré map. Fixed points can be found with a Newton-Raphson iteration procedure as described in [49], [27], [71] or [90]. For the simplest walker, we usually find zero or two fixed points, as elaborated in [27]. These fixed points represent an equilibrium of the gravitational energy input of the slope and the collisional energy loss at heel strike. The fixed points are the basis for stability research; if away from a fixed point, will the walker return there over a number of steps?

3.2.3 Linearized stability, local stability

Suppose we know the fixed point of the simplest walking model, and start the simulation with these initial conditions. By definition, every subsequent step will be equal. Starting away from the fixed point with small errors $\boldsymbol{\epsilon}_n$ on the initial conditions results in errors on the initial conditions of the next step as $\boldsymbol{\epsilon}_{n+1}$. For small errors, we assume linearity around the fixed point, such that:

$$\boldsymbol{\epsilon}_{n+1} = \mathbf{J}\boldsymbol{\epsilon}_n \qquad with \qquad \mathbf{J} = \frac{\partial \mathbf{S}}{\partial(\theta_n, \dot{\theta}_n)} \tag{3.4}$$

J is the Jacobian of the stride function **S** and is approximately determined by performing the simulation procedure once for both errors ϵ_n, one for each independent initial condition. The stability characteristics are described by the two eigenvalues λ_1 and λ_2 of the Jacobian **J**; if both are smaller then 1 in magnitude, errors decay over subsequent steps. The smaller the eigenvalues, the faster the walker converges toward the fixed point.

Garcia *et al.* [27] performed this linearized stability analysis on the simplest walker, showing that it has one stable fixed point for small slopes up to $\gamma = 0.015$ [rad], and none for steeper slopes, see Fig. 3.3. This concludes the recapitalization of results from literature. It is important to note that these results are only valid for small errors, therefore only describing the *local stability* around the fixed point.

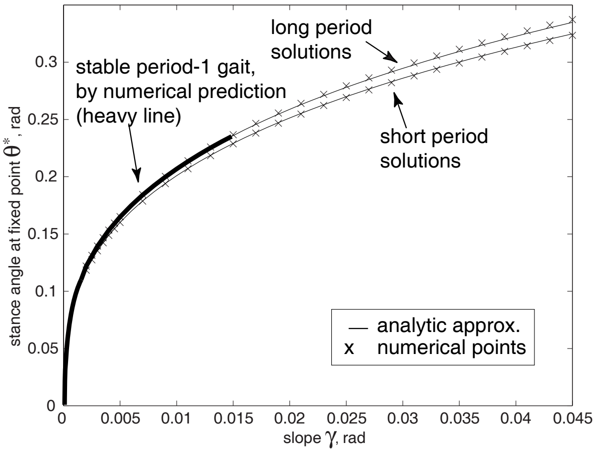

Figure 3.3: *Stance leg angle θ at fixed point versus slope angle γ. In this paper, all simulations are performed with a slope of $\gamma = 0.004$ [rad] leading to a fixed point with stance leg angle $\theta = 0.15$ [rad]. Reprinted with permission from Garcia et al. [25].*

3.2.4 Basin of attraction, global stability

For practical use, one wants to know when the walker keeps walking, and when it falls down. Clearly, the more initial conditions of $[\theta, \dot{\theta}]$ result in continuous walking, the more tolerant is the walker for incorrect launches and in-motion disturbances. The entire collection of initial conditions leading to walking is what is called the *basin of attraction*. We know that there must be some basin of attraction when the walker is linearly stable around the fixed point, but how large is it? Below, we will describe how to find the complete basin of attraction with the cell mapping method [36], and apply this method to the simplest walking model.

The region of feasible initial conditions is subdivided into a large number (N) of small cells. All unfeasible initial conditions (e.g. $\dot{\theta} > 0$) are regarded as a small number (z) of very large cells, so called *sink cells*. The cells are numbered 1 to N+z. By application of the step-to-step function **S** to the center of each cell, all of the N+z cells point to initial conditions inside one of the other cells, except the sink cells which point to themselves by definition. Starting with cell 1, a sequence of cells appears by following the pointers. This sequence either ends in a sink cell or in a repetitive cycle. This cycle can consist of one self-repeating cell (a fixed point), or a number of cells (multiple-period walking, Garcia [25]). The fixed point is identified and all cells in the sequence are labeled as basin of attraction of that fixed point. Then the procedure is repeated with cell 2, then cell 3, etcetera. As soon as a known cell (from a previous sequence) is encountered, the current sequence merges with that of the known cell. The procedure is repeated until all cells are labeled.

Application of the cell mapping method results in a list with all attractors

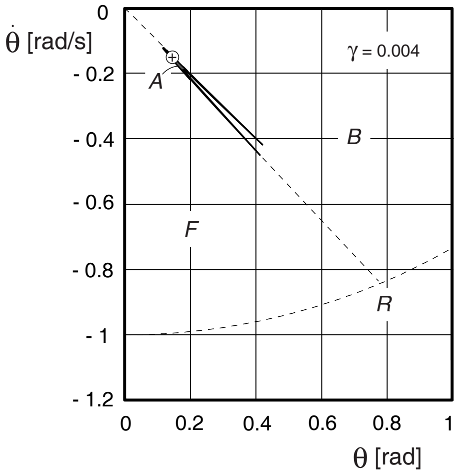

Figure 3.4: *Poincaré section for the simplest walker with initial stance leg angle θ and velocity $\dot{\theta}$ together with failure modes; falling F̲orward, falling B̲ackward and R̲unning, and the basin of A̲ttraction of the cyclic walking motion* $(\theta,\dot{\theta}) = (0.1534, -0.1561)$ [rad] *(indicated with '+') at a slope of* $\gamma = 0.004$ [rad]. *Reprinted from [71]*

(fixed points) and classification of all discretization points into this list. Not only period-one walking gaits can be found, also period-*k* walking gaits. Results of the cell mapping method are as accurate as the discretization, within these tolerances fixed points may come and go. For example, what appears to be a fixed cell might in fact be slowly changing initial conditions (smaller changes than the discretization) of subsequent steps.

With the cell mapping method, the basin of attraction of the simplest walker is calculated in [71], see Fig. 3.4. Although the shape and size of the basin of attraction slightly varies for different slope angles, for this article we have chosen to use a representative slope angle of $\gamma = 0.004$ [rad]. In Fig. 3.4 the basin of A̲ttraction is represented by the very thin area A, otherwise the walker falls F̲orward or B̲ackward, or, if started with high speeds, the stance foot loses compressive ground contact (R̲unning). This analysis describes the *global stability* of the walker. This is the more important stability measure for the robustness of the gait [79].

Note that the calculation of the basin of attraction is a costly business as the number of calculations increases with the power of the number of degrees of freedom. This is one of the reasons that we perform the simulation analysis on the simplest walking model instead of on the more complete model of 'Mike'.

3.3 Swing leg action for a larger basin of attraction

3.3.1 Largest possible basin of attraction

Now that the basin of attraction of the simplest walker is known, some questions arise. Is it a sufficiently large basin of attraction, or is control necessary? Can control of only the swing leg have any substantial positive effect on the basin of attraction? Before answering these questions, we should recognize that any conceivable hip action does not influence the current stance leg motion whatsoever with the assumption of massless legs. The only thing that matters is the hip angle at heel strike. In other words, swing leg control of the simplest walker can only influence the *subsequent* step.

Therefore, swing leg control cannot do anything for the walker if the current hip velocity is not enough to pass the apex of the hip trajectory. The mathematical equivalent of this requirement is the following energy inequality:

$$\frac{1}{2}M(\dot{\theta}l)^2 > Mgl(1-\cos\theta) \tag{3.5}$$

or, rewriting and scaling M, g, and l to unity:

$$|\dot{\theta}| > 2\sin\frac{\theta}{2} \tag{3.6}$$

This inequality is represented in Fig. 3.5 with Line (1). Note that this is the familiar separatrix in the normal simple pendulum phase portrait. Also note that Line (1) does not coincide with the dashed boundary between area B and area F in Fig. 3.4. The area between the two lines represents a set of initial conditions that, for the fully passive walker, does not lead to *immediate* falling backward, but to a short series of successful steps that *eventually* leads to falling backward [71].

The second boundary to the initial conditions for making a successful step is the requirement for compressive foot contact: at high velocities the centrifugal effect overcomes gravity and the stance foot would loose contact. This boundary is represented in Fig. 3.5 as Line (2). The scaled vertical contact force f_v is given in [71] as:

$$f_v = -\cos(\theta)(\dot{\theta}^2 - \cos(\theta-\gamma)) \tag{3.7}$$

Requiring that $f_v > 0$, we get the inequality for Line (2):

$$|\dot{\theta}| < \sqrt{\cos\theta} \tag{3.8}$$

Note that the fact that Line (2) passes through $\{\theta,\dot{\theta}\} = \{0,-1\}$ corresponds to saying that for this nondimensionalized walker the Froude number $\sqrt{v^2/(gl)}$ is equal to 1 (with body speed v equal to stance leg velocity $\dot{\theta}$ due to the unit leg length).

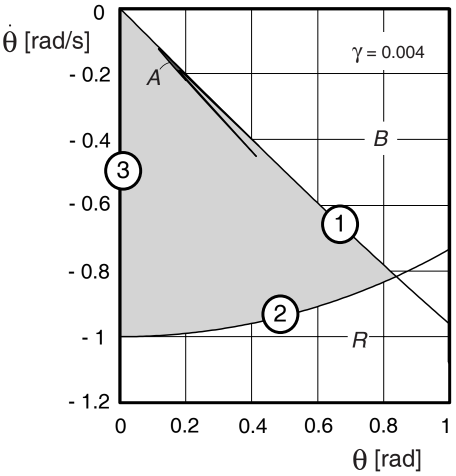

Figure 3.5: *Maximally obtainable basin of attraction (gray area, bounded by Lines 1, 2 and 3, see text) and uncontrolled basin of attraction (thin area A) of the simplest walking model. The entire problem of falling forward can be solved with swing leg control, while the problem of falling backward (area B) remains existent and would need something else than swing leg control.*

The third and last boundary of the maximally achievable basin of attraction is somewhat arbitrary; we only investigate initial conditions with a positive stance leg angle, i.e. starting with the stance foot in front of the swing foot, resulting in Line (3).

Lines (1), (2), and (3) are the outer boundaries for any basin of attraction that swing leg control could possibly achieve for the simplest walker. Therefore we choose to use the area inside these boundaries as a reference for the size of the basin of attraction. Comparing the area of the thin region A in Fig. 3.4 with the large gray area in Fig. 3.5, we find that without control, the basin of attraction is only 0.3% of the maximally achievable. This result justifies the search for a controller to enlarge the basin of attraction.

Summarized so far, we have said that the uncontrolled simplest walker very rarely walks. It mostly falls, either forward or backward. When adding swing leg control, we cannot address the problem of falling backward whatsoever. Therefore, for the swing leg controller we only have to consider the forward falling problem. This makes things easy; as long as we make sure that the swing leg swings forward fast enough, and then just keep it there, the problem should be solved. There is only one extra requirement; the swing leg should not be too far forward, otherwise the walker will fall *backward* at the subsequent step.

3.3.2 The rimless wheel

If for now we stick to the idealized situation of a massless swing leg, we could imagine the swing leg controller putting the swing leg at a preset, constant, forward angle immediately after the step has started. The behavior of the walker would then be exactly equal to the 'rimless spoked wheel', a system that has a number of 'legs' (the spokes) at equal, fixed angles apart (see the inset in Fig. 3.6). This system has been studied in depth by Coleman [16], who concluded that it would always reach a stable cyclic walking motion, provided that the leg angle is small enough for the floor slope angle. For the slope angle of 0.004 [rad] that we use throughout this paper, the inter-spoke angle should be smaller than 0.4 $[\mathrm{rad}]$ [15], otherwise it would slow down and eventually come to a stop and fall backward. We choose a safe value of 0.3 $[\mathrm{rad}]$, i.e. a stance leg angle $\theta = 0.15[\mathrm{rad}]$ at the start of a step, which corresponds to the natural gait of the simplest walking model at this slope (see Fig. 3.3). Fig. 3.6 shows the basin of attraction of the rimless wheel with this inter-spoke angle of $2 \cdot 0.15$ $[\mathrm{rad}]$.

The fixed inter-spoke angle makes it impossible to start the rimless wheel with a larger initial leg angle than 0.15 [rad], unless it were started at the top edge of a table. But even then, it would converge to its fixed point. Other than that, the only important gap in the basin of attraction is the small corner in the top, bounded by a line of constant energy through the point where Line (1) crosses $\theta = -0.15$ $[\mathrm{rad}]$. In that corner, the initial energy of the rimless wheel is enough to make it through the first step, but the fixed inter-spoke angle is too large to make it through the second.

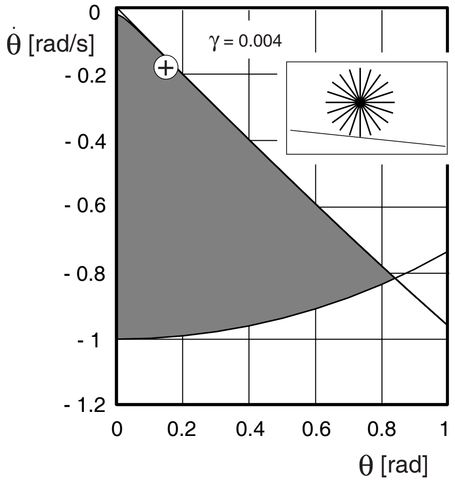

Figure 3.6: *Basin of attraction of the rimless wheel (model: see inset) with an inter-spoke angle of 0.3 [rad]. The initial conditions to the right of the dashed line can only be realized by starting at the top edge of a table. The '+' indicates the fixed point of this model at a slope of* $\gamma = 0.004$ *[rad].*

In conclusion, only considering swing leg control, the maximally obtainable basin of attraction can be achieved with a controller mimicking the rimless wheel.

3.3.3 A realistic actuation model

The previous section indicates that the stability behavior of the rimless wheel is very close to the maximum achievable with swing leg control. So, now it is time to devise a simple but realistic form of actuation that mimics the rimless wheel behavior, acknowledging that instantaneous leg positioning is impossible. We propose to use a spring and a damper at the hip joint with a variable setpoint which can provide for an extra internal torque T to the swing leg, extending the equations of motion to

$$\begin{bmatrix} \ddot{\theta} \\ \ddot{\phi} \end{bmatrix} = \begin{bmatrix} \sin(\theta-\gamma) \\ \sin(\phi)(\dot{\theta}^2 - \cos(\theta-\gamma)) + \sin(\theta-\gamma) + T \end{bmatrix} \tag{3.9}$$

with

$$T = -k(\phi - \phi_{sp}) - c\dot{\phi} \tag{3.10}$$

The setpoint ϕ_{sp} is set to 0.3 [rad] corresponding to the fixed point of the passive walker at a slope of $\gamma = 0.004$ [rad]. The stiffness k is the parameter that we vary, where $k = 0$ corresponds to the fully passive simplest walker and $k = \infty$ corresponds to the rimless wheel. The damping factor c is set as a function of k to provide critical damping:

$$c = 2\sqrt{k} \tag{3.11}$$

Note that a physical realization of this type of actuation requires an active shift of the setpoint after each heel strike from ϕ_{sp} to $-\phi_{sp}$ or vice versa.

Fig. 3.7 presents the stability results for different stiffness values. A higher stiffness results in a faster swing leg motion and thus provides a better resistance against falling forward. The drawback is in energy consumption, but unfortunately the model with its massless feet is too much a simplification of real walking machines to allow for quantitative statements on energy expenditure. With this active hip spring stiffness we can arbitrarily make the basin of attraction as large as necessary up to complete coverage of the maximally obtainable area, so the problem of falling forward can be considered to be solved. Moreover, this is achieved without any feedback control other than a setpoint shift at heel strike.

Remember that this is just one possible way of speeding up the swing leg. It is not this particular implementation that counts, but the main idea behind it that the swing leg should be swung forward quickly, and then kept there at a not-too-large leg angle. We should emphasize here that, although simulated with a floor slope $\gamma = 0.004$ [rad], this control rule works equally well for any slope larger than that. For smaller slopes, the preset leg angle should be decreased accordingly.

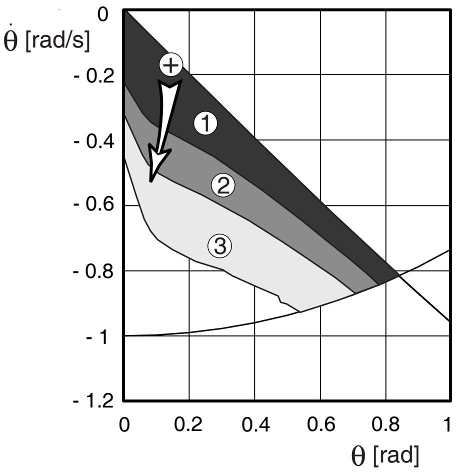

Figure 3.7: *Basin of attraction of the simplest walker with active hip spring. The setpoint of the hip spring is* $\phi_{sp} = 0.3$ *and critical damping is applied. The higher the hip spring stiffness, the larger the basin of attraction;* $k = 25$ *leads to area (1),* $k = 50$ *leads to area (2), and* $k = 100$ *leads to area (3). The fixed point is for all three stiffness settings approximately the same, located at the '+'. A disturbance from a step down in the floor would result in initial conditions away from the fixed point in the approximate direction of the white arrow.*

3.4 Prototype experiments

3.4.1 Mike

We applied the proposed swing leg control to our prototype 'Mike' (Fig. 3.1). An elaborate description of 'Mike' can be found in [94] while movie clips of 'Mike' in action are available at our web site [85]. 'Mike' has four legs symmetrically paired, giving it approximate 2D behavior. It differs from the simplest walking model by having knees, a distributed leg mass, round feet and by walking on a level floor (no slope!), all of which we will discuss in Section V.

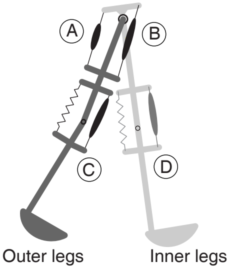

Figure 3.8: *Schematic structure and muscle attachments of 'Mike'.*

'Mike' is actuated with a total of eight McKibben muscles; lightweight pneumatic actuators that act like springs with a stiffness proportional to the internal pressure [14, 76]. The McKibben muscles are arranged according to Fig. 3.8. The hip joint is actuated with an antagonistic pair of muscles (A) and (B) providing a combined joint stiffness. The knees are actively extended with McKibben muscles (C) and (D) which are counteracted by weak passive springs. There is no ankle actuation; the arc feet are rigidly attached to the shanks.

3.4.2 Actuation system

The McKibben muscles are fueled from a 5.8 [MPa] CO_2 container via a two-stage pressure regulator and via electromagnetic valves that are activated by switches underneath the feet. The second-stage pressure regulator output is manually adjustable between 0.1 and 0.6 [MPa] resulting in a hip joint stiffness up to 5 [Nm/rad] and a damping somewhat less than critical damping (estimated by observation). It is not feasible to perform a proper mapping between this stiffness in 'Mike' and the scaled stiffness in the simplest walking model due to the extensive differences between the two, such as leg mass, foot arc radius, muscle non-linearities and significant air flow dynamics. Therefore the comparison between the two will be of qualitative nature only.

If a valve is switched 'on', the muscle is filled from the pressure regulator output; if switched 'off' it reliefs into atmosphere. For example, at activation of the inner leg foot switch, the outer knee muscles (muscle C in Fig. 3.8) are switched 'off' to allow this knee to bend. A manually tuned 400 [ms] later they are switched back 'on', ensuring a properly extended knee for the next step.

The proposed swing leg control in Eq. 3.10 is implemented by alternating the states of the antagonistic hip muscles. When the foot switch of the inner legs is activated, muscle B in Fig. 3.8 is switched 'on' and muscle A is switched 'off'. At the next step this is inverted. As a result, the hip joint has a constant stiffness but a setpoint that alternates between ϕ_{sp} and $-\phi_{sp}$. The joint stiffness can be adjusted without altering the setpoint. We want to emphasize that there is no feedback control other than this once-per-step switching between preset muscle pressures. We dub this 'feet-forward control'.

3.4.3 Stability results

'Mike' walks well. Fig. 3.9 shows a sample of the sustained gait for a hip muscle pressure of 0.55 [MPa], see [85] for video evidence. We would have liked to create a figure of its basin of attraction like Fig. 3.7. However, the combined limitations on the number of experiments to be performed and on the physical possibilities to create controlled disturbances have led us to concentrate on one representative disturbance, namely a step-down. In the experiments the prototype walks steadily and then takes a step down of increasing height, see Fig. 3.10. Such a step down results in a larger stance leg velocity at the subsequent step as sketched with the white arrow in Fig. 3.7. The larger the step down height,

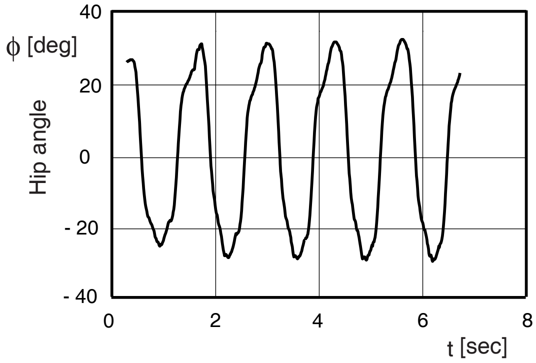

Figure 3.9: *Typical walking result with active hip muscles (0.55 [MPa]) on a level floor. The prototype completes 10 steps in this trial, showing convergence toward its fixed point after a manual launch.*

the larger the arrow. If a larger hip muscle stiffness indeed allows a bigger step down, then our swing leg control rule is validated.

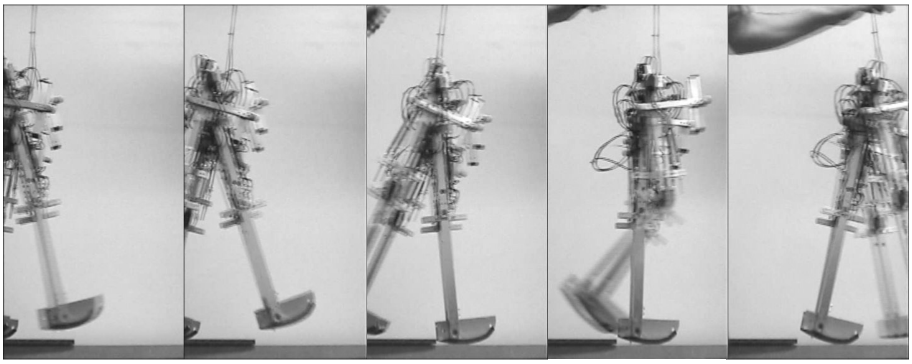

Figure 3.10: *Experiment with 'Mike' walking on level floor and taking a step down as a representative disturbance.*

The stability results are shown in Fig. 3.11. A hip muscle pressure lower than 0.35 [MPa] did not provide stable walking at all, not even without disturbances. When the pressure was increased, a larger step down could be handled. The muscles prohibit pressures higher than 0.55 [MPa]. Fig. 3.11 clearly shows a better robustness against falling forward with a higher hip pressure which corresponds to a higher joint stiffness.

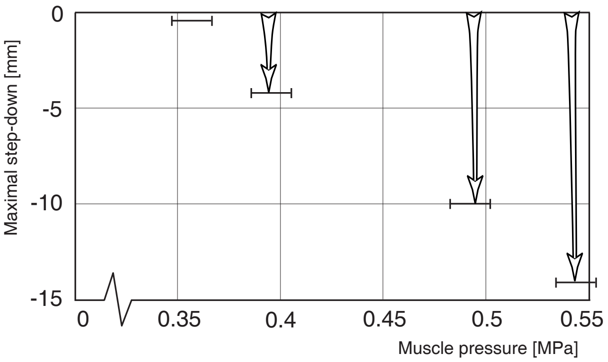

Figure 3.11: *A higher hip muscle pressure setting (corresponding to a higher hip joint stiffness) results in a larger step-down size and thus in a better resistance against disturbances. The arrows are depicted to indicate correspondence with the white arrow in Fig. 3.7.*

3.5 Discussion

3.5.1 Level floor

One of the differences between 'Mike' and the simplest walking model is that 'Mike's legs are not massless. When quickly moving the swing leg forward, it is not only rotated but its center of mass is lifted a little bit. For walkers with non-massless legs, this provides a way of putting energy into the system. For 'Mike' this is sufficient to replace the gravitational energy that the simplest walking model obtained from walking downhill. As a result, 'Mike' can walk on level terrain.

3.5.2 Distributed leg mass

Another difference between 'Mike' and the simplest walking model is that the swing leg has a non-zero moment of inertia. For the simplest walker, any conceivable hip actuation would not influence the stance leg motion. For 'Mike', it does. The actual influence depends on the exact mass distribution of the swing leg. If its center of mass were located at the hip joint, the swing leg acceleration would have the adverse effect of a *forward* stance leg acceleration. With a center of mass more in the middle of the leg, the swing leg acceleration induces a *backward* acceleration (i.e. a deceleration) of the stance leg, which buys the prototype some extra time to place its swing leg. A linearized dynamic analysis of a straight-legged mechanism at mid-stance shows that such advantageous deceleration occurs if

$$I < mc(l - c) \tag{3.12}$$

with the leg moment of inertia I, leg mass m, leg length l and the distance between the hip joint and the leg's center of mass c. From Eq. (3.12) we deduct that most normal constructions ($I \approx \frac{1}{12}ml^2$) result in a slight (advantageous) deceleration of the hip.

3.5.3 Feet

The simplest walking model has point feet, whereas 'Mike's feet have a circular shape. Such feet provide extra robustness against the complementary problem of falling *backward*. As depicted in Figs 3.4 and 3.5, the walker will fall backward if it has not enough velocity to overcome the vertical position. Circular feet smoothen the hip trajectory and thus relax the initial velocity requirement. As a result, the basin of attraction is enlarged in the upper right direction. We believe that round feet are a stability improvement measure complementary to the swing leg control rule proposed in this paper. However, a decisive study on the effect of circular feet on the basin of attraction has yet to be performed.

3.5.4 Knees and muscles

Other differences between 'Mike' and the simplest walking model are the knees and the nonlinear muscle properties. The knees do not essentially change the global behavior [50] as the swing leg starts and ends fully extended. One detail is that a violent knee extension at the end of the swing phase (e.g. as an automatic reaction to toe-stubbing) will decrease the hip angle. As at the end of the swing phase both the knee muscle and the corresponding hip muscle are activated, it seems advantageous to engage a bi-articular muscle at that instant.

The muscles do not behave in an exact linear fashion. Especially the damping and friction losses are strongly dependent on the muscle length, providing much more resistance when the muscle is close to its maximal extension. For 'Mike', this behavior is useful. The swing leg is brought forward without much resistance and is then effectively slowed down by the elongating hip muscle.

3.5.5 Human walking

We claim that any bipedal walking system can be kept from falling forward with a controller like Eq. (3.10). Whatever the exact controller algorithm may be, it should work if it results in speeding up the swing leg to a certain forward position. For that, an accelerating torque is needed at the beginning of the swing phase, and a decelerating torque toward the end. The same patterns are found when measuring human muscle activity during walking (e.g. Inman *et al.* [40], Winter [87]), although these measurements provide no evidence for keeping the swing leg in the forward position. Similarly, it was found that a purely passive model of the human leg would not swing forward as quickly as in reality, indicating that there must be an accelerating hip torque [72]. Kuo [44] suggests that humans might speed up their swing leg to improve walking energetics. We suggest that humans might benefit from the stability improvement that this brings. Probably both suggestions hold.

Another remark is that our proposed swing leg control rule is always active, even if no disturbance is present. A more efficient controller would monitor (or even predict) the size of the disturbances and adjust the applied torques correspondingly. It seems reasonable to compare this to a walking human being who will violently throw forward his swing leg as a reflexive reaction to tripping.

3.6 Conclusion

We started this research asking ourselves the question: “Can we achieve global stability for the simplest walking model with a simple swing leg control rule?” The answer is two-staged.

First, we showed that swing leg control can only address the problem of falling *forward*. If the simplest walker falls *backward*, there is no way that any swing leg control can change this; there is simply not enough energy in the system to move past the vertical position.

Second, we showed that a simple controller can completely solve the problem of falling forward; all it needs to do is to get the swing leg timely in a forward position. A damped hip spring with a forward setpoint already suffices. The specific control and actuation details are not important as the same result can be achieved with any configuration if it is based on the following rule: *“You will never fall forward if you put your swing leg fast enough in front of your stance leg. In order to prevent falling backward the next step, the swing leg shouldn’t be too far in front.”* A controller designed according to this rule is easy to implement, because no a-priori knowledge of the passive dynamic walking motion is needed.

We validated this rule with experiments with an autonomous, two-dimensional (four-legged) prototype with knees. The hip joint was actuated with McKibben muscles which provide a joint stiffness proportional to their internal CO_2 pressure. By using only one muscle of a pair of antagonistic muscles, the hip joint was given a stiffness and a forward setpoint each step. In this manner, the swing leg was accelerated forward according to our proposed control rule. The prototype was made to take a step-down during a steady walk, and the maximal step-down height was recorded as a function of the hip muscle pressure (hip joint stiffness). It was shown that a higher pressure indeed allows a higher step-down. The resultant robust gait can be viewed at [85].

Acknowledgements

This research is funded by the Dutch national technology foundation STW. The mechanical work on ‘Mike’ was done by Jan van Frankenhuyzen, its brain was a LART board provided by Jan-Derk Bakker and Erik Mouw. We would like to thank Jaap Meijaard for his guidance toward the cell mapping method, and

Thomas Platzer for an overview of the reflexes in human walking. Finally, a thanks to Andy Ruina for many helpful comments and Mariano Garcia for supplying Figures 3.2 and 3.3.

Chapter 4

Passive Dynamic Walking Model with Upper Body

M. Wisse, A.L. Schwab and F.C.T. van der Helm
To appear in *Robotica*, 2004.

This paper presents the simplest walking model with an upper body. The model is a passive dynamic walker, i.e. it walks down a slope without motor input or control. The upper body is confined to the midway angle of the two legs. With this kinematic constraint, the model has only two degrees of freedom. The model achieves surprisingly successful walking results: it can handle disturbances of 8% on the initial conditions and it has a specific resistance of only 0.0725(-).

4.1 Introduction

How much of the human walking motion can be modeled with passive dynamics? The more we can, the more likely we are to find simple designs for e.g. walking rehabilitation or entertainment robots. This question arose when Mochon and McMahon [53] discovered that the free swing motion of the human leg can be modeled quite convincingly (though not completely [72]) as a passive double pendulum.

In the late eighties, McGeer [49] showed that passive dynamic modeling is not only suitable for the swing leg motion, but for the stance leg motion as well. He built models and prototypes which he called 'passive dynamic walkers', that can walk down a shallow slope with no actuation and no control. Increasingly complex prototypes (e.g [19]) show that passive dynamic walking results in a particularly elegant and natural bipedal gait.

Passive dynamic walking provides two interesting features: inherent stability and low energy consumption. First, for certain parameter values, the passive models can resist small disturbances without the need for control. If human locomotion is based on passive walking, this could explain why keeping our balance seems so easy for us. Second, the energy consumption of passive walkers (gravitational energy from walking downhill) is much lower than that of conventional bipedal robots, it is actually even lower than that of human walking. All in all, passive dynamic walking is an attractive concept for models of human walking.

However, there is one major shortcoming. Up till now, none of the existing passive dynamic walking models has a fully passive upper body. These models either consist only of a pair of legs, or they have an upper body with active stabilization [51, 79]. In contrast, for applicable results for instance in the fields of entertainment or rehabilitation, the upper body is an essential part of the system. Recognizing this, many researchers work on advanced control paradigms for the hip joint, e.g. [13, 67, 54]. It would be advantageous, however, if the upper body could be stabilized in a completely passive manner. Before we endeavor building a prototype with such an upper body, we will demonstrate theoretically the feasibility with a computer model.

The research aim is to incorporate the upper body in the concept of Passive Dynamic Walking. The goal of this paper is to present a fully passive walking model with an upper body, and to investigate the effects of the parameters of the upper body on the walking characteristics such as stability and energy efficiency.

4.2 Passive walking model with upper body

The goal of this research is a passive walking model with an upper body. This model should be as simple as possible for the sake of a minimal set of parameters, so a natural starting point would be the 'simplest walking model' of Garcia *et al.* [27]. The simplest walking model consists of two rigid massless legs, with small pointmasses m_f as feet and a finite pointmass at the frictionless hip joint. For slopes up to 0.015 (rad), this model performs a stable walk downhill.

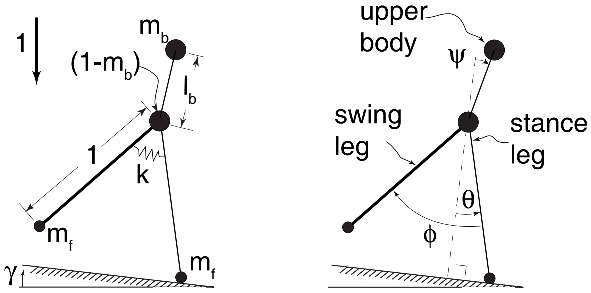

Figure 4.1: *Model of the simplest walker with upper body; parameters (left) and degrees of freedom (right).*

Their model deserves an accordingly simple upper body. A pointmass will do, connected to a rigid, massless stick that rotates around the hip joint (Fig. 4.1). The upper body is parameterized with body length l_b and body mass m_b. The default parameter values are somewhat arbitrarily chosen to have some relevance to human walking or to future prototypes (Table 4.1). We made the parameter values dimensionless for comparison with other models: all sizes are scaled with the leg length, so that the leg length is $1(-)$, and all masses are scaled with the sum of the pelvis mass and the upper body mass, so that the pelvis mass is $1-m_b(-)$. The foot mass is not included in this sum for reasons of compatibility with older models [71]. Time is scaled so that the resulting gravity is $1(-)$. Notice that, because of this scaling, parameters become unit-less, hence the '$(-)$'. There are also two non-human parameters: 1) slope angle γ, with which we can tune the walking speed, and 2) hip spring stiffness k, which allows tuning of the step frequency. The spring will turn out to be necessary for stable walking as will be described in Section IV(C). With the default parameter values according to Table 4.1, the model walks with human-like speed and step length, see Section IV(A).

As such, the model would have three degrees of freedom (Fig. 4.1): absolute stance leg angle θ (counter-clockwise), relative swing leg angle ϕ (clockwise), and absolute body angle ψ (clockwise). However, the upper body is then just an inverted pendulum jointed around the hip. Without any active control acting on it, one can expect that it will not be kept upright passively. To keep a fully passive upper body upright, A. Ruina (personal communication) suggests four possibilities:

1. Use a light upper body that has its actual center of mass *below* the hip. This

Table 4.1: *Default parameter values for the simplest walker with upper body, from a rough estimation of human proportions. The parameters are nondimensionalized by scaling: mass is divided by* $(pelvis\ mass + upper\ body\ mass)$, *length is divided by* $leg\ length$, *time is divided by* $\sqrt{leg\ length/gravity}$.

parameter	symbol	human approx.	scaled
Foot mass	m_f	7 (kg)	0.1 (-)
Upper body mass	m_b	49 (kg)	0.7 (-)
(Pelvis mass)	$(1 - m_b)$	21 (kg)	0.3 (-)
Leg length	-	1 (m)	1 (-)
Body length	l_b	0.4 (m)	0.4 (-)
Hip spring stiffness	k		0.4 (-)
Slope angle	γ		0.0725 (rad)

option is not very useful in realistic prototypes.

2. Use springs that keep the upper body upright [79]: This also has the utility that it should give more efficient walking by making the steps smaller at a given speed [44].
3. Use a compass mechanism: a kinematic coupling that keeps the body midway between the two legs (Fig. 4.2).
4. Keep the model as is, and hope that for some special mass distribution a stable gait emerges.

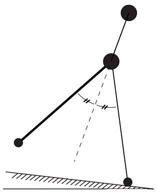

Figure 4.2: *Kinematic coupling of the upper body to the midway leg angle according to Eq. (4.1).*

Intuitively, option three is most promising because the number of degrees of freedom is reduced, which improves the chances of finding stable walking cycles. Human beings do not have such a kinematic coupling, but the assembly of pelvic muscles and reflexes could possibly perform a similar function. Also, such a construction can be found in certain reciprocating gait orthoses [39]. In robot prototypes such a kinematic coupling can be easily realized. In the model

Table 4.2: *Initial conditions that result in a cyclic walking pattern for the simplest walker with upper body, using the default parameter values (Table 4.1).*

θ_0	0.3821 (rad)
$(\phi_0 = 2\theta_0)$	(0.7642 (rad))
$\dot{\theta}_0$	-0.3535 (rad/-)
$\dot{\phi}_0$	0.0736 (rad/-)

it is introduced according to:

$$\psi = \phi/2 - \theta. \tag{4.1}$$

The other options could provide valuable results, although the first is not interesting as a model for human walking. We intend to investigate options two and four in the future, but in this paper we will focus on the behavior of the model with the compass-like kinematic constraint.

4.3 Results

4.3.1 Walking motion

The walking motion is analyzed with the help of the methods as described in the Appendix. With the default parameter values, the model takes something like a human walking step if started with the initial conditions from Table 4.2. However, due to its quintessential nature our model shares some typical non-human characteristics with Garcia's simplest walking model. First, the feet are no more than points, hence the application point of the ground contact force is at a fixed location during one step. Second, there are no actuators, so that the model will only walk if placed on a slope. Third, the legs cannot change length, hence there are not enough degrees of freedom to allow a double support phase.

The step starts and ends immediately after 'heel strike' (Fig. 4.3). The hip moves forward like an inverted pendulum with an almost constant speed, while at the same time the swing leg swings to a forward position. Naturally, the kinematic constraint keeps the upper body at the intermediate leg angle. The motion of the swing leg appears to be that of a free pendulum, while actually it is mainly the result of the dynamics of the upper body and the hip spring.

The trajectories of the various pointmasses are no surprise; the hip moves forward on a circular path (often referred to as 'compass gait' [40], while the swing foot remains close to the floor. The upper body follows a path almost identical to the hip trajectory at a distance l_b above the hip, only slightly smoother at the heel strike discontinuities. There are two peculiarities. First, the hip trajectory equals that of an inverted pendulum, but its speed does not. Due to the influence of the upper body and the hip spring, the speed of the hip is nearly constant, as can be deducted from the nearly constant stance leg velocity in Fig. 4.3. Second, the swing foot travels briefly below floor level. Inevitable for a 2D walker with straight legs, we allow this to happen in our simulation. Human beings and our more sophisticated models [90] and prototypes [94] have knees to solve this problem.

With a step length of $0.746(-)$ and a step time of $1.77(-)$ the model attains a (scaled) walking velocity of $0.42(-)$. Back on a human scale this corresponds to $1.3(m/s)$. The scaled velocity is the same as the familiar Froude number, $\sqrt{v^2/gl}$, where {Froude number = 1} represents the maximum walking speed for any biped. At higher speeds the foot contact force would become negative, so the biped should switch to running or maybe to Groucho walking. With a Froude number of $0.42(-)$ our model is well below that boundary, firmly stepping its way.

The energy consumption of the model at this speed is low. This is usually represented in the non-dimensional form of 'specific resistance': energy consumption per distance traveled per kilogram mass per gravity. For passive dynamic walkers the specific resistance is equal to the slope angle γ as gravity is the only means of energy input. So, our model has a specific resistance of $0.0725(-)$ at a (scaled) speed of $0.42(-)$. This is much more efficient than human beings walking at the same speed with a specific resistance of approximately $0.38(-)$ [65], although the comparison is somewhat unfair as muscle efficiency is unaccounted for. Also, this is much more efficient than the current generation of walking robots.

4.3.2 Inherent stability

To classify the stability of the walking motion there are two useful but essentially different definitions. First, we can regard stability in its most strict way. The basis is a walking motion in cyclic equilibrium, called a 'limit cycle'; a certain combination of initial conditions (Table 4.2) keeps repeating itself for all subsequent steps. If started slightly away from the limit cycle, the walking motion is stable if the subsequent step is closer to the limit cycle. Note that this 'local stability' requires the existence of a limit cycle, and that only small disturbances are investigated. By application of the method as described in Section F of the appendix we found that the model with the parameter values from Table 4.1 and started with the initial conditions from Table 4.2 is indeed stable for small disturbances.

Second, we can regard the stability of walking in the broadest and most intuitive form: 'The robot is stable if it does not fall'. We can even allow ourselves to use the formally incorrect term *'more stable'* for a robot that can handle larger disturbances. Note that this 'global stability' does not require the existence of a limit cycle (every step may be different, as long as the robot doesn't fall), but that it can only be investigated with the costly method of trying out all possible disturbances.

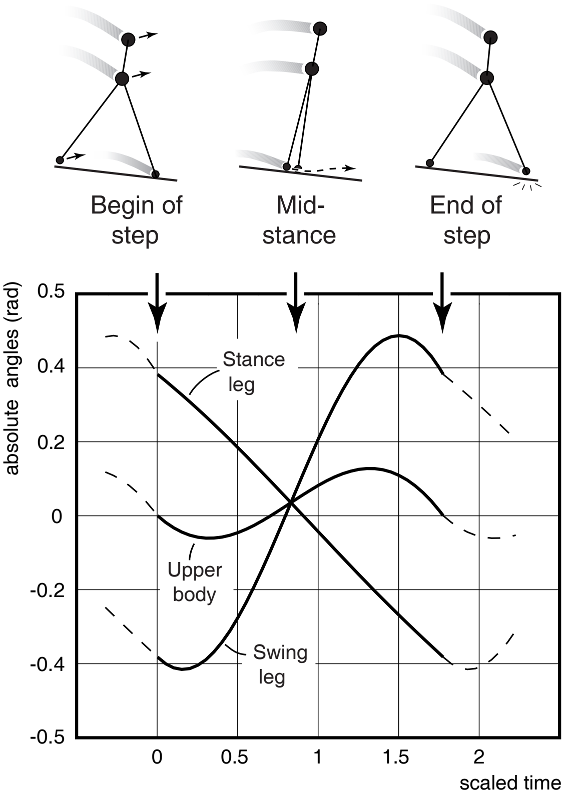

Figure 4.3: *Cyclic walking motion of the model with upper body. Top: stick figure representation, bottom: absolute angles of stance leg, swing leg, and upper body. The simulation is performed using the default parameter values (Table 4.1).*

By application of the cell mapping method as described in Section G of the Appendix, we found that the model performs surprisingly well. The model converges to its limit cycle if started with errors as large as 8% on all initial conditions of Table 4.2, compared to 2% for the simplest walking model [71]. For certain combinations of errors, the errors can even be much larger. This is inspected by evaluation of the *basin of attraction* (Fig. 4.4), the complete set of initial conditions that eventually lead to cyclic walking. For example, the figure shows that cyclic walking with cyclic initial conditions as in Table 4.2 emerges even if the initial step is twice as large, e.g. $\{\theta_0 = 0.75, \dot{\theta}_0 = -0.75, \dot{\phi}_0 = -1\}$.

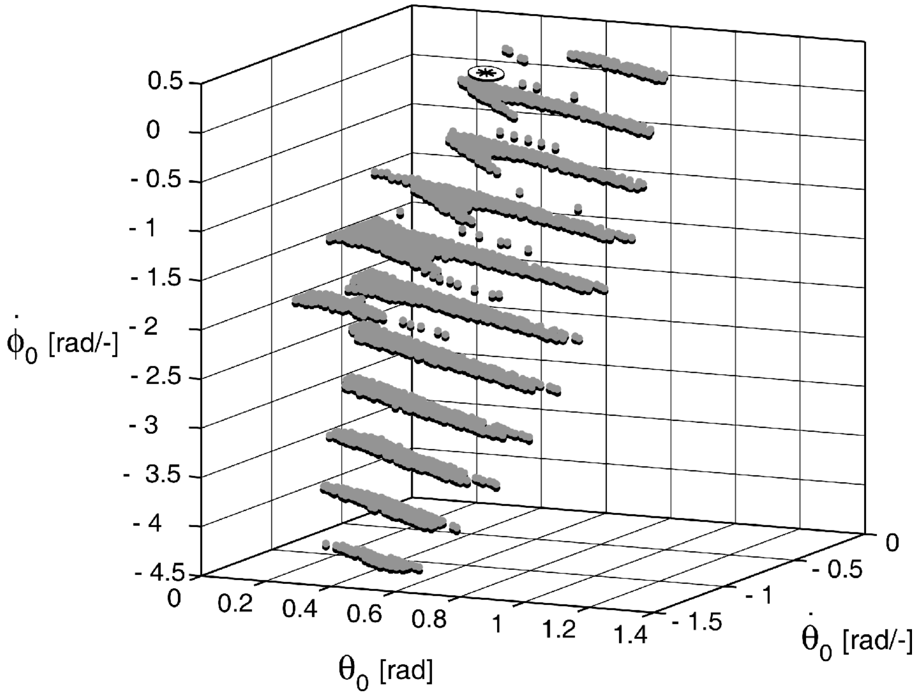

Figure 4.4: *Basin of attraction of the simplest walking model with upper body. The gray layers of points represent horizontal slices of a 3D region of initial conditions that eventually lead to the cyclic walking motion. The cyclic motion (*$\{\theta_0 = 0.3821, \dot{\theta}_0 = -0.3535, \dot{\phi}_0 = 0.0736\}$*, Table 4.2) is indicated with a flat asterisk, just above one of the sample slices.*

4.4 Parameter study

4.4.1 Slope and spring stiffness; speed and step length

As mentioned in Section II, the model has two parameters that are essential to the model's gait: the slope angle and the hip spring stiffness. Together, they determine the step frequency and the step length, thereby also determining the walking velocity.

First, for a fixed set of mass and length parameters, the step frequency is almost completely determined by the hip spring stiffness. It appears that the swing leg amplitude, step length, slope angle or walking speed all have a negligible influence on the step frequency [49, 27].

Then, the step length is directly determined by the slope angle; the steeper the slope, the larger the steps. This is a result of the balance between the gravitational energy input and the impulsive energy losses at heel strike. Although a larger step means more energy input, it leads to even more energy loss at heel strike. As a result, the system will automatically converge to a periodic walking motion with a step length that corresponds to the slope angle.

With the hip spring stiffness and the slope angle together, we were able to set both the speed and the step length to human values. It should be noted that these effects are not unique to our model. In fact, Kuo [44] studied these same effects extensively for the simplest walking model to investigate energy matters of human walking.

4.4.2 Upper body height and weight

The upper body is parameterized with body length l_b and body mass m_b. The body mass and the pointmass at the pelvis together always sum to 1 for the purpose of scaling, while the body length is scaled to the length of the leg. The default parameters of Table 4.1 are chosen so that the model has some relevance to future prototypes. This section investigates the model behavior when the upper body is reduced to nothing or significantly enlarged.

Reduction of the upper body size or mass to zero leads to a model like the simplest walker, except that the simplest walker has no hip spring and an infinitesimally small foot mass. For a very small foot mass, no hip spring is necessary, but for a realistic foot mass as in Table 4.1, stable walking cycles only exist if a spring is applied. As stated earlier, the hip spring and slope angle together determine the walking speed and the step length. If we set them so that speed and step length match the original model (Table 4.1), we find that the 'zero-body-model' needs a slope angle of $\gamma = 0.147$ (rad). In other words, the model with upper body is twice as efficient as the same model without upper body! Apart from that, there is not much difference between the gaits of the two models.

Similarly, an increase in the mass or the size of the upper body will provide an even higher walking efficiency. We found that an increase in m_b has a similar effect as an increase in l_b. As an example, we crudely modeled a person carrying a heavy load on the top of the head by setting $m_b = 0.9(-)$ and $l_b = 1(-)$. The hip spring stiffness and slope angle were again adjusted to obtain human walking speed and step length. The required slope angle is now only $\gamma = 0.0249$ (rad); this model walks about three times more efficient than with the default parameter values! In general it is clear that the presence of an upper body has a positive influence on the walking efficiency.

The changes of the mass or size of the upper body have little effect on the stability. We investigated the three previously mentioned situations: a) zero upper body mass, b) default parameters (Table 4.1), and c) someone carrying a heavy load on the head ($l_b = 1, m_b = 0.9$). In terms of linearized stability, all three situations are stable for small disturbances. In terms of global stability, the allowable errors on all initial conditions are about 8% for all three situations. However, the resultant basins of attraction (as in Fig. 4.4) have different shapes, so that convergence from larger errors occurs for different combinations of errors. It seems odd that the size or mass of the upper body has no apparent influence on the allowable errors (all 8%), whereas there is such a large difference with the simplest walking model (only 2%). We believe that this is a result of the increased speed and step frequency; the simplest walking model walks slower than our model, which we tuned to walk with human speed. We intend to investigate this effect in the near future.

4.4.3 Limits to stability

Our upper-body walker has a remarkably stable gait if provided with the parameter values from Table 4.1. For certain other parameter values, however, the model has unstable gaits or even no cyclic walking motions at all. Usually this can be solved by sufficiently increasing the hip spring stiffness k, with a few exceptions. At slopes steeper than $\gamma \approx 0.35\ (rad)$ the equilibrium speed is so high that the stance foot would loose ground contact and the model should start running. The foot mass m_f and the body size and mass l_b and m_b can be chose arbitrarily small or large; with a high enough value for k the model still walks fine, although this could result in correspondingly small or large step lengths, which in turn could lead to the loss of floor contact.

Inside these boundaries, for each combination of parameter values there exists a minimal value for k that ensures stability. For the model with the default parameter values of Table 4.1, we studied the effect of variations in k on the cyclic walking motion. For $k > 0.218$ we found steady, stable cyclic walking as described in Section III(A). However, for the same value of k there also exists a second, unstable gait. The steps are shorter and faster, and the motion looks like the model is stumbling forward. McGeer and Garcia discovered this second solution for their models and refer to it as the 'short-period gait', as opposed to the normal, stable solution which is termed 'long-period gait'. We are only interested in the last type of gait, the behavior of which we have studied as a function of the parameter value for k.

Above the boundary value, an increase in k results in faster and smaller steps as discussed in section IV(A). If we decrease k below 0.218, we cross a bifurcation to asymmetric gaits, first encountering two-period solutions and for lower k even higher-period solutions. These solutions are still stable. Below $k = 0.162$, we found only unstable gaits or even no cyclic solutions at all. Garcia found a similar bifurcation to chaos for the simplest walking model when increasing the slope above $\gamma = 0.015(rad)$.

We tracked the first bifurcation point over a range of parameter values because that point represents the minimally required value for k to obtain normal, stable walking. The relation between the minimal value for k and the other parameters is not linear, and there is not an obvious and simple non-linear relationship. Qualitatively, the required hip spring stiffness k needs to be increased if l_b, m_b, m_f or γ are increased.

4.5 Conclusion

This paper presented the simplest walking model with a passive upper body. The solution for a fully passive upper body is to confine the upper body angle to the intermediate leg angle with a kinematic coupling. With this kinematic constraint, the model has only two degrees of freedom, similar to the Simplest Walking Model.

The presence of such an upper body results in a better energy efficiency and in a slightly better robustness against disturbances. A spring in the hip joint is essential for stability. An increase in the hip spring stiffness results in a higher step frequency, whereas the slope angle of the floor determines the step length.

These results are convincing enough to commence the construction of a prototype walking robot with a similar upper body construction.

Acknowledgements

This research is funded by the Dutch national technology foundation STW. Thanks to Richard van der Linde, Jan van Frankenhuyzen, Steve Collins and Dick Plettenburg for many helpful comments.

Appendix: Simulation methods and procedures

This appendix describes the methods used to simulate the motion of the simplest walker with upper body. In order of appearance after the start of a new walking step, a simulation contains the following aspects: A) equations of motion, B) numerical integration, C) end-of-step (heel strike) detection, and D) heelstrike impact equations. Then the biped starts a new step. For continuous walking, we must study the step-to-step behavior to E) find periodic solutions and F) determine the linearized stability, and finally G) investigate the basin of attraction of these periodic solutions. This section focuses on the current model; the applied simulation method is elaborated in detail in [71] and [90].

Equations of motion

The configuration of the walker is defined by the coordinates of the four pointmasses (stance foot, hip, swing foot, and upper body), which can be arranged in a global vector $\mathbf{x} = (x_{st}, y_{st}, x_h, y_h, x_{sw}, y_{sw}, x_b, y_b)^T$. In order to obtain a minimal set of equations, the eight coordinates of $\mathbf{x}$ are expressed as functions of the independent coordinates θ and ϕ. To allow inspection of the ground reaction forces, we introduce two more independent coordinates (u and v), representing respectively the x- and y-coordinates (orthogonal to the walking slope) of the stance foot, which will obviously be fixed during the walking motion. The expression of $\mathbf{x}$ as a function of the vector of independent coordinates $\mathbf{q} =$

$(u, v, \theta, \phi)^T$ reads:

$$\mathbf{x} = \mathbf{x}(\mathbf{q}) \rightarrow \begin{bmatrix} x_{st} \\ y_{st} \\ x_h \\ y_h \\ x_{sw} \\ y_{sw} \\ x_b \\ y_b \end{bmatrix} = \begin{bmatrix} u \\ v \\ u - \sin(\theta) \\ v + \cos(\theta) \\ u - \sin(\theta) + \sin(\theta - \phi) \\ v + \cos(\theta) - \cos(\theta - \phi) \\ u - \sin(\theta) - l_b \sin(\theta - \phi/2) \\ v + \cos(\theta) + l_b cos(\theta - \phi/2) \end{bmatrix}. \tag{4.2}$$

Notice the use of the term $(\theta - \phi/2)$ from Eq. (4.1). For the walker the global coordinate related mass matrix is

$$\mathbf{M} = \text{Diag}(m_f, m_f, 1 - m_b, 1 - m_b, m_f, m_f, m_b, m_b), \tag{4.3}$$

The reduced mass matrix M_r is created via

$$\mathbf{M}_r = \mathbf{T}^T \mathbf{M} \mathbf{T}, \tag{4.4}$$

with the Jacobian $T = \frac{\partial \mathbf{x}}{\partial \mathbf{q}}$ from Eq. (4.2), which can be automatically generated with a symbolic math package.

The gravity forces, contact forces and the spring torque are compiled into a reduced force vector $\mathbf{f}_r$ via

$$\mathbf{f}_r = \mathbf{T}^T [\mathbf{f}_g - \mathbf{M} \mathbf{T}_2] + \mathbf{Q}, \tag{4.5}$$

with the convective accelerations $\mathbf{T}_2 = \frac{\partial (\mathbf{T} \dot{q})}{\partial \mathbf{q}} \cdot \dot{\mathbf{q}}$, again obtained automatically. The vector of gravity forces reads

$$\mathbf{f}_g = \mathbf{M} \begin{bmatrix} \sin(\gamma) \\ -\cos(\gamma) \\ \sin(\gamma) \\ -\cos(\gamma) \\ \sin(\gamma) \\ -\cos(\gamma) \\ \sin(\gamma) \\ -\cos(\gamma) \end{bmatrix}, \tag{4.6}$$

and the spring torque and unknown contact forces are represented in the vector with generalized forces $\mathbf{Q}$:

$$\mathbf{Q} = \begin{bmatrix} Q_u \\ Q_v \\ 0 \\ -k\phi \end{bmatrix}. \tag{4.7}$$

This amounts to the reduced equations of motion:

$$\mathbf{M}_r \ddot{\mathbf{q}} = \mathbf{f}_r. \tag{4.8}$$

The contact condition on the stance foot gives the boundary conditions $u = constant$ and $v = 0$. This contact is only valid for compressive vertical contact force, $Q_v > 0$, and will be checked during the simulation. The resulting set of linear equations can be solved for $Q_u, Q_v, \ddot{\theta}$ and $\ddot{\phi}$ by numerical evaluation and subsequent solution.

Numerical integration

The second order differential equations of motion are numerically integrated using the Runge-Kutta method. It must be taken into account that only two of the generalized coordinates are independent (θ and ϕ), the other two are fixed by the boundary condition of keeping the stance foot at the floor, and should therefore not be incorporated in the numerical integration.

Away from round-off errors, the integration accuracy is estimated according to:

$$q^* - q_{\Delta t} \approx \frac{1}{2^n - 1}(q_{\Delta t} - q_{2\Delta t}), \tag{4.9}$$

where q^* is the real state after one walking step, $q_{\Delta t}$ is the numerically calculated state, $q_{2\Delta t}$ is the same calculation with twice the integration step size, and $n = 4$ is the order of the integration scheme. Simulation results show that for an integration step size of $\Delta t = 0.05$ the absolute error in the state variables $\{\theta, \phi, \dot{\theta}, \dot{\phi}\}$ after one walking step is smaller than $1 \cdot 10^{-7}$.

End-of-step detection

The end of a walking step is defined as the instant that the swing foot makes contact with the floor. This is detected during the simulation by monitoring the swing foot clearance (g)

$$g = v + \cos(\theta) - \cos(\theta - \phi), \tag{4.10}$$

which is the sixth element of $\mathbf{x}$ in Eq. 4.2.

However, our model has two straight legs of equal length, and no leg retraction mechanisms. In fact, the model is too simple for the real world. When the swing leg passes the stance leg, the swing foot would inevitably 'scuff' the floor. We have to ignore this instance of foot contact, and continue simulation as if the floor were not there, until the 'real' heel strike occurs. This is detected if all of the following statements are true:

1. g has crossed zero,
2. $\dot{g}$ is negative,
3. the stance leg has passed the vertical position, and
4. the absolute angles of the swing and stance leg have opposite signs.

Now that we know that heel strike must have occurred between the last and the previous integration step (between t_n and t_{n-1}), we must pinpoint the exact instant of contact. This is solved by fitting a third order polynomial through the foot clearance function g, for which we need its derivative which can be automatically generated from the state variables. The polynomial is zero at the time of contact t_c, which we express as the fraction

$$\xi = \frac{t_c - t_{n-1}}{t_n - t_{n-1}}. \tag{4.11}$$

A fast and accurate approach to calculate $\mathbf{q}(t_c)$, as proposed by Meijaard [52], is interpolating $\mathbf{q}$ between t_{n-1} and t_n with a third-order interpolation polynomial, since we know both $\mathbf{q}$ and $\dot{\mathbf{q}}$ at these instants:

$$\mathbf{q}(t_c) = \begin{bmatrix} (1 - 3\xi^2 + 2\xi^3) \\ (\xi - 2\xi^2 + \xi^3)\delta t \\ (3\xi^2 - 2\xi^3) \\ (-\xi^2 + \xi^3)\delta t \end{bmatrix}^T \begin{bmatrix} \mathbf{q}(t_{n-1}) \\ \dot{\mathbf{q}}(t_{n-1}) \\ \mathbf{q}(t_n) \\ \dot{\mathbf{q}}(t_n) \end{bmatrix}. \tag{4.12}$$

The results of this method have the same accuracy as the numerical integration procedure in Section B. The interpolation method is efficient because we avoid solving the equations of motion all together.

Impact equations

We assume that the heel strike behaves as a fully inelastic impact (no slip, no bounce). Also, double stance is assumed to occur instantaneously, which is in accordance with observations on existing passive dynamic walking prototypes. As soon as the swing foot hits the floor the stance foot lifts up, not interacting with the ground during impact. The resulting vertical velocity of the lifting foot should then be pointed upward, which is checked during the simulation. If it points downward, the assumption was incorrect and there actually was interaction between the former stance foot and the floor. Without calculation one can see that in that case the walker comes to a complete stop.

The instantaneous velocity changes during impact can be calculated using the original reduced Equations of motion (4.8). As described in [71], the impact equations read

$$\begin{bmatrix} \mathbf{M}_r & \mathbf{D}^T \\ \mathbf{D} & \mathbf{0} \end{bmatrix} \begin{bmatrix} \dot{\mathbf{q}}^+ \\ \boldsymbol{\rho} \end{bmatrix} = \begin{bmatrix} \mathbf{M}_r\dot{\mathbf{q}}^- \\ -e\mathbf{D}\dot{\mathbf{q}}^- \end{bmatrix}, \tag{4.13}$$

with Newtons coefficient of restitution $e = 0$ and the swing foot contact impulses $\boldsymbol{\rho}$. $\mathbf{D}$ represents the partial derivatives of the impact constraints with respect to $\mathbf{q}$. Since there is no interaction between the old stance foot and the floor during impact, the easiest way to derive the impact equations is by first swapping stance and swing leg coordinates. This must be done anyway before simulating the next step, and by doing this swap immediately before heel strike, the impact constraints become simply $u = constant$ and $v = 0$, resulting in

$$\mathbf{D} = \left[\begin{array}{cccc} 1 & 0 & 0 & 0 \\ 0 & 1 & 0 & 0 \end{array} \right]. \tag{4.14}$$

The impact affects only $\dot{\mathbf{q}}$ and leaves $\mathbf{q}$ constant. With the new velocities and the swapped stance and swing leg, the walker is ready for the next walking step.

Limit cycle analysis

With the above procedure (numerically integrating equations of motion, impact-detection and calculation and stance-swing leg swapping) the initial conditions $\mathbf{v} = (\dot{\mathbf{q}}, \mathbf{q})$ can be mapped from one step onto the next by a step-to-step function $\mathbf{S}$ [51]:

$$\mathbf{v}_{n+1} = \mathbf{S}(\mathbf{v}_n). \tag{4.15}$$

A walking cycle is specified by the requirement that the vector of initial conditions $\mathbf{v}_n$ results in identical initial conditions for the subsequent step:

$$\mathbf{v}_{n+1} = \mathbf{v}_n. \tag{4.16}$$

A vector with initial conditions satisfying this requirement is a cyclic solution $\mathbf{v}_c$, which maps onto itself:

$$\mathbf{S}(\mathbf{v}_c) = \mathbf{v}_c. \tag{4.17}$$

A cyclic solution can be found by a linearization of the step-to-step function

$$\begin{array}{rcl} \mathbf{S}(\mathbf{v} + \Delta\mathbf{v}) & \approx & \mathbf{S}(\mathbf{v}) + \mathbf{J}\Delta\mathbf{v}, \\ \text{with} \quad \mathbf{J} = & \partial\mathbf{S}/\partial\mathbf{v}, & \end{array} \tag{4.18}$$

and applying a Newton-Raphson iteration procedure, starting with a set of initial conditions $\mathbf{v}$ close to the cyclic solution $\mathbf{v}_c$

$$\begin{array}{lrcl} \text{repeat} & & & \\ & \Delta\mathbf{v} & = & [\mathbf{I} - \mathbf{J}]^{-1}(\mathbf{S}(\mathbf{v}) - \mathbf{v}) \\ & \mathbf{v} & = & \mathbf{v} + \Delta\mathbf{v} \\ \text{until} & |\Delta\mathbf{v}| < \epsilon, & & \end{array} \tag{4.19}$$

where $\mathbf{I}$ is the identity matrix. The Jacobian $\mathbf{J}$ is calculated by a perturbation method, which involves simulation of a full walking step for every initial condition. The result of this depends on the model parameters and the initial estimate for the solution. If the parameters are such that no cyclic gait exists or if the initial estimate is poor, then the solution will diverge. If the solution converges we find one of possibly multiple cyclic solutions.

Local stability

If the walker starts a step exactly with $\mathbf{v}_c$, it will walk forever. However, if small errors $\boldsymbol{\epsilon}_n$ appear, the periodic solution needs to be stable for the robot to maintain gait. The stability is described with the Jacobian $\mathbf{J}$ from the previous subsection, which is the linearized multiplication factor for errors from one step to the next:

$$\mathbf{v}_c + \boldsymbol{\epsilon}_{n+1} = \mathbf{S}(\mathbf{v}_c + \boldsymbol{\epsilon}_n) \approx \mathbf{S}(\mathbf{v}_c) + \mathbf{J}\boldsymbol{\epsilon}_n. \tag{4.20}$$

Errors will asymptotically die out if all eigenvalues of the Jacobian $\mathbf{J}$ have an absolute value smaller than 1, and in that case the periodic solution is stable for small disturbances.

Global stability

The global behavior of the step-to-step function $\mathbf{S}$ can be studied with the aid of the cell mapping method [36]. The region of feasible initial conditions is subdivided into a large number (N) of small cells. All unfeasible initial conditions are regarded as a small number (z) of very large cells, so called *sink cells*. The cells are numbered 1 to N+z. By application of the step-to-step function $\mathbf{S}$ to the center of each cell, all of the N+z cells point to initial conditions inside one of the other cells, except the sink cells which point to themselves by definition. Starting with cell 1, a sequence of cells appears by following the pointers. This sequence either ends in a sink cell or in a repetitive cycle. This cycle can consist of one self-repeating cell (a fixed point), or a number of cells (representing an asymmetric gait, Section IV C). The repetitive cycle is identified and all cells in the sequence are labeled as basin of attraction of that cycle. Then the procedure is repeated with all N cells. As soon as a known cell (from a previous sequence) is encountered, the procedure can be stopped, and all cells in that sequence are labeled as basin of attraction of that last cell.

Application of the cell mapping method results in a list with all attractors (cyclic solutions) and classification of all discretization points into this list. Not only period-one walking gaits can be found, also period-*k* walking gaits. Results of the cell mapping method are as accurate as the discretization, within these tolerances fixed points may come and go. For example, what appears to be a fixed cell might in fact be slowly changing initial conditions (smaller changes than the discretization) of subsequent steps.

Chapter 5

Skateboards, bicycles, and 3D biped walkers; Velocity dependent stability by means of kinematic and dynamic lean-to-yaw coupling

M. Wisse and A. L. Schwab
Submitted to *International Journal of Robotics Research*, 2004.

One of the grand challenges in the development of passive dynamic walking robots (useful for an understanding of human gait and for future applications in entertainment and the like) is the stabilization of 3D motions. This is a difficult problem due to the inherent interaction between fore-aft motions and sideways motions. This paper proposes a simple solution. Conceptually, one can avert a sideways fall by steering in that direction, similar to skateboards and bicycles. The paper proposes to implement this concept for walking robots by the introduction of an ankle joint that kinematically couples lean to yaw. The ankle joint has an unusual orientation; its axis points forward and downward, without any left-right component. The effect of the ankle joint is investigated in a simple 3D model with three internal degrees of freedom. It has cylindric feet and an actuator at the hip joint which quickly moves the swing leg to a preset forward position. The simulations show that it is easy to find a stable configuration, and that the resultant walking motion is highly robust to disturbances. Similar to skateboards and bicycles, there exists a critical velocity (as a function of the parameters) above which stable walking motions occur. The critical velocity can be lower for a more vertical ankle axis orientation. As an additional benefit, the ankle joint allows a straightforward implementation for steering; a simple sideways offset of the mass distribution will cause the model to gently steer in that direction. The results show great potential for the construction of a real-world prototype with the proposed ankle joint.

5.1 Introduction

Passive dynamic walking [49] is a well-known concept for the design of energy efficient bipedal (two-legged) robots with a natural looking gait. In their purest form, such walkers are fully unactuated (and thus uncontrolled), while walking stably down a shallow slope. The swing leg moves forward in its natural frequency as a passive pendulum while the stance leg rotates forward as an inverted pendulum, usually rolling on an arc-shaped foot. For passive walkers with lateral constraints (i.e. only possessing two-dimensional dynamics) it has been shown that stable walking motions exist for a wide range of parameter values for prototypes both with and without knees. Moreover, it is straightforward to add elementary hip actuation for level-floor walking with a considerable robustness [93] and to add an upper body through the use of a bisecting hip mechanism [92].

One of the grand challenges is to find the key to stability in three dimensions. In addition to the fore-aft motions (roll), also sideways motions (lean) and rotations around the vertical axis (yaw) are possible. It is the interaction between all three of these that renders the problem of 3D stability so difficult. Consequently, most of the known successful solutions to this problem are successful because they *reduce the interaction* in one way or another:

- Ignore yaw by assuming sufficient yaw resistance in the foot contact [43, 60].
- Apply large moments of inertia against yaw [18, 17].
- Walk with short steps [79, 18, 75].
- Counteract yaw with a counter-rotating body [90] or with counter-swinging arms [19].

In this paper, however, we aim not at a *reduced interaction* between the degrees of freedom, but conversely we show how a *purposefully induced interaction* between lean and yaw can actually benefit the stability of the walking motion. First, in Section 5.2 the related problems of skateboard and bike stability are studied, then in Section 5.3 an elementary walking model is introduced, followed by the simulation results in Section 5.4 and the discussion and conclusion in Sections 5.5 and 5.6.

5.2 Two examples of advantageous lean-to-yaw coupling

5.2.1 Skateboard

The skateboard is one of the most elementary examples of a system with a kinematic lean-to-yaw coupling, hence its treatment here at the start of this paper. In the skateboard, the two sets of wheels are attached to the board via tilted steering axes (Fig. 5.1). Although the main purpose of this construction is to give the rider the ability to steer, here we'll show how this also provides stability. The following analysis is a simplified version of the skateboard stability analysis by Hubbard [37] in 1979.

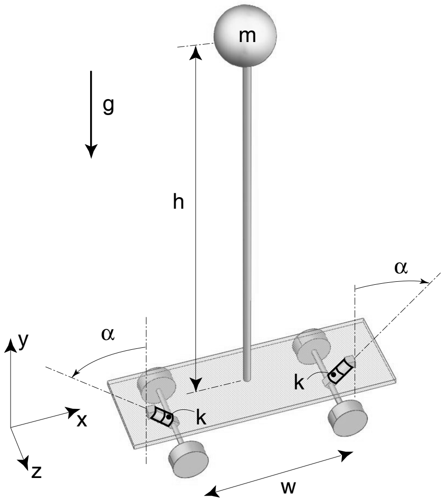

Figure 5.1: *Parameters of the skateboard model.*

The board and wheels are assumed to be massless and the height between the board and the floor is neglected. Also, we assume that there is always contact between all four wheels and the floor; the model cannot tip over. The rider is modeled as a single point mass at height h above the floor, rigidly attached to the skateboard. The distance between the front and rear wheels is w. The steering axes are mounted at an angle α with respect to the vertical such that sideways leaning of the rider results in steering in that direction. The steering axes are equipped with rotational springs with stiffness k. The model has fore-aft and sideways symmetry.

The skateboard is a non-holonomic system, i.e. it cannot slip sideways but it can move to a sideways position by a sequence of steering actions. Therefore it has a smaller velocity space (lean and ride) than coordinate space (lean, x- and y-position and orientation in plane). Here we will consider the linearized equations of motion in which the forward velocity can be considered as a parameter. The linearized model only has one degree of freedom, namely the sideways lean angle of the rider θ (Fig. 5.2). With zero forward velocity, the behavior equals that of an inverted pendulum with a de-stabilizing gravity torque and a stabilizing spring torque. Although the two springs act on the tilted joints, in their projected torques the tilt angle α cancels out.

When riding with a velocity v, the skateboard makes a turn if there is a non-

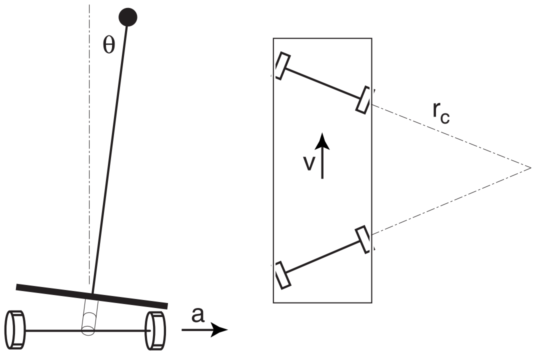

Figure 5.2: *Degrees of Freedom of the linearized skateboard model. Left is a hind view, right a top view.*

zero lean θ. The velocity together with the radius of curvature r_c (Fig. 5.2) determine the sideways acceleration of the board according to

$$a = \frac{v^2}{r} = \frac{2v^2}{w \tan \alpha}\theta \tag{5.1}$$

Therefore, the total system equation describing the linearized model becomes

$$mh^2\ddot{\theta} + (2k - mgh + \frac{2mh}{w \tan \alpha}v^2)\theta = 0 \tag{5.2}$$

This result can be interpreted as follows. If the spring stiffness k is high enough to counteract the inverted pendulum instability, then the system is never unstable. If not, then it can always be made stable by its velocity. The larger angle α, the higher the required velocity. The critical velocity reads:

$$v_{min} = \sqrt{\frac{(mgh - 2k)w \tan \alpha}{2mh}} \tag{5.3}$$

Note that the system can at best only be marginally stable. The introduction of damping in the steering axis could make it asymptotically stable. Also note that Eq. (5.3) suggests that it is best to make angle α equal to zero. In real life there is a lower limit to α dependent on the width of the skateboard because of the unilateral contact between the wheels and the floor.

5.2.2 Bicycle

Most of us know from experience that a bicycle is highly unstable at rest but can easily be stabilized at a moderate speed. Moreover, some uncontrolled bicycles can be asymptotically stable in a certain speed range. To demonstrate this phenomena we will consider one of the simplest bicycle models: an uncontrolled bicycle with a rigid rider attached. This is an example of a dynamically

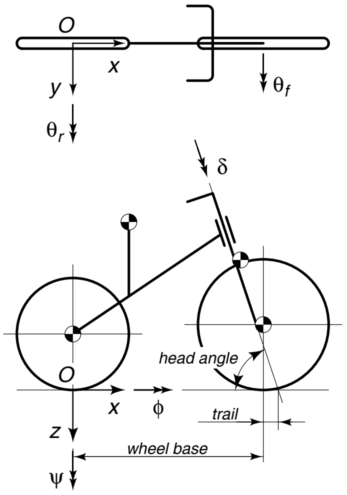

Figure 5.3: *Bicycle model together with the coordinate system, the degrees of freedom, and the parameters from [70].*

coupled lean-to-yaw motion due to the hands-free operation of the bicycle. The following analysis is based on an earlier publication by Schwab, Meijaard, and Papadopoulos [70].

The mechanical model of the bicycle consists of four rigid bodies, viz. the rear frame with the rider rigidly attached to it, the front frame being the front fork and handle bar assembly and the two knife-edge wheels. These bodies are interconnected by revolute hinges at the steering head between the rear frame and the front frame and at the two wheel hubs. The contact between the stiff non-slipping wheels and the flat level surface is modelled by holonomic constraints in the normal direction and by non-holonomic constraints in the longitudinal and lateral direction. There is no friction, apart from the idealized friction between the non-slipping wheels and the surface, nor propulsion and no rider control, the so-called hands free coasting operation. Note that these assumptions make the model energy-conserving.

The mechanical model of the bicycle has three degrees of freedom: the roll angle ϕ of the rear frame, the steering angle δ, and the rotation θ_r of the rear wheel with respect to the rear frame. The forward speed is taken as $v = -\dot{\theta}_r R_{rw}$, where R_{rw} is the radius of the rear wheel. Due to the non-holonomic constraints there are four extra kinematic coordinates which describe, together with the degrees of freedom, the configuration of the system [69]. The four kinematic coordinates are taken here as the Cartesian coordinates x and y of the rear-wheel contact point, the yaw angle ψ of the rear frame, and the rotation θ_f of the front wheel with respect to the front frame. The dimensions and mechanical properties of the benchmark model are those of a regular 18 kg bicycle with an average 76 kg rider. For the precise values we refer to [70].

To investigate the stability of the bicycle in the upright steady motion at constant forward speed we consider the linearized equations of motion expressed in the remaining degrees of freedom $\mathbf{q} = (\phi, \delta)^T$ which takes the form

$$\mathbf{M}\ddot{\mathbf{q}} + [\mathbf{C1} \cdot v]\dot{\mathbf{q}} + [\mathbf{K0} + \mathbf{K2} \cdot v^2]\mathbf{q} = \mathbf{f}\,, \tag{5.4}$$

with a constant mass matrix, $\mathbf{M}$, a "damping" matrix, $\mathbf{C1}$, which is proportional to the forward speed v, and a stiffness matrix which has a constant part, $\mathbf{K0}$, and a part, $\mathbf{K2}$, which is proportional to the square of the forward speed. Typical values for the entries in the matrices are,

$$\begin{aligned} \mathbf{M} &= \begin{bmatrix} 80.812 & 2.3234 \\ 2.3234 & 0.30127 \end{bmatrix}, \mathbf{C1} = \begin{bmatrix} 0 & 33.774 \\ -0.84823 & 1.7070 \end{bmatrix}, \\ \mathbf{K0} &= \begin{bmatrix} -794.12, & -25.739 \\ -25.739 & -8.1394 \end{bmatrix}, \mathbf{K2} = \begin{bmatrix} 0 & 76.406 \\ 0 & 2.6756 \end{bmatrix}, \end{aligned} \tag{5.5}$$

where we use the standard units kg, m, and s. The forces on the right-hand side, $\mathbf{f}$, are the applied forces which are energetically dual to the degrees of freedom $\mathbf{q}$. For the bicycle model the first is M_ϕ, the action-reaction roll moment between the fixed space and the rear frame. In practice such a torque could be applied by side wind, or by 'training wheels' located at the rear wheel hub, or by a parent teaching a child to ride by applying either a pure rolling moment or a lateral force. The second force is M_δ, the action-reaction steering moment between the rear frame and the front frame. This is the torque that would be applied by a rider's hands, or a steering spring-damper, or even an electronic controller. In the case of an ordinary uncontrolled bicycle, both of these moments are taken to be zero.

To investigate the stability of the upright steady motion we start from the homogeneous linearized equations of motion Eq. (5.4). Next we assume for the small variations in the degrees of freedom an exponential motion with respect to time which then takes the form $\mathbf{q} = \mathbf{q}_0 \exp(\lambda t)$. This leads to an eigenvalue problem for which in this case the characteristic equation is a polynomial in the eigenvalues λ of order four. The coefficients in this polynomial are themselves polynomials in the forward speed v, since some coefficients of the linearized equations of motion have a linear or quadratic dependency on v. The solutions of the characteristic polynomial for a range of forward speeds are the root loci of the eigenvalues λ, which are shown in Figure 5.4. Eigenvalues with a positive real part correspond to unstable motions whereas eigenvalues with a negative real part result in asymptotically stable motions. Complex conjugated eigenvalues give rise to oscillatory motions.

For the bicycle model there are two significant eigenmodes, called capsize mode and weave mode. The capsize motion is a non-oscillatory motion in which, when unstable, the bicycle just falls over like a capsizing ship. The weave motion is an oscillatory motion in which the bicycle sways about the headed direction. Both eigenmodes show the dynamically coupled lean-to-yaw motion. At very

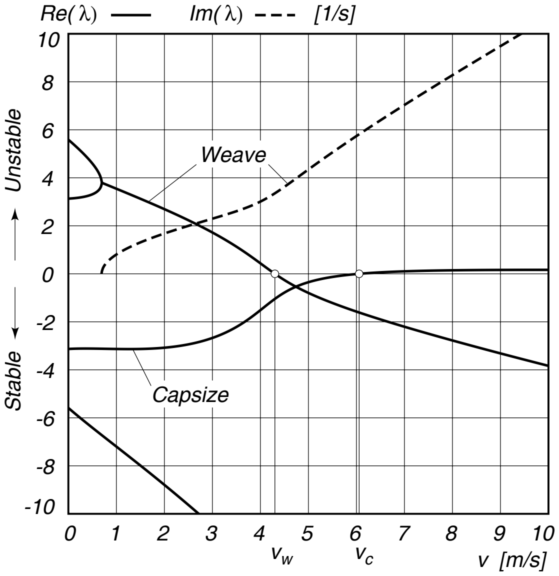

Figure 5.4: *Eigenvalues λ from the linearized stability analysis for the benchmark bicycle from Figure 5.3 and [70] where the solid lines correspond to the real part of the eigenvalues and the dashed line corresponds to the imaginary part of the eigenvalues, in the forward speed range of $0 \leq v \leq 10$ m/s. The zero crossings of the real part of the eigenvalues are for the weave motion at at $v_w = 4.301\,611$ m/s and for the capsize motion at $v_c = 6.057\,011$ m/s, giving the bicycle an asymptotically stable speed range of $v_w < v < v_c$*

low speed, $0 < v < 0.7$ m/s, there are two positive and two negative eigenvalues which correspond to an inverted pendulum-like motion of the bicycle. At $v = 0.693\,713$ m/s two real eigenvalues become identical and start forming a conjugated pair; this is where the oscillatory weave motion emerges. At first this motion is unstable but at $v_w = 4.301\,611$ m/s these eigenvalues cross the real axis in a Hopf bifurcation and the weave motion becomes stable until infinity. After this bifurcation the frequency of the weave motion is almost proportional to the forward speed. Meanwhile the capsize motion, which was stable for low speed, crosses the real axis in a pitchfork bifurcation at $v_c = 6.057\,011$ m/s and the motion becomes mildly unstable. We call a motion mildly unstable when the eigenvalues have a absolute value which is smaller than 2 s^{-1}, in which case it is fairly easy to stabilize the motion manually. With further increase in speed, the capsize eigenvalue approaches zero.

We conclude that the speed range for which the bicycle shows asymptotically stable lean-to-yaw behaviour is $v_w < v < v_c$. In addition, from a practical point of view one could say that the bicycle is easy to balance for all speeds above 3 m/s.

5.3 Simplest passive walking model with lean-to-yaw coupling

5.3.1 Model

The purpose of the simulation model is to show the essential dynamic effects of lean-to-yaw coupling in walking systems. The simplest model for this purpose is a 3D cousin of Garcia's two-dimensional 'Simplest walking model' [27] which consisted of one finite point mass at the hip joint, two infinitesimally small point masses at the feet, and massless rigid links in between, interconnected with a frictionless hinge at the hip. Our model (Fig. 5.5) is a 3D extension of this; the hip has gained a finite width and the hip mass is divided into two point masses at the extremes of the massless hip axle. For numerical reasons the point masses at the feet of our model are not infinitesimally small but just very small. The degrees of freedom are the coordinates and the yaw and lean angles of the center of the hip axle $\{x_h, y_h, z_h, u_1, u_2\}$, the two leg pitch angles $\{u_3, u_4\}$, and the two ankle angles $\{u_5, u_6\}$. The ankle axes are mounted in the x-y plane at an angle α with respect to the vertical. Note that the ankle axes have no component in the z-direction, unlike conventional robot designs or the human ankle. The 'normal' ankle functionality, rotation around the z-axis, is realized by means of the roll-off motion of the feet.

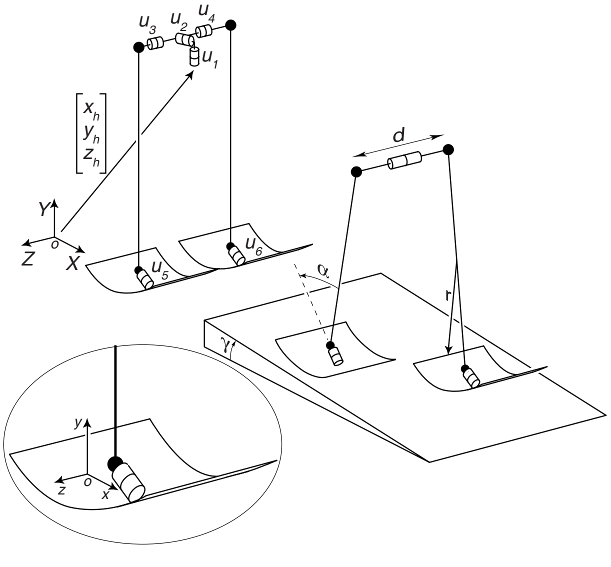

Figure 5.5: *Degrees of freedom (left) and parameters (right) of our simple walking model with ankle joints that couple lean to yaw. The global coordinate system is XYZ whereas the local coordinate system of the foot (inset) is xyz.*

The feet are (partial) cylinder shells with the cylinder axis perpendicular to the ankle axis. They are mounted such that the cylinder axis is in the leg (not displaced forward or backward) and that the total leg length (when standing upright) is independent of the cylinder radius. The foot contact is modeled as a perfectly rigid cylinder-plane contact with only one degree of freedom; roll in a direction perpendicular to the cylinder axis. The width of the feet is not specified and is assumed to be sufficient to prevent sideways tipping over the edge. The feet in the model have a finite size but no inertia, so the foot of the swing leg contributes to the system dynamics only as a point mass. For the detection of heel contact, the swing foot is assumed to preserve its parallel orientation with respect to the floor surface. Heel contact itself is modeled as a rigid plastic impact with immediate and full contact to the floor, while at the same instant the previous stance foot loses contact.

The model walks down a shallow slope γ. All parameters are scaled so that gravity g, the leg length l and the total robot mass ($2m_{hip}$) are all equal to one[1]. The simulation results can be scaled back to obtain results for example for an earthly gravity regime. This scaling exposes the minimal set of adjustable parameters; hip width d, foot radius r, ankle mounting angle α, and slope angle γ as listed in Table 5.1. Additionally, a (small) torque can be exerted at the hip joint to move the swing leg quickly to a forward position, a feature that will prove necessary for stable walking (Section IV).

Table 5.1: *Parameters and their default values.*

hip width	d	0.3
foot radius	r	0.5
ankle mounting angle	α	0.55
slope angle	γ	0.01

5.3.2 Equations of motion

The equations of motion for the system without foot contact constraints were generated with the method of virtual power as described in [71], where the twelve dependent degrees of freedom ($\{x, y, z\}$ for each point mass) were expressed in terms of the nine generalized coordinates $\{x_h, y_h, z_h, u_1..u_6\}$. In addition, there are three coordinates that change value only once per step; the foot roll-off direction ϕ and the foot contact location $\{x_c, z_c\}$. The five foot contact constraints are expressed as follows:

1. No yaw; the foot cylinder axis must remain perpendicular to its initial roll-off heading,

---

[1] Due to the applied scaling, most quantities in this text are dimensionless, which explains the frequent use of seemingly incomplete statements such as 'a velocity of 0.36'.

2. No lean; the foot cylinder axis must remain perpendicular to the normal of the floor,
3. Contact with plane; the center of the foot cylinder axis must remain a distance r (foot radius) above the floor,
4. No lateral slip
5. No forward slip; the forward disposition should match with the roll-off angle.

These constraint conditions (either for the right foot or for the left foot depending on which one is in stance phase) were added to the equations of motion to obtain a system of Differential Algebraic Equations which solves for the 9 generalized coordinates and 5 Lagrange multipliers (one extra unknown per constraint condition).

5.3.3 Simulation procedure

The simulation procedure is a succession of simulations of walking steps which begin and end at the instant immediately after heel strike. Within one step, the system of DAE's is numerically integrated until heel strike is detected, followed by an impact calculation. The end state of the walker is then used as the starting state for a second step. After the second heel strike, the end state ($\{\mathbf{q}, \dot{\mathbf{q}}\}_{n+1}$) is compared to the initial state of the walker ($\{\mathbf{q}, \dot{\mathbf{q}}\}_n$) and the entire two steps can be summarized as the non-linear stride function $\mathbf{S}$ which maps the end states on the initial states:

$$\begin{bmatrix} \mathbf{q}_{n+1} \\ \dot{\mathbf{q}}_{n+1} \end{bmatrix} = \mathbf{S}\left(\begin{bmatrix} \mathbf{q}_n \\ \dot{\mathbf{q}}_n \end{bmatrix} \right) \tag{5.6}$$

Note that we do not apply the common procedure of state-mirroring at the end of the step which is used in most of the 2D analyses to confine the simulation to only one walking step instead of two consecutive steps.

According to the Poincaré Mapping method, if the end state equals the initial state, we have found a *fixed point* representing a cyclic walking motion. The stability is determined by the effect of deviations $\boldsymbol{\epsilon}_n$ in the initial state on deviations $\boldsymbol{\epsilon}_{n+1}$ in the end state. For small deviations, we assume linearity around the fixed point, such that:

$$\boldsymbol{\epsilon}_{n+1} = \mathbf{J}\boldsymbol{\epsilon}_n \qquad with \qquad \mathbf{J} = \frac{\partial \mathbf{S}}{\partial(\mathbf{q}_n, \dot{\mathbf{q}}_n)} \tag{5.7}$$

J is the Jacobian of the stride function **S** and is determined by performing the simulation procedure once for all deviations $\boldsymbol{\epsilon}_n$, one for each independent initial condition. The stability characteristics are described by the eigenvalues $\boldsymbol{\lambda}$ of the Jacobian **J**; if all are smaller than 1 in magnitude, errors decay over subsequent steps. The smaller the eigenvalues, the faster the walker converges toward the fixed point. Note that the definition of eigenvalues here differs from Section II B; the analysis of the walking model is discrete ($-1 < |\lambda| < 1$ is stable) whereas the bicycle analysis is continuous ($|\lambda| < 0$ is stable).

For the stability analysis, there are 6 relevant independent initial conditions $\{\mathbf{q}, \dot{\mathbf{q}}\}_n$ for the start of a step. The 9 independent coordinates for the free model are reduced by 5 foot contact constraints to 4 independent degrees of freedom when one foot is in contact with the floor. The angle of the swing foot is not connected to any inertia, so this leaves only 3 independent degrees of freedom and thus 6 states, namely $\{u_3, u_4, u_6, \dot{u}_3, \dot{u}_4, \dot{u}_6\}$ for left stance. The Poincaré Section removes one state (one of the hip angles) so that there would be 5 independent initial conditions. In addition, there are three coordinates that change only once per step, namely x_c, z_c and ϕ. The linear coordinates x_c and z_c are not relevant to the walking motion, but the foot roll-off direction ϕ is, so it must be added to the set of independent initial conditions. Therefore, in total there are 6 relevant independent initial conditions as listed in Table 5.2.

Table 5.2: *Fixed point initial conditions for left stance, valid for the parameter values in Table 5.1.*

foot roll-off heading	ϕ_2	0.0016
stance leg angle	u_4	0.155
stance ankle angle	u_6	-0.0041
stance leg angular velocity	$\dot{u}_4$	-0.42
stance ankle angular velocity	$\dot{u}_6$	-0.070
swing leg angular velocity	$\dot{u}_3$	-0.42

5.4 Simulation results

This section presents the behavior and stability of five simulation models of increasing complexity. The first model (Fig. 5.6A) is Garcia's two-dimensional 'simplest walking model' [27]. This fully passive model has straight legs with point feet (with infinitesimally small point masses) and a large point mass at the hip. The second model (Fig. 5.6B) is similar except that it has arc feet instead of point feet. The third model (Fig. 5.6C) is equal to the second model except that it is three-dimensional. It has no hip width but it can move out-of-plane. Also, this model is equipped with the proposed ankle joints. The fourth model (Fig. 5.6D) differs in that it has a non-zero hip width, and the fifth model (Fig. 5.6D) has an additional actuator at the hip joint [93].

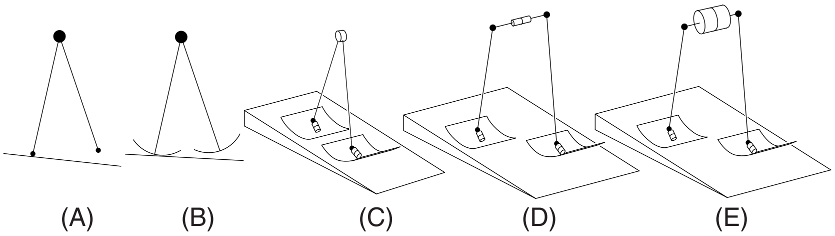

Figure 5.6: *Models with increasing complexity. A) 2D point foot walker [27], B) 2D arc foot walker, C) flat 3D walker (passive or active), D) passive 3D walker with finite hip width, E) active 3D walker.*

5.4.1 Fully passive model

Garcia *et al.* [27] researched the simplest walking model in 2D that could still demonstrate a passive walking motion, Fig. 5.6A. The model consists of three point masses, one of mass 1 at the hip and two infinitesimally small point masses at the feet, with rigid, massless links as legs interconnected with a frictionless hinge. Therefore it has two degrees of freedom when in stance phase and thus $2 \cdot 2 - 1 = 3$ independent initial conditions for a step starting with the hind leg just leaving the floor. With its point feet (no radius of curvature), the simplest walking model is a special 2D case of the model presented in this paper.

The model shows a stable walking pattern when walking on a shallow slope with a downward angle smaller than 0.015 (rad) [27]. For example, Table 5.3 presents the eigenvalues $\boldsymbol{\lambda}$ for the cyclic motion that exists for a typical slope of 0.004 (rad). It has been shown, however, that the simplest walking model is highly susceptible to disturbances [71], and that this sensitivity can be greatly reduced by the application of arc feet with a substantial radius [94]. Therefore we continue this paper with a model with arc feet with a radius of (a somewhat arbitrarily chosen) 0.5 times the leg length. For comparison within this paper and with previous publications [71, 93], the arc foot model is given the same step length and approximately the same velocity as the point foot model by adjustment of the slope angle. The step length is determined by the initial stance leg angle θ_0. On a slope of $\gamma = 0.004$ (rad) the point foot model has a limit cycle with $\theta_0 = 0.15$ (rad). The arc foot walker only needs a slope of $\gamma = 0.00058$ (rad) for the same step length, i.e. it is about 7 times more efficient while walking at the approximate same velocity, see Fig. 5.7. The eigenvalues have moved closer to 1 and thus do not suggest a stability improvement (Table 5.3). However, we performed a crude analysis of the basin of attraction which showed that the arc foot walker can handle deviations from the initial conditions of 8% versus 2% for the point foot walker, indicating a better practical applicability of the model.

An interpretation of the eigenvectors corresponding to the last set of eigenvalues in Table 5.3 has shown that the first three eigenvalues are indeed only related to the fore-aft motions whereas the last three eigenvalues are related to

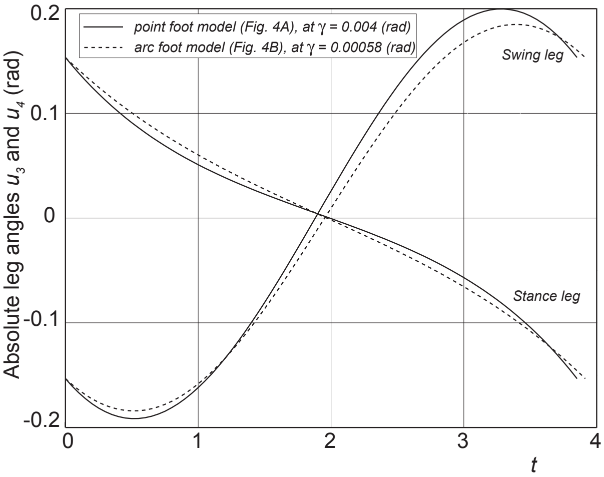

Figure 5.7: *Leg angles versus time for a point foot model (Fig. 5.6A) and an arc foot model (Fig. 5.6B) with a foot radius $r = 0.5$. The displayed cyclic walking motion (only one step is shown) is valid both for 2D models and for 3D models with zero hip width (Fig. 5.6C).*

3D motions in which both the sideways and fore-aft direction are present. The most important conclusion to be drawn from Table 5.3 is that there exists a stable 3D walking motion for our model with no hip width and an almost upright ankle axis ($\alpha = 0.15$ rad).

Further research shows that the eigenvalues are highly sensitive to the orientation of the ankle axis and that only a small region leads to stable motions,

Table 5.3: *Eigenvalues of the cyclic walking motion for the simplest walking model with point feet, a 2D walker with arc feet, and a flat ($d = 0$) 3D walker with ankle axes oriented at $\alpha = 0.15$ (rad). Note that all eigenvalues result from two successive steps.*

eigenvalues	2D point foot walker (Fig. 5.6A) at $\gamma = 0.004$	2D arc foot walker (Fig. 5.6B) at $\gamma = 0.00058$	3D with arc feet (Fig. 5.6C) at $\gamma = 0.00058$
λ_1	-0.3 + 0.27 i	0.69	0.69
λ_2	-0.3 - 0.27 i	0.12	0.12
λ_3	0	0	0
λ_4	-	-	0.72
λ_5	-	-	0.51
λ_6	-	-	0

see Fig. 5.8. The first three eigenvalues are not a function of the ankle axis orientation as it only influences 3D motions. Therefore the figure only shows the last three eigenvalues. The small region of stable values for α is located around the maximal stance leg angle (0.15 rad, see Fig. 5.7). This means that, during the walking motion, the orientation of the ankle axis will move from 0.3 to 0 (rad) with respect to an absolute reference frame, i.e. it will have a completely vertical orientation at the end of each step. This, in turn, means that the model must be in an upright position at that instant, as it has no degree of freedom for sideways lean. This is a problem for realistic prototypes because it would require feet that overlap inward to prevent tipping over on the inside edge of a foot. And such a solution would make the entire exercise of this paper unnecessary!

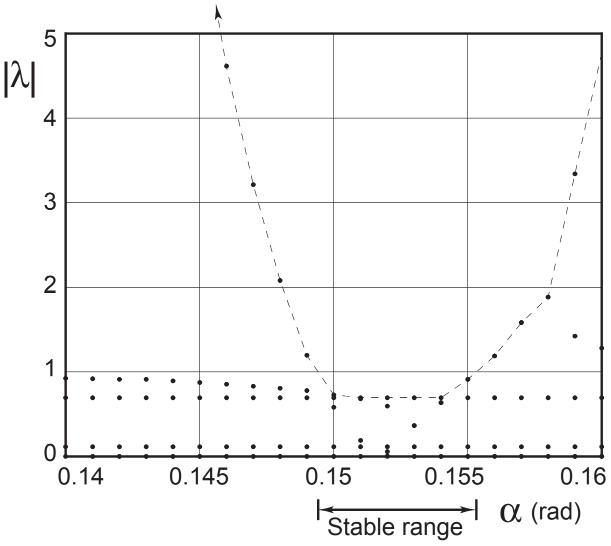

Figure 5.8: *Typical plot of the absolute values of the eigenvalues $|\lambda|$ as a function of the ankle joint orientation α for a fully passive 3D model (Fig. 5.6C). This plot is generated with hip width $d = 0$ and foot radius $r = 0.5$, walking on a slope of $\gamma = 0.00058$ (rad).*

We hypothesized that a finite hip width $d > 0$ might add to stability. A graph of the eigenvalues as a function of both the ankle orientation α and the hip width d is sketched in Fig. 5.9. The sketch is based on a number of cross-sections in the parameter space of α and d. The stable region for α narrows down with an increaseing d up to $d \approx 0.05$, beyond which no stable solutions were found for any α. A search up to $d = 0.2$ provided ever increasing eigenvalues, so we extrapolate the result to conclude that no stable 3D walking motions exist for a hip width of more than 0.05 times the leg length.

Another hypothesis was that a steeper slope might improve the stability; on a steeper slope the passive walker will take larger steps and thus walk faster, and the skateboard and bike models predict a beneficial stability effect for higher velocities. However, the simulation has shown only marginal effects. Up to the maximal slope of 0.046 (rad) beyond which no stable motions exist, the 3D graph in Fig. 5.9 remains similar in shape. The stable region shifts to higher values of α along with the increase in step length. For example, a slope increase from 0.00058 to 0.004 (rad) causes the initial stance leg angle to increase from 0.15 to 0.29 (rad) and also shifts the stable values for α from around 0.15 to around 0.29 (rad).

These marginal stability result, together with the required vertical orientation of the ankle axis, indicate that the fully passive model is not sufficiently applicable for real-world prototypes and warrant a search for a model with stable behavior for larger values of α and d.

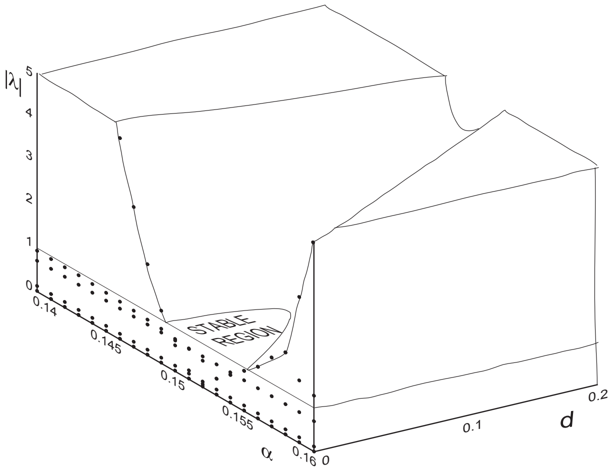

Figure 5.9: *A sketch of the dependency of the eigenvalues as a function of ankle joint orientation α and hip width d for a model (Fig. 5.6D) with foot radius $r = 0.5$ and slope angle $\gamma = 0.00058$ (rad). The left face of the figure is equal to Fig. 5.8.*

5.4.2 Model with hip actuation

In this subsection we propose to improve the overall (3D) walking behavior through the addition of a stabilizing feature that was originally intended for 2D machines. In two dimensions, the most persistent failure is a fall forward which can be averted by simply accelerating the swing leg to bring it quickly to a forward position and subsequently keeping it there [93]. This simple form of swing leg control can be implemented on our 3D model without energy implications; the swing leg is nearly massless, so any control action can be applied (almost) without reaction torques to the rest of the model. Therefore, the model still requires a downhill slope for a sustained walking motion. This also means that the swing leg can be moved arbitrarily fast; in the remainder of this article the swing leg is assumed (and simulated) always to be in the forward position before heel strike occurs.

We can arbitrarily set the forward angle that the swing leg is quickly moved to. Let's maintain the value of 0.15 (rad) as initial stance leg angle in accordance with the passive models described earlier. The controller therefore has to move the swing leg quickly to an inter-leg angle of $2 \cdot 0.15 = 0.3$ (rad). The immediate effect of the controller is that disturbances on the initial swing leg velocity do not affect the end state, thus one of the eigenvalues of the model becomes zero, as shown in Fig. 5.10. The top graph shows that also the active model knows stable values for α in the neighborhood of the initial stance leg angle of 0.15 (rad).

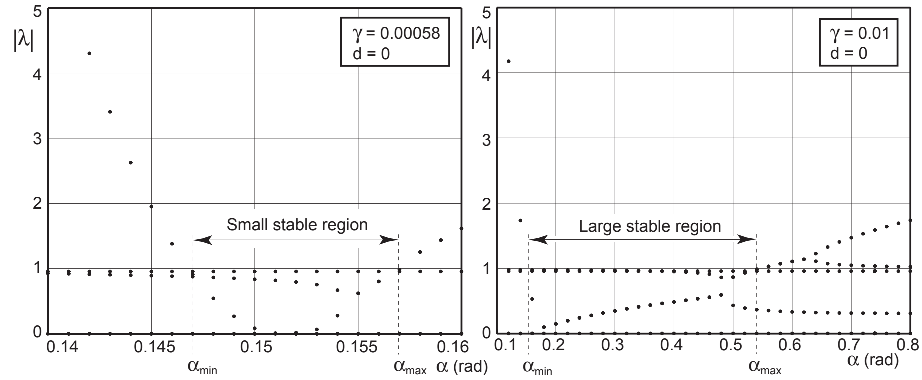

Figure 5.10: *Typical plot of the absolute values of the eigenvalues* $|\lambda|$ *as a function of the ankle joint orientation* α *for a 3D model with simple swing leg control (Fig. 5.6C). This plot is generated with hip width* $d = 0$ *and foot radius* $r = 0.5$*, walking on a slope of* $\gamma = 0.00058$ *(rad) (left) and* $\gamma = 0.01$ *(rad) (right). The two graphs exemplify that the upper boundary for* α *increases with an increasing* γ*; the steeper the slope, the larger the region of stability. Note the difference in scale of the two graphs.*

Looking at the behavior for $\gamma = 0.00058$, there seems to be little difference between the active model (Fig. 5.10, left) and the passive model (Fig. 5.8). The reason is that the main improvements are to be found for larger slopes. For the active model, a change of slope does not lead to a change of step length, while the swing leg control ensures that the model cannot fall forward, so any arbitrarily steep slope can be used. These two effects of the swing leg control together result in a much more favorable behavior. In contrast to the passive model, for the active model an increase of γ does not lead to a *translation* of the stable region for α but rather to an *increase* of this region, shown in the right graph of Fig. 5.10.

The stable region in the right graph of Fig. 5.10 has two independent boundaries. The lower boundary for α is directly related to the step length; if α is lower than 0.15, the ankle axis would reach a vertical orientation at the end of the step which leads to directional instability. With a fixed step length due to the swing leg controller, this lower boundary for α is more or less static. The upper boundary is directly related to the slope angle; the steeper the slope, the higher α can be. Or, in other words, for a given value of α the slope angle must be above a certain critical value for stable walking. In Fig. 5.11 this is depicted for $\alpha = 0.55$, the upper boundary from Fig. 5.10. Note the correlation between the two graphs; the upper boundary $\alpha = 0.55$ in Fig. 5.10 corresponds to the stability boundary $\gamma = 0.01$ in Fig. 5.11.

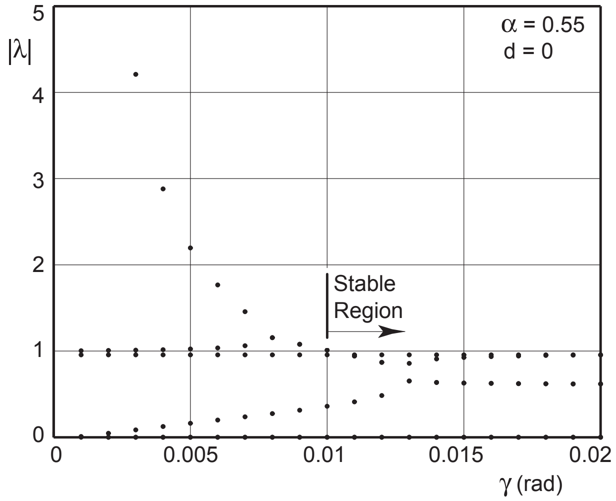

Figure 5.11: *Typical plot of the absolute values of the eigenvalues* $|\lambda|$ *as a function of slope angle* γ *for a 3D model with simple swing leg control (Fig. 5.6C). This plot is generated with hip width* $d = 0$*, a foot radius* $r = 0.5$*, and an ankle joint orientation* $\alpha = 0.55$ *(rad). For* $\gamma > 0.01$ *the model is stable. This boundary corresponds to the the upper stability boundary in the right graph of Fig. 5.10.*

With respect to the passive model, the active model has a much larger stable region; when walking on a slope of $\gamma = 0.01$ (rad), the ankle orientation angle can be anything between $0.15 < \alpha < 0.55$ (rad) for stable walking. This gives good hopes for models with a finite hip width. Fig. 5.12 presents the eigenvalues as a function of both α and the hip width d, where the left front plane equals the right graph of Fig. 5.10. Apparently, for the active model an increase of the hip width is even *beneficial* to the stability, in sharp contrast with the passive model.

5.4.3 Stability versus velocity

For the active model, it is easy to find a parameter combination that results in stable walking. Fig. 5.11 basically suggests that for any parameter combination, it is just a matter of increasing the slope angle past a critical value. This effect has the same feel to it as the velocity relation in skateboards and bicycles, in which for most parameter values there exists a critical velocity above which stable motions occur. Therefore it is interesting to investigate the relation between

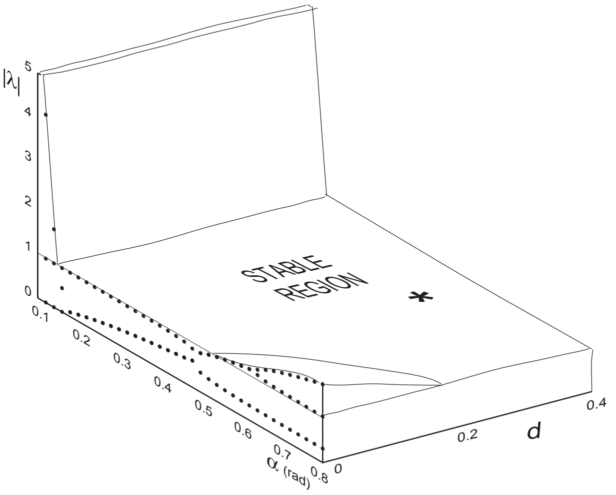

Figure 5.12: *Sketch of the eigenvalues of the active model as a function of ankle joint orientation α and hip width d for a model (Fig. 5.6E) with foot radius $r = 0.5$ and slope angle $\gamma = 0.01$ (rad). The left face is equal to the right graph of Fig. 5.10. The asterisk indicates the parameter set of Table 5.1.*

the slope angle, the walker's velocity, and its stability, with the goal to answer the question: 'Is there a direct relationship between velocity and stability?'

To answer that question, we need to bring r into the equation because the velocity is determined by γ and r for a given step length. For manageability of the model and calculations, we will answer this question only for the *flat* version of the 3D model, i.e. $d = 0$ (Fig. 5.6C). The result is stunning; according to Fig. 5.13 there is almost a one-to-one relationship between the velocity and the stability, irrespective of the specific values of r and γ that cause that velocity!

The result in Fig. 5.13 was obtained as follows. First, the plot contains contour lines of constant velocity. The walking velocity is a result of the gravitational energy input and the energy loss at the heel strike impact which are in balance when the walker is in a limit cycle. An analysis of the energy balance (not shown here for brevity) leads to the following approximate relationship:

$$\mathrm{v} \approx \frac{1}{(1-r)}\sqrt{\frac{\gamma}{\theta}} \tag{5.8}$$

where v is the walking velocity and θ is the stance leg angle at the start of the step (equal to half of the preset inter-leg angle). This approximation ignores the velocity decrease at midstance and therefore slightly overestimates the walking velocity. Eq. (5.8) clearly shows that if r equals the leg length 1, then the walker could have any velocity at a slope of 0 while no equilibrium exists for any other slope angle, because no energy is lost during heel strike. In Fig. 5.13 we used the exact velocities (from the non-linear simulations) rather than the approximation in Eq. 5.8.

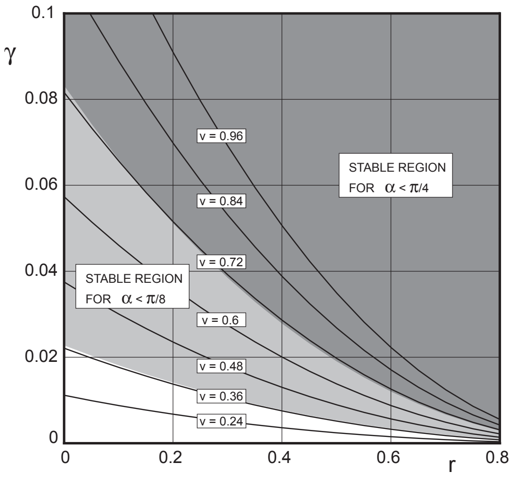

Figure 5.13: *Stability regions and walking velocity as a function of the slope angle* γ *and the foot radius* r *for an active, flat 3D model (Fig. 5.6C). The velocity is determined by the parameters* r *and* γ *and is independent of* α*. The stability is dependent on all three parameters. The graph shows that a more vertical ankle axis (smaller* α*) provides stability for lower velocities; For* $\alpha = \pi/4$ *the critical velocity is* $v \approx 0.72$*, whereas for* $\alpha = \pi/8$ *the critical velocity is* $v \approx 0.36$*. The velocity lines are obtained with the simulation, not with the approximation in Eq. (5.8). Note how the stability boundaries almost completely coincide with lines of constant velocity.*

The second ingredient of Fig. 5.13 is the shape of the region of stability. The figure shows for two different values of the ankle joint orientation α what combinations of values for the slope angle γ and the foot radius r lead to stable walking. The figure shows what was already known from Fig. 5.10; a steeper slope (larger γ) allows for a more horizontal ankle joint (larger α). The additional information in Fig. 5.13 is how the stability boundary depends on both γ and r, which apparently coincides with contour lines of constant velocity. A heuristic formula for the boundary value of α as a function of the velocity v can easily be extracted from the data scattered in this paper. From Figures 5.10 and 5.13 we can extract four data points that show an almost one-to-one linear relationship, $v_{min} \approx \alpha$.

5.4.4 Walking and steering

The previous subsections have shown that it is easy to find stable parameter combinations for the active model. This subsection will investigate the resultant walking motion for one characteristic set of parameter values (Table 5.1).

For a steady walk, the projection of the center of mass and the footprints are shown in Fig. 5.14. The step length of 0.3 times the leg length is a direct result of the swing leg controller. The center of mass makes sideways excursions of

± 0.008 times the leg length.

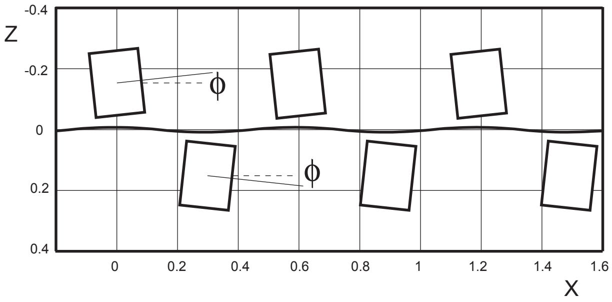

Figure 5.14: *Projection of the center of mass on the floor together with footprints for the full model (Fig. 5.6E). The grid on the floor is in units of leg length. The model walks from left to right in a steady motion. The footprint direction ϕ is exaggerated; the true value $\phi = 0.00155$ (see Table 5.2) would be invisible in the figure.*

The model's inherent stability means that is will react to any (not too large) disturbance by asymptotically moving back to its steady limit cycle. This fact can be used for intentional steering; if the model were placed on the slope in a direction other than steepest descent, it will automatically steer toward that direction. Or, even more useful, a sideways mass offset will also induce steering in that direction. In Fig. 5.15, which contains a sequence of 500 walking steps, the center of mass was displaced slightly (0.006 times the leg length) to the right. The result is that the model asymptotically moves toward a heading direction of 0.64 (rad) with respect to the direction of steepest descent. With its new heading, the model has found balance between the mass offset to the right and the offset effect of the slope to the left.

The model is robust enough to handle a much larger mass offset. Even if the center of mass is sideways displaced with 0.05 times the leg length, a steady (though somewhat limping) walking motion exists. With this offset, the model will turn with a radius of about 8 times the leg length, as shown with the dashed line in Fig. 5.15. It stops and falls not because of the direct effect of the mass offset, but because it has turned more than 90 degrees and thus receives no energy input. If the slope would turn with the walker, it would walk indefinitely in circles.

As a final stability test we investigated the disturbance rejection of the model. The model was started with the initial conditions for the steady walking motion plus an error on one of them. The model is able to recover from an increase of at least 200% or a decrease of 100% on any of the initial conditions, except for the velocity of the stance leg angle. The stance leg's angular velocity can only be decreased with 50%, otherwise the model falls backward. All in all, the model predicts great potential for practically applicable prototypes.

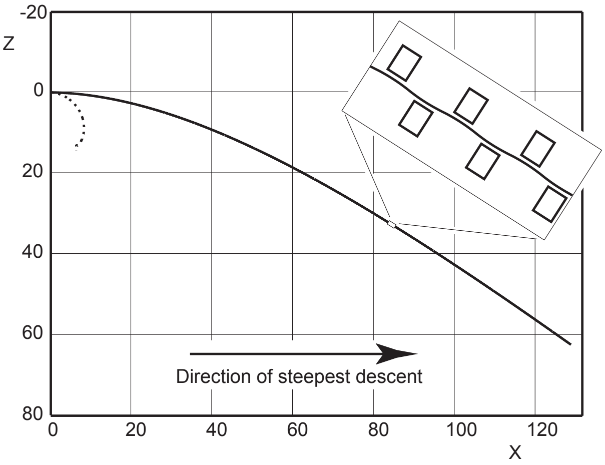

Figure 5.15: *Projection of the center of mass on the floor together with footprints for 500 steps. The model has a mass offset to the right and thus steers asymptotically toward a direction in which the sideways slope effect is in balance with the effect of the mass offset. A much larger mass offset results in a tighter turn as shown with the dashed line. After a turn of more than 90 degrees, the walker receives no energy input and eventually stops and falls.*

5.5 Discussion

5.5.1 Applicability in walking robots

The simulations predict successful walking for prototypes with the special ankle joint that couples falling sideways (lean) to turning in that direction (yaw). The solution to any instability is to increase the walking velocity. There is, however, a practical limit to the walking velocity. The simulation assumes that the (almost massless) swing leg is always in time to catch the walker for its next step, but a physical swing leg with substantial mass cannot move instantaneously. Its velocity is not only limited by practical considerations (actuator capacity), but also by the fact that its reaction torque might exceed the friction torques that the stance foot can supply.

Our model is not equipped with springs in the ankle joints for the sake of simplicity. The skateboard analysis, however, predicts a beneficial influence of such springs. It is recommended for future research to investigate the possible stability benefit that such springs can provide for walking robots.

The implication of this paper for the creation of stable prototypes goes beyond the concept of the tilted ankle joint. Even if proposed ankle joint is not implemented in a prototype, it is still possible to benefit from the idea behind it; any control algorithm anywhere in the body can have similar beneficial stability effects, as long as its effect is a lean-to-yaw coupling. We hypothesize that such an effect is also present in the human body, albeit well disguised by the simultaneous presence of two other control strategies for sideways stability, namely sideways foot placement and inertial reaction torques from the upper body.

5.6 Conclusion

This paper shows that a special ankle joint that couples falling sideways (lean) to turning in that direction (yaw) can lead to stable 3D walking models. A practical robustness against disturbances requires a basic form of swing leg control which moves the swing leg quickly to a forward position. With this control rule in place, the model shows behavior that corresponds to bicycles and skateboards; stable motions exist above a certain critical forward velocity, depending on the tilt angle α of the ankle axis. The more vertical the axis (smaller α), the lower the critical velocity. There is a minimum, however; the tilt angle α must always remain larger than the maximal stance leg angle, otherwise it would have a completely vertical orientation at the end of a step. This does not only lead to instabilities but also requires impractically wide feet to prevent tipping over on the inside of the foot.

The ankle joint provides an effective means for direction control; a slight asymmetry in any of the parameters (such as a sideways mass offset) results in a walk on a curved path. The simulations with the elementary model presented in this paper predict a sufficient robustness against disturbances to warrant the construction of a physical 3D prototype.

Acknowledgements

This research is partially funded by the Dutch national technology foundation STW.

Part II

Prototype experiments

Chapter 6

Design and Construction of 'Mike'; A 2D autonomous biped based on passive dynamic walking

M. Wisse and J. van Frankenhuyzen

International Conference on Adaptive Motion of Animals and Machines (AMAM)
2003; Kyoto, Japan

For research into bipedal walking machines, autonomous operation is an important issue. The key engineering problem is to keep the weight of the actuation system small enough. For our 2D prototype 'Mike', we solve this problem by applying pneumatic McKibben actuators on a passive dynamic biped design. In this paper we present the design and construction of Mike and elaborate on the most crucial subsystem, the pneumatic system. The result is a fully autonomous biped that can walk on a level floor with the same energy efficiency as a human being. We encourage the reader to view the movies of the walking results at http://dbl.tudelft.nl/.

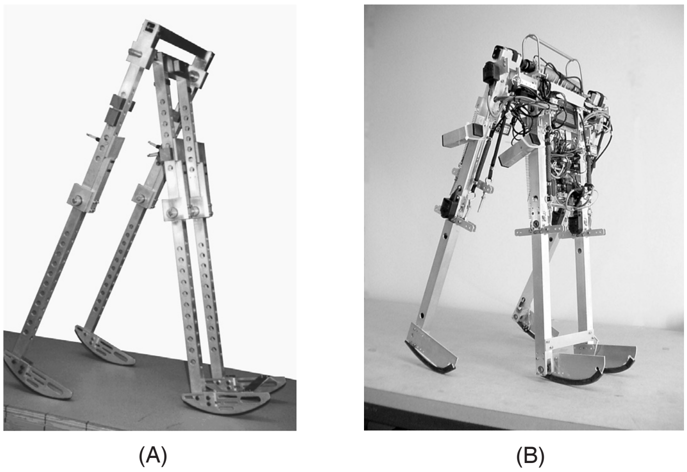
(A) (B)

Figure 6.1: *(**A**) Close copy of McGeer's walker by Garcia et al., (**B**) 2D biped prototype Mike.*

6.1 Introduction

We are performing research into bipedal walking robots with two long-term goals in mind. First, we expect that it increases our understanding of human walking, which in turn can lead to better rehabilitation of the impaired. Second, autonomous walking robots could greatly enhance the entertainment experience for visitors of theme parks and the like. Both long-term goals impose identical requirements on bipedal robots. They should be anthropomorphic in function and appearance, their locomotion should be robust, natural and energy efficient, and they should be easy to construct and control.

A solution for energetic efficiency is the exploitation of the 'natural dynamics' of the locomotion system. In 1989 McGeer [49] introduced the idea of 'passive dynamic walking'. He showed that a completely unactuated and therefore *uncontrolled* robot can perform a stable walk when walking down a shallow slope. His most advanced prototype (Figure 6.1A) has knees and a hip joint, which connect in total four thighs and shanks (with rigidly attached circular feet). The inner two legs form a pair and so do the outer legs, so that the machine essentially has 2D behavior.

We believe that passive dynamic walking should be the starting point for successful biped design. For a human-like robot walking on level ground, a necessity of actuation arises for energy input (instead of walking down a slope), and for stabilization against large disturbances. We propose a robot design that can perform a robust motion as a result of the passive dynamics, while the actuators only compensate for friction and impact energy losses.

We are materializing this combination of passive dynamic walking and actuation in the form of our new prototype 'Mike' (see Figure 6.1B). On top of the specifications of McGeer's machine, Mike is provided with McKibben muscles (pneumatic actuators) in the hip and knee joints that can provide energy for propulsion and control, thus eliminating the need for a slope and providing an enhanced stability. In this paper we will describe the design and construction of Mike, focusing in sections II - V on the key construction elements; foot shape, McKibben muscles, pneumatic system, pressure control unit. Section VI presents walking experiments of Mike walking downhill and on a level floor.

6.2 Foot Shape

6.2.1 Foot shape in literature

The human foot is shaped so that the center of pressure (the average contact point) travels forward during the progression of a walking step. This effect is known as 'foot roll-over'. When replicating the human foot for prostheses or for walking robots, many designers apply a curved foot sole with an approximately circular foot roll-over shape. For contemporary foot prostheses, Hansen *et al.* [31] shows the effective foot roll-over shapes of different makes. From his graphs we conclude that they all have a foot radius of 30-35 cm. Apparently that was empirically determined to be the best foot shape.

In passive dynamic walking robot research, many computer models and prototypes are equipped with circular feet, following McGeer's example. McGeer [49] determined the effect of the foot radius on the local stability (i.e. small disturbances) of his walkers and so concluded that a foot radius of about 1/3 of the leg length would be a good choice. However, we argue that a good local stability does not imply a good disturbance rejection for larger disturbances. As an example, we compare the findings of Garcia *et al.* [27] on the simplest walking model with our own. Their simplest walking model was equipped with point feet (foot radius equal to zero), and showed stable downhill walking for slopes up to 0.015 rad. However, when studying the allowable size of the disturbances for that model [71], we found that even a 2% change of the initial stance leg velocity could make the model fall over. In conclusion, more information is needed about the effect of the foot roll-over shape on the allowable size of the disturbances.

6.2.2 Test machine for foot roll-over shape

We built a test machine (Figure 6.2) to answer the question: 'with what foot radius can the largest disturbance be handled?' The test machine weighs 3 kg and is, with a leg length of 38 cm, approximately half the size of Mike. It has no knees, the only joint is at the hip. The test machine was placed on a shallow slope with a disturbance half-way. The disturbance was realized by lowering the second half of the walkway. The stability was quantified as the largest amount of lowering that the test machine could still recover from and continue walking to the end of the slope.

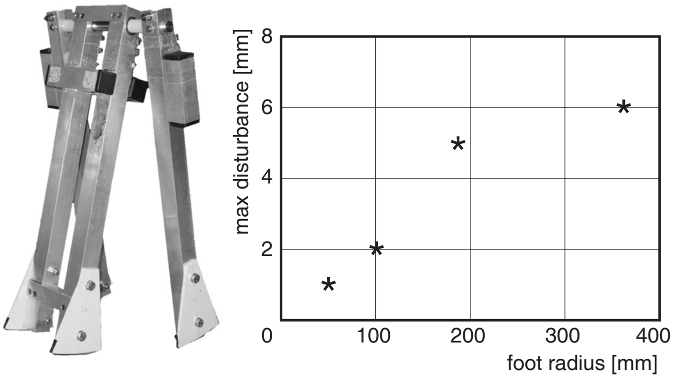

Figure 6.2: *Stability results of the test machine (left) tested with four different foot radii: 50, 100, 190 and 380 mm with a foot length limited to approx. 8 cm. Apparently a larger foot radius is always better.*

We built four different sets of feet with radii from 50 mm to 380 mm, but limited the foot length to about 8 cm. The results are plotted in Figure 6.2. Apparently, the larger the foot radius the better, as coincides with intuition. Of course, when the foot length is limited, there is no gain in increasing the foot radius above a certain value; the walker would just spend more time on the heel and toe.

6.2.3 Construction

Theoretically, Mike needs feet with a radius as large as possible. In practice however, there is a limitation to the length of the foot due to the required foot clearance. If the foot is long, bending the knee will not result in enough clearance for the swing leg, but rather in the opposite. Based on the empirically determined prosthetic foot shape and some experimenting with Mike, eventually we decided on a foot radius of 25 cm and a length of 13 cm. This is pretty close to McGeer's recommended 1/3 of the leg length.

Another practical consideration is the place of attachment of the foot to the shank. McGeer shifted the feet somewhat forward from the center, so that the passive reaction torques would keep the knees locked during the stance phase. We don't need this, for we have muscles to actively extend the knees. However, empirical study showed that the best stability results were obtained indeed with the feet shifted forward about 6 cm, see Figure 6.3.

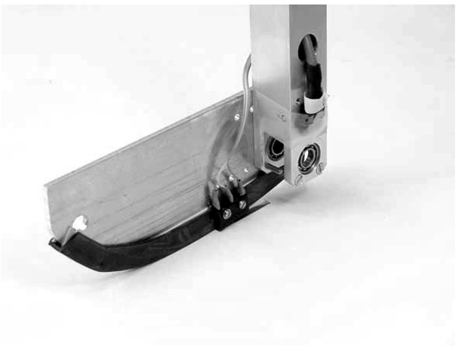

Figure 6.3: *In practice, we obtained the best results with a foot radius of 25 cm, a foot length of 13 cm, and a forward displacement of 6 cm. The foot switch allows the controller to adapt to the actual step time by registering the exact instant of heel strike.*

6.3 McKibben Muscles as Adjustable Springs

6.3.1 Background and requirements

For autonomous systems, it is crucial to apply lightweight actuators. For a passive dynamic walker, another requirement is that the actuators should not interfere with the passive swinging motions of the legs. McGeer says the following about this matter: "The geared motors or fluidic actuators used on most mechanical bipeds do not satisfy this requirement; lift one of their legs, and it will hang catatonically or, at best, grind slowly to a halt at the bottom of its swing." We chose to use pneumatic McKibben muscles as actuators that fulfill these requirements. In comparison to other alternatives, such as commercially available pneumatic cylinders, McGeer's LITHE [51], Direct Drive torque motors, or MIT Leglab's Series Elastic Actuators [61], the McKibben muscles are very lightweight and simple in construction and application.

Under constant pressure the McKibben muscles behave like a spring with low hysteresis. Because the muscles can only provide tension force, we use them in a pair of antagonists, counteracting on the same passive joint (see Figure 6.4). Increasing the internal pressure results in a higher spring stiffness, which in turn increases the natural frequency of the limb.

6.3.2 Operating principle, technical realization and results

A McKibben muscle consists of flexible rubber tube, covered by a weave of flexible yet non-extensible threads, see Figure 6.5. The operating principle is best explained when starting with a non-attached, pressurized muscle. If from that state the muscle is extended, the non-extensible threads are forced into an orientation with a smaller inter-thread angle, thus decreasing the diameter of the muscle. The cumulative effect of muscle extension and diameter reduction is

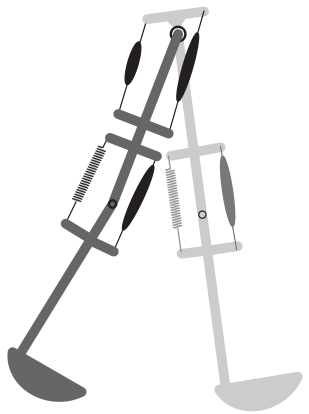

Figure 6.4: *Overview of the McKibben muscles on Mike. Each muscle drawn represents two parallel muscles in the machine.*

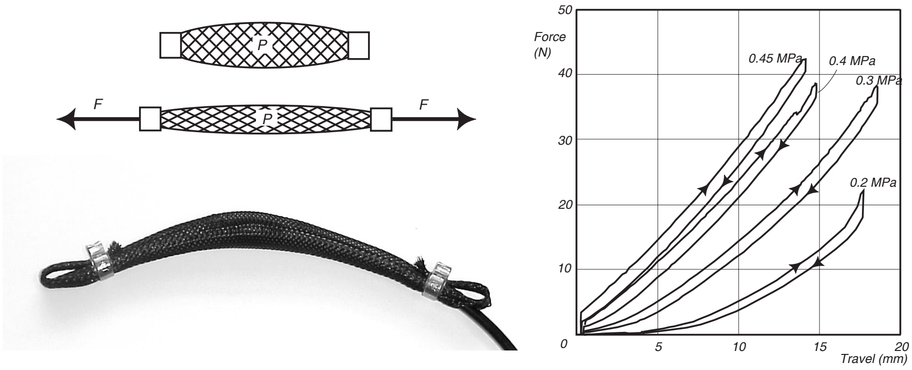

Figure 6.5: *McKibben muscles; (***left top***) operating principle, (***left bottom***) photograph of the Shadow muscle, (***right***) force-length diagram.*

a decrease of muscle volume. Against an assumed constant muscle pressure, reducing the muscle volume costs work. This work can only be supplied by a tension force in the muscle attachments. In other words; muscle extension causes a counteracting force, which makes the muscles act like tension springs. A more detailed study of the McKibben muscle used as an adjustable spring can be found in [77], where the relation between muscle extension and tension force is presented as:

$$F = \frac{b^2 P'}{2\pi n^2 L_0} \Delta L \tag{6.1}$$

with F = muscle force, b = length of weave threads, P' = relative muscle pressure, n = number of turns of a thread, L_0 = muscle rest length, and ΔL = relative muscle extension. This relation reveals the most important characteristics of a

McKibben muscle:

- The muscles behave like linear springs,
- The spring constant is proportional to the muscle pressure.

McKibben muscles are based on a simple concept and are generally easy to construct. However, it is our experience that the choice of materials and connectors is important for the muscle lifetime. Therefore, we use commercially available muscles (Figure 6.5) made by the Shadow Group [4], which they sell at £6 each. The muscles weigh less than 10 grams and can produce a force of 40 N at 0.40 MPa.

Figure 6.5 shows the mechanical behavior of one type of Shadow muscle (6 mm diameter, 150 mm length) at different pressure levels. Note that indeed the muscles behave like linear springs (in this range). Also, note that there is a small but noticeable hysteresis-loop, representing losses mainly due to friction between the scissoring threads and the rubber tube.

6.4 Pneumatic System

6.4.1 Background and presumptions

Because a McKibben muscle needs pressurized gas for functioning, our autonomous biped Mike needs to be provided with an efficient, lightweight and properly working pneumatic system. First of all, we have to carry along our own reservoir of pressurized gas. The gas should be stored at saturation pressure in order to keep the necessary container volume as small as possible. Secondly, the high pressure from this container has to be reduced to various operation pressure levels between 0.1 MPa and 0.4 MPa.

Minimizing gas consumption helps to increase the autonomous operation time. Van der Linde [77] developed the so called 'Actively Variable Passive Stiffness'-system. This system includes a solenoid 3/2 valve that switches the internal muscle pressure between two preset pressure levels. In this way, only a small volume of gas is needed every time the muscle is activated, because the muscle pressure is never completely vented to ambient pressure.

6.4.2 Requirements

To have time for proper experiments, we need a few minutes of autonomous operation time on one gas container. Measurements on the amount of exhaust gas, during a pressure decrease from 0.35 to 0.15 MPa in one muscle, tell us that we need 44 milligrams CO_2 per actuation. During each step 4 muscle activations take place, so that we need 176 milligrams of gas each step. The step time is 0.6 seconds. By choosing an ISI CO_2-bulb [2] with 86 grams of gas, we have an acceptable 5 minutes of continuous experimental time.

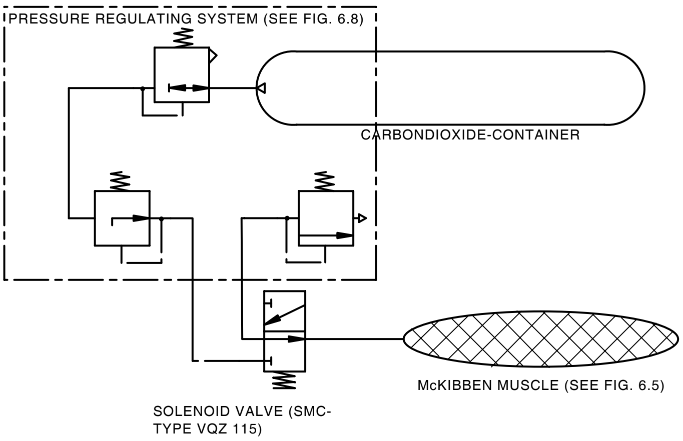
PRESSURE REGULATING SYSTEM (SEE FIG. 6.8)
CARBONDIOXIDE-CONTAINER
McKIBBEN MUSCLE (SEE FIG. 6.5)
SOLENOID VALVE (SMC-
TYPE VQZ 115)

Figure 6.6: *Overview of the pneumatic system on Mike.*

Because our goal is to build a transportable and easy to handle biped, we (intuitively) put the maximum total weight on 7 kg. Regarding the amount (and weight) of the electrical and mechanical sub-systems, a total weight of the pneumatic system of 1 kg seems to be acceptable.

Since the muscle pressure is directly related to the stiffness, it is important to be able to control the pressure levels with high accuracy. A relatively short response time is needed to make it possible to execute control actions during a step time of 0.6 seconds.

6.4.3 System overview

The pneumatic system provides the actuation for our prototype Mike. The pneumatic system receives input from the on-board controller in the form of valve control signals. The controller determines when each muscle is activated or deactivated. The two respective muscle pressures are to be preset manually when tuning the prototype. The output of the pneumatic system obviously has the form of joint torques that influence the passive dynamic leg motions.

To provide for this desired input-output behavior, the pneumatic system consists of four components (see Figure 6.6): 1) gas container, 2) manually adjustable pressure reduction valves, 3) electronically controlled 3/2-way switching valves, and 4) McKibben muscles. The pressure reduction system is the most crucial part of the pneumatic system. We developed this system and will present it in the next section. For the valves we use the pilot pressure operated VQZ 115 valves from SMC [5]. Although these are about the most efficient commercially available valves, they still consume 0.5 Watts each. We are encouraging suppliers to develop more efficient valves. The McKibben muscles have been discussed in the previous section.

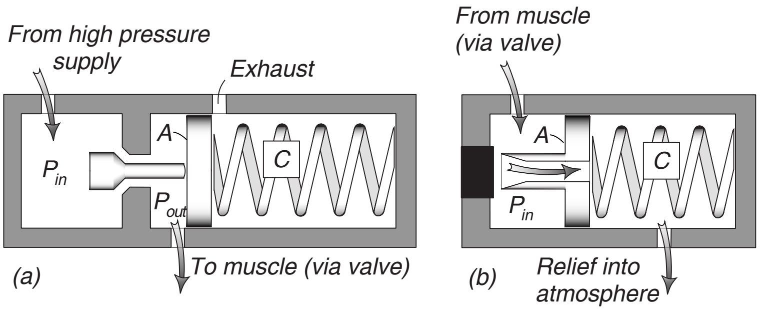

Figure 6.7: *Working principle of (a) pressure regulator valve and (b) pressure relief valve.*

6.5 Pressure Control Unit

6.5.1 Background and requirements

The pressure control unit must be able to regulate the desired muscle pressures accurately and fast (well within the step time of 0.6 seconds). Second, application in an autonomous biped requires a compact, lightweight and gas efficient solution.

There are two commercially available regulator principles, each of which can only fulfill part of the above requirements. The indirectly controlled pressure regulators (flapper-nozzle type) provide fast and accurate pressure control at the cost of a high internal gas consumption and relatively large physical dimensions. Directly controlled pressure regulators (piston type) are generally small and lightweight and need no extra gas supply for internal consumption, but are not sensitive and accurate enough for our application. We used the directly controlled principle, as small size and gas efficiency are the most important requirements, and minimized the disadvantages.

6.5.2 Operating principle

The piston type pressure regulator is drawn in Figure 6.7. A valve separates the input pressure from the output pressure. The output pressure acts on a spring loaded piston, where the manually adjustable spring load represents the output pressure level. If the output pressure falls below this preset value, the spring loaded piston opens the valve and the output pressure level is restored. To ascertain that the pressure regulator is sensitive, it needs to be constructed with a high ratio of A:C (see Figure 6.7) and with low internal friction.

The low preset pressure level is realized by integrating a separate pressure relief valve (see Figure 6.7) in the muscle outlet. The spring loaded piston in the pressure relief valve is open as long as the muscle pressure is higher than the preset level (drawn situation).

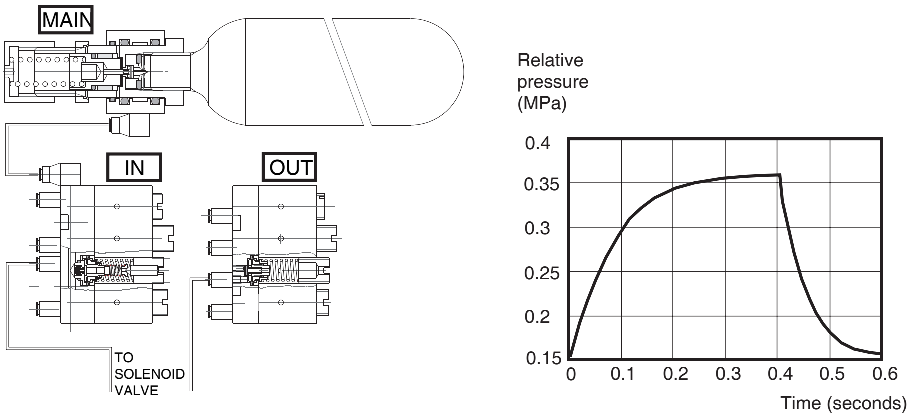

Figure 6.8: *(**left**) technical drawings of pressure reduction system, (**right**) dynamic response of the complete pneumatic system.*

6.5.3 Technical realization and results

The principles discussed above are translated into functioning prototypes. Experiments have convinced us that the required relatively high accuracy cannot be met by a single-stage pressure regulator, due to pressure overshoot and steady state offset. Therefore we have divided the pressure reduction in two stages, see Figure 6.8.

First, one main pressure regulator directly on the gas bulb brings the pressure from 5.8 MPa to about 1.0 MPa. Second, a second-stage reduction from 1.0 MPa to 0.2 – 0.4 MPa, with 4 different preset manually adjustable pressure levels, is realized in the input pressure control block ('IN', Figure 6.8). In these valves, the pistons are equipped with diaphragms to minimize friction effects and to provide the required sensitivity and accuracy. The output pressure control block ('OUT') includes four adjustable pressure relief valves. Basically the same piston construction as in the input pressure reduction valves has been used. The two pressure-control blocks together weigh about 180 gram and have a volume of less than 8 x 5.5 x 1.5 cubic centimeter.

After assembling the complete pneumatic system, it is possible to evaluate the behaviour by measuring the muscle pressure in time, during a switching-action of the described solenoid valve. Figure 6.8 shows the dynamic response of the complete system (see Figure 6.6) when pressurized from 0.15 MPa to 0.35 MPa and back. We obtain an accuracy/repeatability of about 10 kPa, and a relatively slow response as was to be expected with the choice of pressure regulator type. However, the system is fast enough according to the successful walking results.

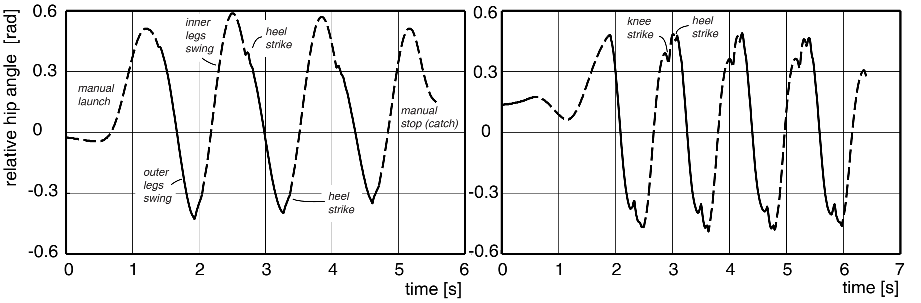

Figure 6.9: *Walking results (left) with stiff knees on a floor with stepping stones on a 0.06 rad slope, (right) with active knees on a 0.06 rad slope. The prototype completes 7 symmetrical steps until the end of the walking surface.*

6.6 Walking Experiments

6.6.1 Downhill walking

We performed walking experiments with an increasing number of active degrees of freedom, starting with walking down a slope with rigid knees. With rigid knees, foot scuffing is inevitable. To eliminate this problem for our initial experiments, we constructed 'stepping stones' at the expected footfall locations. Together with the slope angle this required some tuning, eventually resulting in stable walking with steps of 0.24 m at a slope angle of 0.06 rad.

In this setting, we could start with experiments with rigid knees, similar to the testing machine in Figure 6.2. With the Agilent HEDS-5540 incremental optical encoder on the hip joint, the hip angle was recorded during a successful run as shown in Figure 6.9. As is apparent from the figure, the gait was not symmetrical. When the middle legs were swinging (positive hip angle), the step was much longer in duration. Heel strike only occurred when they were already far on their way back, noticeable by the small bump (impact shock) in the graph. It is not clear whether this asymmetry resulted from a non-perfect launch or from the machine's natural dynamics. A simulation study in the near future should reveal this. Although not symmetrical, the emergent gait was encouraging enough to continue with experiments with bending knees.

By bending the knee for the appropriate time interval during the swing phase of a leg, the prototype can gain just enough foot clearance for continuous walking without stepping stones. As McGeer has shown, it is possible to obtain the appropriate timing with pure passive dynamics by tuning the mechanical properties. In our experience, it is then essential to keep the center of mass of the shank very close below the knee joint. However, we want the ability to actively interfere with the knee motion for future rough terrain walking experiments, so Mike was provided with knee-stretching muscles. Having these muscles there anyway, we decided to actively control the knee motion rather than completely rely on the passive dynamic motion.

The knee is stretched actively with a McKibben muscle counteracted by a passive spring, see Figure 6.4. The default knee muscle pressure is 'high' (0.35 MPa), which is switched to 'low' (0.08 MPa) at the other leg's heel strike, and switched back to 'high' after an empirically determined 400 ms. With this activation pattern we obtained steady walking for the entire length of the slope (5 m) with the appearance to be able to continue to walk indefinitely, see Figure 6.9. It is easy to launch the prototype by hand, so we would call it 'pretty stable'. We have not yet performed experiments to determine the exact stability of the gait.

In these walking experiments Mike has about the same specific resistance as a walking human being, using about 10 W to pull its 7 kg along at a speed of 0.4 m/s. The energy consumption consists of three components. First, the propulsion is obtained from gravity by walking down a 0.06 rad slope, which counts for 1.6 W. Second, the knee muscles use approximately 0.4 MPa CO_2 which accounts for 5.3 W. Actually, to keep the storage volume small, the CO_2 is stored and supplied at the saturation pressure, 5.8 MPa. The inevitable loss of energy in the process of pressure reduction from 5.8 to 0.4 MPa is not taken into account. Third, the prototype is equipped with a number of sensors and a a low power (less then 1 W) Strong-Arm based Linux machine (the LART [3]), which use together about 3 W. Obviously, the bulk of the energy consumption goes to the architecture for improving the stability even when using low-power components. We hope to increase the walking stability without increasing the energy consumption even more by using the timing of the muscle activations as a control parameter [77].

6.6.2 Walking on level floor

Finally, we activated the hip muscles and leveled out the walking surface. That made the robot lose its natural tendency to tilt and walk forward, so we had to shift the center of mass forward with a few centimeters. The hip muscles are the same as the knee muscles, but operate as antagonistic pairs. When heel strike is detected one muscle is set to high, its antagonist to low, so that the swing leg is pulled forward. We have not yet performed accurate measurements on the torque that the muscles exert on the hip, but it is estimated to be below 2.5 Nm, approximately the same as the maximal torque from gravity. This simple form of hip control is sufficient to obtain a robust gait, see [93].

Mike performs a steady walk on a level floor, as demonstrated with video's at http://dbl.tudelft.nl/. It can handle irregularities in the terrain, such as the sidewalk in front of our building.

With the ability to walk on level ground, we finally had the opportunity to perform an endurance test. On the 86 grams of CO_2, Mike can walk 3.5 minutes. After a continuous walk that long, the main pressure regulator is deeply frozen due to gas expansion; apparently it is a little undersized for the actual gas flow.

6.7 Conclusion

We started this research with the question: "How to keep the actuators and energy storage device lightweight enough to enable autonomous operation for a walking biped?" Our solution is provide the biped with a pneumatic actuation system. This form of actuation is successful when applying the following two ideas: 1) use McKibben muscles as adjustable springs and 2) develop a compact and well performing pneumatic system. With these developments we were able to construct a fully autonomous biped. We have succeeded in making it walk in a stable manner on a level floor, see http://dbl.tudelft.nl/.

Now that we have concluded the first phase of this project, we are aiming at the following goals: first to add an upper body while maintaining passive dynamic properties, and finally to extend to three dimensions.

Acknowledgements

This research is funded by the Dutch national technology foundation STW. Thanks to Richard van der Linde, Arend Schwab, Dick Plettenburg, Frans van der Helm, Erik Mouw and Jan-Derk Bakker.

Chapter 7

Adding the upper body to passive dynamic walking robots by means of a bisecting hip mechanism

M. Wisse, D. G. E. Hobbelen and A. L. Schwab
Submitted to *IEEE Transactions on Robotics*, 2004.

Passive dynamic walking is a promising idea for the development of simple and efficient two-legged walking robots. One of the difficulties with this concept is the addition of a stable upper body; on the one hand a passive swing leg motion must be possible, whereas on the other hand the upper body (an inverted pendulum) must be stabilized via the stance leg. This paper presents a solution to the problem in the form of a bisecting hip mechanism. The mechanism is studied with a simulation model and a prototype based on the concept of passive dynamic walking. The successful walking results of the prototype show that the bisecting hip mechanism forms a powerful ingredient for stable, simple and efficient bipeds.

7.1 Introduction

Two-legged walking robots exert a strong attractive appeal due to the resemblance with human beings [66]. Consequently, some major research institutions and private companies have started to develop bipedal (two-legged) robots, which has led to sophisticated machines [59, 68, 46]. To enable economically viable commercialization (e.g. for entertainment), the challenge is now to reduce the design complexity of these early successes, in search for the ideal set of characteristics: stability, simplicity, and energy efficiency.

A promising idea for the simultaneous reduction of complexity and energy consumption, while maintaining or even increasing the stability, is McGeer's concept of 'passive dynamic walking' [49]. On a shallow slope, a system consisting of two legs with well-chosen mass properties can already show stable and sustained walking [19]. No actuators or controls are necessary as the swing leg moves in its natural frequency. An elegant solution indeed, but thus far only the legs have been considered.

The addition of an upper body to passive dynamic walkers remains an active research topic. The problem is that the upper body should be stabilized in the upright position, while at the same time the alternating swing leg should be able to swing passively to a forward position. Previously proposed solutions include McGeer's 'levered isotonic tendons' [51], variable springs [79] or a controllable 'backlash clutch' in the hip joints [56], all fairly complex solutions.

In this paper, we propose to design the hip joint as a passive bisecting mechanism, similar to that in a pair of compasses. First, Section II will give an overview of the main concepts used in this paper. Section III will present the two-dimensional simulation model and prototype (Fig. 7.1) developed for this study. The results will be presented in Section IV followed by a discussion in Section V. Finally, Section VI will conclude that a bisecting hip mechanism indeed provides an elegantly simple solution for stable and efficient walking.

7.2 Main concepts

7.2.1 Passive dynamic walking

In search for simple, stable and efficient walking machines, McGeer pioneered the idea of passive dynamic walking. The concept is analogous to the approach of the Wright Brothers to flying; first they mastered motor-less gliding until they had a design that was intrinsically stable, could be manually controlled, and glided with only a small descent angle (i.e. could travel far on little gravitational energy). Similarly, McGeer focused on finding a completely passive construction that could walk stably and efficiently, requiring only a minimal downward slope in the walking surface. With dynamic simulations, and based on the method of Poincaré Mapping, he analyzed the stability of such walkers and subsequently built increasingly complex prototypes, the most advanced of which had two legs with knees (Fig. 7.2a). With symmetrically paired legs, its

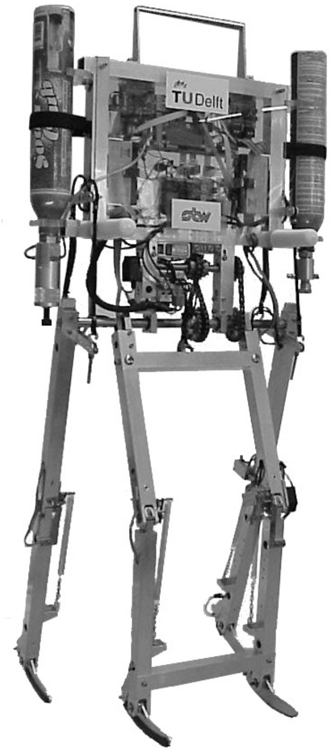

Figure 7.1: *Prototype 'Max'; a 2D passive dynamic walking robot with an upper body connected to a bisecting mechanism at the hip.*

motions were confined to two dimensions, a solution also adhered to in this paper. Since McGeer's work, the idea of passive dynamic walking has gained in popularity [30, 60, 63, 44]. The most advanced fully passive walker yet, constructed at Cornell University, has two legs (genuine three-dimensional dynamics) with knees, and counter-swinging arms [19] (Fig. 7.2b). It has no upper body.

7.2.2 Hip actuation for stability

The purely passive walking prototypes demonstrate convincing walking patterns. However, all prototypes require a smooth and well adjusted walking surface. A small disturbance (e.g. from small errors introduced with a manual launch) can still be handled, but larger disturbances quickly lead to a failure [71]. Two-dimensional models can suffer from three types of failure: collapsing through the stance knee, falling backward, or falling forward. The first type of failure, knee collapse, is related to the ground reaction force. If this force results in a flexing torque in the knee, a knee collapse could occur. The problem is solved

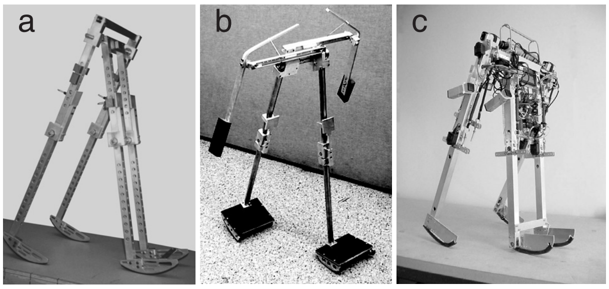

Figure 7.2: *Previous walkers. a) Garcia's copy [26] of McGeer's 2D walker with knees [50], at Cornell University, b) fully passive 3D walker with knees and arms by Collins et al. [19], also at Cornell University c) kneed walker with hip actuation [93], at Delft University of Technology.*

by attaching the feet more forward to the shank, and additionally a knee latch can be installed. The second type of failure, falling backward, is related to the fluctuations in kinetic and potential energy. In the extreme situation of a robot with point feet, the robot's center of mass would make a circular path with midstance as the apex. A shortage of initial kinetic energy could cause a failure to pass the apex, resulting in a fall backward. The problem is solved by applying arc feet with a reasonably large radius. This leaves us with the third type of failure, falling forward.

Falling forward occurs when the swing leg is not timely moved to a forward position where it can catch the robot in preparation for its next step. The solution to this problem is correspondingly straightforward; the faster the swing leg is swung forward (and then kept there), the more robust the walker is against disturbances. The exact motion of the swing leg is irrelevant. This idea was tested in simulation models and in a prototype [93] (Fig. 7.2c). We implemented the idea with a variable spring at the hip joint. The stiffness and damping were kept constant, but the equilibrium angle alternated at each step, always pulling the swing leg forward with respect to the stance leg. As a result, the walker could cope with larger disturbances when the hip spring provided more acceleration, the known trade-off between energy consumption and stability. Note that the prototype in Fig. 7.2c is the direct predecessor of the prototype presented in this paper.

7.2.3 Bisecting hip mechanism

The topic of this paper, a bisecting hip mechanism, was first explored in a simulation model based on Garcia's 'simplest walking model' [27]. Our model consisted of four point masses connected by rigid, massless links [92] (Fig. 7.3). The study revealed the possibility of fully passive walking with an upper body by means of a bisecting hip mechanism; a mechanism which keeps the upper body always at the bisection angle of the two legs. For a lightweight upper body, the dynamic effects of the passive legs are dominant. When the weight of the upper body increases, a hip spring is required to maintain the upright position as the equilibrium position. The study showed that a suitable spring stiffness can be found for any mass distribution.

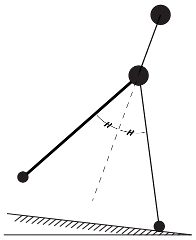

Figure 7.3: *Simple model for preliminary study of passive bisecting hip mechanism [92]. The bisecting mechanism maintains the upper body in the bisection angle of the legs. In addition, the hip joint is equipped with a restoring spring.*

A parameter study with the simple model showed the effects of the upper body on the stability and the energy efficiency of the walking motion. One distinct result is that the fore-aft mass distribution has a strong influence on the existence and the stability of the cyclic walking motion. This matches McGeer's finding of a similar influence of the fore-aft mass distribution in the legs of his walkers. Conversely, the walking motion is very tolerant to changes in the vertical mass distribution. A counterintuitive effect was found, as a higher center of mass provided a slightly better robustness against disturbances. Moreover, elevation of the center of mass also improves the energy efficiency. Altogether, the preliminary study was strongly encouraging to the construction of a prototype with an upper body connected through the proposed bisecting hip mechanism, and thus formed the start for the study presented in this paper.

7.3 Methods

7.3.1 Simulation model

The basis of the present study is a two-dimensional 5-link model (Fig. 7.4). The model has a common topology; the upper body is a single rigid link, whereas each leg consists of a thigh and a shank interconnected through a knee joint. The knees are provided with a hyperextension stop (assuming fully inelastic impacts) and a locking mechanism (latch) which is released just after the start of the swing phase. With the bisecting hip mechanism, the total number of degrees of freedom is at most 3; absolute upper body angle ϕ, inter-leg angle θ, and relative swing knee angle ψ. At the end of a step when the swing knee is fully extended, only two independent degrees of freedom remain (four states; two angles and their velocities). Note that this is the same number of degrees of freedom as for kneed walkers without an upper body ([25]) due to the constraint of the bisecting hip joint.

Ankle joints are not present, as rigidly attached arc feet have proven to be a simple and sufficient solution for stable passive walking. We assume that the links suffer no flexible deformation and that the joints are free of damping or friction. Also, we assume a perfect bisecting mechanical coupling between the legs and the upper body. The contact between the foot and the floor is idealized, assuming perfectly circular feet that do not deform or slip, while the heel strike impact is modeled as an instantaneous, fully inelastic impact where no slip and no bounce occurs. The walker walks on level ground and thus requires a small amount of energy input per step. This is provided by means of the hip muscles which accelerate the swing leg to a forward position. Their main function is to provide fore-aft stability (cf. Section II B), but their secondary effect is the input of just enough energy into the system to maintain the cyclic walking motion. Finally, the floor is assumed to be a rigid, flat, and level surface.

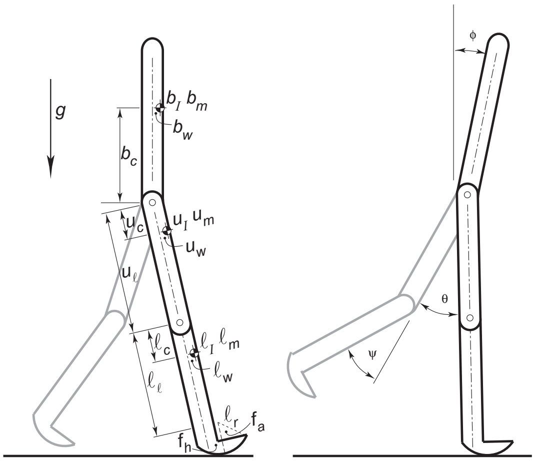

Figure 7.4: *Two-dimensional 5-link model. Left the parameter definition, right the degrees of freedom (ϕ is not measurable in the prototype).*

7.3.2 Simulation procedure

The simulation procedure is similar to that applied in previous researches [71, 93]. The procedure is a succession of nonlinear numerical dynamic simulations of walking steps which begin and end at the instant immediately after heel strike. Within one step, the equations of motion are numerically integrated until an event is detected such as knee strike or heel strike, followed by an impact calculation. After the heel strike impact the simulation of the walking step is ended. The end state of the walker can then be used as the starting state for the next step, or it can be compared to the initial state of the walker. This comparison provides insight in the existence and stability of cyclic walking motions; if the end state equals the initial state, we have found a *fixed point* representing a cyclic walking motion. If a deviation from the fixed point in the initial state results in a smaller deviation in the end state, the cyclic walking motion is stable (this is the Poincaré Mapping method for stability analysis). Additionally, to investigate 'how stable' the walking motion is, we perform an approximate search for the boundaries of the basin of attraction of the fixed point. A walking step is simulated with initial conditions that deviate from the fixed point in different combinations of states (e.g. a positive deviation on the stance leg angle combined with a negative deviation on the angular velocity of the body). We search for the largest allowable deviations that still lead to successful walking. The resulting estimate for the boundaries of the basin of attraction are a measure for the size of disturbances (at the start of a step) that the walker can still recover from.

7.3.3 Default parameter values

A set of physically realistic parameter values that lead to stable walking was readily found. Re-using partial designs from previous research [94] we arrived at a 10 kg machine with a 0.6 m leg length and 1.1 m total height. The physical properties, such as the mass distribution were initially determined by convenient placement of the supplementary electronic and pneumatic components (Section IV). The resultant configuration resulted in stable walking in the simulation, so we have adopted these parameter values as the default values listed in Table 7.1.

Table 7.1: *Default parameter values for the prototype with two full CO_2 canisters.*

	body	upper leg	lower leg
mass m [kg]	8	0.7	0.7
mom. of Inertia I [kgm^2]	0.11	0.005	0.005
length l [m]	0.45	0.3	0.33
vert. dist. CoM c [m]	0.2	0.15	0.16
hor. offset CoM w [m]	0	0	0
foot radius f_a [m]	-	-	0.25
foot hor. offset f_h [m]	-	-	0.01

7.3.4 Construction of the prototype

The central part of the prototype (Fig. 7.1) is its bisecting hip mechanism. Of the many possible forms of implementation we chose to apply an auxiliary axle connected to the legs with one straight and one cross-over chain (Fig. 7.5). In hindsight, it is valuable to report that this solution requires extra attention to the problem of slack in the chains. Also, one must be aware that rather large torques are transmitted through the chainwheels and axles, especially when the prototype occasionally falls. Nonetheless, for our relatively lightweight prototype this solution is satisfactory. Other possible mechanisms include a four-bar linkage, a differential gearbox, or cables and pulleys (as applied in some gait orthoses [39]). Alternatively, the bisecting hip action can also be obtained in fully actuated robots where a sub-controller maintains the upper body in the dissection angle [64, 12].

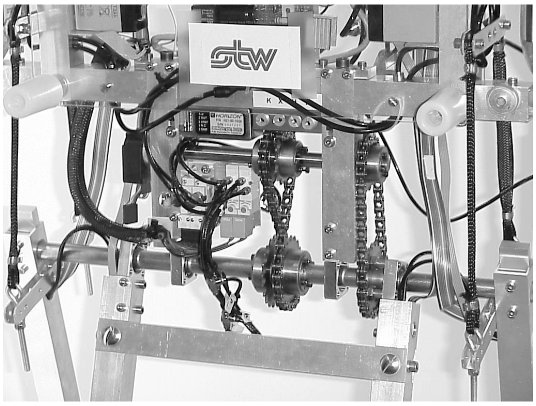

Figure 7.5: *The bisecting hip mechanism in the prototype. The outer legs are rigidly attached to the hip axle, the inner legs can rotate freely. The hip axle is connected through bike chains via an auxiliary axle to the inner legs.*

The prototype is autonomously powered with an on-board pneumatic system. The pneumatic components are displayed in Fig. 7.6, clockwise arranged according to the CO_2 flow through the system. The returnable Alco$_2$jet^{TM} canister (widely available for home soda machines) contains 450 g CO_2 at the saturation pressure of 5.8 MPa and weighs 1.2 kg when completely full. The pressure is reduced in two stages, first to approximately 1.2 ± 0.2 MPa and then to 0.6 ± 0.02 MPa. Both levels are manually adjustable. We developed the regulators specially for this project because they are not commercially available in the required small and lightweight design (the small 40x20x10 mm block in Fig. 7.6 actually contains *four* second stage regulators). The second stage pressure output is fed via low-power SMC^{TM} valves to four tiny SMC^{TM} cylinders that control the knee latches and to four Shadow^{TM} McKibben muscles that act as two antagonistic pairs between the robot's body and the outer legs (attached with a moment arm of 60 mm).

The McKibben muscles are an unorthodox choice of actuators. Their characteristics are quite unlike those of the commonly used DC motors and seem disadvantageous at first. They behave like springs with a stiffness proportional

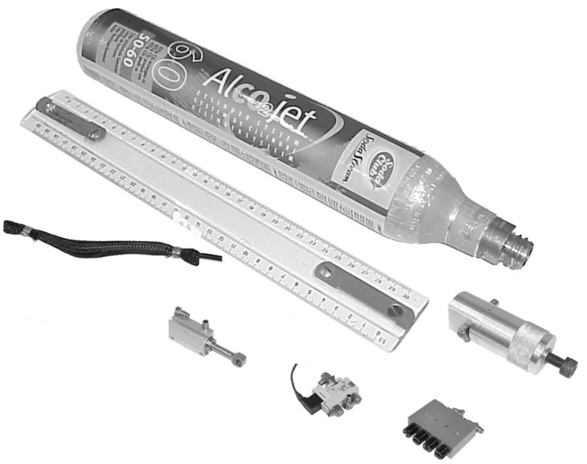

Figure 7.6: *The pneumatic components and a 30 cm ruler to indicate their sizes. The components are clockwise arranged according to the CO_2 flow through the system; 5.8 Mpa CO_2 canister, the first stage pressure regulator to 1.2 Mpa, a block of four second stage regulators to 0.6 Mpa, one of four low-power SMC$^{\mathrm{TM}}$ valves, one of four small SMC$^{\mathrm{TM}}$ cylinders and one of four Shadow$^{\mathrm{TM}}$ McKibben muscles.*

to the internal CO_2 pressure (Fig. 7.7). The use of such muscles is quite energy efficient if they are only required to change pressure once per step, but they are rather unsuitable for continuous control (e.g. to obtain a position servo). The spring behavior is fairly linear for most part of the 30% extension range, but becomes highly non-linear near maximal extension where the stiffness and damping increase dramatically. We modeled this with two stiffnesses as shown in Fig. 7.7, together with a high damping ratio near maximal extension. In addition, the CO_2 flow through our pneumatic system to fill the muscles is a slow first-order system with a time constant of $\tau = 0.25$ s. Altogether, the muscles introduce 5 parameters in the model that cannot be determined exactly because they are linear approximations of a highly non-linear behavior, namely the nominal muscle stiffness, the stiffness near maximal extension, the pre-load, the damping near maximal extension and the time constant. We use these parameters to fit the model behavior to the prototype measurements.

Altogether, McKibben muscles do not seem attractive as robot actuators. For the specific task of walking, however, the spring-like behavior, the non-linearities near maximal extension, and the efficiency when controlled only once per step together with the low weight and flexibility make them highly suitable. With these characteristics, the muscles perform three simultaneous tasks parallel to the three main concepts in Section II:

1. They power the walking motion [77]. A difference of internal pressure between two antagonists results in an asymmetry that pulls forward the swing leg. By alternation of pressures at each step, the muscles inject a

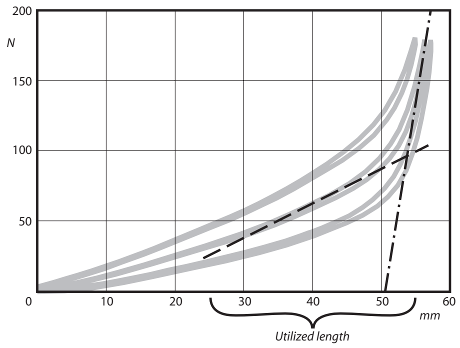

Figure 7.7: *Muscle force-length diagram at different pressures and the approximation used in the simulations. The dashed line represents one instance of the stiffness (variable with muscle pressure) in the normal operation range, whereas the dash-dotted line models the rigid behavior near maximal extension (invariable). The muscles are mounted with a pre-load. By their functioning as antagonistic extension stops, a leg can only rotate between -0.35 and +0.35 radians with respect to the upper body, so that only a part of the muscle's extension range is utilized as indicated in the graph.*

small amount of energy into the system and thus replenishes the energy lost in damping and impacts.

2. They provide robustness against falling forward [93]. Especially the nonlinear behavior near maximal extension is beneficial for this, as the muscles effectively slow down the forward-rushing swing leg and then keep it in that forward position.

3. They provide the required hip spring stiffness for the upper body [92].

Due to this combination of functions, McKibben muscles are a satisfactory choice of actuators for the prototype.

The control system is extremely simple. The prototype has one foot switch per pair of legs which triggers only two valve actions per step. If the inner leg's switch is contacted, the front hip muscles are switched to high pressure and the antagonists to low pressure, effectively pulling the outer legs forward. Simultaneously, the knee latches of the outer legs are released briefly. Then, the system just waits for the outer leg's foot switch to make contact, assuming that knee extension takes place before heel contact. The entire control algorithm is easily implemented in any microcontroller (we have experimented both with a Microchip$^{\mathrm{TM}}$ PIC16f877 and with a LEGO Mindstorms$^{\mathrm{TM}}$ RCX controller).

For measurements, however, a more elaborate electronic system is required. The prototype is equipped with four optical encoders (hip, inner knee, left and right outer knee) and with one gyroscope mounted in the robot's body. The low-level processing (counters and A/D conversion) is still done in a PIC microcontroller, while the data is collected at 50 Hz in a J-stick$^{\mathrm{TM}}$ Java board that can be read out after the experiments. Even with the measurement system active, the entire robot remains fully autonomous.

7.4 Results

7.4.1 Resultant motion and gait characteristics

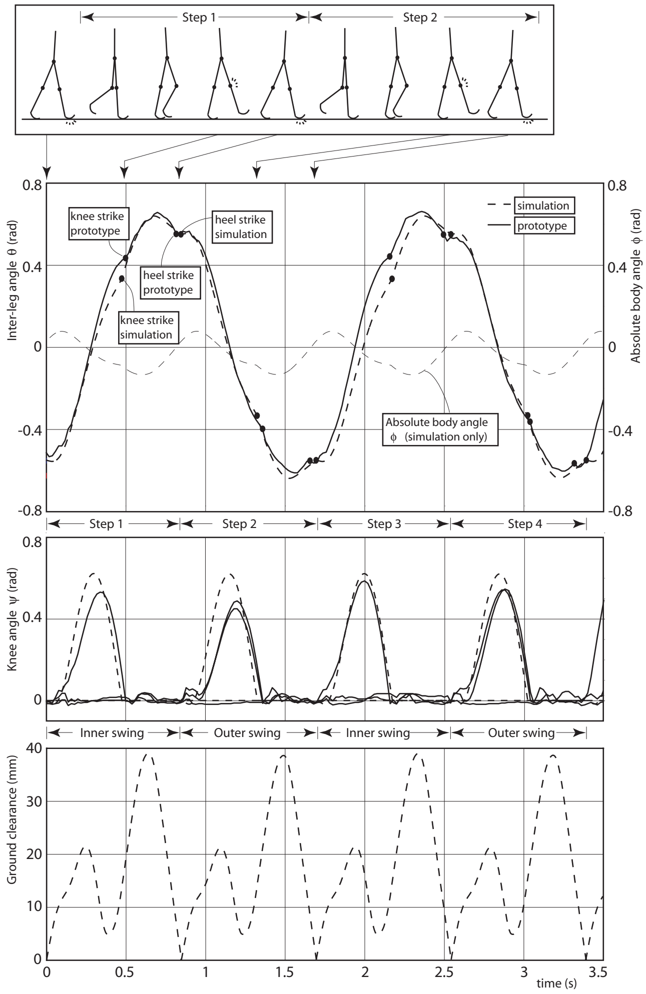

Figure 7.8: *Comparison of the walking motion of the simulation (dashed lines) and the prototype (solid lines). The absolute body angle ϕ and the clearance were not measured in the prototype. The inter-leg angle shows a slight asymmetry in the prototype's gait. The knees of the prototype show approximately 0.05 rad play of the latch.*

The resultant walking motion is depicted in Figure 7.8, in which we have plotted both the simulation results and the actual prototype recordings. The figure presents the absolute body angle (simulation only, not measured in the prototype), the relative hip angle and the knee angles as a function of time, together with the foot clearance (also simulation only). The clearance amounts to 5 mm or more throughout the step. The body remains approximately upright with maximal excursions of ± 0.15 rad. The knee reaches full extension 0.5 s after the start of the swing phase. The maximal inter-leg angle is ± 0.65 rad, but at the time of heel strike this is ± 0.55 rad, leading to a step length of 0.35 m. The model is walking in its limit cycle, taking 1.2 steps per second thus walking at 0.42 m/s (Table 7.2).

Table 7.2: *Gait characteristics when walking with the default parameter values.*

Step length	0.35 m
Step frequency	1.2 Hz
Velocity	0.42 m/s
Nominal clearance	5 mm
Specific resistance	0.2 $\mathrm{J/(kgm^2s^{-2})}$

The differences between the motions of the model and the prototype are small, especially when considering that the model is walking in its limit cycle while the prototype is only *close to* its limit cycle due to constant disturbances; the floor is far from perfectly flat and level. A noticeable difference is in the amount of knee flexion. Especially the knees of the outer legs bend less than predicted by the simulation, probably caused by friction and damping in the knee joint or by a slight delay in the knee latches. The overall effect on the walking motion is small, except for the foot clearance which then decreases significantly and indeed causes most of the failures.

7.4.2 Stability

The stability of the cyclic walking motion is usually analyzed by investigating the initial states of each step in a sustained walking motion. We choose to defer from this and to investigate the *end* states instead of the initial states. The difference is that our analysis is based on the velocities just *before* heel strike in contrast to the tradition of using the velocities just *after* heel strike. The reason is that the velocity measurements in the prototype are unreliable just after an impact due to transient oscillations in the mechanical system.

At the end of a step, with both feet simultaneously on the floor and with both knees extended, there are only three independent states; inter-leg angle θ, its angular velocity $\dot{\theta}$ and the absolute angular velocity of the body $\dot{\phi}$. Their fixed point values given in Table 7.3 are determined with the computer simulation for the parameter values in Table 7.1. A linearized stability analysis with the computer model predicts that the walking motion is stable, i.e. that small errors on the end states in Table 7.3 decay step after step.

Table 7.3: *Fixed point values for the three independent end states just before heel strike, valid for the parameter values from Table 7.1. The difference between simulation and prototype arises from the simplified model for the non-linear muscle behavior.*

		sim.	proto. (aver. ±s.d.)
Inter-leg angle	θ (rad)	0.55	0.55 ±0.06
Inter-leg ang. vel.	$\dot{\theta}$ (rad/s)	-0.58	-1.15 ±0.61
Upper body ang. vel.	$\dot{\phi}$ (rad/s)	1.04	1.03 ±0.17

Fig. 7.9 shows the walking results of over 200 steps (measured in series of 40 steps on average) depicted in the phase plane. The graph only represents two out of the three independent states because the inter-leg angular velocity $\dot{\theta}$ is not relevant; Table 7.3 shows a high variability for this state and the simulations have shown us that even much larger variations on this state can be allowed without resulting in a failure. The reason for this insensitivity is the fact that the inter-leg angle is controlled by the hip muscles toward a fixed end position, independent of the initial velocity. The difference between the measured average and the simulated value for $\dot{\theta}$ is a direct result of the simplified model for the muscle non-linearities at maximal extension.

The experimental results are indicated with black dots in Fig. 7.9. The last step in a series is indicated with an encircled cross, because it is the last step before a fall. These experimental results correspond well with the simulation results, which are indicated in the figure with the gray area. According to the simulation model, the gray area is the basin of attraction; a start outside the area will either lead to a fall Forward or a fall Backward. The average state (indicated in Fig. 7.9 with a white encircled dot) also corresponds neatly to the fixed point from the simulation model (white circle), see also Table 7.3.

The stability results indicate that the prototype can be easily started with a manual launch (illustrated in Fig. 7.10). After such a launch the prototype can walk indefinitely on a level floor until it runs out of power or into a wall. In contrast to the robustness against disturbances in a manual launch, the walker appears to be not too robust against variations in height in the floor surface. The variability of the measurements is quite large. This is a result from the irregularities in the hallway floor. The floor has variations in height of maximally 3.5 mm in one step, amounting to a local slope of ± 0.5°. These irregularities are close to the maximal allowable disturbances as predicted by the simulation model, explaining why some of the measurement points are close to the boundaries of the basin of attraction. The simulation predicts that the walker can handle a step down in the floor of maximally 3 mm. We verified this with an experimental

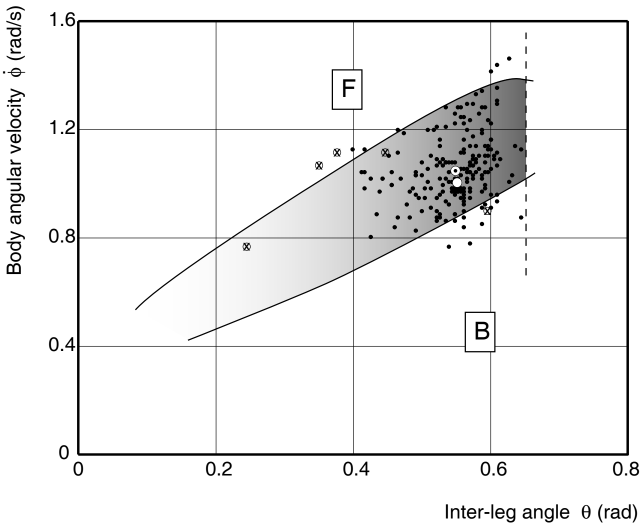

Figure 7.9: *A section of the basin of attraction in the Poincaré map. The figure shows the two most sensitive states at the end of a step, namely the inter-leg angle θ and the angular velocity of the upper body $\dot{\phi}$. The walker is not sensitive to variations in $\dot{\theta}$, the third independent end state, which is therefore not shown. The black dots represent 200 measured states during continuous walking, whereas the last step of each series of steps (the last before a fall) is indicated with an encircled 'x'. The boundaries of the basin of attraction as derived from the simulation are given by the solid black lines. Below the lower boundary, the robot falls Backward, above the upper boundary it falls Forward as a result of foot-scuffing. The dashed line represents maximal extension of the hip muscles. Due to the hip actuation the robot is not likely to arrive in the lower left part of the basin of attraction, but if it would, it would return stably to its limit cycle. The fixed point of the simulation is a white circle, the average measured state is a white circle with a dot.*

setup where it walked on a rigid, flat and level surface (not the hallway floor) and then took a step down. Indeed it could handle not much more than 3 mm.

7.4.3 Parameter sensitivity

The prototype is tolerant to variations in most of the parameters (e.g. 1 kg of extra mass on the upper body has no noticeable effect), except for those parameters that affect the forward velocity. The forward velocity is the net result of the velocity increase during the stance phase and the instantaneous velocity decrease at heel strike. The velocity increase is determined by the amount of time that the robot's center of mass spends *behind* the foot contact point (deceleration) and the amount of time spent *in front of* the contact point (acceleration). Any parameter that influences these has a strong effect on the walking motion; with too much deceleration the walker will have a tendency to fall backward whereas with too much acceleration the resultant walking velocity will be high

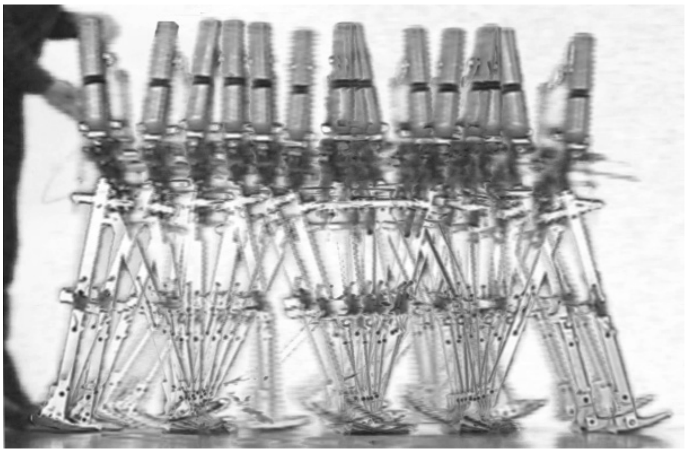

Figure 7.10: *Video stills illustrating the walking motion after a manual launch.*

and thus the chances of falling forward increase.

Parameters with a direct influence are b_w, u_w, and l_w (Fig. 7.4 and Table 7.1) which determine the horizontal position of the center of mass and f_a and f_h which determine the foot contact point. The effect of the position of the center of mass is strong. For our 10 kg walker, a 500 g additional mass that can be attached up to 100 mm in front or behind the hip joint already provides sufficient tuning possibilities. In our opinion, the automatic control of the fore-aft balance will be one of the major improvements for future dynamic walking robots.

The foot radius f_a determines how much the foot contact point travels forward during the stance phase and thus a larger radius has a weakening effect on both the robot's deceleration and acceleration. Previous experiments and simulations [94] have shown that this effect is beneficial to the robot's robustness against disturbances. A forward foot offset $f_h > 0$ creates a forward tilt of the entire robot (best visualized in a drawing of the heel strike state) and thus results in faster walking. Therefore, an increase in f_h should be accompanied by a backward displacement of the center of mass. Note that this observation is only valid for a walker with an upper body with the bisecting hip mechanism and with a substantial mass at a substantial distance above the hip joint. For walkers without an upper body, the effect is reversed.

The hip actuation has an indirect but significant influence on the deceleration and acceleration during the stance phase. For any walker with physically feasible parameter values (also without upper body), the center of mass moves forward when the swing leg is swung forward. This is best verified in a simplified analysis without gravity. If the swing leg is moved quickly by a strong hip actuation, then that forward displacement takes place early in the stance phase, and thus the center of mass will spend relatively more time in front of the foot contact point. In other words, the faster the swing leg is moved forward, the faster the robot will walk. The strength of this effect depends on the amount of inertia (of both the legs and the upper body) that is involved when the hip actuators are engaged.

There seems to be a counterproductive effect here, as the hip actuation was installed in the first place to *reduce* the chances of falling forward and now it appears to *increase* that chance by increasing the walking velocity. This can be resolved easily, however, with a backward adjustment of the robot's center of mass so that the total effect (of hip actuation and mass displacement) is an enlargement of the basin of attraction.

In conclusion, the parameters of the upper body barely influence the walking behavior and the stability. There is almost no effect of an increase of the mass or a vertical displacement of the center of mass. Only the fore-aft position of the center of mass is important, as it regulates the average forward walking velocity, and thus the chances of falling forward or backward.

7.4.4 Energy efficiency

The energy consumption of walking mechanisms is usually expressed with the non-dimensional 'specific cost of transport', i.e. the amount of energy used per unit transported system weight ($m \cdot g$) per distance traveled. For comparison, a walking human being has a specific cost of transport of 0.38 [65], measured by the amount of O_2 uptake. The specific cost of transport of our prototype is calculated with the CO_2 expansion through the muscles from the 0.6 MPa input pressure to 0.24 MPa relief pressure. The prototype uses 208 mg CO_2 per step (allowing it to walk for 30 minutes on a single canister). The exergy (or 'availability'), i.e. the amount of work that could theoretically be done with gas expanding from 0.6 MPa to 0.24 MPa, is 10.6 Joule per step, so the specific cost of transport equals 0.32. Although the specific cost of transport for the prototype resembles that of a walking human being, some deliberations must be taken into account.

On the one hand, one could argue that the prototype is much more efficient than the human. The pneumatic muscles are not optimal for their task, because they have a fairly large 'dead volume' which must pressurized at each action cycle. They use much more pneumatic energy than the amount of work they produce. We determined with the simulation model that the amount of work produced by the muscles (i.e. their force integrated over their elongation) is only 0.5 Joule per step, leading to a very low specific cost of transport of 0.01. Note that this value is in the same range of the fully passive walkers as in Fig. 7.2a and b.

On the other hand, one could argue that the prototype is much less efficient than the human. The specific cost of transport for the human includes the metabolic cost of the entire system, and specifies how well the available energy is used. In that respect, it would be fairer for the prototype calculations to also include the idle pressure reduction from 5.8 MPa to 0.6 MPa. Although exact figures are not available, it is certain that the total amount of available pneumatic energy from the CO_2 canister is factors higher than the energy that is used in the muscles. However, the main cause of this apparent waste of available energy is not in the applied concept of passive dynamic walking but rather in the unavailability of pneumatic components that can use the energy of the high-pressure canister. It is expected that ongoing research in the field of pneumatics will eventually solve this problem.

7.5 Conclusion

This paper reports on the successful addition of an upper body to a walking robot based on the concept of passive dynamic walking. The upper body is connected to the legs by means of a bisecting hip mechanism which forms a passive solution to stabilize the upper body while simultaneously allowing a passive swing leg motion. The prototype walks stably and efficiently. The fore-aft position of the center of mass of the upper body is a powerful parameter for the stability of the walking motion. Conversely, the height of the center of mass, the total mass and the mass distribution have no noticeable influence on the performance. Thus, we conclude that the bisecting hip mechanism forms a practical and simple solution to construct efficient bipedal walking robots, in agreement with the concept of passive dynamic walking.

Acknowledgements

This research is funded by the Dutch National Technology Foundation STW. The mechanical work was done by Jan van Frankenhuyzen.

Chapter 8

Three additions to passive dynamic walking; Actuation, an upper body, and 3D stability

M. Wisse

Submitted to *International conference on Humanoid Robots*, 2004.

One of the main challenges in the design of human-like walking robots (useful for service or entertainment applications as well as the study of human locomotion) is to obtain dynamic locomotion, as opposed to the static form of locomotion demonstrated by most of the current prototypes. A promising concept is the idea of passive dynamic walking; even completely unactuated and uncontrolled mechanisms can perform a stable gait when walking down a shallow slope. This concept enables the construction of dynamically walking prototypes that are simpler yet more natural in their motions than the static bipeds. This paper presents three additions to the concept of passive dynamic walking. First, hip actuation is added to increase the fore-aft stability and to provide power to the system, removing the need for a downhill floor. Second, a bisecting hip mechanism is introduced to allow the addition of a passive upper body without compromising the simplicity, efficiency and naturalness of the concept of passive dynamic walking. Third, skateboard-like ankle joints are implemented to provide 3D stability. These ankles couple the unstable sideways lean motion to yaw (steering), a kinematic coupling which provides sideways stability when walking with sufficient forward velocity. The three additions are investigated both with elementary simulation models and with prototype experiments. All three prototypes demonstrate an uncannily natural and stable gait while requiring only two foot switches and three on/off actuators.

8.1 Introduction

Robots that walk in a human-like manner are a fascinating topic of research. The potential benefits range from robots for entertainment or service jobs via insights in the control of complex dynamical systems to knowledge for the restoration of impaired human locomotion. Currently, one of the major challenges for research on human-like walking robots is to move from *static* walking to *dynamic* walking.

The main difficulty of human-like walking is the unilateral nature of the foot contact. The foot can only exert compressive forces to the floor and thus it can possibly tip over on one of the edges. This makes the system fundamentally underactuated. Moreover, the unactuated degree of freedom is to be operated around an unstable equilibrium position. Therefore such systems are a challenge for classical control techniques. The classical solution is to make sure that the tipping-over does not happen. A very crude method is *static walking* where the center of mass is kept above the floor contact polygon *and* the acceleration forces are kept insignificant. A more sophisticated method is the *Zero Moment Point* approach [81] in which the 'Zero Moment Point' (which coincides with the center of pressure [28, 82]) is kept within a safe area inside the foot edges. With these methods the foot remains flat on the floor allowing the control designer to pretend that the problem of underactuation does not exist. These methods form the basis of today's most sophisticated humanoid robots [68, 46].

Although the extra 'flat-foot'-constraint superficially simplifies the control problem, in reality it might result in unnecessarily complex walking systems. Therefore we will investigate systems which do not ignore the fundamental underactuation and thus show dynamic motion in the passive foot-floor contact. This has been called *dynamic walking*. An extreme example of dynamic walking is McGeer's *Passive Dynamic Walking* [49] in which not only the foot-floor contact is passive but also all other joints in the system. By showing that such systems are potentially capable of stable, human-like walking *without any control*, his work suggests that human-like walking can be realized with much simpler machines than the present-day prototypes.

To move from the relatively basic state of the art in Passive Dynamic Walking (Section 2) toward more versatile and human-like machines, this paper presents three additions to the concept; hip actuation which greatly enhances the 2D stability (Section 3), a bisecting hip mechanism which allows the addition of a passive yet stable upper body (Section 4), and a skateboard-like ankle joint which provides 3D stability (Section 5). Each of the three additions is investigated through a qualitative comparison of elementary model studies and physical prototype experiments.

8.2 Passive Dynamic Walking

8.2.1 Historical background

Biomechanical research has provided several hints toward the possible role of passive dynamic motions in human walking. A remarkably relevant hypothesis posed by Weber and Weber [84] as early as 1836 reads: 'Die Beine können am Rumpfe wie Pendel hin und her schwingen. (...) Unsere aufmerksamkeit wird für diese schwingende Bewegung nicht erfordert.' ('The leg can swing back and forth like a pendulum suspended from the body. ... Our attention is not required to produce this swinging motion.') Mochon and McMahon [53] arrived at the same conclusion after comparing the swing leg motion with a passive double pendulum. Another hint in that direction is given by Ralston [65] who discovered that there exists an optimal walking velocity for humans; at approximately 5 km/h the specific resistance (also termed specific cost of transport, i.e. energy cost per weight per distance traveled) is minimal, a phenomenon that indicates the use of natural frequencies of the mechanical system.

Early toy makers [23] proved the applicability of the ideas by showing that the human walking motion can at least partially be generated with passive mechanisms that move and oscillate in their natural frequencies. In 1989, McGeer [49] proposed that those passive mechanisms could serve as an alternative point of departure for the synthesis of bipedal gait. He parallelled this to the approach of the Wright Brothers, who first mastered passive gliding before they added an engine to their aeroplane. McGeer showed that a completely unactuated and therefore *uncontrolled* robot can perform a stable walk [48] when walking down a gentle slope. Since then, his work has been extended gradually by Ruina's group at Cornell University [15, 24, 19] up to the point where the passive approach can be regarded beyond doubt as a valid starting point for bipedal gait synthesis and robot construction.

The benefits of the passive approach are the inherent efficiency of the walking motion, the natural-looking motions, and the simplicity of the required construction. The development toward a more human-like versatility should be taken step-by-step (figuratively), which can be seen as both a benefit and a drawback of this approach. The drawback is that, although the motions of the early machines are uncannily natural, the general public is quickly disappointed with the incompleteness of the system (e.g. no upper body, lateral constraints to ensure only two-dimensional dynamics, no velocity control). This makes the passive approach unattractive for industrial developers. The required incremental addition of versatility does, however, provide ample opportunities to discover fundamental dynamic properties. As such, the passive approach is the most appropriate point of departure for academic research into gait synthesis.

8.2.2 State of the art

Since McGeer, much research has been done on passive dynamic walking, but even more remains to be done. McGeer left the field after the completion of a biped with knees which was laterally constrained (2D dynamics) by a symmetric construction with two pairs of legs. Simulation studies on fully passive models were performed by Garcia [27] and Goswami [30], whereas Hurmuzlu [38], Spong [73], Van der Linde [78] and Asano [8] added some form of actuation and control. Wisse [90], Piiroinen [60], Adolfsson [6, 7], and Kuo [43] simulated near-3D models, whereas Coleman [17] simulated a fully passive, full 3D model. That last model was one of the few that was matched to a physical prototype [18]. Other prototypes were built by Collins [19], Van der Linde [77], Ono [57, 58] and Tedrake [75], whereas Pratt [62] included passive dynamics in an otherwise active robot.

Almost all walkers in this list consist of legs only, most of them are fully passive, and many exist only as computer models. Also, all of them require a disturbance-free environment. To advance from this state of the art toward human-like walking capabilities, at least the following topics need to be addressed:

- the robustness in 2D must be increased,
- an upper body must be added,
- robustness in 3D must be obtained,
- the walking velocity must be controllable,
- the walker must be able to start and stop,
- the walker must be able to turn,
- the walker must be able to stand up after a fall,

The increase in complexity and actuation must be carried out step-by-step. For each addition, it should be ensured that the beneficial characteristics of passive walking (efficiency, naturalness, and simplicity) are preserved, and that the fundamental dynamic properties and effects in the entire system with the new addition are understood. The current paper focuses on the first three topics; an increased robustness in 2D, the addition of an upper body, and the search for robustness in 3D.

8.2.3 Stability analysis

Dynamic walking requires a special form of stability analysis; not the classical approach with linearized, continuous control, but rather the numerical tools from nonlinear dynamic systems theory. The walking system (e.g. Garcia's 'Simplest Walking Model' [27], Fig. 8.1) is regarded as a dynamic system in a limit cycle; a repetitive motion for all but one of its coordinates (forward progression is non-cyclic). To analyze the stability of such systems the standard method of Poincaré Mapping is applied (originally introduced by Poincaré for the analysis of celestial mechanics and the discovery of chaos). For a well-defined state of the system (the Poincaré Section), usually the state at heel contact, it is analyzed how the cyclic coordinates and velocities progress from step to step. In the limit cycle, the system state is equal at every pass through the Poincaré Section, termed a *fixed point* on the *Poincaré Map*. If errors upon the fixed point decay step after step, the walking motion is asymptotically stable. If on top of that the *basin of attraction* is sufficiently large, the system possesses a practical stability. The basin of attraction (Figs 8.2 and 8.3) is the range of errors for which the system still converges to the limit cycle. If it is sufficiently large, the system under consideration is a candidate for the synthesis of human-like walking machines. These analyses must be performed for each addition to the passive walkers to investigate its practical viability.

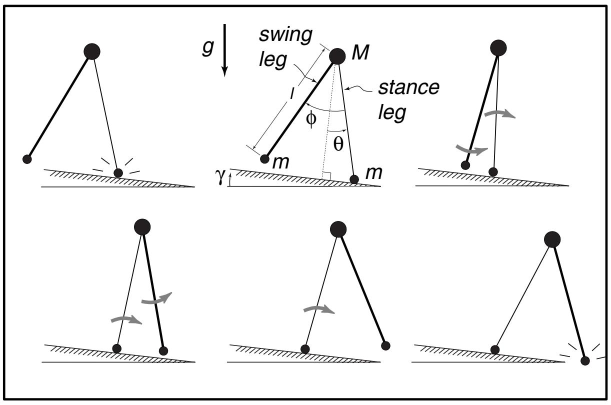

Figure 8.1: *A typical passive walking step. The new stance leg (lighter line) has just made contact with the ramp in the upper left picture. The swing leg (heavier line) swings until the next heelstrike (bottom right picture). The top-center picture gives a description of the variables and parameters that we use. θ is the angle of the stance leg with respect to the slope normal. ϕ is the angle between the stance leg and the swing leg. M is the hip mass, and m is the foot mass. l is the leg length. γ is the ramp slope, and g is the acceleration due to gravity. Reprinted with permission from Garcia et al. [27].*

8.3 Hip actuation for power input and stability

8.3.1 Elementary model study

The first addition to the concept of passive dynamic walking is actuation in the hip joint which greatly enhances the 2D (forward) stability. Although the purely passively walking prototypes demonstrate convincing walking patterns, they all require a smooth and well adjusted walking surface. A small disturbance (e.g.

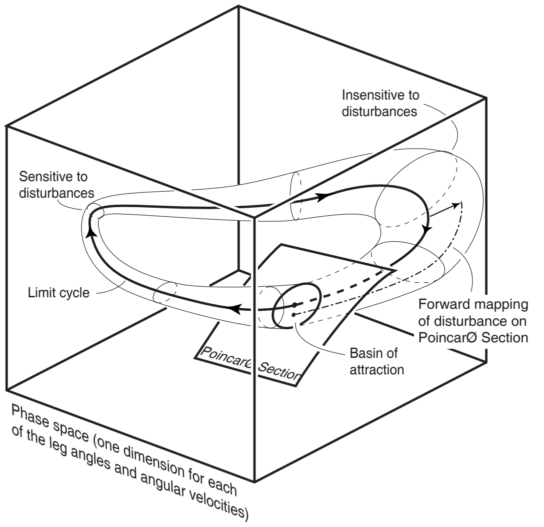
Insensitive to
disturbances
Sensitive to
disturbances
Limit cycle
Forward mapping
of disturbance on
PoincarØ Section
Basin of
attraction
PoincarØ Section
Phase space (one dimension for each
of the leg angles and angular velocities)

Figure 8.2: *Stylized phase graph of walking motion. The dimensionality of the graph is usually much higher than the three dimensions drawn here, so this figure should be considered only as a sketch to convey the ideas behind the stability analysis of cyclic (walking) motions.*

from small errors introduced with a manual launch) can still be handled, but larger disturbances quickly lead to a failure [71], see Fig. 8.3. The most distinct failure is a fall forward; the swing leg is not timely in a forward position to catch the robot for its next step. A second type of failure is an instability that manifests itself as a diverging alternation of short and long steps. This is the result of the interaction between step length, energy input, and energy loss at the heel strike impact.

Both types of failures can be prevented by means of a simple control rule which accelerates the swing leg to a preset forward position [93]; the faster the swing leg is swung forward, the more robust the walker is against disturbances. The exact motion of the swing leg is irrelevant which allows for a wide variety of possible implementations. In the most extreme (and theoretical) case, the swing leg is instantaneously brought to its forward position, making the dynamic behavior comparable to that of a *rimless wheel* [16], i.e. a cart wheel without the rim, walking on its spokes.

For practical robots, instantaneous positioning is impossible because the legs have a non-zero inertia. We investigated the stability improvement as a function of different levels of actuation. The hip actuation is implemented in the model with a critically damped spring with a forward setpoint, where a higher spring stiffness means a higher level of actuation. Fig. 8.3 shows that the basin of attraction increases as a function of the level of actuation, leading to the conclusion that the faster the swing leg is brought forward, the better the model is resistant against disturbances. Another important effect of the leg inertia in real

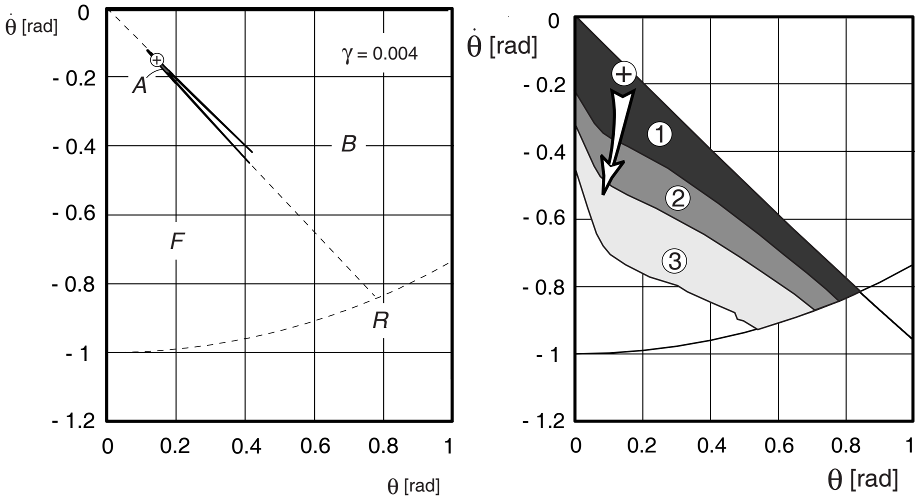

Figure 8.3: ***Left:*** *Poincaré section for the simplest walker (Fig. 8.1 with initial stance leg angle* θ *and velocity* $\dot{\theta}$ *together with failure modes; falling* *Forward, falling* *Backward and* *Running, and the basin of* *Attraction of the cyclic walking motion* $(\theta, \dot{\theta}) = (0.1534, -0.1561)$ [rad] *(indicated with '+') at a slope of* $\gamma = 0.004$ [rad]. *Reprinted from [71].* ***Right:*** *Basin of attraction of the simplest walker with active hip spring. The setpoint of the hip spring is* $\phi_{sp} = 0.3$ *and critical damping is applied. The higher the hip spring stiffness, the larger the basin of attraction;* $k = 25$ *leads to area (1),* $k = 50$ *leads to area (2), and* $k = 100$ *leads to area (3). The fixed point is for all three stiffness settings approximately the same, located at the '+'. A disturbance from a step down in the floor would result in initial conditions away from the fixed point in the approximate direction of the white arrow. Reprinted from [93].*

prototypes is the fact that the hip actuation also provides an energy input into the system. This side-effect eliminates the need for downhill walking and thus drastically increases the usability of the concept of passive dynamic walking.

8.3.2 Prototype experiments

We applied the proposed swing leg control to our prototype 'Mike' (Fig. 8.4a). Mike weighs 7 kg and measures h x b = 0.7 x 0.4 m. An elaborate description of Mike can be found in [94] while movie clips of Mike in action are available at our web site [85]. Mike has four legs symmetrically paired, giving it approximately 2D behavior. It differs from the simplest walking model by having knees, a distributed leg mass, round feet and by walking on a level floor (no slope!).

Mike is actuated with a total of eight McKibben muscles; lightweight pneumatic actuators that act like springs with a stiffness proportional to the internal pressure [14, 76]. The McKibben muscles are arranged according to Fig. 8.5. The hip joint is actuated with an antagonistic pair of muscles (A) and (B) providing a combined joint stiffness. The knees are actively extended with McKibben mus-

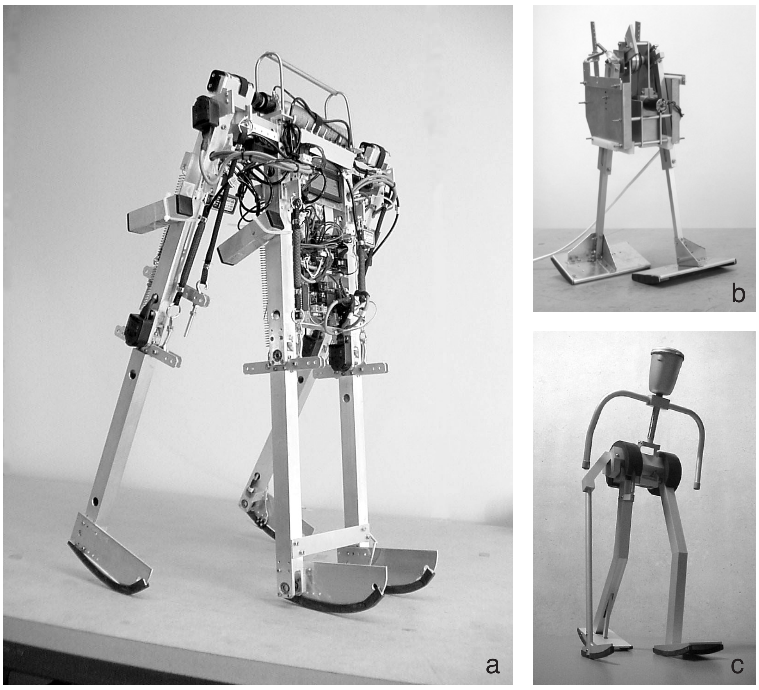

Figure 8.4: *2D machines built during the project: (a) Mike, (b) Latch Walker, (c) Museon Walker.*

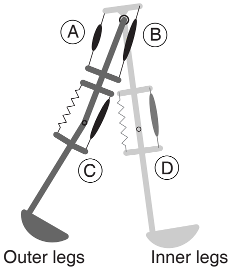

Figure 8.5: *Schematic structure and muscle attachments of Mike.*

cles (C) and (D) which are counteracted by weak passive springs. There is no ankle actuation; the arc feet are rigidly attached to the shanks.

The McKibben muscles are fueled from a 5.8 [MPa] CO_2 container via a two-stage pressure regulator and via electromagnetic valves that are activated by switches underneath the feet. The second-stage pressure regulator output is manually adjustable between 0.1 and 0.6 [MPa] resulting in a hip joint stiffness up to 5 [Nm/rad] and a damping somewhat less than critical damping (estimated by observation). It is not feasible to perform a proper mapping between this stiffness in Mike and the scaled stiffness in the simplest walking model due to the extensive differences between the two, such as leg mass, foot arc radius, muscle non-linearities and significant air flow dynamics. Therefore the comparison between the two will be of a qualitative nature only.

If a valve is switched 'on', the muscle is filled from the pressure regulator output; if switched 'off' it reliefs into atmosphere. For example, at activation of the inner leg foot switch, the outer knee muscles (muscle C in Fig. 8.5) are switched 'off' to allow this knee to bend. A manually tuned 400 [ms] later they are switched back 'on', ensuring a properly extended knee for the next step.

The proposed swing leg control is implemented by alternating the states of the antagonistic hip muscles. When the foot switch of the inner legs is activated, muscle B in Fig. 8.5 is switched 'on' and muscle A is switched 'off'. At the next step this is inverted. As a result, the hip joint has a constant stiffness but a setpoint that alternates between ϕ_{sp} and $-\phi_{sp}$. The joint stiffness can be adjusted without altering the setpoint. We want to emphasize that there is no feedback control other than this once-per-step switching between preset muscle pressures. We dub this 'feet-forward control'.

Mike walks at 0.4 m/s (0.6 s per step), see [85] for video evidence. We would have liked to create a figure of its basin of attraction like Fig. 8.3. However, the combined limitations on the number of experiments to be performed and on the physical possibilities to create controlled disturbances have led us to concentrate on one representative disturbance, namely a step-down.

In the experiments the prototype walks steadily and then takes a step down of increasing height, see Fig. 8.6. Such a step down results in a larger stance leg velocity at the subsequent step as sketched with the white arrow in Fig. 8.3. The larger the step down height, the larger the arrow. If a larger hip muscle stiffness indeed allows a bigger step down, then our swing leg control rule is validated.

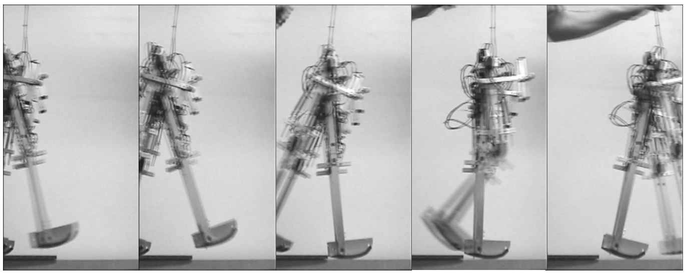

Figure 8.6: *Experiment with Mike walking on level floor and taking a step down as a representative disturbance.*

The stability results are shown in Fig. 8.7. A hip muscle pressure lower than 0.35 [MPa] did not provide stable walking at all, not even without disturbances. When the pressure was increased, a larger step down could be handled. The muscles prohibit pressures higher than 0.55 [MPa]. Fig. 8.7 clearly shows a better robustness against falling forward with a higher hip pressure which corresponds to a faster swing leg motion.

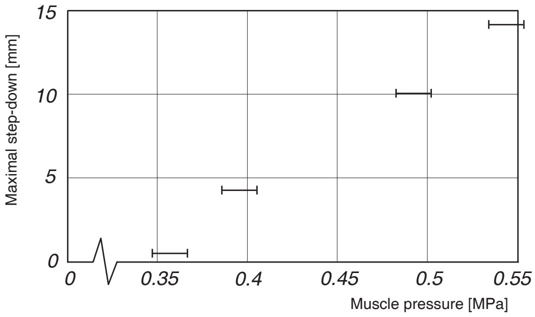

Figure 8.7: *A higher hip muscle pressure setting (corresponding to a higher hip joint stiffness) results in a larger step-down size and thus in a better resistance against disturbances.*

After these successful results, the same form of stabilization by means of an accelerated swing leg was used to construct two demonstration prototypes. The 'Latch Walker' (Fig. 8.4b) walks on level floor using a single, uncontrolled DC motor (its constant energy input is regulated by means of a wind-up spring and a latch in the hip joint). The 'Museon Walker' (Fig. 8.4c), which was on display in a hands-on technical exhibit, requires a sloped walking surface and obtains its swing leg acceleration from a mechanism at the hip joint which effectively lowers the center of mass to provide energy to the swing leg.

8.3.3 Conclusion

Both the elementary simulation and the prototype experiments demonstrate that a simple controller can solve the problem of falling forward; all it needs to do is to get the swing leg timely in a forward position. Both the elementary simulation and the prototype experiments show a similar qualitative effect; the higher the level of actuation, the better the robustness against disturbances. For implementation of this form of control, a damped hip spring with a forward setpoint already suffices. The specific control and actuation details are not important as the same result can be achieved with any configuration if it is based on the following rule: *"You will never fall forward if you put your swing leg fast enough in front of your stance leg. In order to prevent falling backward the next step, the swing leg shouldn't be too far in front."* A controller designed according to this rule is easy to implement, because no a-priori knowledge of the passive dynamic walking motion is needed.

8.4 Bisecting hip mechanism for passive yet stable upper body

8.4.1 Elementary model study

The second addition to the concept of passive dynamic walking is a bisecting hip mechanism for the addition of a passive upper body. The bisecting hip mechanism was first explored in a highly simplified model consisting of four point masses connected by rigid, massless links [92] (Fig. 8.8). The study revealed the possibility of fully passive walking with an upper body by means of a bisecting hip mechanism. For a lightweight upper body, the dynamic effects of the passively swinging legs are dominant. When the weight of the upper body increases, a hip spring is required to maintain the upright position as the equilibrium position. The study showed that a suitable spring stiffness can be found for any mass distribution.

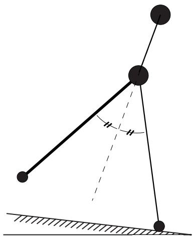

Figure 8.8: *Simple model for preliminary study of passive bisecting hip mechanism.*

A parameter study with the simple model showed the effects of the upper body on the stability and the energy efficiency of the walking motion. One clear result is that the fore-aft mass distribution has a strong influence on the existence and the stability of the cyclic walking motion, matching McGeer's finding of a similar influence of the fore-aft mass distribution in the legs of his walkers. Conversely, the walking motion is very tolerant to changes in the vertical mass distribution. A weak but counterintuitive effect was found, as a higher center of mass provides a better robustness against disturbances. Moreover, elevation of the center of mass also improves the energy efficiency. Altogether, the preliminary study was strongly encouraging to the construction of prototypes with an upper body connected through the proposed bisecting hip mechanism.

8.4.2 Prototype experiments

The idea is validated in the prototype 'Max' [89] (Fig. 8.9), which weighs 10 kg, measures h x b = 1.1 x 0.5 m and walks at 0.4 m/s (0.8 s per step). Max is the direct successor of Mike (Fig. 8.4a); the design and the applied components are more or less identical except for the addition of an upper body and some minor

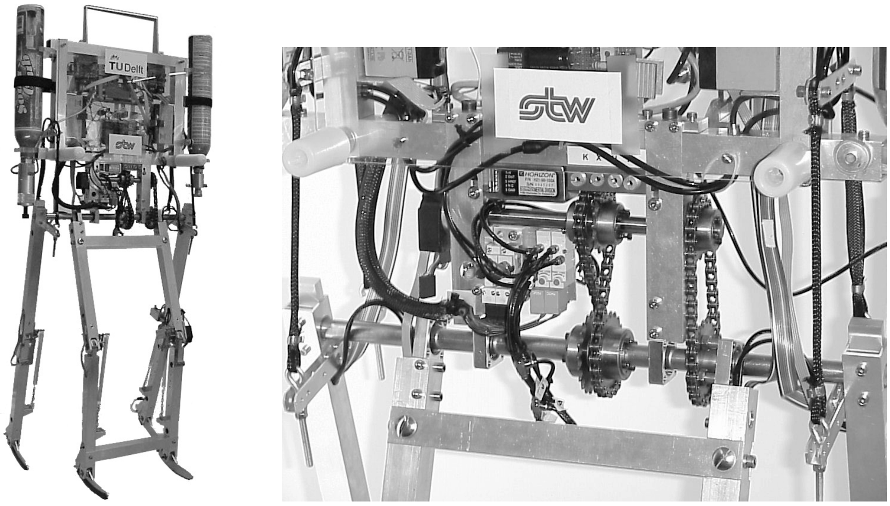

Figure 8.9: ***Left:*** *Prototype Max; a 2D passive dynamic walking robot with an upper body connected to a bisecting mechanism at the hip.* ***Right:*** *The bisecting hip mechanism in the prototype. The outer legs are rigidly attached to the hip axle, the inner legs can rotate freely. The hip axle is connected through bike chains via an auxiliary axle to the inner legs.*

improvements. The improvements include 1) switchable knee latches which remove the need for knee muscles, 2) ankle joints which are frozen now but allow ankle actuation in the near future [34], and 3) a much larger on-board CO_2 storage (two canisters of 450 grams, each of which enables 30 minutes of continuous walking).

The bisecting hip mechanism is implemented with an auxiliary axle connected to the legs with one straight and one cross-over chain (Fig. 8.9). In hindsight, it is valuable to report that this solution requires extra attention to the problem of slack in the chains. Also, one must be aware that rather large torques are transmitted through the chainwheels and axles, especially when the prototype occasionally falls. Nonetheless, for our relatively lightweight prototype this solution is satisfactory. Other possible mechanisms include a four-bar linkage, a differential gearbox, or cables and pulleys (as applied in some gait orthoses [39]). Alternatively, the bisecting hip action can also be obtained in fully actuated robots where a sub-controller maintains the upper body in the bisection angle [64, 12]. We would like to emphasize that any of these solutions, mechanical or controlled, are simple in that they only require *local* information, i.e. the absolute angle of the body or legs are irrelevant, only the relative angles between the three.

Fig. 8.10 illustrates the walking motion after a manual launch. On a reasonably flat and level floor (height variations of less than 3 mm per step), the prototype could easily perform sustained walking with series of over 50 consecutive

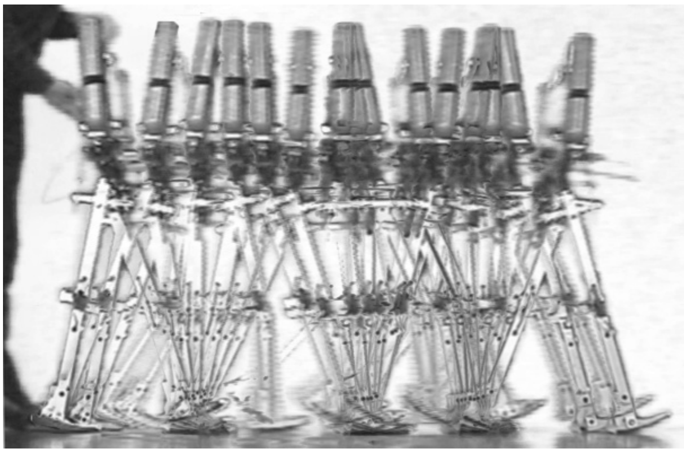

Figure 8.10: *Video stills illustrating the walking motion after a manual launch.*

steps. While tuning the prototype for optimal performance, we found the same parameter influences as predicted by the elementary simulation model. The prototype is tolerant to variations in most of the parameters (e.g. 1 kg of extra mass on the upper body has no noticeable effect), except for those parameters that affect the forward velocity. The forward velocity is the net result of the velocity increase during the stance phase and the instantaneous velocity decrease at heel strike. The velocity increase is determined by the amount of time that the robot's center of mass spends *behind* the foot contact point (deceleration) and the amount of time spent *in front of* the contact point (acceleration). Any parameter that influences these has a strong effect on the walking motion; with too much deceleration the walker will have a tendency to fall backward whereas with too much acceleration the resultant walking velocity will be high and thus the chances of falling forward increase. For our 10 kg walker, a 500 g additional mass that can be attached up to 100 mm in front or behind the hip joint already provides sufficient tuning possibilities. In our opinion, the automatic control of the fore-aft balance will be one of the major improvements for future dynamic walking robots.

8.4.3 Conclusion

In conclusion, the bisecting hip joint allows a straightforward addition of a passive upper body to the concept of passive dynamic walking. Both the elementary simulation model and the prototype show that the parameters of the upper body barely influence the walking behavior and the stability. There is almost no effect of an increase of the mass or a vertical displacement of the center of mass. Only the fore-aft position of the center of mass is important, as it regulates the average forward walking velocity, and thus the chances of falling forward or backward.

8.5 Skateboard-like ankle joint for 3D stability

8.5.1 Elementary model study

The problem of lean instability (the walker is an inverted pendulum in the frontal plane) is usually approached in an isolated fashion; researchers find solutions for the inverted pendulum problem *per se* such as sideways foot placement or reaction torques from the upper body [43]. However, when the full 3D system is regarded, another solution presents itself. Similar to skateboards and bicycles, one could use *steering* (yaw) to stabilize *lean*, at least as long as the system is moving forward with sufficient velocity. The same principle is applicable for walking, and can be implemented in walking robots with an ankle joint that kinematically couples lean to yaw.

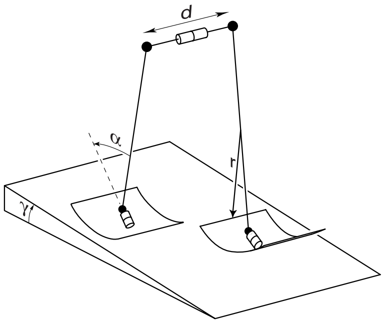

Figure 8.11: *Simplified point-mass model used to analyze the stabilizing effect of a tilted ankle axis that couples lean to yaw.*

We investigated the concept with a simulation study [91]. The simplest model for this purpose is a 3D cousin of Garcia's two-dimensional 'Simplest Walking Model' [27] which consisted of one finite point mass at the hip joint, two infinitesimally small point masses at the feet, and massless rigid links in between, interconnected with a frictionless hinge at the hip. Our model (Fig. 8.11) is a 3D extension of this; the hip has gained a finite width and the hip mass is divided into two point masses at the extremes of the massless hip axle. The degrees of freedom are the coordinates and the yaw and lean angles of the center of the hip axle, the two leg pitch angles, and the two ankle angles. The ankle axes are mounted in the x-y plane at an angle α with respect to the vertical. Note that the ankle axes have no component in the z-direction, unlike conventional robot designs or the human ankle. The 'normal' ankle functionality, rotation around the z-axis, is realized by means of the roll-off motion of the feet. The feet are (partial) cylinder shells with the cylinder axis perpendicular to the ankle axis. The foot-floor contact is modeled as a perfectly rigid cylinder-plane contact with only one degree of freedom; rotation (pitch) in a direction perpendicular to the cylinder axis. The width of the feet is not specified and is assumed to be sufficient to prevent sideways tipping over the edge.

The simulation results can be summarized in four conclusions. First and foremost, the ankle joint indeed provides stability for the 3D walking model. Moreover, the simulation study [91] shows that it is highly robust against disturbances (allowing a 100% deviation on most of the initial conditions) and against parameter changes (allowing a sideways center of mass offset of 5% of the leg length). Second, the simulation study shows that these stability results can only be achieved if the ankle joint is applied in combination with the hip actuation as described in Section 2. Without that, the (fully passive) model is barely stable. Third, the model is stable only if the forward walking velocity is above a certain critical value, a behavior which is similar to that of a skateboard or a bicycle. The critical velocity is a function of the orientation of the ankle joint. The more vertical the joint is oriented, the lower is the critical velocity. Fourth, the ankle joint provides an effective means for direction control; a slight asymmetry in any of the parameters (such as a sideways mass offset) results in a walk on a curved path. All together, the simulations with the elementary model predict a sufficient robustness against disturbances to warrant the construction of a physical 3D prototype.

8.5.2 Prototype experiments

The ankle joint is tested in the prototype ‘Denise’ (Fig. 8.12), which weighs 8 kg, measures h x b = 1.5 x 0.3 m and walks at 0.4 m/s (0.8 s per step). Denise is a direct successor of Max (Fig. 8.9) and has the same hip actuation, bisecting hip mechanism and controllable knee latches. The prototype has five internal degrees of freedom (Fig. 8.12); two ankles, two knees, and one at the hip (the arms are mechanically connected to the opposing leg). The ankle joints are mounted in the non-human orientation as proposed above, namely pointing forward and downward without a component in the lateral direction (Fig. 8.13, making an angle $\alpha = 25^o$ with the leg. The ankles are provided with a high torsional stiffness (Fig. 8.13).

The contact between the foot and the floor is meant to constitute one degree of freedom, namely forward rotation on the foot’s cylindric shape. The foot dimensions are given in Fig. 8.13. The foot has two equal contact rails on the sides to provide as much yaw torque resistance as possible for a given foot width. The degree of freedom in the ankle allows for ground contact with both rails in all situations, but due to the ankle spring it is still possible that the foot tips over sideways on one of the rails (suddenly adding two more degrees of freedom, namely lean and yaw of the foot). Because the stabilizing effect of the ankle joint only exists with full foot contact, we tuned the ankle spring so that this undesired loss of contact does not occur normally.

The main result to report is that Denise walks stably. An illustration of the walking motion is given in Fig. 8.14. With a velocity of 0.4 m/s (0.8 s and 0.3

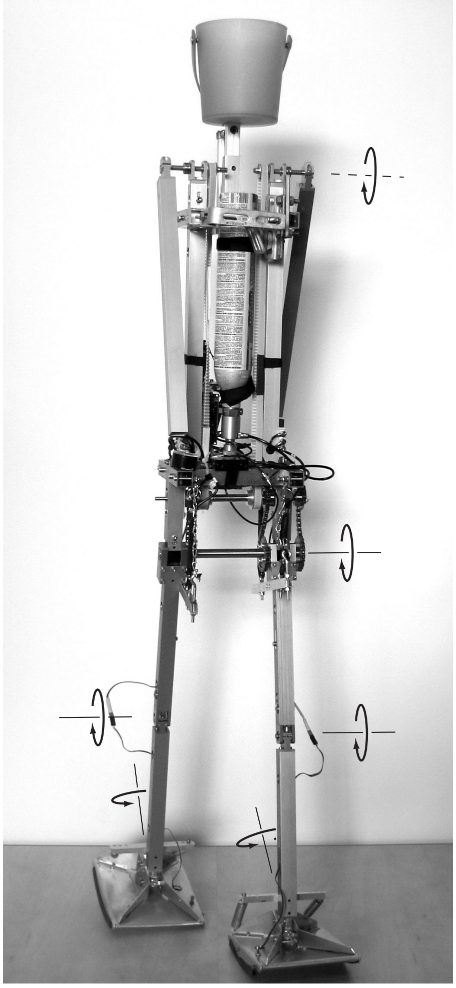

Figure 8.12: *Denise, a 3D dynamic walking robot with 5 degrees of freedom; two ankles, two knees, and one at the hip. The arms are rigidly coupled to the hip angle.*

m per step), it is slower than a human being. It uses 0.3 gram CO_2 per step which allows it to walk for 20 minutes on a single canister. From observations during the experiments we conclude that the prototype is not optimal yet. The prototype demonstrates more frequent failures than the prototypes Mike and Max (Figs 8.4a and 8.9). First, the ankles of Denise had to be equipped with torsional springs and with purposeful friction in the joint before stable walking was achieved. These two features were not part of the elementary simulation model and should not be necessary. We hope to study the influence of the spring and friction in the near future. Second, the foot contact is not entirely yaw-free; at the instant of knee strike of the swing leg, the asymmetric impulse cannot be

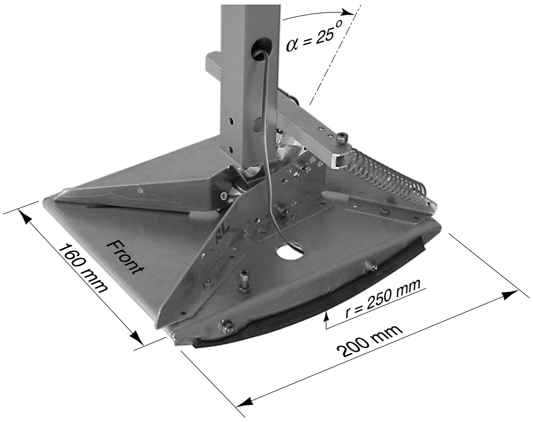

Figure 8.13: *Details of the (right) foot.*

resisted by the friction torque of the stance foot. The prototype is observed to change heading at some of the knee strikes, which is a source of disturbances. Therefore, one of the first directions for future research is to decrease the mass of the foot to decrease the adverse impulse at knee strike. Third, the prototype falls approximately one out of twenty steps due to irregularities in the floor, and when this occurs it is always a fall forward. The solution to this problem has already been presented in Section 3 of this article; apply more power to the hip actuators to bring the swing leg forward more quickly. Unfortunately, we have currently reached the upper power limit of our pneumatic system. A redesign is required before we can increase the level of hip actuation and thereby the stability of the prototype. This current limitation is the reason that we can only crudely recognize the effects that were predicted with the elementary simulation model; the prototype does *not* walk stably 1) when using less than maximal pneumatic power (with the current system) to bring forward the swing leg, 2) when using a less vertical ankle joint (we tried ankle joints of 45^o and 25^o with respect to vertical, it failed with the first and succeeded with the latter), 3) when walking slower than maximally possible (which we tune with the fore-aft mass distribution). A more powerful actuation system is required before we can obtain more quantitative results.

8.5.3 Conclusion

Both the elementary simulation model and the prototype demonstrate 3D stability. The skateboard-like ankle joint forms a simple mechanical ingredient for the design of stable dynamic walking bipeds. The stabilizing effect is only present when walking with a substantial forward velocity and requires the presence of hip actuation as proposed in Section 3 of this article.

Although the idea is strongly linked to a mechanical implementation in the

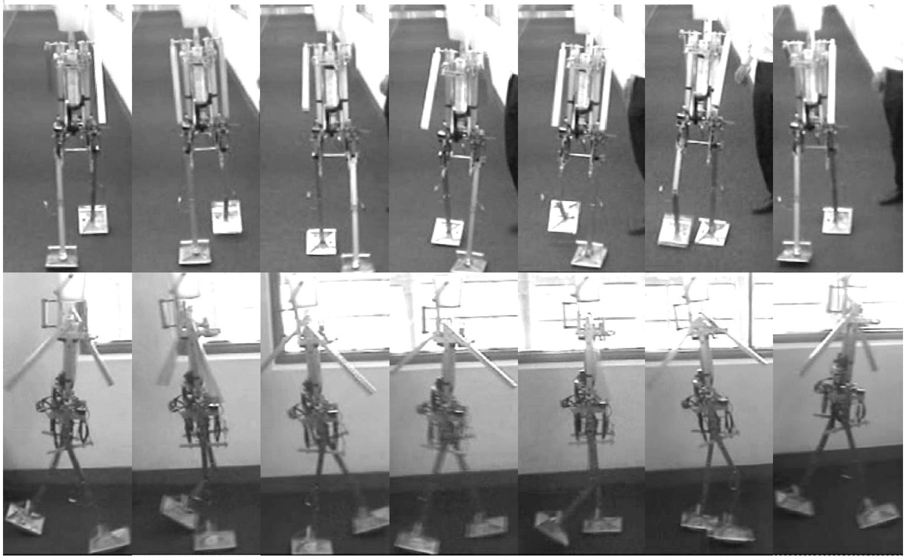

Figure 8.14: *Video stills of Denise walking, two steps (one stride). The video shows a slight turn to the right as a result of a disturbance in the floor.*

form of a tilted ankle axis, there are many alternative ways of implementation, either mechanically or via control, in the foot, ankle, leg, or hip. The central idea is that, if there exists a forward velocity, a sideways fall can be averted by steering in that direction.

8.6 General conclusions

In this article we propose three additions to the concept of passive dynamic walking:

- Actuation at the hip joint results in a drastic increase of the 2D stability of the walkers; the faster the swing leg is brought to a predefined forward position, the smaller the chance that the walker falls forward (the most frequent failure). Additionally, this form of actuation provides sufficient energy to the system to remove the need for a downhill walking surface.
- A bisecting hip mechanism allows the addition of a passive upper body without compromising the efficiency, stability, or simplicity of the concept of passive dynamic walking,
- Skateboard-like ankle joints (which point forward and downward without a lateral component) provide stability for 3D bipeds. The ankle joints are only effective when in combination with the proposed hip actuation and when walking with sufficient forward velocity.

The three additions have enabled us to construct a prototype with a human appearance (two legs with knees, upper body, arms) and a stunningly natural gait. The most significant achievement is that these results were obtained while using a minimal control system; the entire control system consists of two foot switches which trigger three on/off actuators (one hip actuator and two knee latches). Dynamic walking can be obtained with elegantly simple machines.

Acknowledgements

The author wishes to express his gratitude to Jan van Frankenhuyzen who engineered most of the robots, Arend Schwab who advised on multibody dynamics, Richard van der Linde who initiated the project, Frans van der Helm who advised on biomechanics and John Dukker who produced many of the high-quality mechanical components. The research project was funded by the Dutch Technology Foundation STW.

Chapter 9

Discussion, conclusions, and future directions

9.1 Essentials of dynamic walking

The topic of this thesis is the search for the essentials of dynamic, human-like walking. The previous chapters present design solutions for the three *specific* problems that this thesis focuses on: 1) how to increase the robustness of 2D walking motions, 2) how to add a passive yet stable upper body, and 3) how to obtain a stability for 3D walking motions. The goal of the current chapter is to find the overarching effects of the specific solutions to these problems with respect to stability (Sections 9.2 and 9.3), to actuation (Section 9.4), to simulations (Section 9.5) and with respect to human walking (Section 9.6). Section 9.7 will summarize the overarching conclusions of the research in this thesis, followed by future directions in Section 9.8.

9.2 On general design guidelines for stability

The design solutions in this thesis are strongly focused on the specific problems that are treated: 1) hip actuation is a solutions for increasing the robustness of 2D motions, 2) a bisecting hip mechanism is a solution to add a passive upper body, and 3) a skateboard-like ankle joint is a solution for 3D stability. In addition, throughout the thesis arc feet are used as another mechanical feature that provides stability. One of the most intriguing questions now is how these solutions fit together, what general ideas lie behind them, and how do they provide stability to the walking motion?

Stability is one of the main issues in bipedal walking because of the fundamental problem of underactuation at the stance foot. The cause of this is the limited size of human-like feet combined with the fact that only compressive forces can be exerted between the foot and the floor. As a result, only limited torques can be transmitted between the foot and the floor, so that there exist two degrees of freedom (fore-aft rotation and sideways lean) that can barely be actuated. This is a cause for instability because the biped system as a whole is operating around the unstable equilibrium of these fundamentally underactuated degrees of freedom; it can be regarded as an inverted pendulum pivoting at the foot.

To understand how stability of the walking motion is achieved, the term 'stability' must be specified more precisely. Walking is a periodic motion in all degrees of freedom (except for forward travel). Therefore, in the phase space (excluding forward travel) the walking motion forms a closed orbit, see Fig. 9.1. The walking motion is stable if there is orbital stability, i.e. if a deviation from the orbit decreases over time. It is important to note that there is a discrete event in the orbit, namely the change-over of foot support (heel strike). Stabilizing effects can occur during the continuous motion and during the discrete event of heel strike. For example, the 'classical' biped control approach (e.g. Vukobratovic [81]) focuses mainly on stabilizing the orbit during the continuous motion. The robots follow a prescribed trajectory (the continuous part of the orbit) and use control to return to this trajectory after a disturbance. Compare this type of control to a thightrope walker who uses his upper body (plus balancing beam) to stabilize his unstable inverted-pendulum configuration pivoting around the feet. A contrasting example is given with the passive dynamic walkers. Here, or-

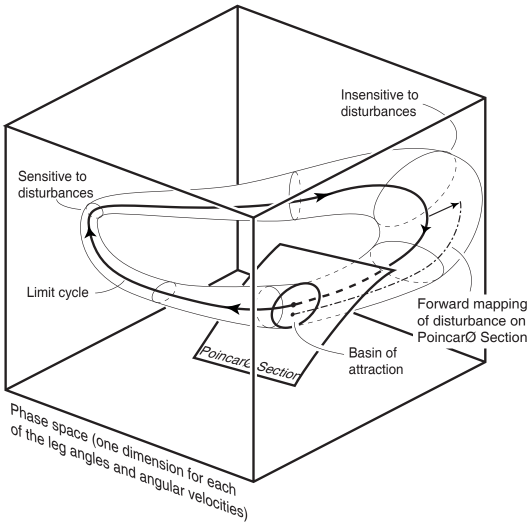
Insensitive to
disturbances
Sensitive to
disturbances
Limit cycle
Forward mapping
of disturbance on
PoincarØ Section
PoincarØ Section
Basin of
attraction
Phase space (one dimension for each
of the leg angles and angular velocities)

Figure 9.1: *Stylized phase graph of walking motion. The dimensionality of the graph is usually much higher than the three dimensions drawn here, so this figure should be considered only as a sketch to convey the ideas behind the stability analysis of cyclic (walking) motions.*

bital stability is mainly obtained from the discrete event at heel strike. The stabilizing effect is the fact that the energy loss at impact is dependent on the forward velocity; if the velocity is too high, more energy is dissipated in the impact and so it provides a stabilizing effect. The stabilizing effect of this impact is stronger than the instability of the inverted-pendulum configuration during the continuous motion. In effect, a small error at the beginning of a step increases during the continuous motion, but the impact strongly brings the motion back to the nominal orbit and thus there is orbital stability. These two extremes (the classical approach versus the concept of passive dynamic walking) illustrate that orbital stability can be realized both by measures during the *continous* motion and during the *discrete event* at heel strike.

The specific solutions presented in this thesis can all be seen as contributions to stability in the two categories:

- **Stabilizing effects during continuous motion.** In the search for simple and efficient mechanical solutions for stability, we do not apply the classical solution. The classical solution is to stabilize the unactuated and unstable degrees of freedom at the feet through intensive control of the actuated degrees of freedom (hip and upper body). This solution is control intensive and requires much energy and high-grade components. In contrast, our approach is to allow a mild instability in the degrees of freedom at the foot, and to focus on implementing features that reduce the rate of divergence from the nominal trajectory after a disturbance to an acceptable level:
  - Arc feet reduce the rate of divergence; the walker is still an unstable inverted pendulum but deviations from the nominal orbit grow slower than in a walker with point feet.
  - The addition of the upper body increases the mass moment of inertia around the foot and thus also reduces the rate of divergence.
  - The ankle joint couples yaw to lean and thus the inertia around the vertical axis is added to the lean degree of freedom, which reduces the rate of divergence of this unstable lean degree of freedom. Note that this requires zero slip in the foot-floor contact. It only works as long as a sufficiently large foot-floor contact can be maintained; if the foot would tip over and make ground contact only at a single point, there would be no yaw friction torque between the foot and the floor.
  - All robots in this thesis are actuated such that they walk at a slightly faster pace than they would if fully passive. As a result, the rate of divergence is slightly decreased *relative to the walking pace*.

  In addition to these effects which are all related to the unactuated degrees of freedom at the foot, our design solutions also affect the remaining degrees of freedom. These remaining degrees of freedom, e.g. the hip joint, pose no fundamental instability problem as they can be actuated and controlled directly. The work in this thesis presents simple and efficient ways to keep these degrees of freedom under control, all in the form of constraints in one form or another:

  - The ankle joint couples yaw to lean and so it constrains the yaw degree of freedom; it is no independent degree of freedom and thus it requires no control. Basically, this reduces the dimension of the phase space.
  - The bisecting hip mechanism also forms a rigid constraint in such a way that the addition of the upper body does not lead to the addition of any degrees of freedom.
  - The knee latches as used in most prototypes lock the knee at the end of the swing phase and all through the stance phase. This is also a reduction of the phase space dimension during an interval at every step.
  - The swing leg control as implemented in the prototypes has the effect that the swing leg is quickly brought to a fixed forward position *and then kept there*. By keeping it in that prescribed position at the end of the step, again the phase space dimension is reduced during the final part of the step.

  All together, in our robots at the end of the step all degrees of freedom are locked or fixed by control so that only the unactuated degrees of freedom at the foot remain. Hence, all other degrees of freedom do not pose a stability risk.

- **Stabilizing effects during the discrete event at heel strike.** To enable a stabilizing effect during the discrete event at heel strike, it is required that this event actually takes place. In our walker designs, several features have been built in to increase the chances that this occurs:

  - The swing leg control has the effect that the swing leg is *quickly* brought to a forward position. This increases the chances of catching the walker for its next step and prevents a fall forward.
  - The arc feet decrease the chances of falling backward and so they help with ensuring the completion of the step.

  The stabilizing effects during the discrete event at heel strike are the following:

  - The impact at heel strike dissipates more energy when the walking velocity is higher and vice versa, and so it provides a regulating effect.
  - The ankle axis results in a steering motion toward the side that the robot leans to. Effectively, this ensures that the next foothold is in a favorable position so that the discrete event at heel strike puts the walker back on the nominal walking orbit.

One of the directions for future research is to investigate how exactly do features such as the arc feet contribute to the orbital stability. As described above, they reduce the rate of divergence due to the inverted-pendulum instability. However, they might also influence the stabilizing effect of the heel strike impact. These effects were not studied in this thesis and warrant further research.

To find and investigate new features that can enhance the stability of the walkers, we advise to regard the stability problem as sketched above; stable walking requires orbital stability which can be obtained both during the continuous motion and through the discrete event at heel strike. The walking orbit can be subdivided in various sub-regions, where a disturbance in each of the sub-regions requires a different approach to obtain stability. An example of this can be found in a recent research result on the human reaction to a tripping disturbance [20]. If the disturbance takes place early in the swing phase it is best to use the swing leg muscles to quickly bring it back into its normal forward motion. However, if this disturbance takes place late in the swing phase, it is better to finish the step without undertaking any special corrective action, and just use the stabilizing effects during the discrete event at heel strike. In this manner, it should be possible to obtain highly robust walking machines using only a handful of simple stabilizing features.

9.3 On stability measures and disturbances

Throughout this thesis, the stability of the walkers is analyzed by means of a Poincaré mapping analysis; how well do they respond to changes in the initial conditions of a step? Although this analysis has proven to be both practical and successful, it should be noted that it is only a limited representation of the complete stability problem in dynamic walking robots. The goal of this subsection is to indicate the limits of the stability analysis as used in this thesis and to point to future directions of research.

Before discussing the limitations of the stability analysis in this thesis, it is useful to briefly recapitulate the essence of the cyclic walking motion. Fig. 9.1 shows a stylized phase space graph of a cyclic walking motion. The axes of the graph contain the states of the walker, for example the leg angles and their angular velocities (note that even for the simplest walker, this is already 4-dimensional, which is why Fig. 9.1 is 'stylized' into a 3D figure). A perfect cyclic walking motion (a *limit cycle*) is represented in this graph with a closed orbit which is followed once per stride (two steps). The Poincaré mapping method uses only one point of that orbit; the point where it crosses a predefined surface, the *Poincaré Section*. For walking systems, this surface is usually defined as the instant of heel strike, a condition that occurs only once per step. If the walker is in a limit cycle, the crossing with the Poincaré Section constitutes a point that maps onto itself stride after stride; a *fixed point*. If the walker is not in a limit cycle, it will cross the Poincaré Section at another point. Following the walking motion stride after stride, one will observe a sequence of points in the

Poincaré Section which either converges toward a fixed point or diverges until a fall occurs and the sequence stops.

In this thesis, all stability analyses were performed in the Poincaré Section. We used two forms of analysis, namely a linearized stability analysis of the fixed point, and an analysis of the *basin of attraction*, i.e. the set of all points in the Poincaré Section that converge to the fixed point. The first form, the linearized analysis, has become common for the stability analysis of walking motions since Hurmuzlu [38] first applied it. For small deviations from the fixed point, this analysis provides insight into wether the fixed point (and the belonging limit cycle) is stable or not, and how fast these small disturbances decrease from stride to stride. In addition to the linearized analysis, this thesis applies the analysis of the basin of attraction. This analysis provides valuable insight into what happens after larger deviations from the fixed point. We learned to which deviations the walkers were relatively sensitive, and what type of fall would follow. Most importantly, the analysis of the basin of attraction pointed us toward the idea for stabilization by means of hip actuation in Chapter 3.

However, one of the important questions is: is the basin of attraction, or any abstraction thereof, useful as an objective measure for robustness? In this thesis, we have pretended that it is, first by measuring the total area of the basin of attraction in Chapters 2 and 3, and subsequently by measuring (over the principal axes) the smallest distance from the fixed point to the boundaries of the basin of attraction in Chapter 4 and 5. The main objection to the first method, measuring the total area of the basin of attraction, is the fact that it wrongfully attaches value to parts of the basin of attraction far away from the fixed point. For example, assume that the original basin of attraction of a walking motion has the shape of a triangle, and that the fixed point is located somewhere close to the top corner. Then, imagine a design change that results in a downward enlargement of basin of attraction, and simultaneously in an upward shift of the fixed point, bringing it even closer to the top corner. Obviously, the outcome of the area measurement of the basin of attraction wrongfully predicts a better robustness against disturbances.

To avoid the wrongful predictions of the measurement of the area of the basin of attraction, our second approach was to measure the distance from the fixed point to the boundaries of the basin of attraction. Starting in the fixed point, the state variables were varied one by one to find the largest allowable deviations both in positive and in negative direction. In this way, we found the distance between the fixed point and the boundary of the basin of attraction in the direction of the principle axes. After having done this for all the states, the smallest value was taken as a measure for the robustness of the walking motion. Although this measure represented an improvement compared to the area measurement, it is still not an objective measure for robustness. The main objection is that the result of the measure depends on how the state variables have been chosen. One could try to make the comparison between two walking models somewhat fair by applying a standardized scaling (as we have done in Chapters 4 and 5 where the models are scaled to unit gravity, leg length and body mass).

However, even with such scaling, the outcome of the comparison would still be different if the state variables were chosen differently. In other words, the 'fixed point to boundary'-measurement is not an objective measure for robustness.

So, if the measures for robustness as applied in this thesis were not objective measures, does there *exist* any objective measure for robustness of the walking motion? To our knowledge, the answer appears to be negative. Following suggestions by Ruina [personal communication], the best approach appears to be to first devise a classification of all possible disturbances that can occur during the walking motion, and then to produce a robustness score for each of the different kinds of disturbances. So, a discussion on the robustness of a certain walking motion should always have a reference to what type of disturbance is considered. Such a classification has not been made in this thesis, except for the establishment of the 'step-down' experiments in Chapters 3 and 6. A step-down can be regarded as one kind of disturbances for which an objective measure can be created (such as step-down height scaled by leg length). A further classification is recommended for future research, which should incorporate all possible deviations from the limit cycle, and not only those in the Poincaré Section, see Fig. 9.1.

9.4 On actuation

A central theme in this thesis is adding actuation to passive dynamic walkers. The underlying principles and concepts are more important than the actual physical form of actuation. Therefore, the choice for pneumatic McKibben actuators as used in Chapters 7, 8 and 9 was not based on an elaborate consideration of all candidate actuation principles but rather on practicality; as a result of the preceding research by Van der Linde [79] our lab had operational knowledge of the McKibben muscles and the required pneumatic systems. The original choice was based on the following benefits of these muscles:

1. High power-to-weight ratio.
2. High efficiency (almost no damping).
3. Compliance which allows passive joint motions.
4. Controllable, linear stiffness which allows modification of system eigenfrequencies.
5. Cheap because they can be easily self-made.
6. Easy to install.

Strangely enough, none of the above benefits (except the last) really holds. First, the power-to-weight ratio for the muscles alone is fairly high indeed, but this should be put in the perspective that a range of other components (pressure canister, regulators, valves, electric valve control system) are required. Also, the

McKibben muscles operate only at moderate pressures (up to 0.6 MPa) which limits their power output. Even a lighter piston cylinder operating at higher pressures could easily outperform the muscles [Plettenburg, private communication]. Second, the high efficiency claim is only valid when a muscle is operated as a spring (at constant pressure) in the linear range. At maximal extension, the damping increases dramatically. When used as an actuator, the efficiency remains questionable because the muscles have a fairly large ’dead volume’ which must be filled at every actuation cycle. Moreover, as reported in Chapter 8, the entire pneumatic system is distinctly inefficient because of the idle pressure reduction from 5.8 to 0.6 MPa. The third feature, compliance, is not a very special feature. Any other actuator can be given compliance through control or through the combination with mechanical springs. However, the compliance is a disadvantage rather than an advantage as soon as some control is to be implemented. Even the very basic swing leg control applied in the prototypes in this thesis (a quick forward swing followed by a static position) is already difficult to obtain with compliant actuators. Fourth, the stiffness of the muscles is not as linear as was hoped for, see Fig. 7.7. In addition, the miniaturized pneumatic system that we apply in the prototypes results in fairly slow muscle dynamics; filling up a muscle is a first-order system with a time constant of 0.25 s in some cases. If this time constant is compared to the average step time of 0.6 s, it is clear that the stiffness is highly variable over one step, so one can hardly speak of a ’controllable’ stiffness. Even research dedicated to the control of pneumatic muscles [21] has resulted thus far in only slow to moderately fast responses. Fifth, the muscles are not that easy to produce, as especially the connectors at both ends are a source of trouble such as leakage or structural weakness. For that reason, all prototypes in this thesis have been equipped with commercially available muscles [4] which are more reliable although even these still break frequently. Furthermore, the choice for McKibben muscles also implies a choice for portable pneumatics. The lack of sufficiently lightweight commercially available components means that many must be specially developed for the research project, which makes the choice for McKibben muscles not so cheap after all. All together, it is not recommended to use McKibben muscles for future biped robot projects.

Even more strangely, it appears that precisely the originally undesired muscle properties of non-linearity and damping at maximal extension are the main factors for the success of the prototypes in this thesis. As stated above, with compliant actuators it is difficult to perform the relatively simple control task of Chapter 3; bringing the swing leg forward quickly and then keeping it there. However, thanks to the non-linearity of the muscles (they cannot extend beyond 30% of their length and show a high stiffness near that boundary) they act as extension stops to the hip joint. Whatever the precise torque on the hip joint is, the swing leg is always brought forward to the position of maximal muscle extension. Subsequently, thanks to the relatively high amount of damping in that position, the leg bounces back only mildly, thus fulfilling the second part of the control rule (i.e. staying there). Prototype experiments and simulations such as presented in Chapter 8 have consistently shown that the more of a rebound the swing leg makes, the less stable is the walking motion. Much experimenting effort has therefore gone into tuning the pneumatic system and muscle configuration toward minimal swing leg rebound. For future research it is recommended to investigate wether the same performance is easier to achieve with alternative, more controllable actuators, for example electrical DC motors combined with controllable passive elements (brakes, springs, dampers).

9.5 On foot contact in simulations

The core of the research is formed by numerical simulations of both irreducibly simple models and more realistic models correlating to the prototypes. Although the basics of multibody modeling and simulation are considered common knowledge, there are some details that have required special attention for the walking models. The most complex issue is the foot contact, especially during heel strike where an impact occurs. Most commercial software packages for multibody simulations cannot be trusted; in one of our attempts the model would take off and fly away at high speed after its first heel strike impact due to a numerical instability. A mild adjustment of the mysterious contact parameters would suddenly result in a more normal motion, but who is to say that that solution is anywhere near reality?

For the development of our simulation equations, it was decided to model the foot contact as completely rigid, which implies the requirement for impact calculations at heel strike. The alternative, ’soft’ contact with the use of stiff unilateral springs and dampers underneath the foot, is less attractive due to the additional stiff degrees of freedom to the model. Not only does this cost calculation time during the smooth stance phase, but it is especially disruptive for the stability calculations where all the model states at the beginning of two successive steps have to be compared with each other. Our choice for hard contact with impacts however brings its own peculiarities.

Throughout this thesis, the models are assumed to have an instantaneous double stance phase; as soon as the swing foot hits the floor at heel contact, the former stance foot loses contact with the floor and does not participate in the actual impact (an assumption which is verified if the hind foot ends up with a positive vertical velocity). Thanks to this instantaneous double stance phase and to the persistent use of arc feet, there is always only a single contact point between the robot and the floor. This makes the impact calculations deterministic and generally solvable. This would not be the case if we would have allowed impacts with multiple simultaneous contacts in our models. The problem is that the impact cannot be regarded as a simple instantaneous event, because the outcome is highly affected by the interaction between the contact forces in the multiple contact points (which are affected by the exact contact stiffness and damping and by how shockwaves travel through the system). We briefly made an excursion toward this more complicated situation in an attempt to capture behaviors such as falling and stopping more realistically. To solve the impact indeterminacies we used an algorithm by Chatterjee [11] which generally provides a likely result in a reasonable amount of time. However, the amount of discussion and uncertainty that result from such calculations are too much of a distraction from the main focus of the research. Therefore, a strong recommendation for future research is to continue to work with the simple impact calculations to avoid the above deliberations, even if it requires mild adjustments to the prototype under investigation.

9.6 On human walking

The research in this thesis was performed on the basis of biomechanical knowledge (e.g. [42, 87, 40]). So, how much do the resulting prototypes resemble a walking human being? The mechanical construction is quite different but the dynamic principles behind it appear to be the same, as revealed by the natural appearance of the motions.

First, Chapters 3 and 6 propose to obtain fore-aft stability by accelerating the swing leg to move faster than a fully passive leg. The required actuator activity for this corresponds neatly with measurements on muscle activity [40] and with calculations with inverse-dynamic models [42, 72]. Moreover, the required feedback control loop in the prototypes is a simple state machine where a switch underneath the foot signals the transfer to the subsequent state. This can be regarded as a very basic replica of how human walking is governed by a Central Pattern Generator (a neural oscillator in the spinal cord which oscillates in the walking frequency under strong influence of feedback signals). It also correlates to the influential role of foot skin reflexes [80] in human walking.

Second, Chapters 4 and 7 propose the use of a bisecting hip mechanism to obtain a stable upper body. Although the same mechanism can be found in some orthotic devices [39], this is obviously not a good model of the human locomotive system. In our prototypes, the bisecting mechanism is implemented with bicycle chains which could be regarded as tendons or muscles under permanent tension. However, this is a very unattractive solution for biology because of the metabolic energy consumption by the muscle fibers under tension even if no mechanical work is done. As a result, the models and prototypes in this thesis show relatively large excursions of the upper body whereas the human upper body remains almost vertical. Nevertheless, the prototype results indicate that (at least for 2D motions) a simple and local mechanism (or control loop) around the hip joints already suffices for a stable walking motion; there is no need for more ’system-wide’ information such as gyroscopic sensory readings or processed visual information, or even information on which leg is the current stance leg. Therefore, even though the human body does not contain a mechanical bisecting hip joint, it is hypothesized here that the muscles around the hips and pelvic body might very well operate largely on local feedback (reflex) loops alone, as far as the fore-aft motion is concerned.

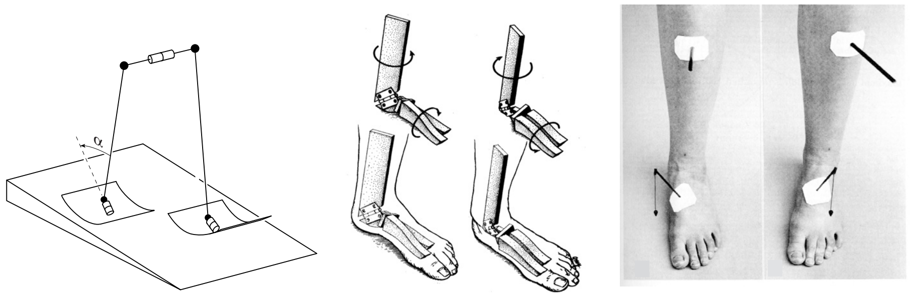

(A) (B) (C)

Figure 9.2: *Robot ankle axis (A) [91] versus human ankle joints (B and C, from Inman [40]). The robot ankle axis points forward and downward whereas the human ankle axis points forward and upward. However, it appears that the overall effect is the same; leaning to the left (or shifting the foot pressure to the left side) results in steering to the left. More research is required for insight into the precise nature of the differences and similarities between the two.*

Third, Chapters 5 and 8 propose the use of a tilted ankle axis for 3D stability. This axis is mounted in a completely different orientation than in the human ankle, see Fig. 9.2. Nevertheless, the effect is similar; a lean angle to the left results in steering to the left. Again, it is not the physical shape of the design but rather the conceptual idea behind it that could be of interest to the biomechanics research community. The idea is that sideways stability can be obtained by coupling lean to yaw; a potential fall to the right is averted by steering to the right. The success of bicycles and skateboards underlines the power of the concept. It is possible that the human ankle or the entire foot construction contribute to such an effect, but it is equally likely that an active control loop in the hip region induces such an effect. It will be a difficult task to find such effects in human locomotion, as the human body is always applying multiple solutions simultaneously. In the case of sideways stability, it has been found already that humans apply sideways foot placement as one strong factor of influence and inertial reaction torques (cf. tightrope walking) as the other. This thesis adds a new possibility; changing the walking direction as a means for sideways stability. It remains as a recommendation for future research in biomechanics to affirm or to negate its use in human locomotion.

9.7 General conclusions

This thesis set out to answer three issues:

1. **How can the robustness of 2D walking motions be increased?**
   In 2D the stability problems are manifested in either a fall forward or backward (Chapter 2), as long as a knee collapse is prevented through the use of knee latches or a proper mechanical design. The chance of both to occur

can be decreased by applying arc feet with a large radius and by increasing the walking velocity. However, an even stronger effect is obtained with the application of a simple form of swing leg control, where the swing leg is quickly brought to a forward position and subsequently kept there until the end of the step. This form of control can theoretically avert all chances of falling forward, although this represents a tradeoff between stability and energy consumption (Chapter 3). This conclusion was validated with the successfully walking prototype 'Mike' as presented in Chapter 6.

2. **How can an upper body be added?**
   The simplest and most straightforward solution is the implementation of a bisecting hip mechanism. It does not decrease the stability and robustness with respect to the original passive walkers while the efficiency in terms of energy per meter traveled per unit of weight is even increased (Chapter 4). This conclusion was validated with the successfully walking prototype 'Max' in Chapter 7.

3. **How can robustness for 3D walking motions be obtained?**
   The 3D walking motion is liable to instabilities in the sideways direction. Chapter 5 shows that these instabilities can be addressed by coupling the lean degree of freedom to yaw; a fall to the side is averted by steering in that direction. This solution only works when walking with a certain minimal velocity which depends on the design of the vehicle, just as with bikes and skateboards. Chapter 5 shows that a reasonable amount of disturbance rejection can be expected for a simple model with an ankle joint that provides this coupling between lean and yaw. This conclusion was validated with the successfully walking prototype 'Denise' in Chapter 8.

All three solutions preserve the main attractions of the concept of passive dynamic walking, namely a low energy consumption and an extremely simple control structure.

9.8 Future directions

The introductory chapter of this thesis lists a number of topics that need to be addressed to make the concept of passive dynamic walking practical for applicable walking robots:

- the robustness in 2D must be increased,
- an upper body must be added,
- robustness in 3D must be obtained,
- the walking velocity must be controllable,
- the walker must be able to start and stop,

- the walker must be able to turn,
- the walker must be able to stand up after a fall.

The first three topics have been addressed in this thesis. However, the robustness that has been achieved is not yet sufficient to cope with rough (outdoors) terrain. Therefore, in addition to the remaining points of the above list, future research must address the issue of robustness of the walking motion.

With respect to the current prototypes, it appears that the robustness of the walking motion cannot be increased significantly by means of purely mechanical components. The next logical step will be the inclusion of simple, local reflex-like control loops. We expect that such control loops can help especially with sideways stability; robot research has shown that this is a problem where mechanical solutions alone are not sufficient while there is also biological evidence for the necessity of control to solve this problem. It is known that human beings use sideways foot placement as a control parameter for sideways stability. The sensors with the strongest relation to the sideways stability appear to be the vestibular organ and the pressure distribution sensors underneath the feet. A first research topic could be to find a simple and straightforward control rule that uses these sensors to control the sideways foot placement.

Another issue that might be resolved with local reflex loops is a proper reaction to tripping. Human beings use, depending on the progression of the step, one out of two possible strategies [20], namely 1) quickly setting down the tripping swing foot (shortening the step), or 2) quickly lifting up the tripping swing foot to overcome the obstacle (elongating the step). Possibly, both of these reflexive actions plus the choice between them can be implemented with a simple and straightforward solution (by proper choice of actuator, sensor, and control algorithm).

However, such feed-back stability solutions will probably provide only so much of extra robustness. Human beings obtain much of their robustness from feed-forward control; mostly through visual input an estimate of the upcoming obstacles is made, which is incorporated in advance in the muscle control. The applicability of visual input for walking robot control should be investigated in a two-way approach; 1) How accurate can the upcoming obstacles be predicted with a vision system and what are the key visual cues? 2) What accuracy is required for the predictive information?

As soon as some of the proposed control algorithms are implemented, the issue of tuning the control parameters must be addressed. Manual tuning will be necessary initially but automation is inevitable. In our opinion, the best approach is to provide the system with a set of initial parameter values that are sure to result in stable walking on a smooth floor, probably at the cost of energy expenditure and velocity. Then the system should adapt its control parameters to optimize for stability, efficiency, and velocity. The research challenge is to find the proper adaptation or learning algorithms, and to find which parameters should be tuned in which sequence and on the basis of which measurements.

It will take many man-years of research effort to arrive at a system with sufficient robustness for confidential use in real-world applications. However, we believe that this may happen sooner than one would think; the research community pursuing the approach in this thesis is quickly gaining momentum with each successful prototype because of the stunningly human impression that these machines leave when strolling along in their natural cadence, while at the same time industrial interest is growing because of the elegant simplicity of the robot designs.

Appendix A

First steps in Passive Dynamic Walking

M. Wisse and A. L. Schwab
To appear at *International conference on Climbing and Walking Robots*, 2004,
Madrid.

Passive dynamic walking is a promising concept for the design of efficient, natural two-legged walking robots. Research on this topic requires an initial point of departure; a stability analysis can be executed only after the first successful walking motion has been found. Experience indicates that it is difficult to find this first successful walking motion. Therefore, this paper provides the basic tools to simulate a simple, two-dimensional walking model, to find its natural cyclic motion, to analyze the stability, and to investigate the effect of parameter changes on the walking motion and the stability. Especially in conjunction with the accompanying MATLAB[1] *files, this paper can serve as a quick and effective start with the concept of passive dynamic walking.*

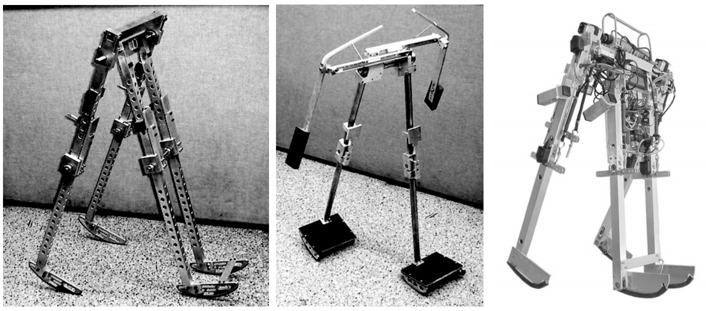

Figure A.1: *Prototypes of passive dynamic walking bipeds that have been developed over the years. Left: Copy of Dynamite, McGeer [49], middle: 3D walker, Collins et al. [19], right: Mike, Wisse and Frankenhuyzen [94].*

A.1 Introduction

This text is written for prospective researchers of 'Passive Dynamic Walking'. Passive Dynamic Walking is an approach to investigate bipedal (two-legged) walking systems, be it humans or other bipedal animals, or bipedal walking robots that you want to build or control. Passive Dynamic Walking is a way to look at bipedal walking. Instead of seeing it as a continuous struggle to keep balance, bipedal walking is much better understood when regarding it as a continuous passive fall, only intermittently interrupted by a change of foot contact. A steady succession of steps can then be analyzed as a cyclic motion.

The approach of Passive Dynamic Walking as originally proposed by McGeer [49] has led to various insights regarding human walking [44], and has produced a number of natural and efficient walking machines [19, 49, 94], see Figure A.1. It is our opinion that huge progress can be made in both fields using the approach of Passive Dynamic Walking. However, experience indicates that it is rather difficult to get started with Passive Dynamic Walking, as one can start analysis only after at least one successful walking motion has been found. This text serves as a guide to that first start.

We will present the complete simulation procedure for a simple, two-dimensional passive dynamic walker. The model is realistic enough to enable the construction of a physical prototype with corresponding behavior. Section II describes the required algorithms for a computer simulation that will predict a walking motion after a proper launch of the biped. This section includes the model description, the derivation of the equations of motion, numerical integration, heel strike detection and the derivation of the impact equations. Section III focuses on the analysis of the step-to-step progression of disturbances on the walking motion, encompassing the selection of a Poincaré section and a linearized stability analysis.

---

[1] For availability of the accompanying files, please try `http://dbl.tudelft.nl` or contact the first author.

The text is accompanied by a set of MATLAB (version 5.2 or higher) files that will provide an operational programming example for a quick start. The following sections will guide you through the functions and background of each of the files.

A.2 Forward dynamic simulation

Model

The simplest system that can perform a Passive Dynamic Walking motion consists of two rigid legs interconnected through a passive hinge. We will study a two-dimensional model for the sake of simplicity. A real-world prototype can be made to behave (more-or-less) two-dimensional through the construction of two symmetric pairs of legs, see Figure A.2. The corresponding dynamic model is shown in Figure A.2.

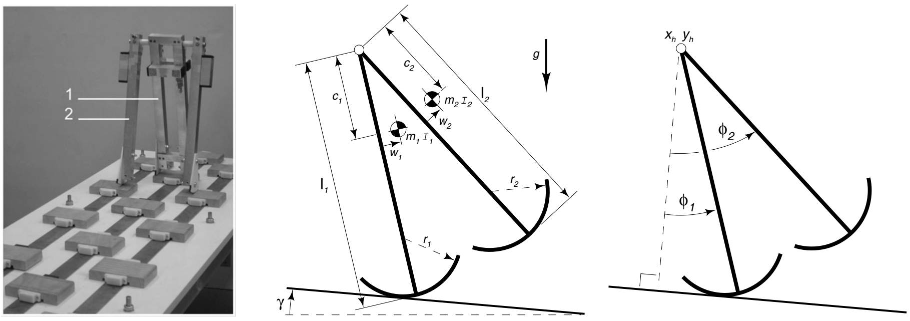

Figure A.2: *Left: Prototype Passive Dynamic Walking robot with four legs (two-dimensional walking behavior), walking on a checkerboard surface to prevent foot-scuffing at mid-stance. Middle: Parameters of the simulation model. Right: four degrees of freedom of the simulation model; the position of the hip and the absolute leg angles.*

We will make a number of assumptions to keep the simulation manageable. First, we assume that the legs suffer no flexible deformation and that the hip joint is free of damping or friction. Second, we idealize the contact between the foot and the floor, assuming perfectly circular feet that do not deform or slip, while the heel strike impact is modeled as an instantaneous, fully inelastic impact where no slip and no bounce occurs. Finally, the floor is assumed to be a rigid and flat slope with a small downhill angle.

There is one problem due to oversimplification of the model. Contrary to humans who have knees, the legs of the model cannot extend or retract, which inevitably leads to foot-scuffing at mid-stance. In a real-world prototype this problem is solved by covering the floor with a checkerboard pattern of tiles that provide foot clearance for the swing foot, see Figure A.2. In the computer simulation, we will simply assume that there is no interference between the floor and the swing foot under certain conditions, as described in the section 'Heel strike detection'.

Based on these assumptions, the model is defined with 14 parameters, which is done in the file wse_par.m. The world is parameterized with gravity g and slope angle γ. A leg must be parameterized as a single rigid body with a mass m, a moment of inertia I, the coordinates for its center of mass with respect to the hip in vertical direction c and in horizontal direction w, the leg length l and the foot radius r. An idealized model consists of two completely equal legs. However, we have noticed that a small difference in parameter values between the legs can strongly influence the walking behavior, so the model will be prepared for legs with different parameter values. All parameters are summarized in Table A.1 in which we have also provided a set of default parameter values that should lead to a successfully walking model or prototype.

World			
gravity	g	9.81	m/s^2
slope angle	γ	0.01	rad
Leg 1 and 2			
length	l	0.4	m
foot radius	r	0.1	m
CoM location	c	0.1	m
	w	0	m
mass	m	1	kg
mom. of inertia	I	0.01	kgm^2

Table A.1: *Parameters for a simple passive dynamic walking model corresponding to Figure A.2. The given default parameter values were chosen to 1) comply with a realistic prototype, and 2) provide stable simulation results.*

The number of degrees of freedom of this model requires some attention; although the two legs each have two position and one orientation coordinate in a two-dimensional world resulting in a total of six degrees of freedom (twelve states when including the velocities), only three states are independent at the start of a step. We get from twelve to three by successively considering the hip joint constraint, the foot contact, and the Poincaré section. First, the hip joint constrains two degrees of freedom (four states) so that the model has only four independent generalized coordinates, x_h, y_h, ϕ_1 and ϕ_2, see Figure A.2. Second, the foot contact constrains two more degrees of freedom (again four states), leaving only ϕ_1 and ϕ_2 as independent coordinates. The hip coordinates depend alternatingly on the one or the other foot contact, which is calculated in the file wse_dep.m. Third, we take a Poincaré Section of the cyclic walking motion. This means that we will focus our attention on the start of each step defined as the instant just after heel strike when both feet are in contact with the floor, which makes one more state dependent; only one leg angle is independent, the other is the same but opposite in sign. Together with the two independent velocities, there are three independent initial conditions that completely define the state at the start of a step, see Table A.2. The definition of the initial conditions takes place in the file `wse_ic.m`. The values in Table A.2 together with the default parameter values in Table A.1 will result in a cyclic and stable walking motion.

Independent initial conditions			
Stance leg (leg 1) angle	ϕ_1	0.2015	rad
Stance leg (leg 1) angular velocity	$\dot{\phi}_1$	-1.4052	rad/s
Swing leg (leg 2) angular velocity	$\dot{\phi}_2$	-1.1205	rad/s
Dependent initial conditions (`wse_dep.m`)			
Swing leg (leg 2) angle	ϕ_2	-0.2015	rad
Hip horizontal displacement	x_h	0.0802	m
Hip vertical displacement	y_h	0.3939	m
Hip horizontal velocity	$\dot{x}_h$	0.5535	m/s
Hip vertical velocity	$\dot{y}_h$	0.0844	m/s
Initial foot contact coordinates			
Foothold location stance leg (leg 1)	xf_1	0	m
Foothold location swing leg (leg 2)	xf_2	0	m

Table A.2: *Initial conditions for a simple passive dynamic walking model corresponding to Figure A.2. Leg 1 is chosen as the initial stance leg. The given default values will, in combination with the default parameter values in Table A.1, result in a stable cyclic walking motion.*

Next to defining initial conditions for the model coordinates, we also need to define the foot contact coordinates. The actual foot contact point travels forward as the model 'rolls' forward over the sole of its circular feet. Therefore we appoint a single, fixed location as foot contact coordinate for the entire duration of a step. This location is defined as the actual point of contact if the leg angle is zero. The piecewise non-holonomic nature of walking systems requires that the foot contact coordinates are re-evaluated after each step. The initial values for the foot contact locations are set rather arbitrarily to zero in Table A.2.

Derivation of equations of motion

The equations of motion are the heart of the computer simulation. For our model we will first derive the generalized equations of motion for the two legs plus hip joint, then derive the algebraic equations that describe the alternating foot contact, and finally put these together in a system of DAE's - Differential Algebraic Equations. The equations in this section correspond to the file `wse_eom.m`.

Let's first consider the system of legs and hip without foot contact. As explained above, that system has four independent *generalized* coordinates $\mathbf{q}$. Their accelerations are calculated with the set of equations

$$\overline{\mathbf{M}}\ddot{\mathbf{q}} = \overline{\mathbf{f}} \tag{A.1}$$

with the generalized mass matrix $\overline{\mathbf{M}}$ and the generalized force vector $\bar{\mathbf{f}}$. They are constructed with the principle of virtual power and d'Alembert inertia forces (the so-called TMT-method) resulting in

$$\overline{\mathbf{M}} = \mathbf{T}^T\mathbf{M}\mathbf{T}, \qquad \bar{\mathbf{f}} = \mathbf{T}^T[\mathbf{f_g} - \mathbf{M}\mathbf{h}]. \tag{A.2}$$

In this $\mathbf{M}$ and $\mathbf{f_g}$ are the terms from 'normal' Newton-Euler equations of motion, i.e. without hip joint constraints and thus for six coordinates. The matrix T transfers the independent generalized coordinates $\dot{\mathbf{q}}$ into the velocities of the center of mass of the bodies $\dot{\mathbf{x}}$. The vector $\mathbf{h}$ holds the convective accelerations. $\mathbf{T}$ and $\mathbf{h}$ are generated by running `wse_sde.m` once, which creates the file `wse_mat.m` containing all necessary matrices.

With equation (A.2) we can calculate the accelerations for the two legs while ensuring that they remain connected at the hip. However, the system is in free fall like this as we have not yet incorporated the contact between the feet and the floor. This contact is described with two equations per leg. First, the foot should be at floor level. Since we apply circular feet, the vertical constraint equations becomes

$$g_y = y_h - (l - r) * cos(\phi) - r \tag{A.3}$$

where g_y must be zero to fulfill the constraint. Second, the horizontal displacement of the foot must be related to the leg angle plus some initial offset (x_f) depending on where the foot has landed,

$$g_x = x_h + (l - r) * sin(\phi) + r * \phi - x_f \tag{A.4}$$

where g_x must be zero to prescribe pure rolling without slip.

To construct the complete set of DAE's we must first determine which foot is in contact, as only one set of foot contact constraints is active at a time. We will need the second derivative of these constraint equations (in the form of $\mathbf{D}$ and $\mathbf{D2}$) to allow a combination with the equations of motion in the total system of equations

$$\begin{bmatrix} \overline{\mathbf{M}} & \mathbf{D}^T \\ \mathbf{D} & \mathbf{0} \end{bmatrix} \begin{bmatrix} \ddot{\mathbf{q}} \\ \mathbf{F_c} \end{bmatrix} = \begin{bmatrix} \overline{\mathbf{F}} \\ \mathbf{D2}(\dot{\mathbf{q}}, \dot{\mathbf{q}}) \end{bmatrix} \tag{A.5}$$

Solving these equations at any instant will provide the generalized accelerations $\ddot{\mathbf{q}}$ and the foot contact forces $\mathbf{f_c}$ at that instant.

Numerical integration

The next step is to go from accelerations at any instant to a continuous motion. To obtain that motion numerical integration is needed, which is done in the file `wse_rk4.m`. We use the classical Runge-Kutta 4 method, which calculates in four intermediate steps the positions and velocities at time $t + \Delta t$.

One of the problems of numerical integration is the accumulation of numerical errors. The overall error can be checked by inspection of the energy content of the system, as the sum of kinetic and potential energy should be constant for a passive walker. An example of such energy checks is given in the file wse_ech.m. Otherwise, one could check stride characteristics such as stride time or stride length, and investigate how much these change by halving the integration step Δt.

Next to the overall error, there is the problem of non-satisfied constraint conditions. The accumulating numerical errors easily lead to a foot that sinks into the ground or flies away. The source of this type of errors is the fact that in equation (A.5) there are only second derivatives of the constraint equations, which only impose that the *acceleration* of the foot is zero. A small round-off error leads to huge position displacements after a while. Therefore, the file wse_rk4.m frequently calls the file wse_dep.m which recalculates the hip coordinates and velocities as a function of the independent leg angles and angular velocities so that the foot constraints are met.

Heel strike detection

During normal walking some events take place every step, whereas in the case of a fall a few other events could take place. To start with the latter, falling forward, falling backward, and losing ground contact (too high velocity) are three possible events. At every step, the file wse_evd.m checks for each of these terminal events and reacts by stopping the simulation.

During continuous locomotion, at every step a heel strike impact occurs, followed by a change of stance foot. This event is detected by monitoring the clearance of the swing foot (equation A.3). Zero clearance means that either a genuine heel strike has occurred or that the swing leg has briefly reached floor level during mid-stance. To distinguish between the two, the file wse_evd.m contains a four-level decision tree; `IF`

- the vertical distance between the swing foot and the floor has changed sign, `AND`
- the stance leg has passed mid-stance (i.e. its direction of motion is away from the vertical position), `AND`
- the swing foot is currently below floor level, `AND`
- the legs are not parallel but in a spread configuration

`THEN` there must have been a valid heel-strike somewhere between the previous and the current integration time step.

If this is detected, an interpolation is necessary to determine the exact instant of heel contact. We approximate the motion between the timesteps t_{n-1} and t_n with a third order polynomial and determine when this polynomial passes

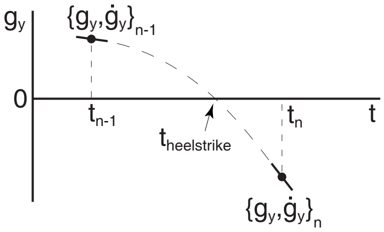

Figure A.3: *Interpolation with third order polynomial to find the instant of heel strike between to integration steps. The clearance function* g_y *is given by equation A.3.*

through zero, see Figure A.3. This is done in `wse_int.m`. After this operation we know the precise instant of heel contact and the state of the model at that instant.

Derivation of impact equations

We assume that heel strike is a fully inelastic impact between the forward foot and the floor. During the heel-strike impact there are very high forces for a very short time. This process can be interpreted as an impulsive motion, an instantaneous event in which the velocities change but not the positions of the model elements. To calculate this we can use the same equations of motion as eq. (A.5) if we apply an integration over the impact duration and take the limit of this duration to zero. The result is a system of impact equations with much resemblance to eq. (A.5):

$$\begin{bmatrix} \overline{\mathbf{M}} & \mathbf{D}^T \\ \mathbf{D} & \mathbf{0} \end{bmatrix} \begin{bmatrix} \dot{\mathbf{q}}^+ \\ \mathbf{f_c} \end{bmatrix} = \begin{bmatrix} \overline{\mathbf{M}}\dot{\mathbf{q}}^- \\ \mathbf{0} \end{bmatrix} \tag{A.6}$$

The D matrix again represents the foot constraints, and is equal to the D used in equation A.5. We must carefully decide which foot constraints are active during heel strike and which are not. At heel strike, both feet are at floor level, so both could possibly participate in the impact. However, the contacts are unilateral which means that only compressive forces can occur. We should only incorporate those constraint equations that result in a compressive impulse. For our model during normal walking, it turns out that only the forward foot does participate whereas the hind foot does not. Presumably the hind foot will obtain an upward velocity as a result from the impact calculation. If it doesn't, the assumption was wrong and we should have incorporated *both* feet in equation A.6, which would have resulted in a full stop. The file `wse_evd.m` checks for this.

Walking cycle

Now we have sufficient tools and algorithms to simulate a continuous walking motion. Let's give the model some initial conditions and see how many steps it will take or how it might fall. The file wse_scw.m ties all previously mentioned files together. Use it by first setting the appropriate parameter values and initial conditions in wse_par.m and wse_ic.m and then running wse_scw.m. The simulation results are then stored in the large matrices `t_t`, `q_t`, `qd_t`, `f_t`, and `g_t`, accessible from MATLAB's base workspace as global variables. To visualize the results, one can use and modify wse_fig.m which plots some basic graphs (Figure A.4), or wse_ani.m which displays a simple animation of the resulting motion, see Figure A.5.

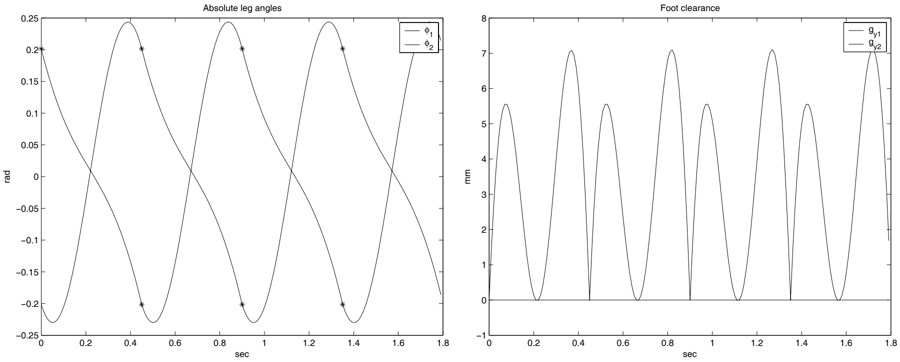

Figure A.4: *Result figures produced by `wse_fig.m`.*

A.3 Step-to-step stability analysis

Stability

The most important characteristic of a walking machine is its stability; it should not fall down. According to the classical interpretation, this requires postural control at every instant of the motion, aimed to keep the center of gravity above the support polygon. We believe that this static approach (and related approaches such as 'ZMP' control [83]) are suitable for *standing* but not for *walking*. As said before, walking should be regarded as a continuous passive fall with intermittent changes of foot contact. Instead of analyzing the balance at every instant we should analyze the stability of the entire cyclic motion in a step-to-step analysis.

A step-to-step analysis allows us to concentrate on the initial conditions only; the rest of the step is then a predictable passive motion. We can present the initial conditions in a phase-space graph (a plot of ϕ versus $\dot{\phi}$), where any point in the graph represents one specific combination of values for the three independent

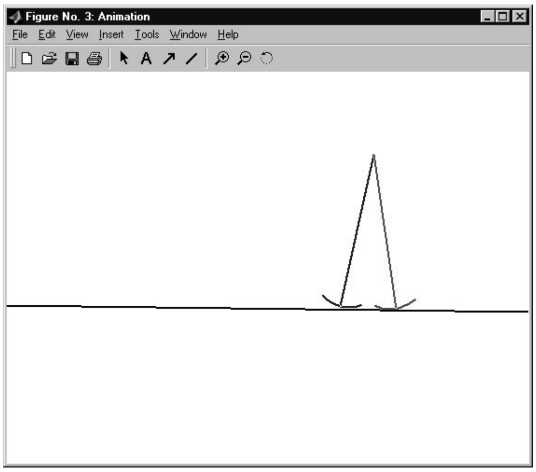

Figure A.5: *Animation screen produced by* `wse_ani.m`.

initial conditions. All points lead to a subsequent motion, but only some of them are successful steps. The end of a successful step is the start of a new one, and so some points in the graph map to some others. This is called 'Poincaré mapping'.

With a little bit of luck (depending on the model parameter values) there are one or two points in the graph that map onto themselves. These are called *fixed points*. They represent a continuous walking motion with all identical steps, which is called a *limit cycle*. With some more luck, one of the fixed points is stable; if the initial conditions are a small deviation away from the fixed point, this deviation disappears over a number of steps until the walker is back in its limit cycle. This stability for small errors is analyzed in the next section. A question that remains is 'how small is small'; for what initial conditions will we still find convergence to the limit cycle? That question is answered with an analysis of the basin of attraction, but that is outside the scope of this paper.

Linearized stability

We need to *find* a fixed point and to *analyze its linear (small-error) stability*. This is easiest understood in reverse order, so for now let's assume that we already know a fixed point. Actually we do, see Table A.2. The three independent initial conditions are represented with $\mathbf{v} = [\phi_1, \dot{\phi}_1, \dot{\phi}_2]^T$, whereas we'll call the fixed point $\mathbf{v}_{fp}$. The Poincaré mapping is represented with the nonlinear function S, so that

$$\mathbf{v}_{n+1} = \mathbf{S}(\mathbf{v}_n) \tag{A.7}$$

where S is a short notation for the complete simulation of one walking step including the heel strike impact and a mirroring of the legs to compare $\mathbf{v}_{n+1}$

with $\mathbf{v}_n$. All initial conditions can be written as a sum of the fixed point plus some deviation:

$$\mathbf{v}_n = \mathbf{v}_{fp} + \Delta\mathbf{v}_n \tag{A.8}$$

Although S is highly nonlinear, for small deviations from $\mathbf{v}_{fp}$ we can approximate the mapping with a linearization according to

$$\begin{array}{rcl} \mathbf{v}_{fp} + \Delta\mathbf{v}_{n+1} = \mathbf{S}(\mathbf{v}_{fp} + \Delta\mathbf{v}_n) & \approx & \mathbf{S}(\mathbf{v}_{fp}) + \mathbf{J}\Delta\mathbf{v}_n \\ with \quad \mathbf{J} = & \frac{\partial \mathbf{S}}{\partial \mathbf{v}} & \end{array} \tag{A.9}$$

This equation simplifies to $\Delta\mathbf{v}_{n+1} = \mathbf{J}\Delta\mathbf{v}_n$. The Jacobian (matrix of partial derivatives) $\mathbf{J}$ here is the key to our linearized stability analysis. Basically it multiplies the errors at step n to produce those at step $n+1$. If the multiplication factor is between -1 and 1, errors decrease step after step and the walker is stable. The multiplication factors are found in the eigenvalues of $\mathbf{J}$ that should all three have a modulus smaller than 1. In the case of the parameter values of Table A.2 the eigenvalues are 0.65, 0.22 + 0.30i, and 0.22 - 0.30i, so the model is linearly stable.

Unfortunately, the Jacobian $\mathbf{J}$ is not readily available. It must be obtained by numeric differentiation by means of four full-step simulations; once for the initial conditions of the fixed point and three times to monitor the effect of a small perturbation on each of the initial conditions. This is done in the file $\boxed{\text{wse\_lca.m}}$. The resulting eigenvalues of $\mathbf{J}$ tell us whether a fixed point is stable or not. However, more than a simple 'yes' or 'no' cannot be expected, as the actual eigenvalues and eigenvectors do not provide much more insight. To determine which model is 'more stable', one should investigate the maximally allowable disturbance size, which can be found by analysis of the basin of attraction (not in this paper).

Finding a fixed point

Now we know how to analyze a fixed point, but how do we *find* it? The approximation of equation (A.9) can also be applied to a set of initial conditions *close to* the fixed point (which we need to guess). This will provide an estimate for $\mathbf{J}$. With that estimate and with the difference between the beginning ($\mathbf{v}$) and the end ($\mathbf{S}(\mathbf{v})$) of a step, a Newton-Raphson iteration can be performed that will quickly converge to the fixed point. The iteration procedure as used in $\boxed{\text{wse\_lca.m}}$ is as follows:

```
repeat
    $\Delta\mathbf{v} = [\mathbf{I} - \mathbf{J}]^{-1}(\mathbf{S}(\mathbf{v}) - \mathbf{v})$
    $\mathbf{v} = \mathbf{v} + \Delta\mathbf{v}$
until $|\Delta\mathbf{v}| < \epsilon$                                    (A.10)
```

where we can set ϵ according to the desired accuracy. If this procedure is started for example with $\{\phi_1, \dot{\phi}_1, \dot{\phi}_2\} = \{0.15, -1, -1\}$, it takes 7 iteration steps (± 20 seconds on a 2GHz PC) to arrive at the fixed point with $\epsilon < 10^{-12}$.

Note that the file `wse_lca.m` always simulates only a single step. In order to compare the end state with the begin state, the end state must be mirrored. This is the standard procedure used in most passive dynamic walking researches, although it is not entirely realistic. In case the model has two legs with different mass properties or in some other special situations [27], the limit cycle analysis should be performed on two subsequent steps which eliminates the necessity for mirroring. The drawback of this is that there is more chance of a fall and thus more difficulty in finding (unstable) cycles with a bad initial guess for the initial conditions.

A.4 Conclusion

This paper provides the basic tools to simulate a simple, two-dimensional walking model, to find its natural cyclic motion, to analyze the stability, and to investigate the effect of parameter changes on the walking motion and the stability. Especially in conjunction with the accompanying MATLAB files, this paper can serve as a quick and effective start with the concept of passive dynamic walking.

Appendix B

Video material

Martijn Wisse.

The topic of this thesis, walking robots, is one of those fields of research in which video material plays an essential role, especially when the claim is that the *motions look natural*. Therefore, the text of the thesis is accompanied by a collection of video clips of the various prototypes that were developed during the course of the PhD-research. This appendix provides a quick introduction to the video material.

The thesis presents three additions to the concept of passive dynamic walking, a design concept for the development of human-like walking machines that require no actuation or control. The state of the art in this field in 2001 was a 3D walker with knees and counter-swinging arms (**`Collins_Video6_Armed1.mpg`**), which could walk stably without any actuation on a slight downhill slope. The benefits of such passive walkers, as opposed to the more traditional 'static' designs (e.g. Honda's ASIMO) are the low energy consumption, the low control requirements (resulting in simple designs) and the natural motions. The main disadvantage is the relatively early state of development; the stability of the current machines is still meager, and the versatility (number of degrees of freedom) is still low. For example, in 2001, no passive walker existed with an upper body, all prototypes consisted of legs only. This thesis aims to address three of such shortcomings.

First, the fore-aft stability is increased. The basic problem is that the inherent stability of purely passive walkers only works for a very limited strength of the disturbances. Larger disturbances quickly lead to a fall, which is in most cases a fall forward, as demonstrated with one or our first experimental walkers in **`wissejandouwe.avi`**. The solution to the problem is to accelerate the swing leg so that it quickly reaches the forward position, ready for the next step. We implemented this idea in a passive walker which obtained the swing leg acceleration through a mechanism in the hip. The primary goal of the mechanism is to lift the swing foot to provide clearance (the prototype has no knees), but a secondary effect is a lowering of the center of mass early in the swing phase, which

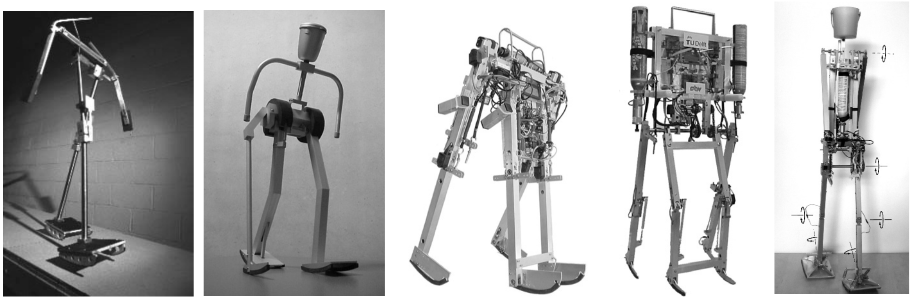

Figure B.1: *In order of appearance: State of the art passive dynamic walker (Cornell University, 2001), Demonstration robot for Museon, Mike, Max, Denise.*

in turn provides energy to accelerate the swing leg. The resultant robustness of the walking motion as shown in `museonside.mpg`, `museonfront.mpg`, and `museonkick.mpg`, enabled the presentation of the prototype in a hands-on exhibition of a local museum. The idea of swing leg acceleration is also implemented in a powered walking robot, the 7 kg autonomous prototype 'Mike'. The actuation at the hip by means of pneumatic McKibben muscles not only provides extra stability but also provides sufficient power to the system to remove the need for a downhill walking surface. The prototype walks robustly on a level floor, see `mikelonghall.mpg`, `mikechangefloor.mpg`, or `mikestart.mpg`, and even on the more uneven surface of an outdoors sidewalk as shown in `mikeoutside.mpg`. With this prototype, the idea of hip actuation for an increased stability is validated.

Second, an upper body is added. The basic problem is the fact that the upper body is an inverted pendulum with its pivot at the hip joint. To stabilize it, a torque should be applied between the upper body and the stance leg. Most researchers revert to active control to deal with the complication of the continuous alternation of leg function between stance phase and swing phase. In contrast, our solution is purely mechanical and requires no additional actuation or control. The hip is equipped with a bisecting mechanism so that the upper body always remains at the dissection angle of the two legs. As a result, the upper body adds no extra degrees of freedom to the system. The mass and inertia of the upper body do not significantly change the governing dynamics of the (almost) passive walking motion. The concept is proven with the successor of 'Mike', the 10 kg autonomous prototype 'Max', see `maxtotaalfilmlego.mpg`.

Third, a solution for 3D stability is presented. The previous machines are all two-dimensional (by means of their four-legged symmetrical construction) and thus they do not suffer from sideways instabilities. The last robot of the series, the 8 kg autonomous prototype 'Denise' shown in `denise_collage.mpg`, is much more human-like with only two legs. To obtain more resistance against disturbances than possible with the fully passive machine in 2001, a special ankle joint is introduced. The ankle joint couples the unstable sideways lean motion to a yaw motion; the prototype steers in the direction that it is falling. When walking faster than a critical velocity, this coupling provides stability to the motion similar to the stability of a riding bicycle.

The three solutions together make it possible to build stable, efficient, and natural looking human-like walking machines such as ‘Denise’ while requiring only a minimal amount of control technology and actuation.

References

[1] `http://www.humanoid.rise.waseda.ac.jp/`. Waseda Humanoid Project.

[2] `http://www.isi-group.com`. ISI.

[3] `http://www.lart.tudelft.nl/`. LART board; a strong-Arm based low power linux machine, developed at TU Delft.

[4] `http://www.shadow.org.uk`. Shadow Group.

[5] `http://www.smcusa.com`. SMC pneumatics.

[6] J. Adolfsson. *Passive control of mechanical systems; Bipedal walking and autobalancing*. PhD thesis, Royal Institute of Technology, Stockholm, Sweden, 2001. ISSN 0348-467X.

[7] J. Adolfsson, H. Dankowicz, and A. Nordmark. 3d passive walkers: Finding periodic gaits in the presence of discontinuities. *Nonlinear Dynamics*, 24(2):205–229, 2001.

[8] F. Asano and M. Yamakita. Virtual gravity and coupling control for robotic gait synthesis. *IEEE Trans. on Systems, Man and Cybernetics, Part A*, 31(6):737–745, 2001.

[9] G. A. Borelli. *On the Motion of Animals (De Motu Animalum)*. 1680.

[10] W. Bräune and O. Fischer. *The Human Gait*. Springer-Verlag, Berlin, 1987 (orig. published 1895-1904).

[11] A. Chatterjee and A. Ruina. A new algebraic rigid body collision law based on impulse space considerations. *J. of Applied Mechanics*, 65(4):939–951, 1998.

[12] C. Chevallereau, G. Abba, Y. Aoustin, F. Plestan, E. R. Westervelt, C. Canudas-De-Wit, and J. W. Grizzle. Rabbit: a testbed for advanced control theory. *IEEE Control Systems Magazine*, 23(5):57–79, October 2003.

[13] C.-M. Chew and G. A. Pratt. Dynamic bipedal walking assisted by learning. *Robotica*, 20(5):477–491, 2002.

[14] C. P. Chou and B. Hannaford. Measurement and modeling of mckibben pneumatic artificial muscles. *IEEE Trans. on Robotics and Automation*, 12(1):90–102, February 1996.

[15] M. J. Coleman. *A Stability Study of a Three-dimensional Passive-dynamic Model of Human Gait*. PhD thesis, Cornell University, Ithaca, NY, 1998.

[16] M. J. Coleman, A. Chatterjee, and A. Ruina. Motions of a rimless spoked wheel: A simple 3d system with impacts. *Dynamics and Stability of Systems*, 12(3):139 – 160, 1997.

[17] M. J. Coleman, M. Garcia, K. Mombaur, and A. Ruina. Prediction of stable walking for a toy that cannot stand. *Physical Review E*, 64(2):022901–1 – 022901–3, august 2001.

[18] M. J. Coleman and A. Ruina. An uncontrolled toy that can walk but cannot stand still. *Physical Review Letters*, 80(16):3658 – 3661, April 1998.

[19] S. H. Collins, M. Wisse, and A. Ruina. A two legged kneed passive dynamic walking robot. *Int. J. of Robotics Research*, 20(7):607–615, July 2001.

[20] A. Forner Cordero. *Human gait, stumble and... fall?* PhD thesis, University of Twente, Enschede, The Netherlands, 2003. ISBN 90-365-1912-8.

[21] F. Daerden and D. Lefeber. Pneumatic artificial muscles: actuators for robotics and automation. *Eur. J. of Mechanical and Environmental Engineering*, 47(1):10–21, 2002.

[22] H. Elftman. The measurement of the external force in walking. *Science*, 88:152–153, 1938.

[23] G. T. Fallis. Walking toy ('improvement in walking toys'). U. S. Patent, No. 376,588, January 17 1888.

[24] M. Garcia. *Stability, Chaos, and Scaling Laws: Passive–Dynamic Gait Models*. PhD thesis, Cornell University, Ithaca, NY, 1998.

[25] M. Garcia, A. Chatterjee, and A. Ruina. Speed, efficiency, and stability of small-slope 2d passive-dynamic bipedal walking. In *Proc., IEEE Int. Conf. on Robotics and Automation*, pages 2351–2356, Piscataway, NJ, 1998.

[26] M. Garcia, A. Chatterjee, and A. Ruina. Efficiency, speed, and scaling of two-dimensional passive-dynamic walking. *Dynamics and Stability of Sytems*, 15(2):75–99, 2000.

[27] M. Garcia, A. Chatterjee, A. Ruina, and M. J. Coleman. The simplest walking model: Stability, complexity, and scaling. *ASME J. Biomech. Eng.*, 120(2):281–288, April 1998.

[28] A. Goswami. Foot-rotation indicator (fri) point: A new gait planning tool to evaluate postural stability of biped robots. In *Proc., IEEE Int. Conf. on Robotics and Automation*, pages 47–52, 1999.

[29] A. Goswami, B. Espiau, and A. Keramane. Limit cycles and their stability in a passive bipedal gait. In *Proc., IEEE Int. Conf. on Robotics and Automation*, Piscataway, NJ, 1996.

[30] A. Goswami, B. Thuilot, and B. Espiau. A study of the passive gait of a compass-like biped robot: symmetry and chaos. *Intern. J. Robot. Res.*, 17(12):1282–1301, December 1998.

[31] A. H. Hansen, D. S. Childress, and E. H. Knox. Prosthetic foot roll-over shapes with implications for alignment of trans-tibial prostheses. *Prosthetics and Orthotics International*, 24:205–215, 2000.

[32] Hippocrates. *On the Articulations. Parts 52 and 60*. 400 BC. Available at `http://classics.mit.edu//Hippocrates/artic.html`, translated by Francis Adams.

[33] K. Hirai, M. Hirose, Y. Haikawa, and T. Takenaka. The development of honda humanoid robot. In *Proc., IEEE Int. Conf. on Robotics and Automation*, pages 1321–1326, May 1998.

[34] D. G. E. Hobbelen and M. Wisse. Ankle joints and flat feet in dynamic walking. to appear at *Int. Conf. on Climbing and Walking Robots*, Madrid, 2004.

[35] J. K. Hodgins and W. L. Wooten. Animating human athletes. In Y. Shirai and S. Hirose, editors, *Robotics Research: The Eighth International Symposium*, pages 356–367, Berlin, 1998. Springer-Verlag.

[36] C. S. Hsu. *Cell-to-cell mapping; a method of global analysis for nonlinear systems*. Applied mathematical sciences 64. New York: Springer, 1987. ISBN 0-387-96520-3.

[37] M. Hubbard. Lateral dynamics and stability of the skateboard. *J. of Applied Mechanics*, 46:931–936, December 1979.

[38] Y. Hurmuzlu. Dynamics of bipedal gait; part ii: Stability analysis of a planar five-link biped. *ASME J. of Applied Mechanics*, 60(2):337–343, 1993.

[39] M. J. Ijzerman, G. Baardman, H. J. Hermens, P. H. Veltink, H. B. K. Boom, and G. Zilvold. The influence of the reciprocal cable linkage in the advanced reciprocating gait orthosis on paraplegic gait performance. *Prosthetics and orthotics international*, 21:52–61, 1997.

[40] V. T. Inman, H. J. Ralston, and F. Todd. *Human Walking*. Williams & Wilkinns, Baltimore, 1981. ISBN 0-683-04348-X.

[41] K. Kaneko, F. Kanehiro, S. Kajita, K. Yokoyama, K. Akachi, T. Kawasaki, S. Ota, and T. Isozumi. Design of prototype humanoid robotics platform for hrp. In *Proc., IEEE/RSJ Int. Conf. on Intelligent Robots and System, Vol.3*, pages 2431 – 2436, 2002.

[42] H. F. J. M. Koopman. *The three-dimensional analysis and prediction of human walking*. PhD thesis, University of Twente, Enschede, The Netherlands, 1989. ISBN 90-9003075-1.

[43] A. D. Kuo. Stabilization of lateral motion in passive dynamic walking. *Int. J. Robot. Res.*, 18(9):917–930, September 1999.

[44] A. D. Kuo. Energetics of actively powered locomotion using the simplest walking model. *J. of Biomechanical Engineering*, 124:113–120, February 2002.

[45] R. Kurazume, T. Hasegawa, and K. Yoneda. The sway compensation trajectory for a biped robot. In *Proc., IEEE Int. Conf. on Robotics and Automation*, pages 925 – 931, 2003. Vol. 1.

[46] Y. Kuroki, M. Fujita, T. Ishida, K. Nagasaka, and J. Yamaguchi. A small biped entertainment robot exploring attractive applications. In *Proc., IEEE Int. Conf. on Robotics and Automation*, pages 471–476, 2003.

[47] E.-J. Marey. *Le Mouvement*. 1894.

[48] T. McGeer. Powered flight, child's play, silly wheels, and walking machines. In *Proc., IEEE Int. Conf. on Robotics and Automation*, pages 1592–1597, Piscataway, NJ, 1989.

[49] T. McGeer. Passive dynamic walking. *Intern. J. Robot. Res.*, 9(2):62–82, April 1990.

[50] T. McGeer. Passive walking with knees. In *Proc., IEEE Int. Conf. on Robotics and Automation*, pages 1640–1645, Los Alamitos, CA, 1990.

[51] T. McGeer. Passive dynamic biped catalogue. In R. Chatila and G. Hirzinger, editors, *Proc., Experimental Robotics II: The 2nd International Symposium*, pages 465–490, Berlin, 1992. Springer–Verlag.

[52] J. P. Meijaard. Efficient numerical integration of the equations of motion of non-smooth mechanical systems. *Zeitschr. der Angew. Math. Mech.*, 77(6):419–427, 1997.

[53] S. Mochon and T. A. McMahon. Ballistic walking. *J. Biomechanics*, 13:49–57, 1980.

[54] X. Mu and Q. Wu. Synthesis of a complete sagittal gait cycle for a five-link biped robot. *Robotica*, 21(5):581–587, 2003.

[55] E. Muybridge. *The Human Figure in Motion*. Dover Publications, New York, 1955, 1985, 1995. ISBN 0486202046.

[56] M. Okada, T. Shinohara, T. Gotoh, S. Ban, and Y. Nakamura. Double spherical joint and backlash clutch for lower limbs of humanoids. In *Proc., IEEE Int. Conf. on Robotics and Automation*, pages 491–496, 2003.

[57] K. Ono, R. Takahashi, and T. Shimada. Self-excited walking of a biped mechanism. *Int. J. of Robotics Research*, 20(12):953–966, 2001.

[58] K. Ono, F. Takasahi, and R. Takahashi. Self-excited walking of a biped mechanism with feet. *Int. J. of Robotics Research*, 23(1):55–68, 2004.

[59] F. Pfeiffer, K. Löffler, and M. Gienger. The concept of jogging johnnie. In *Proc., IEEE Int. Conf. on Robotics and Automation*, pages 3129 – 3135, Washington DC, May 2002.

[60] P. T. Piiroinen. *Recurrent Dynamics of Nonsmooth Systems with Application to Human Gait*. PhD thesis, Royal Institute of Technology, Stockholm, Sweden, 2002.

[61] G. Pratt and M. Williamson. Series elastic actuators. In *Proc., Int. Conf. on Intelligent Robots and Systems*, Pittsburgh, PA, 1995.

[62] J. Pratt and G. Pratt. Exploiting natural dynamics in the control of a 3d bipedal walking simulation. In *Proc., Int. Conf. on Climbing and Walking Robots*, Portsmouth, UK, 1999.

[63] J. E. Pratt. *Exploiting inherent robustness and natural dynamics in the control of bipedal walking robots*. PhD thesis, Massachusetts Institute of Technology, Cambridge, MA, 2000.

[64] J. E. Pratt, C.-M. Chew, A. Torres, P. Dilworth, and G. Pratt. Virtual model control: An intuitive approach for bipedal locomotion. *Int. J. of Robotics Research*, 20(2):129–143, 2001.

[65] H. J. Ralston. Energy-speed relation and optimal speed during level walking. *Int. z. angew. Physiol.*, 17:277–283, 1958.

[66] R. Regele, W. Bott, and P. Levi. Prorobot - predictions for the future development of humanoid robots. In R. Dillmann, H. Wörn, and T. Gockel, editors, *Autonome Mobile Systeme*, pages 292–303. Springer, Berlin, 2003.

[67] T. Saidouni and G. Bessonnet. Generating globally optimised sagittal gait cycles of a biped robot. *Robotica*, 21(2):199–210, 2003.

[68] Y. Sakagami, R. Watanabe, C. Aoyama, S. Matsunaga, N. Higaki, and M. Fujita. The intelligent asimo: System overview and integration. In *Proc., Int. Conf. on Intelligent Robots and Systems*, pages 2478–2483, 2002.

[69] A. L. Schwab and J. P. Meijaard. Dynamics of flexible multibody systems with non-holonomic constraints: A finite element approach. *Multibody System Dynamics*, 10(12):107–123, 2003.

[70] A. L. Schwab, J. P. Meijaard, and J. M. Papadopoulos. Benchmark results on the linearized equations of motion of an uncontrolled bicycle. In preparation, 2004.

[71] A. L. Schwab and M. Wisse. Basin of attraction of the simplest walking model. In *Proc., Int. Conf. on Noise and Vibration*, Pennsylvania, 2001. ASME. Paper number DETC2001/VIB-21363.

[72] R. Selles, J. B. J. Bussmann, R. C. Wagenaar, and H. J. Stam. Comparing predictive validity of four ballistic swing phase models of human walking. *J. of Biomechanics*, 34:1171–1177, 2001.

[73] M. W. Spong and F. Bullo. Controlled symmetries and passive walking. In *IFAC Triennial World Congress*, Barcelona, Spain, 2002.

[74] K. Tanie. Humanoid robot and its application possibility. In *Proc., IEEE Int. Conf. on Multisensor Fusion and Integration for Intelligent Systems*, pages 213 – 214, 2003.

[75] R. Tedrake, T.W. Zhang, M.-F. Fong, and H.S. Seung. Actuating a simple 3d passive dynamic walker. In *Proc., IEEE Int. Conf. on Robotics and Automation*, 2004.

[76] R. Q. van der Linde. Active leg compliance for passive walking. In *Proc., IEEE Int. Conf. on Robotics and Automation*, pages 2339–2344, May 1998.

[77] R. Q. van der Linde. Design, analysis and control of a low power joint for walking robots, by phasic activation of mckibben muscles. *IEEE Trans. Robotics and Automation*, 15(4):599–604, August 1999.

[78] R. Q. van der Linde. Passive bipedal walking with phasic muscle contraction. *Biological Cybernetics*, 81(3):227–237, September 1999.

[79] R. Q. van der Linde. *Bipedal walking with active springs, gait synthesis and prototype design*. PhD thesis, Delft University of Technology, Delft, The Netherlands, November 2001. ISBN 90-370-0193-9.

[80] B. M. H. van Wezel, F. A. M. Ottenhoff, and J. Duysens. Dynamic control of location-specific information in tactile cutaneous reflexes from the foot during human walking. *J. of Neuroscience*, 17(10):3804–3814, 1997.

[81] M. Vukobratovic. How to control the artificial anthropomorphic systems. *IEEE Trans. System, Man and Cybernetics SMC-3*, pages 497–507, 1973.

[82] M. Vukobratovic and B. Borovac. Zero-moment point - thirty five years of its life. *Int. J. of Humanoid Robotics*, 1(1):157–173, March 2004.

[83] M. Vukobratovic, B. Borovac, D. Surla, and D. Stokic. *Biped Locomotion: Dynamics, Stability, Control and Applications*. Springer–Verlag, Berlin, 1990.

[84] W. Weber and E. Weber. *Mechanik der Menschlichen Gehwerkzeuge*. 1836.

[85] Website. Delft biorobotics laboratory. `(http://dbl.tudelft.nl/)`.

[86] E. R. Westervelt, J. W. Grizzle, and D. E. Koditschek. Hybrid zero dynamics of planar biped walkers. *IEEE Trans. on Automatic Control*, 48(1):42–56, 2003.

[87] D. A. Winter. *Biomechanics and motor control of human movement*. John Wiley & Sons, Inc., 1990. ISBN 0-471-50908-6.

[88] M. Wisse. Passive dynamic biped with knees. Master's thesis, Delft University of Technology, Delft, The Netherlands, June 2000.

[89] M. Wisse, D. G. E. Hobbelen, and A. L. Schwab. Adding the upper body to passive dynamic walking robots by means of a bisecting hip mechanism. Submitted to *IEEE Trans. on Robotics*, 2004.

[90] M. Wisse and A. L. Schwab. A 3d passive dynamic biped with roll and yaw compensation. *Robotica*, 19:275–284, 2001.

[91] M. Wisse and A. L. Schwab. Skateboards, bicycles, and 3d biped walkers; velocity dependent stability by means of lean-to-yaw coupling. Submitted to *Int. J. of Robotics Research*, 2004.

[92] M. Wisse, A. L. Schwab, and F. C. T. van der Helm. Passive dynamic walking model with upper body. to appear in *Robotica*, 2004.

[93] M. Wisse, A. L. Schwab, R. Q. van der Linde, and F. C. T. van der Helm. How to keep from falling forward; elementary swing leg action for passive dynamic walkers. To appear in *IEEE Trans. on Robotics*, 2004.

[94] M. Wisse and J. van Frankenhuyzen. Design and construction of mike; a 2d autonomous biped based on passive dynamic walking. In *Proc., Conference on Adaptive Motion of Animals and Machines, AMAM*, Kyoto, Japan, 2003. Paper number WeP-I-1.

Samenvatting

Mensen kunnen stabiel en efficient lopen op allerlei soorten ondergrond, zonder dat dit veel moeite lijkt te kosten. Vanuit een technisch oogpunt is deze klaarblijkelijke moeiteloosheid merkwaardig, omdat de loopbeweging in feite een zeer complex dynamisch verschijnsel is. Bij het lopen op twee benen is sprake van niet-lineaire en multi-variabele dynamica, beperkingen in het voet-vloer contact (er zijn geen trekkrachten mogelijk), een ingebouwde instabiliteit (het systeem is een omgekeerde slinger met het draaipunt bij de standvoet), discrete gebeurtenissen (zoals het neerkomen van het zwaaibeen) en een variabele configuratie (door de afwisseling van stand- en zwaai-functie van de benen). Om deze complexe loopbeweging kunstmatig te kunnen nadoen, bijvoorbeeld om mensen met een handicap weer te laten lopen of voor de ontwikkeling van lopende robots, is het noodzakelijk om de essentie te begrijpen van het menselijke voortbewegingssysteem.

Om de essentie van menselijk lopen te achterhalen, wordt in dit proefschrift gebruik gemaakt van synthese (het bouwen van kunstmatige loopsystemen) in tegenstelling tot het vaker voorkomende analyseren van het bestaande, menselijke loopsysteem. Het kunstmatige loopsysteem wordt elementsgewijs opgebouwd. Deze aanpak heeft als groot voordeel dat het de nadruk legt op de essentie van het lopen op twee benen; voor ieder element is het precies duidelijk waarom het noodzakelijk is en hoe het bijdraagt aan de gehele loopbeweging.

De aanpak in dit proefschrift verschilt van de meeste andere looprobotprojecten. Meestal baseert men het ontwerp en de regeling voor looprobots op de standaard robottechnologie zoals bekend van de industriële robot-armen; krachtige motoren en stijve verbindingselementen zorgen samen met ingewikkelde regelalgoritmes ervoor dat die robot-armen met hoge naukeurigheid een voorgeschreven traject kunnen volgen. Wij stellen dat deze aanpak leidt tot onnodig complexe, zware, en inefficiënte loopsystemen, omdat de hoge nauwkeurigheid bij de loopbeweging niet noodzakelijk is. Het belangrijkste inzicht hier is dat de stabiliteit niet persé binnen één stap verkregen hoeft te worden, zolang de loopbeweging *als serie van opeenvolgende stappen* maar stabiel blijft. Anders gezegd, de loopbeweging moet beschouwd worden als een periodieke beweging welke slechts als geheel stabiel hoeft te zijn. Dus, de fundamentele instabiliteit die er bestaat binnen één stap (het systeem is een omgekeerde slinger) hoeft eenvoudigweg niet te worden weggeregeld!

Ons onderzoek is gebaseerd op het bestaande concept van ’passief dynamisch lopen', een concept waarmee op overtuigende wijze gedemonstreerd kan worden wat de mogelijkheden zijn van het inzicht dat de loopbeweging als geheel gezien moet worden. Passief dynamische loopsystemen zijn constructies van puur mechanische componenten die een stabiele, periodieke loopbeweging kunnen maken wanneer ze op een flauwe neerwaartse helling worden gezet. Met onaangedreven heup- en kniescharnieren vertonen deze lopers stabiel gedrag zonder dat daar enige regelactiviteit voor nodig is. Dit soort loopsystemen zijn niet alleen uiterst eenvoudige constructies, maar de loopbeweging is ook nog eens zeer natuurlijk en efficiënt; het zwaaibeen slingert naar voren in zijn natuurlijke frequentie, iets wat geen energie vereist en natuurlijk aandoet. Alleen aan het einde van een stap wordt een beetje energie verloren doordat het zwaaibeen met een klap op de grond neerkomt. Deze botsingsverliezen worden bij de meeste passief dynamische loopsystemen aangevuld door van een lichte helling af te lopen. De stabiliteit van deze lopers is een resultaat van het regulerende effect van die botsingen tussen voet en vloer, een effect dat afhankelijk is van de parameterwaarden van het loopsysteem. Om de stabiliteit te onderzoeken wordt doorgaans gebruik gemaakt van methode 'Poicaré mapping'. Bij deze methode wordt de toestand van het systeem eenmaal per stap bekeken (op het moment van neerkomen van het zwaaibeen). Vervolgens wordt geanaliseerd hoe die toestand verandert stap na stap. Als een bepaalde toestand zichzelf iedere stap herhaalt, is er sprake van een 'limit cycle' (grenskringloop). De stabiliteit hiervan wordt geanaliseerd door te kijken naar de gelineariseerde effecten van kleine afwijkingen bovenop de zich herhalende toestand. Dit is de methode die in eerdere onderzoeken al is gebruikt voor de stabiliteitsanalyse van lopende systemen, en als zodanig vormt het de basis voor het stabiliteitsonderzoek in dit proefschrift.

Het doel van dit proefschrift is om de essentie te achterhalen van dynamisch, menselijk lopen, met het concept van passief dynamisch lopen als startpunt. De vraag is nu, wat zijn de beperkingen van de huidige stand van onderzoek op dit gebied? Het antwoord bestaat uit een lange lijst van kenmerken en vaardigheden die nog niet zijn toegevoegd of bestudeerd: stabiliteit bij grote verstoringen, een bovenlichaam, stabiliteit in 3D, starten en stoppen, opstaan na een val, traplopen, enzovoort. Dit proefschrift concentreert zich drie elementen uit deze lijst. Ten eerste, alhoewel de pure passieve lopers stabiel zijn bij kleine verstoringen, leiden grote verstoring al snel tot een val. Daarom moet er eerst een methode komen om het gedrag bij grote verstoringen te analyseren, met behulp waarvan we in staat zouden moeten zijn om eenvoudige en efficiénte regelalgoritmes of mechanische oplossingen te vinden om het gedrag bij grote verstoringen te verbeteren. Ten tweede, een belangrijke beperking van de huidige passieve lopers is dat ze allemaal alleen maar bestaan uit benen, omdat er nog geen passieve oplossing bestaat om er een bovenlichaam aan toe te voegen. Ten derde, qua stabiliteit in 3D zijn de resultaten tot nog toe erg mager. Bijna alle bestaande prototypes zijn slechts 2D; ze kunnen niet zijwaarts 'uit het vlak' bewegen door hun constructie met vier benen in een dubbele, symmetrische configuratie (vergelijkbaar met het lopen met krukken). De weinige prototypes die echte 3D dynamica hebben (ze kunnen ook zijwaarts bewegen en vallen omdat ze maar twee benen hebben), zijn slechts ternauwernood stabiel. Samengevat, het doel van dit proefschrift is om de volgende drie problemen op te lossen:

1. het begrijpen en verbeteren van het gedrag bij grote verstoringen,
2. het toevoegen van een bovenlichaam,
3. het verkrijgen van stabiliteit voor 3D loopsystemen.

Ten eerste, om het gedrag bij grote verstoringen te bestuderen, introduceren we de analyse van de zogenoemde 'basin of attraction' (aantrekkingsgebied) van de limit cycle. De basin of attraction is de verzameling van alle toestanden van de loper die uiteindelijk leiden tot de limit cycle, de periodieke loopbeweging. Alle toestanden buiten de basin of attraction leiden uiteindelijk tot een val. We hebben de basin of attraction van het meest elementaire loopmodel geanalyseerd, een 2D model met rechte benen en puntmassa's op de heup en voeten. Uit de analyse volgt dat het gedrag bij grote fouten voornamelijk is op te delen in een val achterover (niet voldoende energie om over het dode punt halverwege de stap te komen) en een val voorover (het zwaaibeen is niet tijdig naar voren om de loper op te vangen voor de volgende stap). De computersimulatie leidde tot de volgende conclusies:

- Vergeleken bij de oorspronkelijke, lineaire stabiliteitsanalyse zorgt de analyse van de basin of attraction voor een beter inzicht in het gedrag bij grote verstoringen, en dus wordt het beter mogelijk om te voorspellen of een bepaald loopsysteem succesvol al zijn in realistische omstandigheden.
- Voor de passieve (puur mechanische) loopsystemen is de basin of attraction erg klein, wat duidt op een zeer lage tolerantie voor verstoringen.
- Het meest voorkomende gedrag bij grote verstoringen is een val voorwaarts. Het (nu nog) volledig passive zwaaibeen beweegt in zijn natuurlijke frequentie en heeft dus een onveranderlijke hoeveelheid tijd nodig om volledig naar voren te zwaaien. Als de loper door een verstoring tijdelijk te snel beweegt, is het zwaaibeen niet op tijd om de robot voor de volgende stap op te vangen.

Om het gedrag bij grote verstoringen te verbeteren, stellen we voor om het onderzoek niet meer te richten op volledig passieve loopsystemen, maar voegen we aandrijving toe aan het heupscharnier. Met een actuator in de heup is het mogelijk om het zwaaibeen te versnellen om zeker te stellen dat de voorwaartse zwaaibeweging tijdig is voltooid. Met een computersimulatie is aangetoond dat deze oplossing in principe ieder risico om voorover te vallen wegneemt, alhoewel dit wel wat extra energie vergt. Belangrijker nog is het feit dat er voor deze stabiliteitswinst geen ingewikkelde regelalgoritmes nodig zijn; het volstaat om het zwaaibeen iedere stap snel naar een vooraf ingestelde voorwaartse positie te zwaaien. Daarvoor zijn geen metingen nodig van de werkelijke toestand van de rest van het systeem, de aandrijving mag elke stap identiek zijn. Een eenvoudige veer-demper combinatie in het heupscharnier is al voldoende; het enige dat hoeft te gebeuren is het omschakelen van de nulstand van de veer aan het begin van elke nieuwe stap. Een bijkomend voordeel van het voorgestelde systeem voor aandrijving is dat het juist voldoende energie aan het loopsysteem als geheel toevoegt om niet langer van een helling af te hoeven lopen.

De voorgestelde oplossing is gevalideerd door middel van de bouw en het testen van een autonoom 2D prototype met knieën. Het prototype weegt 7 kg, is 0.7 m lang, en loopt met een snelheid van 0.4 m/s (0.6 s per stap). Het heupscharnier is aangedreven met zgn. 'McKibben muscles', pneumatische kunstspieren die de heup een veerstijfheid geven die proportioneel is met de interne CO_2-druk in de spieren. Door om beurten telkens slechts één van de twee spieren uit een paar van antagonisten in te schakelen, krijgt het heupscharnier iedere stap opnieuw een veerstijfheid met een voorwaarts gerichte nulstand. Op deze manier wordt het zwaaibeen naar voren versneld zoals we hierboven hebben voorgesteld. Om het effect hiervan te testen, hebben we het prototype van een afstapje laten lopen, waarbij de maximaal mogelijke afstap-hoogte werd uitgezet tegen de druk in de heupspieren. Zoals verwacht, bleek inderdaad dat een hogere druk (ofwel een hogere heup-veerstijfheid) ervoor zorgt dat het prototype stabiliteit kan behouden bij hogere afstapjes. Dus, de voorgestelde heupaandrijving zorgt inderdaad voor een betere stabiliteit bij grote verstoringen.

Ten tweede, om een bovenlichaam toe te voegen hebben we een hoekdelingsmechanisme in de heup geintroduceerd. Dit mechanisme is een verbinding tussen het bovenlichaam en de twee benen die ervoor zorgt dat de hoek van het bovenlichaam (vanaf de zijkant bezien) altijd het midden houdt van de hoeken van de twee benen. Op deze manier zorgt de toevoeging van een bovenlichaam niet voor een vergroting van het aantal vrijheidsgraden. Het bovenlichaam is zo niet een instabiele omgekeerde slinger (scharnierend om de heup), maar het is meer alsof de massa en massatraagheid van het bovenlichaam over de twee benen is verdeeld. Daarom is er geen extra stabiliteitsregeling nodig en kunnen we het eenvoudige systeemontwerp van de originele passieve lopers behouden. Een computersimulatie wijst uit dat de aanwezigheid van zo'n gekoppeld bovenlichaam de energie-efficiëntie nog verder verhoogt terwijl het geen nadelige invloed heeft op de stabiliteit. Hieruit concluderen we dat het hoekdelingsmechanisme in de heup een praktische en eenvoudige oplossing is om efficiënte tweebenige lopers met bovenlichaam te construeren, goed passend bij het concept van passief dynamisch lopen.

De voorgestelde oplossing is gevalideerd door middel van de bouw en het testen van een tweede prototype. De looprobot is een autonoom 2D prototype met knieën en een bovenlichaam. Het prototype weegt 10 kg, is 1.1 m lang (0.7 m beenlengte), en loopt met een snelheid van 0.4 m/s (0.8 s per stap). De aandrijving en het merendeel van het ontwerp zijn een verbeterde kopie van het eerste prototype. Dit nieuwe prototype loopt stabiel en efficiënt, en het gedrag bij verstoringen klopt nauwkeurig met voorspellingen van een gedetailleerde computersimulatie van het prototype. De resultaten geven aan dat de positie van het zwaartepunt in voor- en achterwaartse richting een zeer krachtige parameter is voor de stabiliteit van de loopbeweging. De rest van de massaverdeling daarentegen (massatraagheidsmoment en hoogte van het zwaartepunt) hebben geen merkbaar effect op de stabiliteit. De experimenten met het tweede prototype valideren het gebruik van een hoekdelingsmechanisme om een passief bovenlichaam op eenvoudige wijze toe te voegen aan dynamisch lopende systemen.

Ten derde, om stabiliteit voor 3D loopbewegingen te verkrijgen hebben we een bijzonder enkelscharnier voorgesteld. Dit scharnier heeft een as die vanaf achter op de hiel schuin naar voren en naar beneden loopt (niet zijwaarts), nogal afwijkend van het enkelscharnier bij de mens. Het effect van dit scharnier is een dynamische stabiliteit; het zorgt voor een stabiele loopbeweging in 3D, maar alleen wanneer de robot voldoende voorwaartse snelheid heeft. Dit effect is vergelijkbaar met de stabiliserende dynamische effecten bij fietsen en skateboards. In al deze systemen is er een (statische of dynamische) koppeling tussen een zijwaartse scheefstand (de belangrijkste oorzaak van instabiliteit in 3D loopsystemen) en de richting waarin het systeem stuurt. Hierdoor stuurt het systeem automatisch in de richting waarin het valt. Bij voldoende voorwaartse snelheid zorgt deze koppeling voor stabilisatie tegen zijwaarts omvallen. Een computersimulatie wijst uit dat de orientatie van het bijzondere enkelscharnier een belangrijk effect heeft op de stabiliteit. De algemene regel hier is dat hoe meer horizontaal dit scharnier is gericht, hoe groter de kritische snelheid is waarboven stabiliteit verwacht kan worden. De simulatieresultaten laten ook zien dat de hierboven voorgestelde heupaandrijving een vereiste is om stabiliteit te verkrijgen voor 3D loopsystemen met zulke enkels. Een laatste resultaat is dat dit bijzondere enkelscharnier het zeer eenvoudig maakt om (flauwe) bochten te maken; een asymmetrie in de massaverdeling leidt automatisch tot het maken van een bocht, omdat de asymmetrie feitelijk gezien kan worden als een continue zijwaartse verstoring die gecorrigeerd wordt door (automatisch) in die richting te sturen. Kort samengevat laten de simulatieresultaten overtuigend zien dat het voorgestelde bijzondere enkelscharnier voor stabiele 3D loopbewegingen kan zorgen.

Het idee van een bijzonder enkelscharnier voor 3D stabiliteit is gevalideerd door middel van de bouw en het testen van een derde en laatste prototype. Het prototype weegt 8 kg, is 1.5 m lang (0.7 m beenlengte) en loopt ook met een snelheid van 0.4 m/s (0.8 s per stap). Het prototype laat een veel natuurlijker indruk achter dan alle voorgaande machines. Het heeft twee benen (dus niet, zoals bij de 2D prototypes, vier benen in twee symmetrische paren) met knieën en de bijzondere enkelscharnieren, en een bovenlichaam (met daarop een lichtgewicht hoofd en armen die tegen de beenrichting in zwaaien, maar deze onderdelen zitten er voorlopig meer voor de sier). Het mens-achtige voorkomen is bijzonder sterk wanneer het prototype loopt; de natuurlijke zwaaibeenbeweging inclusief het passieve kniebuigen en -strekken, de lichte zijwaartse oscillatie van stap tot stap, en de schijnbaar moeiteloze voortbeweging verschaffen het prototype een zeer natuurlijk voorkomen. Door de succesvolle loopbewegingen is met dit derde prototype het idee gevalideerd dat 3D stabiliteit verkregen kan worden door middel van een bijzonder enkelscharnier dat zijwaarts vallen koppelt aan sturen in diezelfde richting.

Het belangrijkste van wat er bereikt is met het werk in dit proefschrift is het feit dat de drie prototypes stabiel, natuurlijk, en efficiënt kunnen lopen met slechts *een zeer minimaal regelsysteem*; het complete regelsysteem bestaat uit slechts twee schakelaars onder de voeten op basis waarvan slechts drie aan/uit actuatoren (één vergrendeling in elke knie en één uit McKibbenspieren samengestelde actuator in de heup) geregeld worden, en dit slechts éénmaal per stap. Met deze resultaten hebben we aangetoond dat kennis van de essentie van het dynamisch, menselijk lopen een goede basis is voor het ontwerp van uiterst eenvoudige en toch zeer natuurlijk lopende systemen.

Martijn Wisse, 2004

Dankwoord

Een klein deel van het belastinggeld gaat naar onderzoek. Zo heb ik dankzij uw bijdrage vier jaar onderzoek kunnen (leren) doen op het gebied van lopende robots, waarvoor mijn dank. Hieronder wil ik mij richten tot de direct betrokkenen.

De belangrijkste bijdragen aan dit proefschrift komen van Arend Schwab, Jan van Frankenhuyzen, en Richard van der Linde. Arend, eigenlijk heb jij mij leren rekenen en schrijven (multibody dynamica berekeningen en het schrijven van wetenschappelijke artikelen). Je bent niet voor niets co-auteur van bijna alle tot hoofdstukken omgedoopte artikelen in dit proefschrift. Ik ben vooral zeer dankbaar voor de voor jou zeer arbeidsintensieve feedback op mijn schrijfsels; als je kritiek had, ging dat altijd gepaard met een voorbeeld of uitleg hoe het wél zou kunnen. Dat is een zeer motiverende manier van begeleiden, ik hoop dat ik dat ooit ook zo zal kunnen. Jan, jouw bijdrage aan dit onderzoek is van onschatbare waarde; het is je gelukt om op basis van mijn conceptmatige ontwerpen drie goed werkende robots te maken, en daarmee al onze theoretische gedachtenspinsels te valideren. Petje af! Ik vond het geweldig om met jou te mogen samenwerken, waarbij vooral ons veel te korte reisje naar Japan als een van de hoogtepunten geldt (ze hebben het in Japan nu nóg over ons optreden daar). Met name wil ik de aandacht vestigen op de voortreffelijke manier waarop jij je rol als 'ondersteunend technicus' hebt ingevuld; zelfs als mijn plannen volledig onhaalbaar leken, en op niet meer gebaseerd waren dan een intuïtie, gaf je toch altijd de volle inzet. Daardoor zijn de meeste van die onhaalbare plannen toch gelukt. Richard, jij bent natuurlijk de meester in onhaalbare plannen die toch lukken, jij hebt immers zes jaar geleden dit onderzoek gestart. Ik ben daarnaast vooral dankbaar voor je ongelofelijke hoeveelheid energie, ambitie en enthousiasme enerzijds, en anderzijds voor het feit dat je, door na je eigen promotie een ander onderwerp te kiezen, mij de gelegenheid hebt gegeven het looprobotonderzoek zelfstandig vorm te geven. Arend, Jan, en Richard, ik hoop dat we nog veel zullen samenwerken in de toekomst!

Binnen onze vakgroep Mens Machine Systemen hebben velen een rol gespeeld in mijn onderzoek. De belangrijkste daarvan zijn natuurlijk mijn promotoren Frans van der Helm en Henk Stassen. Frans, bedankt voor de scherpe opmerkingen en inzichten, voor je aanhoudende maar deels tevergeefse pogingen om mijn onderzoek richting biomechanica te sturen, en voor de openheid en onaflatende steun die je me desondanks hebt gegeven. Henk, jouw rol kan ik niet beter verwoorden dan dat Richard dat heeft gedaan. Jij was ook voor mij de perfecte ‘ballistische’ regelaar; ik kreeg vrijheid wanneer dat mogelijk was en effectieve feedback wanneer ik dat nodig had. Verder gaat mijn dank naar John Dukker voor de altijd hoogwaardige onderdelen, naar Dick Plettenburg voor zijn rol als (milde) advocaat van de duivel, naar Ad van der Geest, Leo Brinkman, Dineke Heersma en Tjeerd Jongeling voor verschillende vormen van ondersteuning, en naar de rest van de vakgroep en verschillende mensen daarbuiten voor hulp, een goede werksfeer, en een inspirerende omgeving. Wat dat betreft nog speciale aandacht voor mijn zeer gewaardeerde collega’s van ons ‘Delft Biorobotics Laboratory’, namelijk Richard van der Linde, Jan van Frankenhuyzen, Daan Hobbelen, Erik Fritz, Göran Christiansson, en sinds kort André Schiele. Het is een buitengewoon genoegen om met jullie te kunnen samenwerken en van jullie te leren. Ik heb grote verwachtingen voor de toekomst van het lab dat we vormen, zeker nu door de komst van Daan het toekomstperspectief van het looprobotproject een enorme vlucht heeft genomen. Daar ben ik heel blij mee, Daan, en daarnaast vooral ook met je inhoudelijke bijdrage in de vorm van nauwgezet simulatiewerk en in de vorm van zeer waardevolle feedback op al mijn goed of minder goed doordachte bedenksels.

De inhoud van dit proefschrift rust direct en indirect op het werk van vele studenten (wat in een enkel geval meer het werk werd van kundige adviseurs zoals Erik Mouw en Jan-Derk Bakker zich dat zullen herinneren). De belangrijkste studentenbijdrage is het werk van Thomas Platzer. Thomas, jouw gedegen simulatiewerk was een cruciale stap voor het 3D gedeelte van mijn proefschrift. En onze trip door Californië (met Jan en Richard) was natuurlijk geweldig! Verder mijn grote dank voor de inspanningen en bijdragen van Guus Raaphorst, Pieter Verhage, Danny Ooijen, Heidi Witteman, Joyce Verwijs, Bert de Vries, Gerrit de Waard, Stephan Tobé, Bart van der Velde, Umberto Scarfogliero, Yutaro Takahashi, Geert-Jan Thijssen, Piet-Willem Chevalier, Sai-Kit Liu, Sander Minnoye, Jasper Schuurmans, Karlijne van Liebergen, Ralph Beckers, Marijn van der Zee, en Eric Wictor.

Voor de financiële randvoorwaarden voor het onderzoek gaat mijn dank uit naar de Technologiestichting STW, met als externe projectcommissieleden Bart Koopman, Lex Lemmens, Peter van Lith, Peter Beek, Nils van Leerdam, Nico Boots, en Ton van Lunteren. Tevens ben ik zeer erkentelijk voor de interesse en financiële steun van de Anna Stichting, en voor de (nog voortdurende) samenwerking met FESTO BV.

Het laatste jaar is ook een jaar geweest van plannen voor de toekomst, en die is nu duidelijk: we gaan humanoid robots bouwen!! (Het is alleen nog niet helemaal zeker wanneer we precies gaan beginnen). Mijn dank voor alle (soms zeer grote) inspanningen die hiervoor al geleverd zijn door Daan Hobbelen, Pieter Jonker, Maja Pantic, Ioannis Patras, Thom Warmerdam, Robert Babuska, Michel Verhaegen, Frans van der Helm, Jurjen Caarls, Peter Wieringa, Peter van Lith, Just Herder, Rufus Fraanje, Henk Stassen, Marc Brinkman (jouw op ontwerpkennis gebaseerde tekenkunsten zijn echt heel indrukwekkend!), en op de achtergrond de overige collega’s van het Delft Biorobotics Laboratory. Het vooruitzicht naar deze toekomstplannen heeft voor mij een enorme motiverende werking!

Tenslotte een gebaar van dank/verontschuldiging aan mijn vrienden en familie, voor wie ik tegen het einde van mijn promotieonderzoek bijna helemaal onbereikbaar ben geworden (dat hoort kennelijk bij promoveren). Maar natuurlijk gaat de meeste lof, dank, en genegenheid naar mijn grote liefde Marrigje. Speciaal voor jou heb ik dit dankwoord zo kort mogelijk gehouden...

Curriculum Vitae

February 16, 1976
Born in Delft

1988 - 1994
Gymnasium cum laude at Sint-Stanislascollege in Delft.

1994 - 2000
MSc. study at Delft University of Technology, Mechanical Engineering. The final project concerned the design and simulation of a two-legged robot. Part of the MSc. training was a three-month internship with prof. Ruina at Cornell University, USA.

2000 - 2004
PhD. study at Delft University of Technology, Mechanical Engineering. The title of the thesis is 'Essentials of dynamic walking; Analysis and design of two-legged robots'.

2004
Recipient of a research grant for 2.5 years of Post-doc research via the Dutch 'Innovational Research Incentives Scheme' ('VENI vernieuwingsimpuls'). The research focuses on robust dynamic walking by combining the concept of 'passive dynamic walking' with biologically inspired reflexive control.